SCIENCE • TECHNOLOGY • RESEARCH HIGHLIGHTS • VISIONS •

Dissertation
48

A measurement-based statistical model to evaluate uncertainty in long-range noise assessments

Panu Maijala

VTT

VTT SCIENCE 48

A measurement-based statistical model to evaluate uncertainty in long-range noise assessments

Panu Maijala

Thesis for the degree of Doctor of Technology to be presented with due permission for public examination and criticism in Festia Building, Auditorium Pieni Sali 1, at Tampere University of Technology, on 3 January 2014, at noon.

ISBN 978-951-38-8109-2 (Soft back ed.)
ISBN 978-951-38-8110-8 (URL: http://www.vtt.fi/publications/index.jsp)

VTT Science 48

ISSN-L 2242-119X
ISSN 2242-119X (Print)
ISSN 2242-1203 (Online)

JULKAISIJA – UTGIVARE – PUBLISHER

VTT
PL 1000 (Tekniikantie 4 A, Espoo)
02044 VTT
Puh. 020 722 111, faksi 020 722 7001

VTT
PB 1000 (Teknikvägen 4 A, Esbo)
FI-02044 VTT
Tfn. +358 20 722 111, telefax +358 20 722 7001

VTT Technical Research Centre of Finland
P.O. Box 1000 (Tekniikantie 4 A, Espoo)
FI-02044 VTT, Finland
Tel. +358 20 722 111, fax +358 20 722 7001

Kopijyvä Oy, Kuopio 2013

Abstract

CAREFULLY validated long-range sound propagation measurements with extensive meteorological instrumentation were continued for 612 days without interruption, around the clock, resulting in a database with millions of files, terabytes of sound and environmental data, and hundreds of pages of documentation. More than 100 environmental variables were analysed by statistical means, and many statistically highly significant dependencies linked to excess attenuation were found. At a distance of 3 km from the source, excess attenuation was spread over a dynamic range of 80 dB, with differences of 10 dB between individual quarters of the year; also, negative excess attenuation at frequencies below 400 Hz existed. The low frequencies were affected mainly by the stability characteristics of the atmosphere and the lapse rate. Humidity; lapse rate; sensible heat flux; and longitudinal, transverse, and vertical turbulence intensities explain excess attenuation at higher frequencies to a statistically highly significant extent. Through application of a wide range of regression analyses, a set of criteria for frequency-dependent uncertainty in sound propagation was created. These criteria were incorporated into a software module, which, together with a state-of-the-art physical sound propagation calculation module, makes it possible to perform environmental noise assessments with known uncertainty. This approach can be applied to the short-term measurements too and it was shown that some of the most complex meteorological variables, among them atmospheric turbulence, can be taken into account. Comparison with two standardised noise modelling methods showed that the statistical model covers well a range of uncertainty not matched with the standardised methods and the measured excess attenuation fit within the limits of predicted uncertainty.

Academic dissertation

Instructor Professor Risto Kuivanen
VTT Technical Research Centre of Finland
P.O. Box 1000
FI-02044 VTT
Finland

Supervisor Professor Jouko Halttunen
Tampere University of Technology
P.O. Box 692
FI-33101 Tampere
Finland

Reviewers Dr Michel Bérengier
French Institute of Science and Technology for Transport
Centre de Nantes, Route de Bouaye
CS4 44344 Bouguenais Cedex
France

Dr David Waddington
Science & Engineering University of Salford
Acoustics Research Centre School of Computing
Salford M5 4WT
UK

Opponent Dr Lars Hole
Meteorologisk institutt
Allégaten 70
5007 Bergen
Norway

Contents

Preface

It was autumn 1997 and I had just finished my master's thesis[1]. My thesis adviser, Professor Matti Karjalainen, asked whether I was interested in development work for a military surveillance system. The Department of Defence Scientific Board (MATINE) had suggested that the technology developed in my thesis project[2–7] could perhaps enhance the capabilities of an underwater surveillance system[8, 9]. The problematics of detecting, locating, and recognising helicopters and aeroplanes were also on the table, and soon we were developing robust acoustic sensors, wind screens for microphones, and novel sensor materials (electro-mechanical film)[10–12] for the Finnish Air Force.

The modelling of the medium was found to be the bottleneck for further development of sensors, and the performance of the state-of-the-art models turned out to be unsatisfactory[13] (see Subsection 2.2.6). To obtain a sufficiently good sound propagation model for our use, we commenced many studies:

- Modelling of the effect of the height of the sound source on detection distance, and comparison to field measurements[14, 15].
- A comprehensive literature review surveying the measurement of atmospheric sound propagation[16].
- A military aircraft as a sound source, sound power measurements for a flying aircraft, and modelling of the short-distance propagation[17, 18].
- Plans for long-term measurements[19, 20] and development of the signal analysis for the relevant sound propagation measurement[21].
- Initial description of the propagation model software interface[22], implementation[23], and functional description[24].
- Full description of the long-term measurement set-up[25–27] and publication of the first results, in 2006[28, 29].
- Final implementation of the Atmosaku software with built-in statistical module in 2007[30] and publication of some results in 2008[31].

Atmosaku has been further developed and utilised in evaluation of environmental noise in both classified and public projects[32, 33].

This work has been rewarding, and it has taken me literally around the world — from Shanghai to Hawaii — and even to publicity: I was featured in the MTV3 lead newscast in 2005, presenting the measurements.

The number of people involved has been huge, and it would be impossible to list all of them here. I made a list of people who have made contributions through e-mail, and it ended up with more than a hundred names! The most intensive communication, involving more than 600 e-mail messages, was with Dr Ossi Ojanen, from the Defence Forces Technical Research Centre. He also was of remarkable help with the measurements — great thanks, Ossi! Much communication was conducted also with Dr Jari Hartikainen (European Defence Agency), and I am particularly thankful for his reviewing of my papers and reports.

I started the work for this dissertation under the supervision of Professor Matti Karjalainen (Helsinki University of Technology), and he was the most important person guiding me in the world of science. Matti encouraged me and pushed me onward until he passed away, in May 2010. Matti, your work effort was not in vain — thanks! In autumn 2012, Professor Jouko Halttunen (Tampere University of Technology) took the role of supervisor and Professor Risto Kuivanen (VTT Technical Research Centre of Finland) promised to advise me as a mentor. I found their comments and critique very useful and reassuring.

I wish also to thank all of my colleagues at VTT but especially Kari Saarinen, M.Sc.; Velipekka Mellin, M.Sc., who took part in my lengthy measurement trips to Sodankylä; and Dr Seppo Uosukainen, who went through all of my Atmosaku code and made many improvements. The assistance provided during the kick-off phase by Mervi Karru, M.Sc., was greatly appreciated. All the great meteorologists with the Finnish Meteorological Institute who were involved in this project, thank you very much — in particular, Dr Ivan Mammarella and Mr Reijo Hyvönen, who validated the meteorological data. I would also like to thank the staff of the Sodankylä Geophysical Observatory, and special thanks go to Dr Esa Turunen and Dr Antti Kero — you were my right and left hand while I was not in Sodankylä. And, of course, I value the pleasure and honour I had of enjoying the day-to-day company of people at the ASE department of TUT during my final sprint in writing this thesis.

I had the opportunity to participate in development of the Common Noise Assessment Methods in Europe, in the work of the CNOSSOS-EU Technical Committee. I especially appreciate the discussions with the members of WG5, the sound propagation group. I would like to offer my special thanks to Dr Guillaume Dutilleux (CETE de l'Est, France) for his voluntary work in the comparison between models.

Most of the work for this research was carried out in projects financed by the Finnish

Air Force. I would like to show my humble appreciation for the confidence in my work to the staff of Air Force Headquarters, along with very special thanks for the support and encouragement I received from Kari Tanninen, M.Sc.

The writing phase of this manuscript was made possible in part by a grant from the Industrial Research Fund at Tampere University of Technology and in part by the financial support of the VTT Technical Research Centre of Finland.

Finally, I wish to thank my friends, parents, brothers, sisters, and other family for all of your love and support! My dearest wife Mira and children Jere, Tomi, Lari, Ella, and Aapo, without your love and the joy of your existence, I would find work meaningless. Thank you for your patience during my most intense work period; I hope I can pay you back for this time.

In 2008, we received substantial EU funding for a project covering environmental noise, and the completion of this thesis began seeming concretely possible, so I promised not to cut my hair until the thesis had been submitted and approved. However, annoyance issues took the main role in the project and my growing hair began to get attention. Pekka Simojoki, a musician friend of mine from Kangasala, asked a couple of years ago, grinning, whether I had taken a Nazarite vow, as the Bible says in Numbers 6:5 (KJV): '*All the days of the vow of his separation there shall no razor come upon his head: until the days be fulfilled, in the which he separateth [himself] unto the Lord, he shall be holy, [and] shall let the locks of the hair of his head grow.*' Sounds appropriate, but my issue was more worldly — to force myself to remember every time I looked in the mirror that I should finish the job... Now, as I write these final words, I'm starting to believe that I can finally get rid of my long braid.

Kangasala, summer 2013

Panu Maijala

Chapter 1

Introduction

ENVIRONMENTAL noise, defined as unwanted or harmful outdoor sound created by human activities[34, Art. 3], can be generated by traffic, industry, construction, and recreation activities[35, p. 12]. Airports, (wind) power plants, rock-crushing, shooting ranges, and motorsport tracks are examples of noise sources from which the noise propagates several kilometres from the place of origin.

The uncertainty in environmental noise assessments increases rapidly with the distance from the source, and all assessment methods have their limitations: for example, the distance limit of the most commonly used one, following ISO 9613-2:1996, '*General method of calculation*', is 1000 m[36, Clause 9] and Nordic environmental noise prediction method Nord2000 is validated only to 200 m[37, p. 18]. It is challenging to include all the uncertainty, the limits, and the error when one is preparing noise maps[38].

Environmental noise has both direct and indirect social impacts. In addition to restricting land use and causing real estate to lose value, environmental noise has become a health issue: cardiovascular disease and cognitive impairment are among the identified effects of environmental noise[35, 39]. Including disturbance and annoyance, the social significance of this question is of major economic importance today. The annual costs arising from harm caused by noise are enormous: in the EU, € 13,000,000,000 *per annum*[40, p. 72]. However, the associated economic valuation is challenging[41].

1.1 Significant milestones

1.1.1 The phenomenon becoming harmful

A relatively large amount of literature on the topic exists (see Table 1.1) and publications on the subject[42, 43] can be found even from 350 BC. Aristotle (Ἀριστοτέλης) (384–322 BC) is often credited with being the first to write about propagation of sound as compression waves[44, p. 288], and Roman engineer Marcus Vitruvius Pollis was the first known to report the analogous relationship between sound waves and surface waves

on water[44, p. 307] — the wave theory of sound. However, both Aristotle[42, p. 175] and, according to Cohen and Drabkin, Archytas (Ἀρχύτας ο Ταραντίνος) (410–350 BC) came to an incorrect conclusion as to the speed of sound: Archytas wrote that '*high-pitched sounds move more swiftly and low-pitched more slowly*'[44, p. 288].

Table 1.1: The number of related publications found by Google Scholar, from fetching on 19 March 2013 (in brackets are figures for the same search limited to publications before 1997, when the work for this thesis began)

Search words	Search results
sound propagation	1,310,000 (260,000)
noise weather	609,000 (99,800)
noise uncertainty weather	91,900 (16,500)
sound propagation uncertainty	78,900 (19,500)
noise uncertainty meteorological	50,400 (13,000)
sound propagation uncertainty meteorological	14,700 (3780)
statistical model sound propagation uncertainty meteorological	9460 (1850)

It took more than 2000 years to correct the false assumption about the speed of sound. In *Opera Omnia*, Petri Gassendi (1592–1655) wrote '*... tranſlationem eiuſ per ſpatium eſſe ſemper æqui-velocem.*'[45, p. 418], freely translated as '*... travels always with the same speed.*'. According to Lindsay, Gassendi was the first to measure sound propagation[46], but Lenihan claims that he never made any measurements[47]. Though Gassendi did refer to measurements made by friend Marin Mersenne (1588–1648), a monk of the Franciscan Order. Lenihan's argument is based on the fact that no numerical measurements have been found in Gassendi's writings. If Lenihan is right, Mersenne was the first scientist to measure sound propagation. In any case, some credit was given by Gassendi himself: '*Quo loco tacenda non eſt Merſenni noſtri obſervatio, qui velocitatem ſoni ſtudioſè emenſuſ*'[45, p. 418], in English: '*We must not fail to mention the observations of our friend Mersenne who studied the velocity of sound diligently*'.

Mersenne carried out experiments with gunfire, and his result, 230 Ts per second[48, p. 44] (448 m/s), indicates that the measurement accuracy was not very good. It took 100 years more to gain the accuracy needed for determination of the sound speed value used today and for the temperature-dependence to be noticed[49].

The theory of sound propagation was first stated in mathematical form by Sir Isaac Newton (1642–1727) in his *Principia*[50, pp. 369–372]. His derivation of the numerical value of the speed of sound for sea level is fascinating: the initial data he needed were the mass ratio between quicksilver and rainwater ($13\frac{2}{3}$) and the mass ratio between rainwater and air (870) when the quicksilver barometer is at 30 inches. Then he calculated the height of uniform air (9 km) and imagined a pendulum of that length. It was com-

monly known that the frequency for a pendulum 1 m in length is 0.5 Hz, and Galileo Galilei (1564–1642) had demonstrated in his *Dialogues* that the time period of a pendulum is directly proportional to the square root of the length[51, p. 96]; this indicated a 191-second oscillation for a pendulum 9 km long. The circumference of a circle with 9 km radius is about 57 km, so the speed of the pendulum is 57 km / 191 s ≈ 300 m/s (in Fig. 1.1, 979 feet/s). If one assumes the sound propagates in solid particles '*instantaneously*' and every ninth particle in the air is solid[52, p. 182], $979/9 = 109$ has to be added to yield the real speed of sound: $979 + 109 = 1088$ ft/s (see Fig. 1.1), which is the same value used today in 0 °C conditions. A more useful solution can be found in later editions of *Principia*[52, p. 180]: the analytical solution for the speed of sound $c = \sqrt{P/\rho}$, where P is the gas pressure and ρ the corresponding density. Newton considered also the effects of weather on sound propagation, speculating thus: '*But in winter, when the air if condenſed by cold, and itſ elaſtic force if ſomewhat remitted, the motion of ſoundſ will be ſlower in a ſubduplicate ratio of the denſity; and on the other hand, ſwifter in the ſummer*'[52, p. 183].

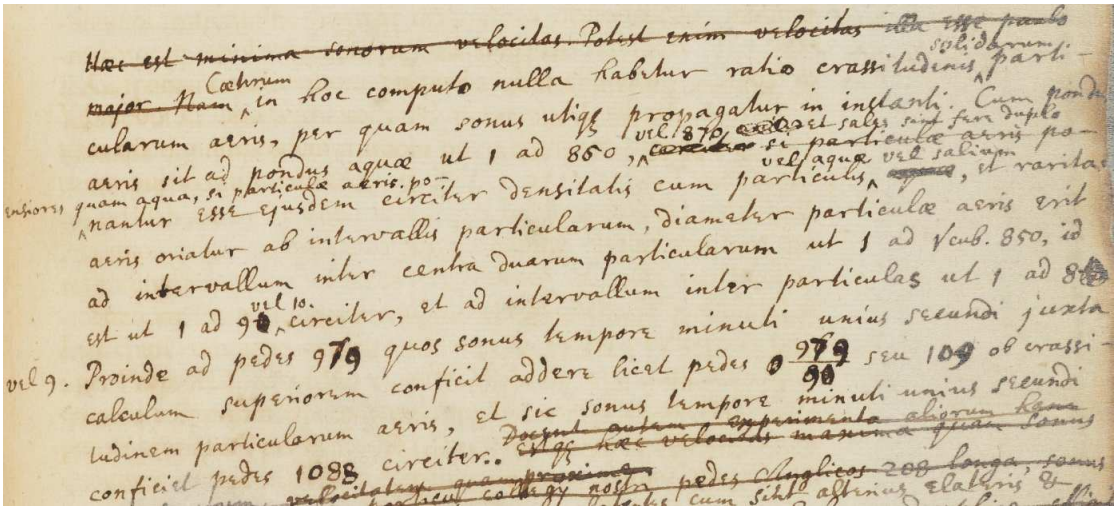

Fig. 1.1: The speed of sound, from Newton's hand-written notes[50, sheet facing p. 370]. Reproduced by kind permission of the Syndics of Cambridge University Library, classmark: Adv.b.39.1.

Leonhard Euler (1707–1783) too made great contributions to the theory of sound propagation. At the age of 20 years, he depicted in *Dissertatio physica de sono*[53] how air consists of small compressible globules and sound is transferred to other places by a compression force acting on some globules, which, in turn, compress others, further away (on pages 210–211). Further, in that treatise he presents an expression for the speed of sound in air (on pages 213–214). Euler and Joseph Louis Lagrange (1736–1813) penned much criticism of Newton's theory, but later Euler obtained Newton's result himself and wrapped up the state-of-the-art theory for sound propagation in *De la propagation du son*[54] — including the theoretical foundation for **the wave equation**

in the air[1],

$$\left(\frac{ddy}{dt^2}\right) = 2gh\left(\frac{ddy}{dx^2}\right), \tag{1.1}$$

in Euler's original syntax, where y is the variable to be solved for (sound pressure), t time, x distance, h the '*height of a column of air*', and g the '*height by which a heavy body falls in a second*'.

In his calculations, Lagrange too ended up with Newton's equation, but Pierre Simon Laplace (1749–1827) developed Newton's result further and pointed out[56] that the adiabatic ratio, γ, was needed for correction[57, pp. 119–120] of the excessively low values in Newton's equation: $c = \sqrt{\gamma P/\rho}$. Later, Laplace's theory was found to be so precise that γ for gases is commonly defined via measurement of the speed of sound in the gas.

Sixty years after Euler's wave equation in one dimension[54, 58], Siméon Denis Poisson (1781–1840) published a 56-page introduction to the propagation of a compression wave in a three-dimensional fluid medium[59]. Pierce states, that Euler presented[61] the three-dimensional wave equation also[60, p. 18], but, according to Lindsay, Poisson's presentation was the first correct one[46, p. 637].

Kurze and Anderson claim[62, p. 119] that the first scientific modelling of outdoor sound propagation was performed by Rayleigh, Reynolds, and Kelvin — this calculation of acoustic refraction is described in Rayleigh's *Theory of Sound*[63, pp. 129 *ff*]. Rayleigh also introduced Fermat's principle in modelling of sound propagation with ray theory[63, p. 126].

The term 'environmental noise' is relatively new — it has been recognised as an adverse environmental effect for less than a hundred years[64]. In 1933, Edward Elway Free wrote[65]: '*A dozen years ago no one thought of measuring noise.*' The first studies of environmental noise can be traced back to the first issues of scientific journals on acoustics. The Acoustical Society of America was established in 1929, and the first issue of their journal's Volume 2 was dedicated to environmental noise[66–71], because Shirley Wynne — a health commissioner of New York City — asked[66] them to address the growing problem of noise. Rogers Galt was among the first scientists to test the recently developed '*acoustimeter*'[67] — a sound pressure meter with the weighting of an average human ear[2] — in environmental noise measurements[68], though without any concern about the uncertainty caused by the weather.

MIT Professor Emeritus Karl Uno Ingard was one of the earliest acousticians to consider the uncertainty in environmental noise assessments that is caused by changing meteorological conditions. In 1953, he wrote that '*[i]nvestigations of the effect of weather on sound propagation can be traced back with certainty to the years around 1700. People were almost as concerned about noise and sound then as today. At that*

[1] The wave equation was derived for a continuous string slightly earlier by Jean Le Rond D'Alembert (1717–1783)[55].

[2] Very close to what was later standardised as A weighting[72].

time the primary problem was to make sound audible as far away from the source as possible' [73].

Known sources of environmental noise are usually planned for locations far from residential areas. As cities spread out to more and wider regions, a remote industrial plant or airport soon ends up surrounded by residential areas. This century's typical environmental noise assessment might be for the rock-crushing station depicted in Fig. 1.2 and nearby habitation. This scenario would certainly lead to complaints and later to assignments for environmental consultants. Such a consultant, when visiting the site and averaging sound pressure levels over a short time, might obtain ambivalent results, as shown in Fig. 1.3. The actual measurements presented in the figure are from different dates at different distances from the source. The overrun value 60 dB at a distance of 300 metres from the station could lead to costly noise-reduction actions or the authorities could even withhold permission for operation of the station. The world is full of these short-time overrun stories, annoyed people, and arguments in the courts. Another good example is from Phoenix Valley, Arizona, where a sound level increase of 8 dB at distances 400 m and greater from the freeways was found from October to March and led to expensive investigations, reports, and solutions. According to the environmental consultants, the overruns were due to night-time thermal inversion conditions [74].

1.2 Fragmentation in modelling

Aircraft were the first sources of environmental noise to be the subject of a dedicated computer-based tool for calculation of sound propagation. In January 1978, the US Federal Aviation Administration (FAA) released version 1 of the Integrated Noise Model (INM) [76, p. 18]. It would be many years before the calculation tools became available to environmental consultants. Environmental Noise Model was among the first software to run on low-cost personal computers — it was released in 1987 [77].

Many computational tools for calculation of sound propagation became available during the 1990s [78]. There are now analytical solvers; standardised ray-tracing-based techniques [36], which include interaction with a complex impedance boundary; Gaussian beam ray trace algorithms [79]; and many methods for approximately solving the full wave equation, such as the parabolic equation (PE) [80–82], the fast field program (FFP) [83], and hybrid combinations thereof [84, 85].

Even the most recent and complete models of sound propagation lack information on accuracy. If a comparison of accuracy is made between models [78], the models can be categorised as, for example, simple, as in the case of the ray-tracing-based, or more complex, such as solvers of the wave equation. Typically, the results from simple models differ from those of complex models with certain input parameters but are very close to those of other models in the category in question. However, the uncertainty of the

Fig. 1.2: A rock-crushing station has many distinct noise sources, among them cone and jaw crushers, stone screening and conveyor systems, excavators, front-loading shovels, dozers, and haulage vehicles[75]. Image © 2003 V. Mellin; used with permission.

models still cannot be determined without comparison to reality. With some evaluations, it is possible to use scale models[86], which aids in addressing this issue.

1.3 Harmonisation of abatement-related methods

The first part of the international standard for assessment of environmental noise was published in 1982[87] and described the basic quantities and procedures. However, one individual but significant environmental noise source — aircraft — had received an international standard just a few years before, in 1978[88]. With advances in computer technology, the computational approach became more interesting. ISO 9613[36, 89] defined an empirical octave-based ray-tracing calculation method for point sources with a defined sound power level. This method became the most important standard for environmental noise assessments and was implemented in practically all commercial calculation software. However, the method is very limited and its uncertainty is almost impossible to manage[90].

Research activity in the field of outdoor sound propagation started to increase no-

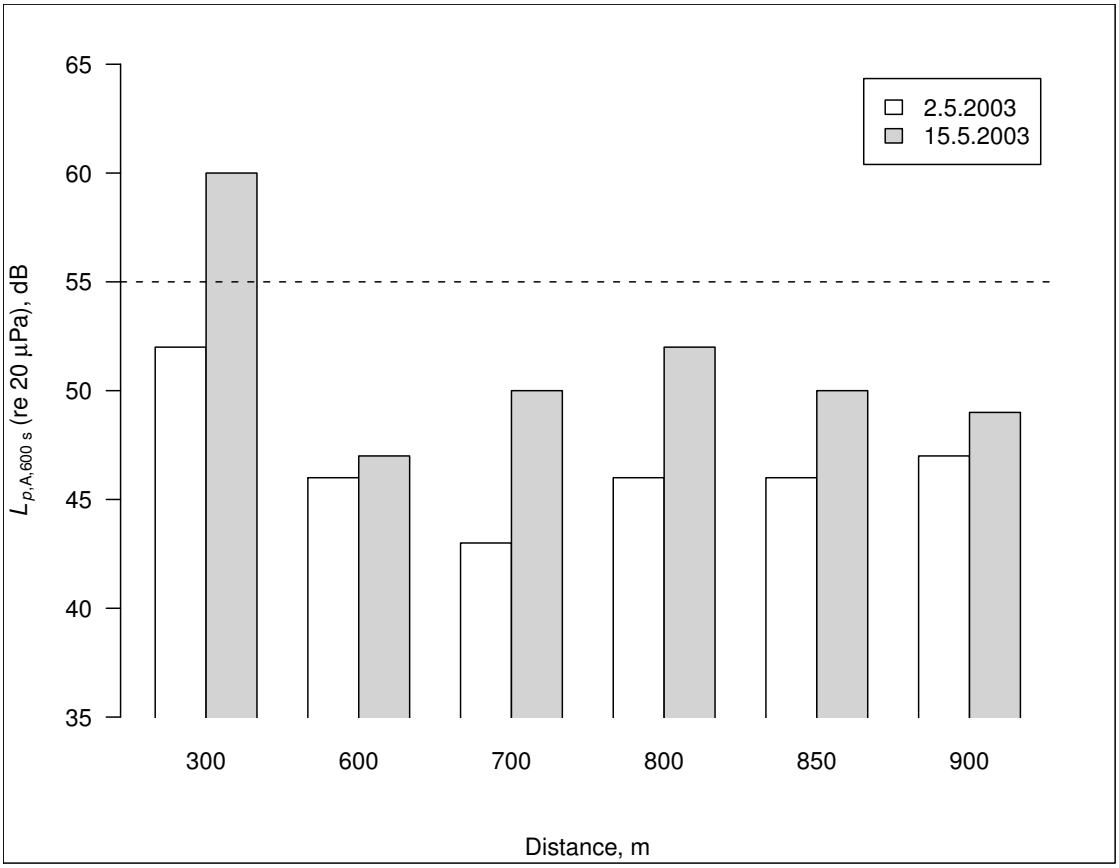

Fig. 1.3: Variation of 10-minute-equivalent sound pressure levels at certain distances near a rock-crushing station: 2 May 2003, with a headwind of 3 m/s and all values below the 55 dB statutory limit, and 15 May, with a 2 m/s tailwind and an overrun at 300 metres from the station.

ticeably at the beginning of this century. The importance of weather conditions for sound propagation was recognised, and serious research campaigns were implemented. In the European Union, the Environmental Noise Directive (2002/49)[34] (END), related to the assessment and management of environmental noise, gave impetus to work[91] on harmonising the computational noise mapping methods[92] and presenting the state of the art[93] and guidelines[94, 95].

CNOSSOS-EU[96–99] is the framework intended for use by the EU member states (MS) for noise mapping and action planning. In the initial phase of the development of the CNOSSOS-EU framework, only seven of the 27 MS were assessed as being in compliance with the requirements of the assessment methods in the END[34, Art. 6]. Comparability and reliability of assessments were cited among the CNOSSOS-EU objectives, and improvement in meeting of the objectives is expected if all the MS migrate to this framework. However, there will always be sources of *uncertainty*, some well-known and others unknown[38].

The French method of assessing noise propagation, NMPB 2008[100], was selected as the propagation part of the CNOSSOS-EU framework and translated into the AFNOR

NF S 31-133:2011 standard[101, p. 78]. The maximum distance at which the NMPB 2008 framework is valid is 800 m[100, p. 7].

A framework such as CNOSSOS-EU is a collection of compromises, but there is also an ongoing review and development process — better means can be implemented once they become available.

The most important historical milestones in sound propagation and environmental noise assessments can be found in Table 1.2.

Table 1.2: The main line of milestones in sound propagation and noise assessments

350 BC	The first scientific publications by Aristotle[42, 43].
1637	The first scientific measurements by Mersenne[48].
1687	The first theory in mathematical form from Newton[50].
1759	Theoretical foundation of the wave equation in air by Euler[54].
1820	Three-dimensional wave equation in fluids by Poisson[59].
1877	The first mathematical modelling of outdoor sound propagation[63, pp. 129 *ff*].
1953	The first paper on meteorological effects in noise abatement[73].
1982	The first international standard for assessment of environmental noise[87, 102, 103].
1990s	Breakthrough of various computational tools[78].
2003	The first cross-border project to harmonise assessment methods[91].
2000s	Various methods for management of uncertainty.

1.4 What it's all about

The weather conditions can dramatically alter the propagation of sound outdoors. The environmental variables must be included in the sound propagation models, but which are the most important of these to consider?

The theory of atmospheric sound propagation is well presented in the literature, and good reviews of the basics can be found[62, 104–107]. According to said literature, the most important physical phenomena in outdoor sound propagation are *absorption*, *refraction*, and *scattering* (see Fig. 1.4). Outdoors, sound almost never propagates along straight paths. The sound is refracted by both wind and temperature gradients and is *scattered* by *turbulence*. Scattering is a common umbrella concept referring to several phenomena that change the propagation direction of a sound wave. Scattering involves, for example, diffraction or reflection according to Snell's law. However, because refraction is a consequence not of the effect of obstacles on the propagation path but of the *lapse rate*, it is not covered by scattering. The lapse rate has an effect on turbulence. If the temperature rises as a function of height, there is a positive temperature gradient; this meteorological situation is called *inversion*. Upward-oriented sound rays are bent

toward the ground during inversion and scattering is decreased because the mechanisms maintaining turbulence are eliminated. In contrast, with a negative temperature gradient, the turbulence is usually strong.

A highly simplified depiction with only the most basic environmental interactions is presented in Fig. 1.4. Sound propagation in the atmosphere is affected also by many other variables, and all of these come together in a more or less complex way, often changing rapidly as a function of time. The effect of all these variables together on sound propagation can be expressed as A_{total}

$$A_{\text{total}} = A_{\text{div}} + A_{\text{env}}, \tag{1.2}$$

the total attenuation at a given distance (the location of noise *immission*) from the source (noise *emission*), and it is the sum of the geometric divergence A_{div} and the fluctuation, left to the term A_{env}, for the *excess attenuation* or environmental attenuation. Depending on the purpose, the A_{env} term may be separated into attenuation due to atmospheric absorption (A_{atm}), ground effect (A_{gr}), barriers (A_{bar}), and miscellaneous other effects (A_{misc}) [36]. In this thesis, the latter separation was not performed; rather, excess attenuation A_{env} was explained by all the measurable environmental quantities, such as ground properties and lapse rate, as shown in Chapter 4.

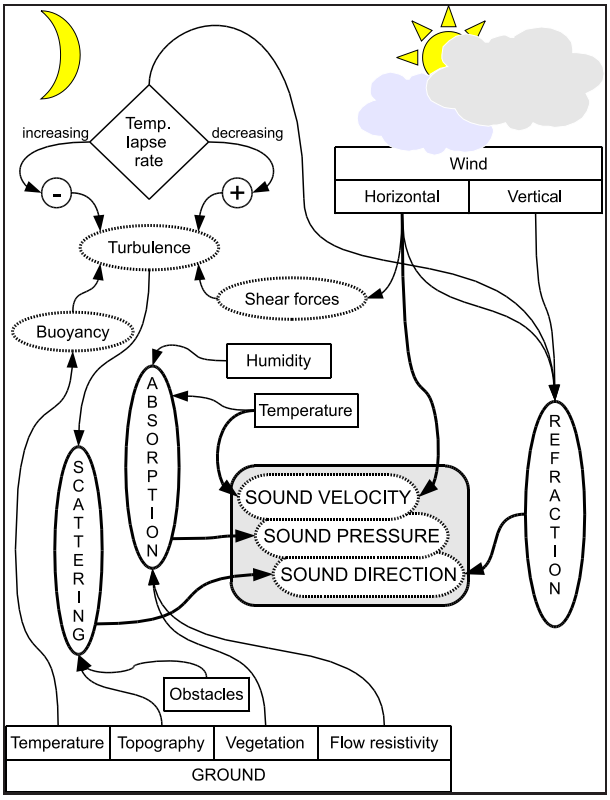

Fig. 1.4: The most important variables and their interactions with sound propagation outdoors. [30]

1.5 Research questions and objectives

The driving forces for this research have been both civilian and military needs for computational atmospheric acoustics and the unknown link between the modelling and the real world — the uncertainty. The **main research problem** was defined thus: *What are the most important meteorological variables that should be taken into account in modelling of the long-range sound propagation, and what is the effect of the variables on uncertainty in noise assessments?* Many detail-level questions were identified:

- Are all the major meteorological variables that affect long-range sound propagation known?
- What are the main variables of uncertainty and their effect on the magnitude?
- How may one evaluate the uncertainty caused by various meteorological variables — what are the interdependencies among the noise and meteorological variables?
- What could be the role of the statistical means in determination of the uncertainty in long-range sound propagation?

The main objective of this work was to complete an extensive measurement campaign with simultaneous measurements of environmental variables and sound propagation, to identify the most important meteorological variables, and to create a model based on statistical analysis of the results. This measurement-based statistical model was implemented as a software module to evaluate the uncertainty in noise assessments due to changing meteorological conditions. In the course of the project, also a state-of-the-art physical model was implemented (see Section 2.1) and the statistical module became a part of the software, called *Atmosaku*.

1.6 The contribution of the research

More than a hundred people were involved in this project in one way or another during the 15 years in which the author was developing the original idea of a sound propagation model capable of meeting the objectives set. Most of them are experts in several fields and people whom the author asked to participate as advisers at the seminars and meetings wherein the work was developed further. Almost 30 of these people were involved in the long-term measurements in Sodankylä, Finland, with five of them together responsible for the most significant amount of hands-on support. The knowledge work involved four people, whose work has been documented. *Development of Signal Analysis for the Sound Propagation Measurement*[21], master's thesis by Karru, shows the implementation of the signal analysis, referred to in Section 4. The analysis was further developed (see Section 5.2), and a technical report, *Measurements of Nonlinear*

and Time-Variant Acoustical Systems[108], was written by Kero. The work of Mammarella and Hyvönen was documented as a technical report, *The Structure of the ABL at Sodankylä*[109], and it is discussed in Section 4.10.

The **main contributions** made by the author are the following:

- Introduction of the original idea of a hybrid model, *Atmosaku*, in which a measurement-based statistical model was coupled with a state-of-the-art physical model to make possible the evaluation of uncertainty.
- Planning of the pre-processing of the meteorological and acoustic data, signal analysis, and the automation tasks needed for carrying out the measurements. Also accomplishment of more than 95% of the programming needed for the automation, as described in Chapter 3.
- Performance of all the measurements, as described in Chapter 3.
- All of the statistical analysis of the meteorological and acoustic data, as described in Chapter 4.
- Drawing of all conclusions described in this thesis.
- Implementation of the Atmosaku physical and statistical models alike, as described in sections 2.1 and 4.8.
- All of the Atmosaku simulations and the analysis of the results as described in this thesis.

1.7 Limitations

Whilst a wide variety of noise source types, with diverse properties and propagation paths, are examined in environmental noise assessments, some limitations apply to this work.

- Only linear acoustics are considered, no high sound pressures, shock waves, or high temperatures: The emission from some environmental noise sources can exceed the limits of linear acoustics, but in most cases the majority of the propagation path will be linear.
- One stationary point source at rest near the ground is used: the source is described as a fixed location with a known sound power level and directivity in one-third-octave frequency bands.
- One constant receiver is assumed: There is a fixed propagation distance, but other distances can be approximated, within the limits discussed in the thesis.

- The frequency range is limited to 40–1600 Hz: The propagation distance imposes a limit on higher frequencies, due to atmospheric absorption, and the lowest frequencies were limited by the output capabilities of the subwoofer.
- The uncertainty of measurement devices (IEC 61672-1:2002[72]) and the standard method for expression of uncertainty in measurement (JCGM 100:2008[110]) were excluded from this analysis.

Depending on the context, the *long-term measurements* refer to different time spans. A long-term environmental noise measurement takes longer than the ordinary environmental noise measurement period, which is 10 minutes for a stationary noise source[111]. The long-term measurements mentioned in the literature have ranged from hours to years (see Section 2.2), and there exist fixed noise-measurement installations in many airports and urban areas. For a typical case of environmental noise, both the source and the propagation path change with changes in the environment. Meteorological conditions may affect the most common environmental noise source — road traffic — by changing the road surface from dry into wet. During the wintertime, spiked or studded tyres also have their effect on this noise source. It is of primary importance to know how much the environment changes and over what time the change extends, before one concludes that any rules of minimum averaging periods are representative of the values for the year. In this thesis, the changes in environmental noise sources are not discussed further in this connection, nor are the time periods of measurements for the yearly averages required under the END[34].

1.8 The structure of the thesis

The bulk of this thesis focuses on the long-term measurements, preparation of the database, and the phases of the statistical analysis. The purpose of this 'Introduction' chapter is to give an overview of the problematics and the motivation for this work. The findings are situated along the time-continuum (see Table 1.2) through presentation of a brief historical survey from the standpoint of measurements and modelling, meteorological phenomena, and uncertainty, linked to the sound propagation and environmental assessments. New perspectives are opened through explication of the process of development whereby the great men of history, through failures, eventually reach the correct conclusion. Chapter 2 provides the background and a review of the state of the art in this field. Then, the main contribution is presented in chapters 3 and 4. The outcome of the thesis project and some ideas for future work are discussed in Chapter 5. Finally, the main conclusions and the contributions of the thesis are summarised in Chapter 6. To assist in the reading, a glossary is provided, starting on page 141, and an index, which begins on page 177.

Chapter 2

Background and the state of the art

INTERNATIONAL standard ISO 1996[112] describes basic assessment procedures and methods. Initial data for assessments are usually obtained through measurements or modelling. It is practically impossible to measure all possible distances and atmospheric conditions from the noise source, also, if one applies the general guidelines in the European Union, around the clock, with averaging over the years of measurement. EU Directive 2002/49/EC[34] states: '$L_{p,\mathrm{A,eq}}$ *should be determined over all the day periods of a year which is a relevant year as regards the emission of sound and an average year as regards the meteorological circumstances.*' On the other hand, there is no model that explicitly is adapted to this statement.

In general, it is possible to define the average meteorological year on the basis of existing long-term weather observations and climatological statistics. The standard normal period, preferred by the World Meteorological Organization (WMO), is based on the years 1961–1990, and the next internationally recognised standard normal period will be 1991–2020.[113]

New guidelines and regulations may give rise to new problems, if the objectives and means do not meet: Denmark has recently lowered the limit for noise from wind turbines to a 20 dB A-weighted indoor sound pressure level[114] (from 45 dB), which poses a clear challenge to measurement — not only because it is below the noise floor of most measurement microphones.

2.1 Physical modelling

The most common modelling methods were introduced in Section 1.2. One of the most widely used, a state-of-the-art physical model for calculation of long-range sound propagation, is the parabolic equation method. One of the strengths of this numerical method is that it is not confined to a layered atmosphere or homogenous ground surfaces. With the PE method, the lapse rate and surface impedance values can be functions of loca-

tion. Additionally, topography and turbulence can be addressed in the same model and solved for simultaneously, interacting with each other.

In the PE method, the sound field is solved for by means of the parabolic equation. In the calculation of outdoor sound propagation, the elevation angle of the source emission is small and other directions of emission can be ignored — the wave equation can be simplified to the parabolic equation. In the PE method, the widest elevation angle can vary between 10° and 70°. In practice, depending on the PE method employed, the result is accurate up to an angle of 35°.[115]

The physical part of the Atmosaku software is based on the PE method. Next, an introduction to the PE method is presented; a more comprehensive presentation is given by Salomons[115]. Cylindrical co-ordinates (r, z, ϕ) and the notation $\partial_z \equiv \partial/\partial z$ are used. Note the departures from the notation usually presented in mathematical papers — the notation here follows the literature on physical acoustics: r is the distance, and z is the variable for height.

The co-ordinate transforms for Cartesian ↔ cylinder are:

$$x = r\cos\phi, \quad y = r\sin\phi, \quad z = z \tag{2.1}$$

and

$$r = \sqrt{x^2 + y^2}, \quad \phi = \arctan(y/x), \quad z = z. \tag{2.2}$$

Gilbert and White (1989)[116] were the first to suggest use of the Crank–Nicolson PE method (CNPE) in connection with sound propagation in the atmosphere[116]. The method is based on the Helmholtz equation (Eq. 2.3), with k referring to the wave number and p_c to the complex pressure amplitude

$$\nabla^2 p_c + k^2 p_c = 0, \tag{2.3}$$

written in three-dimensional cylinder co-ordinates (2.4) thus:

$$\frac{1}{r}\frac{\partial}{\partial r}\left(r\frac{\partial p_c}{\partial r}\right) + k_{\text{eff}}^2 \frac{\partial}{\partial z}\left(k_{\text{eff}}^{-2}\frac{\partial p_c}{\partial z}\right) + \frac{1}{r^2}\frac{\partial^2 p_c}{\partial \phi^2} + k_{\text{eff}}^2 p_c = 0. \tag{2.4}$$

The equation uses the effective[1] value of wave number, which is calculated from effective sound speed c_{eff} at frequency f by means of $k_{\text{eff}} = 2\pi f/c_{\text{eff}}$. The sound source is assumed to be an axisymmetric monopole source, and the variable p_c is replaced in accordance with

$$q_c = p_c\sqrt{r}. \tag{2.5}$$

This way, the three-dimensional Helmholtz equation is simplified to two-dimensional form (2.6).

[1] 'Effective' refers to total, consisting of everything that affects the quantity. For the sound speed, it is the sum of the adiabatic speed (due to temperature) and air movement (due to wind and turbulence).

$$\frac{\partial^2 q_c}{\partial r^2} + k_{\text{eff}}^2 \frac{\partial}{\partial z}\left(k_{\text{eff}}^{-2}\frac{\partial q_c}{\partial z}\right) + k_{\text{eff}}^2 q_c = 0 \tag{2.6}$$

If the term $k_{\text{eff}}^2 \partial_z \left(k_{\text{eff}}^{-2}\partial_z q_c\right)$ in Eq. 2.6 is approximated by the term $\partial_z^2 q_c$, the two-dimensional Helmholtz equation can be written in the form of Eq. 2.7, subject to the condition that k_{eff} does not strongly depend on z:

$$\frac{\partial^2 q_c}{\partial r^2} + \frac{\partial^2 q_c}{\partial z^2} + k_{\text{eff}}^2 q_c = 0. \tag{2.7}$$

This approximation (2.7) is the basis for various PE models. The error due to the simplification above is negligible, as can be shown by numerical calculations.

In the CNPE method, the sound field is solved for in the rz plane and calculation starts from the point $r = 0$ at the time moment $p(0,z)$, which presents the monopole source. The function is extrapolated to positive r direction, and we solve for the complete sound field $p(r,z)$. Next, we define the following: $k_{\text{eff}} \equiv k$, $c_{\text{eff}} \equiv c$, and $q_c \equiv q$. The step of extrapolation from distance r to distance $r + \Delta r$ is defined as

$$q\,(r,z) \rightarrow q\,(r+\Delta r, z)\,. \tag{2.8}$$

In other words, the values of q at the distance $r + \Delta r$ are calculated from the values at distance r. Both horizontal step Δr and vertical step Δz have to be less than $\lambda/10$[115], where λ is the wave's length. In this two-dimensional PE method, the calculation grid is defined as a slice of the atmosphere. The horizontal grid size is the calculation coverage (extent) distance divided by the sound speed and multiplied by frequency times the 'oversampling' coefficient mentioned just above — usually 10. The same applies to the calculation of the vertical grid size, but the sound ray path and the sound speed profile of the atmosphere have to be taken into account in estimation of the vertical coverage or extent; see Subsection 2.1.1.

2.1.1 Models for the boundary conditions

The calculation grid is of finite length and height. The boundary condition at the bottom of the grid is the complex impedance of the ground. The most practical way to determine the impedance is to calculate it from the *flow resistivity*. Flow resistivity is, in general, a real and quite easily measured parameter, though measuring the flow resistivity of the soil is challenging[117]. There exist many models for determination of the impedance from the flow resistivity, one of the most widely used of which is the Delany–Bazley model[118], involving a direct and a reflected wave (2.9):

$$Z = 1 + 0.0571\left(\frac{\rho_0 f}{\sigma_{\text{r}}}\right)^{-0.754} + i0.087\left(\frac{\rho_0 f}{\sigma_{\text{r}}}\right)^{-0.732}, \tag{2.9}$$

where σ_r is the flow resistivity in Pa $\cdot$ s/m^2, f is the frequency, and ρ_0 is the static air density. Embleton et al. refined[119] the work of Delany and Bazley by taking into account also the ground wave. This resulted in more accurate values for time-dependent ($e^{-i\omega t}$) models (2.10):

$$Z = 1 + 9.08\left(\frac{f}{\sigma_r}\right)^{-0.75} - i11.9\left(\frac{f}{\sigma_r}\right)^{-0.73}. \tag{2.10}$$

The values of the flow resistivity are quite well documented in the literature, and a compilation from some of these sources can be found in Table 2.1. As a reference, the typical flow resistivity for a light mineral wool is 10 kPa $\cdot$ s/m^2. In 2012, Pohl et al. published the open database openMat for acoustic properties of materials and objects[120]. It is directed mainly at room acoustics, but some data are usable also for modelling of environmental acoustics.

The top of the calculation plane is more problematic. An infinite boundary condition (ρc) is not enough, because only vertically propagating plane waves will be absorbed. An artificial absorbing layer has to be defined to eliminate the reflections downward. For just below the top of the grid, Salomons[82] proposes an imaginary coefficient to the wave number for a narrow layer, $z_t \leq z \leq z_M$, of which z_M is the top and z_t the bottom[82]. The proposed coefficient is

$$iA_t \frac{(z - z_t)^2}{(z_M - z_t)^2}, \tag{2.11}$$

where A_t is a constant. Experiments have proved that a softer layer (see Eq. 2.12) behaves better[30]:

$$iA_t \left(\frac{z - z_M + z_t}{z_t}\right)^2. \tag{2.12}$$

The best results were obtained when A_t was changed as a function of frequency. Good experimental values for the frequencies 1000, 500, 125, and 30 Hz are $A_t = 1$, 0.5, 0.4, and 0.2, respectively. Linear interpolation can be used for the frequencies between these values. A safe layer for this absorbing layer $z_M - z_t$ is 50 wave lengths. There are other possibilities too in definition of this boundary condition[122].

The height of the calculation plane should be defined so as to be great enough that the absorbing layer does not affect the results. A general rule for z_M cannot be stated, because the optimal height depends on geometry, frequency, and the lapse rate[82]. Typically, z_M is at least 1000 vertical grid steps high[24].

In the case of refracting weather conditions, the possibility should be provided for all of the rays bending downward from the source to the receiving point to do this below the absorbing layer. For example, a logarithmic lapse rate

$$c(z) = c_0 + b\ln(1 + z/z_0), \tag{2.13}$$

Table 2.1: Flow resistivity for some soil surface types[119, 121]

Description	Flow resistivity, $kPa \cdot s/m^2$
Layers of dry new snow (10 cm) on an old 40 cm snow layer	10–30
'Sugar snow'	25–50
Soft forest floor with twigs and moss	40–
Forest floor covered by weeds	63–
In forest, pine or hemlock	25–80
Sparse vegetation and dense shrubbery, 20 cm high	100–
Soft forest floor covered with pine needles, leaves, and twigs, agricultural field	160–
Airport and grass (rough-pasture-type land)	150–300
Pasture, lawn seldom stepped on, and earth covered with sawdust	250–
Roadside dirt, ill-defined, with small rocks up to 0.1 mesh	300–800
Soccer field, gravel, earth and sparse grass, and mixed paving stones and grass	630–
Sandy silt, hard packed by vehicles	800–2500
Gravel car park, hard soil, sandy forest floor, and gravel road with small stones	2000–
'Clean' limestone chips, thick layer	1500–4000
Old dirt roadway, fine stones with interstices filled	2000–4000
Earth, exposed and rain-packed	4000–8000
Quarry dust, fine, very hard-packed by vehicles	5000–20,000
Asphalt, sealed by dust and light use	–30,000
Theoretical upper limit (thermal conductivity and viscous boundary layer)	200,000–1,000,000

where z_0 is not to be confused with the height parameter of the calculation grid. Parameter z_0 is the aerodynamic roughness value for the surface. Typical z_0 values are 0.001 to 0.1 m for grass, 10^{-4} to 10^{-3} m for the surface of water[123], and ≈ 1 m for forest land. Usually, the value $z_0 = 0.1$ m is used, if the value is not otherwise specified. When $b > 0$, the atmosphere is refractive. If the source and the receiving point are near the ground, the ceiling for the rays can be approximated as $h \approx r/\sqrt{2\pi c_0/b}$. A typical value for b is 1 m/s, yielding $h \approx 0.02r$. For example, if $r = 10$ km, then $h = 200$ m.[82, p. 47]

2.1.2 A general solution

To obtain a general solution for PE method, we start with substitution of a general solution into Eq. 2.7:

$$q(r,z) = \psi(r,z)\, e^{ik_a r}, \tag{2.14}$$

where k_a is a value for the wave number $k(z)$ at a certain height (or at the ground). The term $e^{ik_a r}$ in Eq. 2.14 presents the propagating plane wave in positive r direction and changes rapidly as a function of r. Function $\psi(r,z)$ changes slowly with z. By substitution, inserting Eq. 2.14 into Eq. 2.7, we obtain

$$\frac{\partial^2 \psi}{\partial r^2} + 2ik_a \frac{\partial \psi}{\partial r} + \frac{\partial^2 \psi}{\partial z^2} + \left(k^2 - k_a^2\right)\psi = 0. \tag{2.15}$$

Because, in practice, ψ changes slowly with distance, the first term can be eliminated and the equation simplifies to the form seen in Eq. 2.16, which is referred to as a parabolic equation for a narrow elevation angle.

$$2ik_a \frac{\partial \psi}{\partial r} + \frac{\partial^2 \psi}{\partial z^2} + \left(k^2 - k_a^2\right)\psi = 0 \tag{2.16}$$

The differential equation (2.16) can be solved via numerical difference methods.

In 1995, Sack and West presented their Generalized Terrain Parabolic Equation method (GTPE), wherein topography can be taken into account[81]. On a flat surface, the GTPE method reduces to the CNPE method. Atmosaku includes both a CNPE and a GTPE solver, and a detailed description is given by Maijala (2007)[30]. The performance of the physical part of Atmosaku is addressed in Section 4.9, below.

2.1.3 The turbulence factor

The lowest part of the atmosphere, known as the *atmospheric boundary layer* (ABL), is characterised by turbulence, which is caused by the interaction between the atmosphere and the ground surface or the change in the atmospheric flows to adapt to the characteristics of the ground. In reality, the turbulence is generated both *mechanically* (from the friction between ground and air) and *thermally* (through the buoyancy forces created by the temperature differences between the ground and the air). Close to the ground, a wind speed of 1 m/s is sufficient to generate turbulence. The size of the vortices of the turbulence can range from kilometres to millimetres, and, depending on this magnitude, the explanatory variables are the roughness of the ground surface, the heat flux, the pressure gradient, and Earth's rotation (Coriolis forces).[124]

The boundary layer can be divided into the surface layer and the Ekman layer[2]. In the surface layer, turbulent fluxes are almost constant. The height is typically about

[2]The Ekman layer is named after Swedish marine scientist V.W. Ekman. He discovered that sea currents are formed into a spiral shape as a function of depth, and the same happens in the atmosphere as a function of height.

10% of the boundary-layer height[124]. Above that, in the Ekman layer, the typical wind direction is clockwise in the northern and anti-clockwise in the southern hemisphere, and it gradually adapts to the prevailing geostrophic wind above the boundary layer. The divergence between the wind direction in the surface layer and the geostrophic wind direction is usually 5°–50°[125].

The strengt of wave-equation-based models such as the PE approach is that they can account for the effect of all known physical phenomena, including atmospheric turbulence. Turbulence is the most complicated phenomenon to be taken into account, but, on the other hand, implementation of the turbulence factor in this PE framework is very easy. An example of a GTPE calculation for 2000 Hz, using the von Kármán spectrum to simulate the turbulence, is shown in Fig. 2.1. The topography and the propagation condition for the example calculation are explained in Section 4.9, and the turbulence initialisation parameters are shown in Table 4.9. The same propagation condition, averaged for frequencies between 40 and 1600 Hz, is depicted in Fig. 4.19 (a).

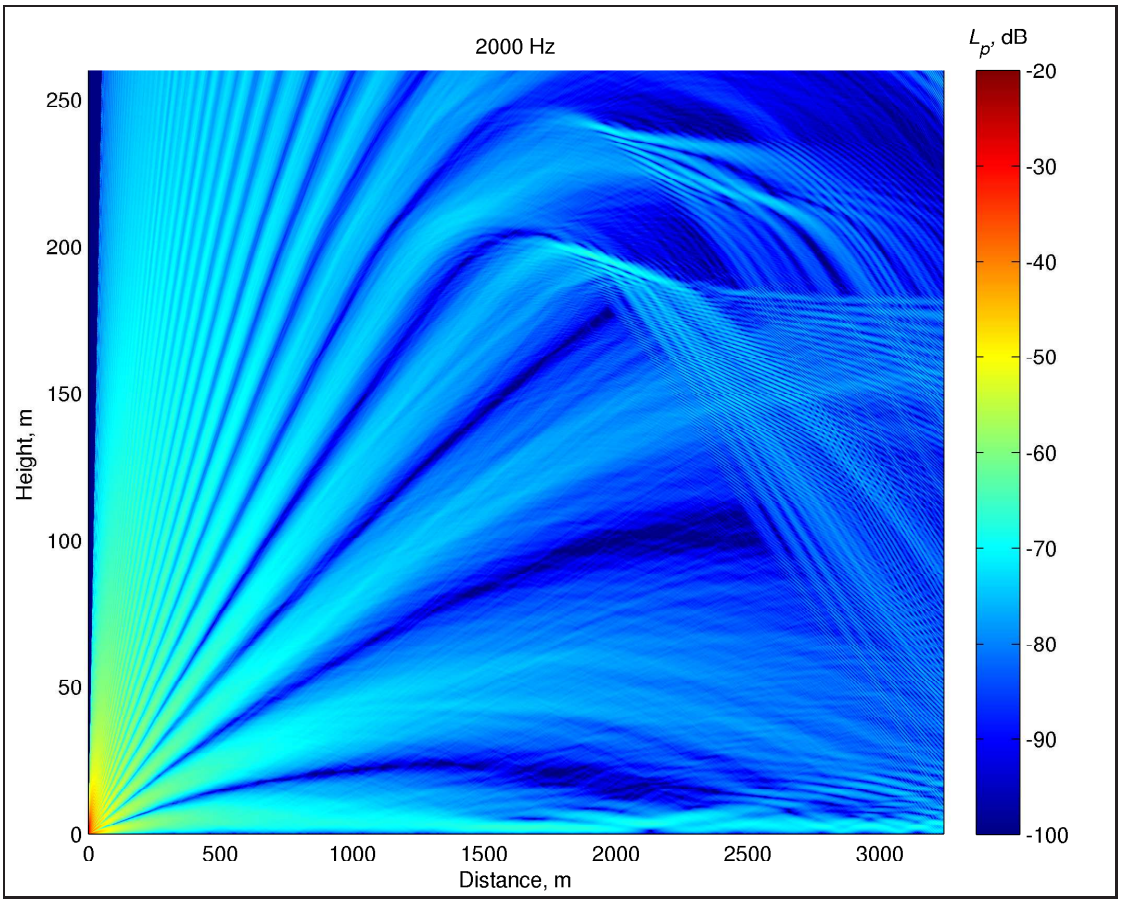

Fig. 2.1: GTPE calculation for the Sodankylä site, 6 February 2005 at 23:00 UTC.

Proper turbulence models do not exist. There has been research into scattering due to turbulence, and one of the best overviews of this issue has been provided by Wilson et al.[126]. Three of the turbulence models most commonly used in atmospheric

acoustics are the *Gaussian*[127, 128], *Kolmogorov*[129, 130], and *von Kármán*[131] turbulence models, presented by Salomons (2001)[115, pp. 211–219]. The most typical approach to estimation of the sound scattering arising from turbulence is based on the turbulence wave number (the vortex size). The scattering detected in the direction of the θ angle from the x-axis is caused by turbulence with wave number $\mathbf{k}_t$,

$$\begin{aligned} \mathbf{k}_t &= k\left(\frac{r}{|r|} - \mathbf{e}_x\right) = k_t \mathbf{e}_\theta \\ k_t &= 2k\sin\left(\frac{\theta}{2}\right), \end{aligned} \tag{2.17}$$

where $\mathbf{e}_\theta$ is a unit vector in the direction of θ. The turbulence wave number, k_t, can be presented as L, the length of the turbulence:

$$k_t = \frac{2\pi}{L}, \tag{2.18}$$

and from Eq. 2.17, the relationship of the frequency, turbulence length, and direction of turbulence radiation can be derived:

$$\begin{aligned} \sin\left(\frac{\theta}{2}\right) &= \frac{c_0}{2Lf} \\ L &= \frac{c_0}{2f\sin\left(\frac{\theta}{2}\right)}. \end{aligned} \tag{2.19}$$

The scattering due to turbulence is dominated by eddies with sizes on the order of the wavelength of the sound waves. This can happen in the *drive* or *inertial* sub-ranges (see Fig. 2.2), depending on the geometry and the atmospheric conditions. The dissipation sub-range is negligible because the eddies are very small in comparison with the acoustic wavelengths.

The theoretical turbulence models do not apply very well to real atmospheric turbulence, for many reasons. The Gaussian and von Kármán spectra are valid only if the turbulence is homogenous and isotropic. In the real atmosphere, the scale of the turbulence varies as a function of height from the ground. One reason the actual atmospheric turbulence is always anisotropic is that the correlation length parallel to the wind vector is greater than the correlation length perpendicular to the wind vector.[115, p. 219]

2.1.4 Addition of noise sources

Wilson et al.[133] considered the practical problems in implementation of the source in PE models: The disadvantage of these PE methods is the assumption that each source can be regarded as an equivalent point source. Therefore, care must be taken to define the noise source in such a way that it is possible to estimate its acoustic centre (the position of a point source yielding the same sound pressure level in the environment as the noise source under testing). One workaround for overcoming this point source

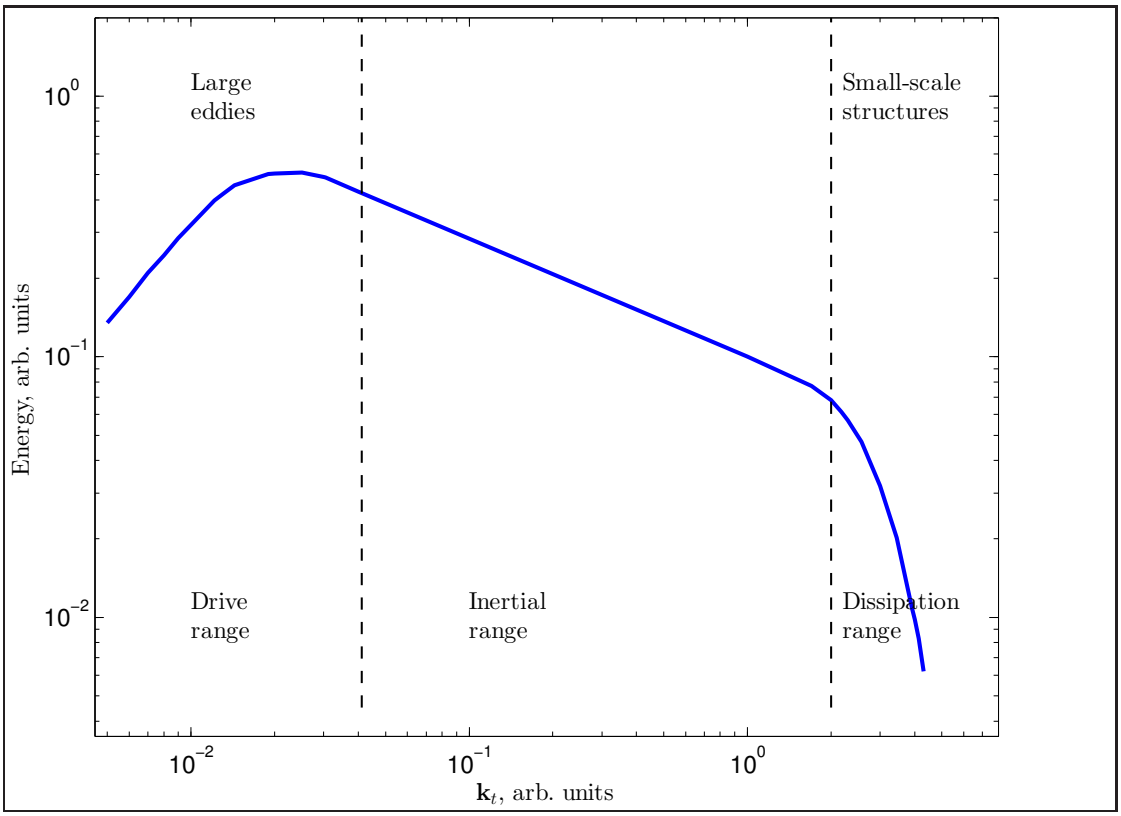

Fig. 2.2: The Kolmogorov wave number spectrum of the kinetic energy of turbulence, figure modified from the work of Müller and Biskamp (2003)[132]. The x-axis shows not the k value, the wave number of the sound, but the wave number of the turbulence $\mathbf{k}_t$, defined in Eq. 2.17.

limitation is to approximate line sources as a series of point sources. Also, the directivity of the noise sources should be taken into account.[133]

Vecherin et al.[134] proposed two methods for PE algorithms, wherein the directivity of the source varies considerably along the horizontal axis. In the equivalent source method (ESM), a distribution of omnidirectional point sources is defined such that the far sound field is as desired. This does not mean that the sound field should be calculated for all of these point sources separately; instead, the field starter function can be constructed by breaking down the directivity into a spherical harmonic series and then constructing the equivalent source distribution as a vertical or horizontal source distribution. The other method is referred to as a directional starter method (DSM). In this DSM, a closed-form expression is obtained via a single Fourier transform from the directivity function $D(\theta,\phi)$ as a starter function for the PE field.[134]

2.1.5 Integration with meteorology

Hole and Mohr showed how sound propagation forecasts could be carried out[135]. They used the output of a mesoscale meteorological model as input to an acoustic model.

Although they were able to perform the calculation for only low frequencies (≤ 100 Hz), they were able to demonstrate differences as great 16 dB between upwind and downwind at a 1 km distance from the source[135].

2.1.6 Weaknesses and problems

Sound propagation in canyons, in cities, or near any reflecting boundaries other than the ground is usually beyond the scope of 2D models. One approach is to rotate the 2D grid from vertical to horizontal, but then the propagation over the obstacles has to be neglected[136]. The most common approaches involve the ray-based models, but the task is not straightforward with these models either when street canyons are involved — even changing the geometrical boundary to diffuse alters the propagation situation considerably[137, 138].

The wave-equation-based methods of calculating outdoor sound propagation are still quite computationally intense today — especially for higher frequencies than a few hundred hertz and for distances longer than 1 km. For example, the single-frequency result shown in Fig. 2.1 for a distance of 3 km required a computer with 1.5 TB of RAM and took 160 days of CPU time (five days for a PC with 32 cores). The calculation times can be reduced to a fraction of this by means of a graphics processing unit (GPU) with thousands of parallel data-processing units. Inexpensive GPU cards have been available for years and can be installed for a standard workstation. Albert et al.[136] implemented a two-dimensional finite difference time domain (FTDT) sound propagation algorithm on a GPU and showed up to 240 times faster calculation than with MATLAB® code running on a CPU[136].

Schiff et al. showed that the PE method can be successfully used in an urban environment also.[139]

2.2 Previous measurements

There are many measurable quantities and interactions behind the physical phenomena. Topography and obstacles, flow resistivity of surfaces, temperature, humidity, individual wind components, and lapse rate are the most evident measurable quantities. Horizontal and vertical wind components and turbulence parameters also are among the important variables. Both the wind and lapse rate can change the sound wave propagation path and usually explain the fastest changes in the time domain.

However, neither the topography nor the varying ground impedances are responsible for the major sources of uncertainty in sound propagation models; instead, the biggest deviations between the calculations and measurements arise from the deficient implementation of meteorological variables. Meteorological aspects of sound propaga-

tion modelling have received focus since the very beginning of this century[28, 140, 141]. Measurements are needed both for development of new models and for evaluation of the existing models.

As long as there have been computational models, there have been long-term measurements, unfortunately too often not properly organised. It is always very expensive and complicated to arrange sound propagation measurements that suffice for scientific purposes. Not just the generation of well-known emission of sound power in ever-changing environmental conditions is challenging; also, the data are useless without proper monitoring of the atmosphere. Common flaws include taking measurements without any information about environmental changes or changes in the source of sound, and the most typical problem is inadequate meteorological data. Depending on the distance between the source and receiver(s), there should be enough instrumentation capable of characterising both the vertical and horizontal gradients of wind and temperature in the ABL. To enable this, meteorological towers, wind profilers (SODAR, LIDAR, and RASS), and real soundings must be exploited.[27]

Heimann et al.[142] underscore the issue of representativeness of the meteorological measurements. If the target site is topographically flat and the terrain is homogenous, the meteorological observations can be transferred slightly off the site, but in the case of mountains, valleys, or coasts the representativeness is normally not stated, even if the station is not very distant.[142]

Automatic weather stations have made it possible to acquire much more comprehensive weather data both temporally and spatially. In Finland, just 15 years ago, observations were carried out every three hours at best, but today the typical temporal resolution is 10 minutes. Also, automatic weather stations can be placed in unpopulated areas.[143]

It is unacceptable that the quantity of measurement data is insufficient for testing and validation of the new models. Some authors have validated their models against other models[78], and some of them[144, 145] have used the data collected by Parkin and Scholes[146, 147] half a century ago, from which the former reference[146] was the first article in the first Journal of Sound and Vibration, published in 1964.

Quite a few properly conducted, well-documented, and publicly reported sets of long-term measurements exist. Next, a review of some typical long-term measurements is presented. In some publications, comparison between the measurements and models is made; these measurements are referred to in Section 2.3.

2.2.1 Measurements in Spain, in 1980–1990

A typical example of long-term tracking of noise levels in an urban environment is the work done by García and Faus[148], in one of the noisiest countries in the world: Spain. In Spain, about 23% of the population is exposed to $L_{p,\mathrm{A}} > 65$ dB. This study is completely lacking the meteorological perspective, but so are practically all the other

long-term measurements in an urban environment: the propagation distances are so small that the atmosphere can be disregarded in most cases.

This study is worth mentioning because it is unusually comprehensive. García and Faus carried out noise level recordings in several Spanish cities from 1980 to 1990. The survey covers several 24 h measurement periods and, in total, 4200 hours of A-weighted noise levels. The results of the work present several good rules for noise assessments in urban areas — for example, for freely flowing traffic,

$$L_{10} - L_{\mathrm{eq}} \approx 3 \text{ dB}. \tag{2.20}$$

On the other hand, the results show clearly that in high-traffic urban areas the variation of the maximum (L_1) levels between day and night or by day of the week is negligible. Furthermore, the authors found that the correlation between L_{eq} and L_1 or L_{10} is very strong, and, finally, they suggest that the $L_{p,\mathrm{A},900\mathrm{s}}$ measured between 17:00 and 18:00 is enough to produce all of the relevant information for general-purpose noise surveys in urban areas.[148]

2.2.2 The USA, 1983–1984 and 2000–2001

One way to apply the statistical approach is to rely just on sound level measurements, but over long distances this approach should be questioned. Schomer[149] conducted experiments with C-4 explosives, measured the sound pressure levels at a distance of 8 km, and carried out statistical analysis of the data. He proposed as a statistical approach that the mean level and its standard deviation are sufficient descriptors for noise assessments. He claims that two decay curves for mean sound levels as a function of distance are enough: Over land, this decay is -29 dB, and over water it is -15 dB, per decade of the distance. His standard deviation curves start from 0 at a distance of 10 m and increase over the water by 1 dB and over land by 1.3–2.6 dB per decade of distance, depending on the atmospheric conditions.[149]

In 2006, Schomer and White[150] reported on experimental studies with sources at two heights: 0.6 m and 31 m. The measurements for the higher source height were performed in a flat area over the course of 50 days and for the lower over 40 weeks, with 25 individual measurement days, on each of which measurements took up to 12 hours. Measurement distances ranged from 50 to 1600 m. The authors were able to fit linear regression lines to all the data such that the distance explains the sound pressure levels well.[150]

2.2.3 Japan, 1989–1990

A long-term and long-range measurement with basic acoustical and meteorological instrumentation was organised by the Japanese. The measurements were carried out over

a 14-month period. The signal was emitted from a fixed point on an artificial island at sea and received on the coast about 5 km from the source. Measurements were carried out every hour. The Japanese found that the propagation path could show variations of 20–30 dB within half an hour in total sound pressure level. The maximum variations in one-day periods were found to be 50 dB or more. Further, daily variation patterns showed that the noise-reduction value is low at night and high in the daytime from autumn to winter, but this cannot be seen in other seasons.[151]

2.2.4 Norway, 1994–1996

The first serious, publicly reported, extensive measurement with proper meteorological characterisation was organised in Norway. The 'Norwegian Trials' consist of four large-scale outdoor sound propagation experiments performed between 1994 and 1996. During the field experiments, acoustic measurements were carried out in conjunction with meteorological, seismic, and ground characterisation measurements. Sound propagation was measured over distances from 0.1 to 24 km. The results were compared with various theoretical predictions. Unusual is that microphone masts with a height of up to 30 m were used.[152]

2.2.5 France, 2002–

Gauvreau[153] reported in 2013 on some results from a long-term monitoring station situated in a canyon in Saint-Berthevin, France. The measurements reported upon were performed in 2002–2007, and the site is still active and capturing data. There were four meteorological towers and many microphones, at various distances (up to 300 m) from a highway and a railway. The researchers measured the basic meteorological data at three sensor heights: 3 m, 10 m, and 25 m. Additionally, they used rainfall and 'solar insulation' (probably a typo for 'insolation') measurements. The original acoustic data were not saved at all (in waveform), so the reasons for any anomalies cannot be determined. Some kind of filter was used that prevented other than road traffic noise being saved in the database. The monitoring mission required daily efforts from all of the project's participants: pre-processing, averaging, synchronising, zipping, transferring, and validating the data. The amount of manual work always is associated with the risk of human error and in this case could have been reduced dramatically through a fully automated measurement chain[28]. Because the researchers did not have a controlled sound source, they used a reference microphone 5 m above ground level, next to the highway. So far, they have reported some statistics for the sound pressure levels: regardless of the microphone location, the SPL dispersion increased with frequency, varying from 8 dB for 100 Hz to 20 dB for 4 kHz. The six-year continuous measurement period assures the statistical significance of the results.[153]

2.2.6 Finland, 2004–2005

Finland has mainly been a silent follower of the remainder of the scientific world in the field of outdoor sound propagation. Measurement campaigns have been organised, but details of only a few have been published.[154, 155]

In the late 1980s, the Finnish Defence Forces began the development of sound propagation models and evaluations based on measurements from mass detonations[3]. Signals from several microphones and meteorological data were available to aid in evaluation of the computational methods developed by Ojanen[156]. However, the applied ray theory did not take into account some important wave phenomena, and more sophisticated tools were needed.

In 2001, Maijala et al. evaluated three commercial noise-modelling software applications by comparing the modelling results to measured data. Also, *in situ* impedance measurement techniques were developed for parameterisation with the software. Four quite distinct test cases were prepared and measured. Three types of approach were represented by the software evaluated: state-of-the-art PE-based software ('SALPE'), BEM software (LMS Sysnoise), and ray tracing software ('ENM'). The BEM implementation had to be limited to frequencies below 100 Hz in consequence of its high memory requirements, and it was omitted from the final comparison. The pieces of software showed similar modelling results with short distances but differed from field measurements at all distances; see Fig. 2.3.[13] The performance of this commercial wave-equation-based state-of-the-art software turned out to be unsatisfactory, on account of many deficiencies in the software, the challenging special elements of *Nordic climate conditions*, and lack of knowledge as to the effect of weather conditions on sound propagation. In the SALPE software, a single flow resistivity value was used to characterise the ground along the entire sound propagation path and only one profile for the atmosphere. Also, the capabilities of the software were limited: the maximum modelling frequency was 400 Hz, and only a very simple turbulence model was implemented, without the option of employing a more sophisticated one in its place. These difficulties were addressed by development of the model described in this thesis.

2.2.7 The Harmonoise project, 2006

The European Harmonoise project preceded the CNOSSOS-EU work (see Section 1.3), and one of the objectives of the project was to develop the noise propagation models to be used in MS for noise mapping. The Harmonoise models (engineering model[157] and reference model[158]) suggested many meteorological variables to be taken into account, and some measurements lasting 19–32 days were made to validate the models[141, 158–162].

[3] Destruction of obsolete ammunition through large-scale explosions.

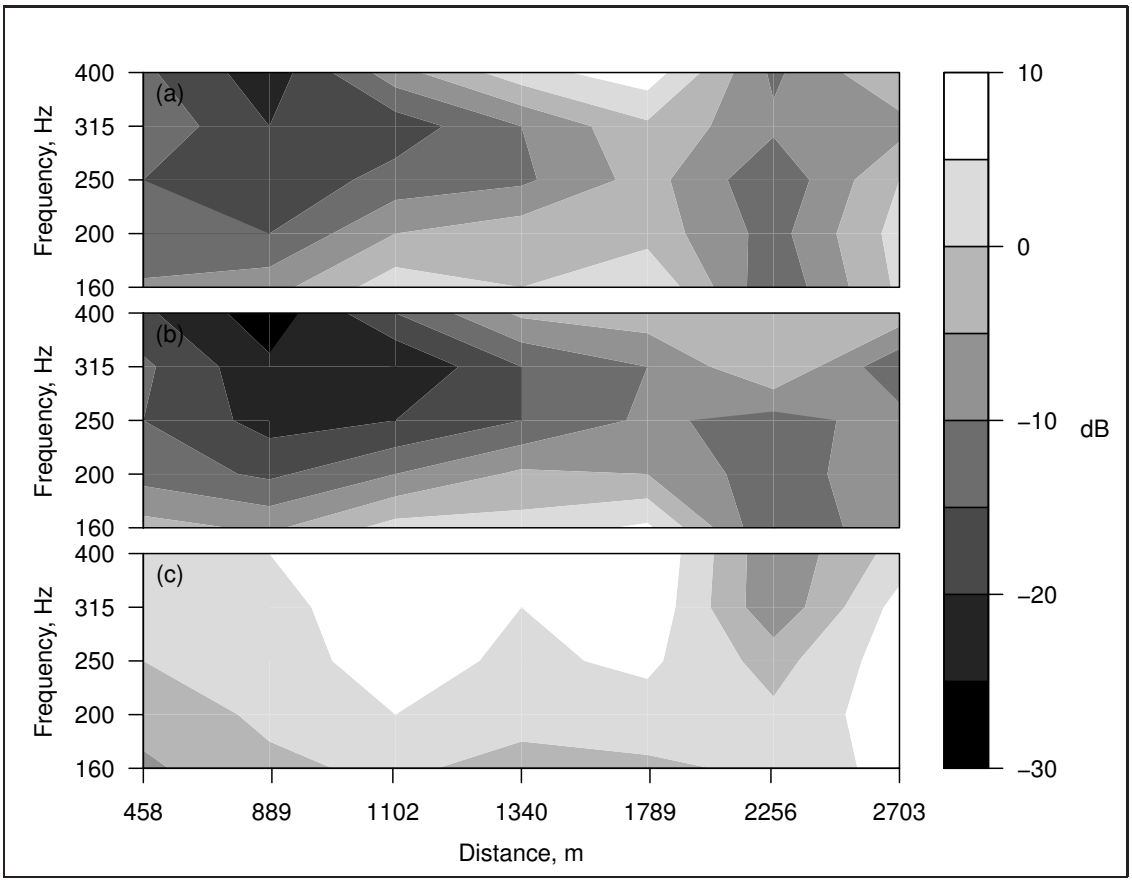

Fig. 2.3: Difference between the measurements and SALPE (a), and ENM modelling results (b). In pane c, the difference between the pieces of software is shown (SALPE−ENM).[13]

2.2.8 Problematics of the measurements

The measurement of real noise sources is challenging. In an urban environment, noise is received from many simultaneous noise sources. Usually only one microphone (or a sound level meter) is used and the separation of a specific noise source from the urban background noise is often impossible. Various attempts to overcome this problem of separation are documented in the literature, some of them based on increasing the directivity of the sensor with beam forming and cross-correlation algorithms[163, 164] and others based on classification employing fuzzy logic[165], support vector machines (SVM) and k-means clustering[166], or hidden Markov models (HMMs)[167]. In separation between cars, trucks, mopeds, aircraft, and trains, source recognition rates of up to 95% were reported[167], which corresponds to average human ability to distinguish among these sources. However, this kind of test is performed with pre-processed sound libraries and the classification algorithms are trained on limited sound samples. The real world tends to change all the time, and so does its environmental noise. An automatic recognition system should adapt to the changes by monitoring the environment and organising the observed activity in a meaningful way. Härmä et al. have reported

an experiment wherein a detection algorithm was based on continuous estimation of background noise and two criteria for triggering the recording of sound events[168].

2.3 Comparison between measurements and modelling

Yokota et al.[169] performed a series of measurements on an asphalt runway and in a grass field and compared the results to the PE simulations. They used the measured wind properties as an input to a logarithmic wind profile (see Eq. 2.21, below):

$$u(z) = \alpha \ln\left(\frac{z}{z_0}\right)\cos\theta, \tag{2.21}$$

where u is the wind speed at a height of z from the ground, z_0 is the roughness length of the ground, α is the gradient of the wind speed profile, and θ is the angle between horizontal wind and the sound propagation directions. The distances were as great as 300 m. The results show that it is possible to evaluate the order of magnitude of variations in the excess attenuation with the simulations. The researchers found the values of excess attenuation to vary more strongly when the wind speed rises, and the variation became larger as the distance and frequency rise; see Fig. 2.4 and Fig. 2.5.[169] Over the runway, the calculated values were quite consistent with the measurements except with the strong upwind conditions. Values for the grass field too were quite well estimated by the modelling, but the frequency 1 kHz displayed more differences, leading the authors to conclude that their boundary condition for that frequency was not correct.

A comparison between the sound propagation measurement and a model was done by Lam[170] in 2001. He had a mast with a weather station at two discrete heights (8 and 28 m). The temperature gradient was calculated by division of the temperature difference between the two sensors by their vertical distance. Lam found the sound propagation data to correlate better with the vector wind speed than the temperature gradient — the conclusion was that the linear difference between the two sensors does not offer an adequate estimate of the vertical temperature profile of the sound propagation path. Also, comparison with the measured data and a heuristic ray tracing model was conducted and the model was found to perform poorly, especially under strong refractive conditions.[170]

The data from the meteorological equipment, such as profilers, should be fitted properly for sound propagation models. Heimann et al.[142] examined whether it is possible to determine the vertical sound speed profiles (SSPs) from meteorological measurements at only one height above the ground. They compared two theoretical-empirical flux-gradient functions and a simplified logarithmic-linear approach to the data from a meteorological tower and found that the log-linear model approximated the directly measured profiles 'fairly well'.[142]

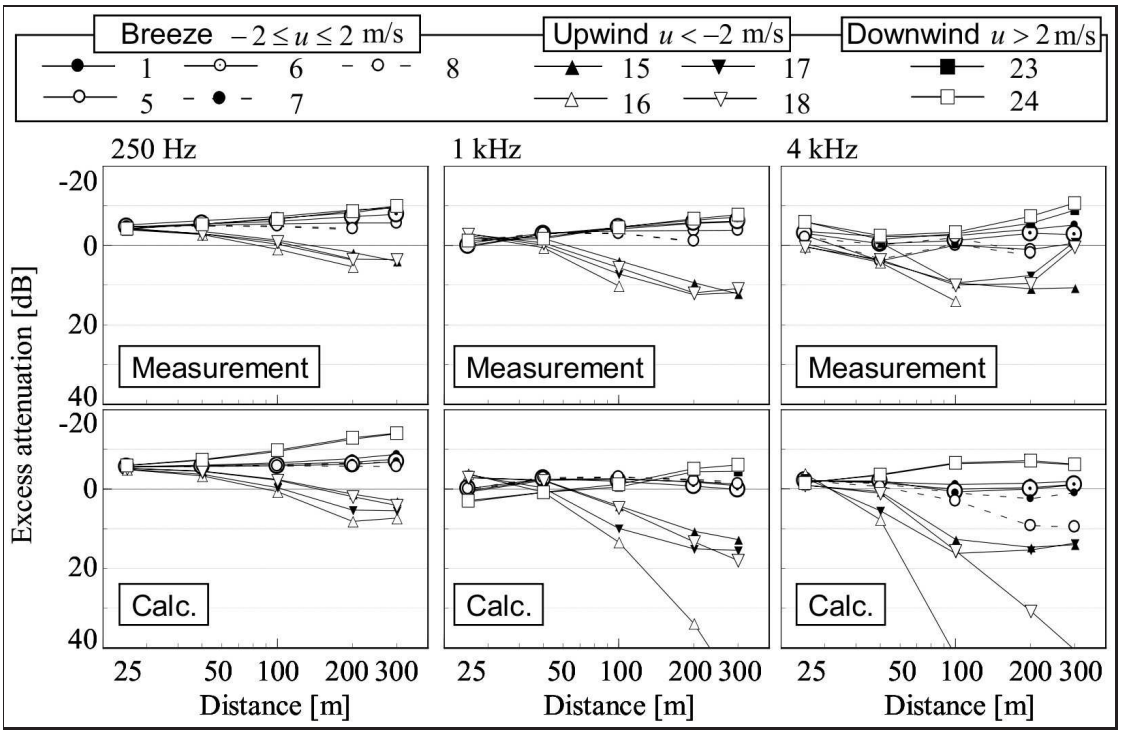

Fig. 2.4: Runway, differences between measurements and calculations. Figure from Yokota et al. (2006)[169, Fig. 5]; © 2006 the Institute of the Noise Control Engineering, USA; used with permission.

Bradley et al.[171] evaluated the applicability of the logarithmic-linear approximation to 15 distinct stability classes, ranging from very convective in low winds to very stable in low winds. They compared SSPs measured by a Bragg's-scattering-based RASS[172, pp. 9–14] and could not find any SSPs characteristic of certain stability classes. They saw a large amount of deviation in their observed data, probably due to the use of fast averaging (30 s instead of 10 minutes). Also, the lack of data below 43 m might have been the reason for the badly fitting profiles. The equation was of the form shown in Eq. 2.22:

$$c(z) = \eta + a \ln z + \varepsilon(z), \tag{2.22}$$

where c is the sound speed at height z, a and η constants throughout a particular profile, and $\varepsilon(z)$ the residual between the actual profile and the log-linear approximation.[171]

2.4 Uncertainty

2.4.1 Some approaches

Statistics is a practical way — and usually the most effective — to describe ever-changing environmental phenomena, such as noise propagation in the atmosphere. The

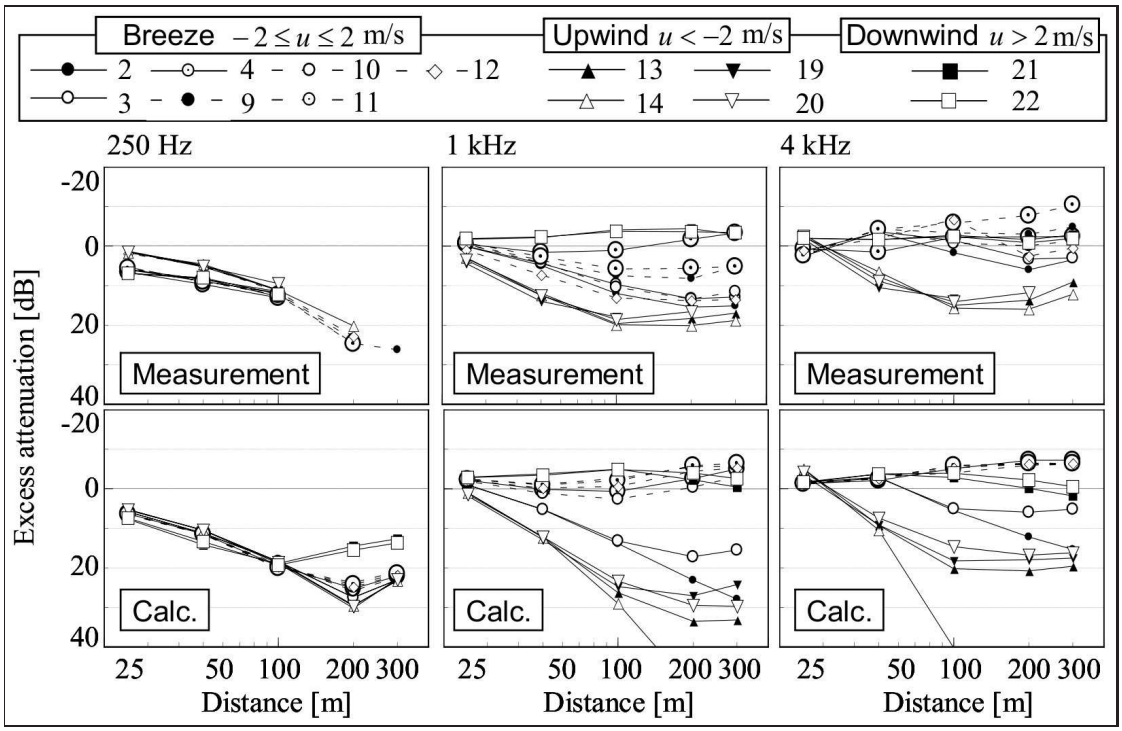

Fig. 2.5: Grass field, differences between measurements and calculations. Figure from Yokota et al. (2006)[169, Fig. 6]; © 2006 the Institute of the Noise Control Engineering, USA; used with permission.

uncertainty related to the assessment of environmental noise can be roughly divided into that arising from the modelling or measurement of the source, from the transmission path, and from the immission (or measurement at the evaluation point). In the modelling, the immission is defined from the calculated value at the evaluation point and the only uncertainty that applies is the computational uncertainty — which is negligible. The uncertainty related to the measurements of environmental noise (sound pressure signals) is very small when compared to the other sources of uncertainty, and it is not considered in this review.

The original goal of the approach presented in this thesis was to evaluate the uncertainty of modelling, although it also applies to the evaluation of the uncertainty in measurement. In turn, the uncertainty in measurement is a much discussed topic and good guidance exist. Both the good practice guide (GPG) by Craven and Kerry [173] and the ISO 1996-2:2007[174] provide means for handling the uncertainty in the measurements. The GPG is a very comprehensive guide for evaluation of the uncertainty and it consists of a number of practical examples, tables, useful notes, guidelines, and rules of thumb. The GPG advise on how to set up an 'uncertainty budget', in which the uncertainty of sources, the propagation path, and measurement processes can be combined. A short summary of this 'uncertainty budget' is also presented by Kerry and Waddington.

The paper gives much attention to uncertainties due to meteorological effects, and the authors' budget indeed shows that the weather is the largest source of uncertainty.[175] The ISO 1996-2:2007 is a fully rewritten version of its predecessor from 1987. It is an attempt to quantise weather conditions and derive uncertainty of measurement by robust rules. However, it is based upon a knowledge of the sound ray curvature and there are several restrictions limiting its use. For example, the measurement uncertainty due to weather is valid for measurement time intervals from 10 minutes up to a few hours and for specific sound-propagation conditions. Also, it only applies to short-term measurements and to the weather conditions stated.

Knowledge of the *reliability* of the mappings and predictions is vital for well-informed decision-making. Wilson and Pettit propose the use of special expert decision-support tools (DSTs) in characterising the effects of the terrain and atmospheric conditions on sound propagation. The DSTs expose both the possible problems with the model and also whether the source data are sufficient for reliable predictions.[176]

The words '*reliability*' and '*validity*' are frequently referred to in scientific research. *Internal reliability* measures whether we can repeat the test and get the same result, and *external reliability* indicates whether someone else can repeat the test, in another situation, and obtain the same result. Validity refers to how well the test measures what it is meant to measure. *Internal validity* represents whether the test performed was done as documented, and the test is valid externally (i.e., shows *external validity*) if other scientists understand the test and results as documented.[177–179]

Reliability and validity can also be explained in terms of the concepts of *uncertainty*, *accuracy*, and *precision*. Probst says[180]: '*Accuracy of a calculation method describes the deviation of calculated results from the values obtained by an ideal measurement. An ideal measurement is characterized by negligible uncertainty. Precision of a calculation method describes the differences between results that are obtained if different experts apply the calculation method in exactly the same case. Transparency is an expression for the ability to understand and to retrace calculations in each step.*' Using the definitions above, we can say that accuracy corresponds to internal validity, precision to external reliability, and transparency to external validity. All of these definitions can be covered by the word 'uncertainty'. Uncertainty can be divided into sub-categories such as *aleatory uncertainty*, resulting, for example, from random signal generation and scattering effects, and *epistemic uncertainty*, linked to the state of the environment[176].

The uncertainty of modelling results did not arouse much attention until the last few years. In the days of the scale models, it was evident that computer models were imperfect[181], but today surprisingly many experts believe the uncertainty in noise mapping can be handled without unpleasant and laborious real measurements. The most popular way to study uncertainty has been comparing individual models to each other[78, 182]. Uncertainty at another level appears if the calculated results are compared to human

responses[183]. Studies of the uncertainty have appeared in increasing numbers in the last few years[176, 184], including well-adapted statistical methods, based on *in situ* measurements[185].

2.4.2 Uncertainty of the source

There have been statistical prediction models for traffic noise since the 1950s, but the approach of these models has changed many times since the earliest models. In the beginning, the models were based on linear sound pressure level measurements from a single constant-speed vehicle, as a single point source[186, p. 191]. Bolt et al. remind of the accuracy in the following words: '*Only when the traffic rate approaches 100 vehicles/min does the noise level at a distance of 20 to 30 ft become constant within a total variation as small as 5 dB, even when all vehicles are identical*' [186, p. 191].

Later, A-weighted equivalent sound pressure levels L_{eq} over a chosen period of time were introduced and research addressed the variation by means of more advanced descriptors, such as percentile levels (L_{10} to L_{99}); nevertheless, all of the modern source models are deserving of criticism[187]. Makarewicz and Gałuszka tried to overcome the criticism by developing a method for road traffic noise prediction that was based on the average speed of freely cruising vehicles, the capacity of the traffic flow, traffic speed at that traffic flow capacity, and the slope of the decrease in traffic speed versus traffic flow[188]. Makarewicz continued the formulation to estimate annual average sound levels[189]. As a result of this work, source models have become highly complicated and require huge quantities of initial data to be utilised. Fortunately, more and more data are acquired and made available by the authorities.

2.4.3 Uncertainty of the propagation path

Rapid and large fluctuations in the sound pressure field received from a source of constant strength is a noteworthy phenomenon in outdoor sound propagation. These rapid fluctuations are induced by the atmospheric turbulence[128, 190]. Experimental studies[146, 147, 191, 192] show that there are changes of about 10 dB at distances less than 100 m. At longer distances, the fluctuations increase. However, Salomons et al. have suggested that the effects of turbulence on the time-averaged sound pressure level may be ignored if the source and the receiver are very close to the ground[190].

There are many methods of categorising the stability of a region of the atmosphere. *Pasquill stability index* is one of these. While this index[193, 194] can be used to estimate the atmospheric turbulence[195], Heimann et al. state that the way Pasquill index is determined gives only a very rough estimate, one that is inaccurate in many cases[142].

The Pasquill indices, or classes, are determined by a simple table lookup route, wherein wind speed, cloud cover, and solar radiation are used as input parameters (see

Table 2.3). The solar radiation, or insolation, was defined as a function of solar altitude but is today determined from the radiation balance, or sensible heat flux (see Table 2.2).

Table 2.2: Insolation and example values for sensible heat flux, *mhf*, at the surface as a function of solar altitude, h[196, 197]

	Daytime insolation			Near neutral	Night	
	Strong	Moderate	Slight		$\geqslant \frac{4}{8}$ cloud	$\leqslant \frac{3}{8}$ cloud
h	$\beta > 60°$	$35° < \beta \leqslant 60°$	$15° < \beta \leqslant 35°$	$\beta \leqslant 15°$	$\beta \leqslant 15°$	$\beta \leqslant 15°$
mhf, W m^{-2}	+164	+91	+20	0 to −50	−60 to −80	−90 to −115

Pasquill suggested six classes[194], and Turner, modifying Pasquill's scheme, defined seven categories[197]. Both of these approaches assume an open area and apparently a roughness parameter z_0 of 3 cm — Golder proposed a method of transferring Pasquill categories to areas with different surface roughness[198], and Hasse and Weber extended this approach even to the roughness of a sea[196]. Low Pasquill values (classes A=1, B=2, and C=3) indicate that the atmosphere is unstable and that sound scattering due to thermal turbulence and convection is strong. The most frequently occurring class is D, equivalent to value 4; this refers to an atmosphere that is neutral, with possible weak, sporadic buoyancy but often a windy day or night, which causes scattering that provides mechanical turbulence. High values (classes E=5 and F=6) indicate that the atmosphere is stable and buoyancy forces are weak. Class A refers to a very unstable atmosphere and corresponds to hot, calm days, while class F indicates very stable conditions and corresponds to nights with low winds.

Table 2.3: Pasquill stability classes[193, 194]

Wind speed, m/s	Daytime insolation			Near neutral	Night	
	Strong	Moderate	Slight		$\geqslant \frac{4}{8}$ cloud	$\leqslant \frac{3}{8}$ cloud
< 2	A	A–B	B	D	(G)	(G)
2–3	A–B	B	C	D	E	F
3–5	B	B–C	C	D	D	E
5–6	C	C–D	D	D	D	D
> 6	C	D	D	D	D	D

Wilson et al.[199] assessed the uncertainty of outdoor sound propagation by comparing CNPE calculations in simulated atmospheric fields. The atmospheric fields were obtained via large-eddy simulations (LES), and the CNPE calculations were performed for downwind, upwind, and crosswind directions. The calculation range was 1 km at the frequencies 50, 150, and 250 Hz. The authors defined four types of vertical profiles:

a) *Ensemble-mean*: spatial average of each LES volume (temporal snapshot of the horizontal plane) and, finally, averaging over the time domain.

b) *Instantaneous, along-path mean*: the spatial average of the profiles over the propagation path.

c) *Instantaneous, midpoint*: the profile from the middle of the propagation distance — calculation for each LES volume, with averaging and conversion to decibels.

d) *Instantaneous, displaced*: the same as the preceding profile type except that the collection point of the profile is moved an additional 500 m in the positive crosswind direction.

Bias error b and mean-square error σ^2 from the sound pressure level predictions $\hat{\phi}_i$ of N LES snapshots were calculated by

$$b = \frac{1}{N}\sum_{i=1}^{N}(\hat{\phi}_i - \phi_i), \sigma^2 = \frac{1}{N}\sum_{i=1}^{N}(\hat{\phi}_i - \phi_i)^2, \tag{2.23}$$

where ϕ_i is the actual sound pressure level, as determined from the fully resolved LES fields. The authors found that the error is greatest near the ground (see Fig. 2.6), especially for events of brief duration. However, the mean sound pressure levels can be predicted from the mean profiles, except in refractive shadow regions, with good accuracy.

Taking turbulent scattering into account would reduce the error in the calculations based on mean profiles (*ensemble-mean*) seen in Fig. 2.6 (a). The *instantaneous, displaced* vertical profiles approach is similar to the method proposed by Yokota et al. [169]. With the latter approach, however, the scattering is too strong, because the method assumes that the turbulent eddies extend much further spatially than the propagation path.

Also, four stratification conditions were determined: very unstable, unstable for sunny days, neutral for windy and cloudy conditions, and stable stratification of clear nights. Of these conditions, the bias error with a fixed receiver height of 2 m is greatest for very unstable stratification in upwind propagation (see Fig. 2.7). [199]

Considering the root mean square error as a function of frequency and distance reveals the effect of wind direction. In crosswind and upwind directions, the error values tend to increase without saturation when either frequency or distance increases, but in downwind conditions the 150 Hz and 250 Hz cases seem to saturate at the 8 dB level (as demonstrated in Fig. 2.8).

Often, the ground surface is overlooked as a source of uncertainty. Krajewski studied [200] the significance of ground effect on uncertainty. In addition to the characteristics of the ground surface and the terrain topography, the ground effect depends in a complicated way on the source–receiver geometry, atmospheric turbulence, and their random

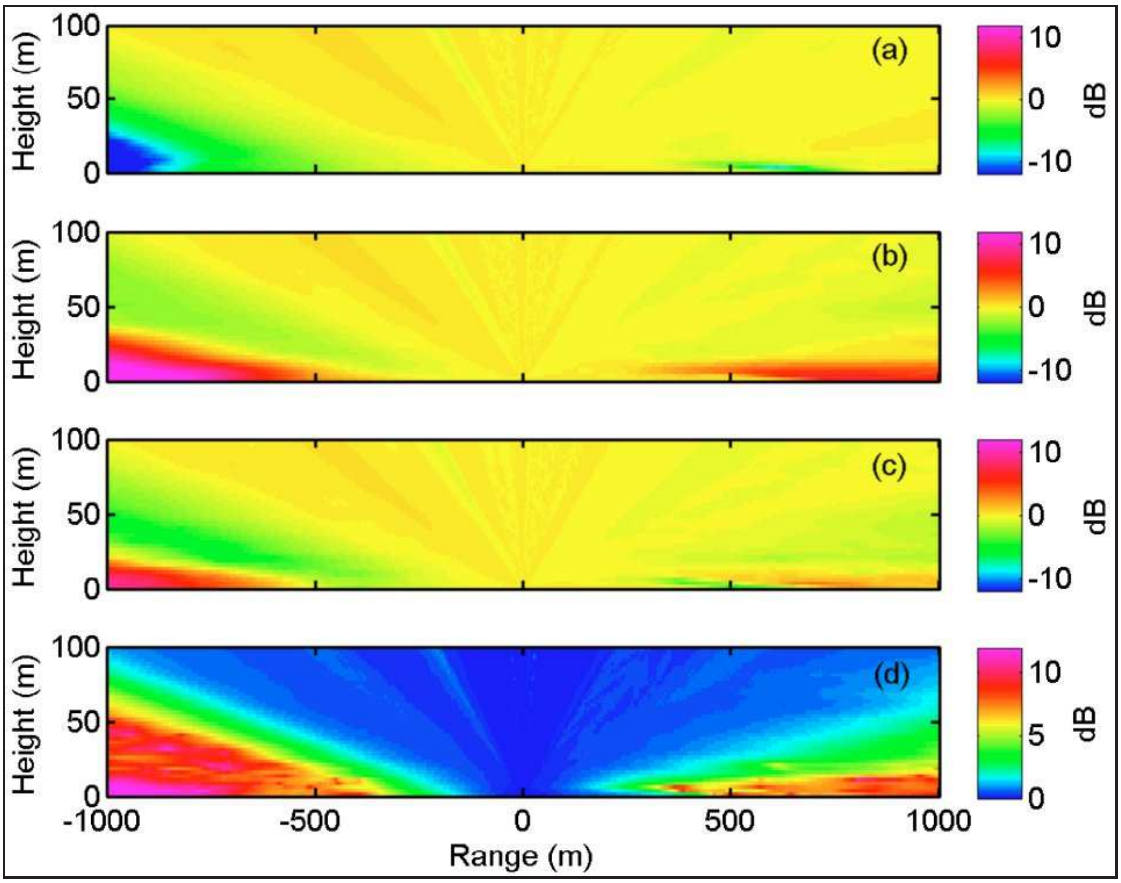

Fig. 2.6: Error values for mean sound pressure level estimates at 150 Hz in unstable stratification to upwind (negative range) and downwind (positive range) direction. a) Bias error for ensemble-mean, b) bias error for instantaneous displaced, c) bias error for a randomly selected set of vertical profiles, and d) σ of c) — see body text and Eq. 2.23. Reprinted with permission from Wilson et al. (2007)[199, Fig. 1]. © 2007, Acoustic Society of America.

variations. He showed variations of up to 14 dB at different frequencies and 10 dB variation in total attenuation between the results from different ground absorption models, at distances as great as 300 m[200].

Finally, Kühner demonstrated that, by capturing noise data over a sufficiently long time, one can decrease the uncertainty to a negligible level — even at a distance of 1200 m from a large motorway. He conducted measurements for up to 12 weeks at five distances from roads, rail lines, and loudspeakers. The data thus obtained were sorted — by means of various parameters, among them time of day and wind direction — into classes or strata, and the uncertainty was reduced to ± 0.4 dB by means of this stratified data-evaluation scheme. More than one week was needed for reaching uncertainty of less than ± 1 dB.[159]

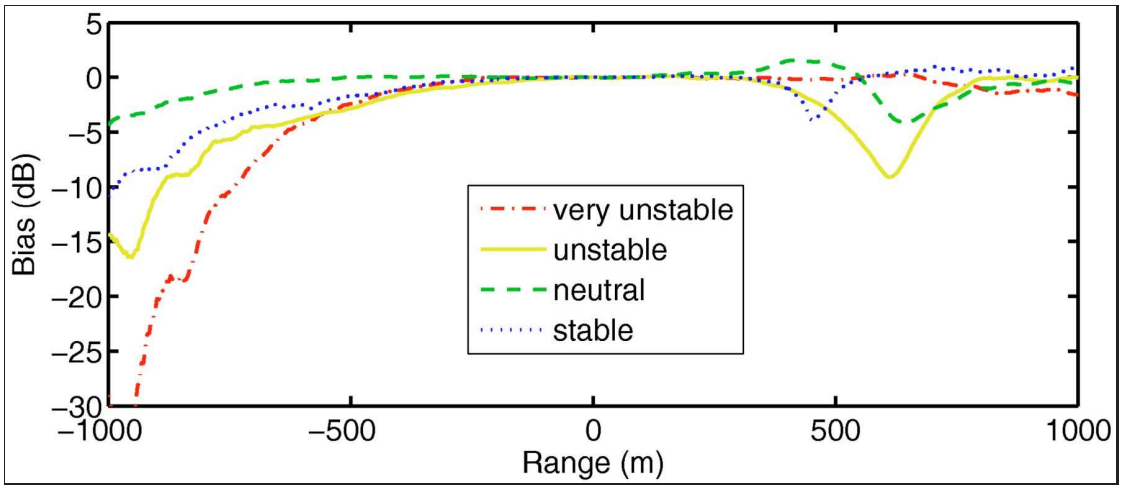

Fig. 2.7: Bias error for mean sound pressure level estimates at 150 Hz based on ensemble-mean vertical profiles in four distinct atmospheric stratification conditions. Receiver height is 2 m. Reprinted with permission from Wilson et al. (2007)[199, Fig. 2]. © 2007, Acoustic Society of America.

2.5 Summary of the background and the state of the art

The basic principles of one of the most widely used physical methods for long-range sound propagation was introduced. The parabolic equation method provides means to take most of the physics of the environment into account, but, there are weaknesses too: the method is computationally intense and turbulence models do not apply very well to real atmospheric turbulence. Also, a brief review of past long-term measurement campaigns was made. Only a few publicly reported measurements with satisfactory acoustical and meteorological instrumentation exist. The modelling approaches showed that the sound levels were quite well estimated for distances up to a few hundred metres. Finally, the concept of uncertainty and the sources of uncertainty in environmental noise assessments were considered. The largest source of uncertainty is the weather mainly affecting the uncertainty of the propagation path. An example of assessing the uncertainty by the means of parabolic equation method was shown.

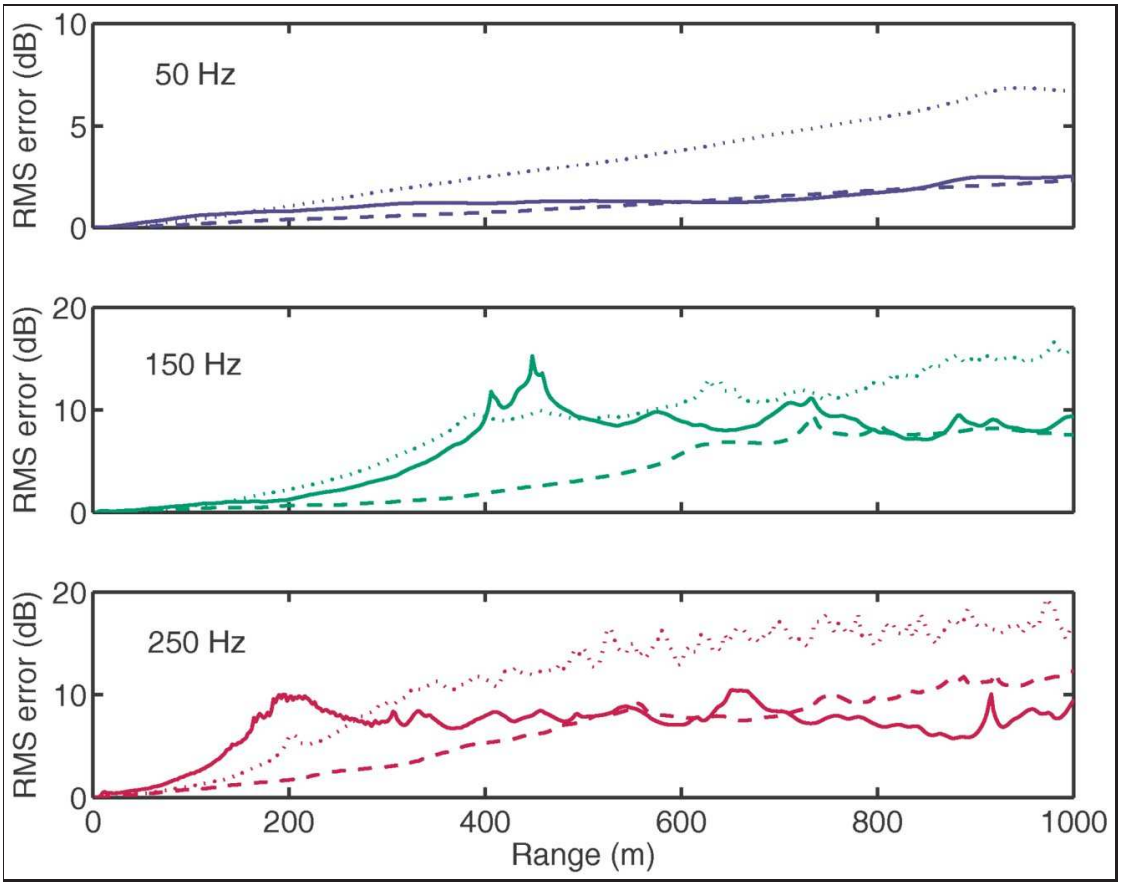

Fig. 2.8: The root mean square error as a function of frequency and range with different vertical profiles. Solid lines: downwind propagation, stable stratification. Dashed lines: crosswind propagation, neutral stratification. Dotted lines: upwind propagation, unstable stratification. Receiver height is 2 m. Reprinted with permission from Wilson et al. (2007)[199, Fig. 4]. © 2007, Acoustic Society of America.

Chapter 3

Measurements

CAREFUL and extensive data acquisition was required as a basis for the formation of the statistical model. It was the statistical model that demanded the majority of the research resources, with less than 5% left to the implementation of the physical model. Thorough planning, hardware testing, and software programming preceded the realisation of the measurements. More than a hundred people took part in this process, and research facilities were obtained from several organisations. Also, the management and control of the output of the measurements — many terabytes of sound and environmental data — was demanding. All of this work was diligently documented in a 339-page report[25]. This chapter provides an overview of the measurement environment, procedures, and methods.

The primary topic of interest was changes in excess attenuation due to environmental (mainly meteorological) effects, but also of key interest were changes in sound propagation delay and changes in angles of incident sound energy at the receiver location. Initially, it was planned to have many measurement points on the sound propagation path, but the delivery of electrical power for this end was found to be highly demanding and a point-to-point (P2P) approach was selected. On account of the temperature range expected in the research area (-50 to 30°C), the amount of electrical power needed for stabilising the temperature of the measurement equipment was several kilowatts, and the use of batteries had to be rejected. Also, a fast network connection was needed between the emission and immission points; this too was found to be challenging in the planning phase, in 2003.

In addition to the sound propagation measurements, background noise measurements were carried out. The environmental data consist of versatile observations of the environment and the atmosphere. The continuous measurements were launched as background noise measurement on Saturday, 13 March 2004, at 02:10 UTC. Background noise measurements were carried out every 10 minutes in the beginning, later every 15 minutes. The first successful sound propagation measurement was captured at 04:00 UTC on the same date, and another was completed every hour. The measurements

were stopped on 14 November 2005 at 07:42 UTC, which means there exist continuous data for 612 days — for 14,688 sound propagation measurements in the database in all.

Coordinated universal time (i.e., time in UTC) has been used in all the documentation of this work. The timestamps follow the rules of ISO 8601[201]: for example, 1 March 2005 at 15:45:17 had the timestamp 20050301T154517 (or 0503011545 in the brief presentation, leaving the seconds and century out).

Fig. 3.1: The Nordic region of Europe. The measurements were carried out in Northern Finland's Sodankylä, located in Finnish Lapland. Image © 2013 Google; © 2013 TerraMetrics, US Department of State Geographer; and © 2009 GeoBasis-DE/BKG. Reproduced with permission.

3.1 The measurement environment

Most attempts to produce experimental material for evaluation of sound propagation lack adequate data from the environment. In this project, we decided to concentrate on one case, capture all possible data, and document said data as well as possible. The selection of the measurement area was a sum of many compromises: far enough from settled areas not to disturb people with measurement signals yet providing all of the facilities an extensive sound propagation measurement campaign requires. With the absolute amount depending on the distance between source and receiver(s), there should

be enough instrumentation capable of characterising both the vertical and the horizontal gradients of wind and temperature in the atmospheric boundary layer. To allow this, meteorological towers, wind profilers, and real soundings were exploited.

A relatively homogenous area in acoustic terms, mostly with low vegetation and practically no difference in altitude but still very close to state-of-the-art meteorological measurement facilities, was found near the Arctic Research Centre of the Finnish Meteorological Institute (FMI) in Sodankylä, in Finnish Lapland (see figures 3.1, 3.2, and 3.3), at 67° 22′ N, 26° 38′ E, 180 m. One of the challenges was the 800 km distance to the author: the measurements had to take place fully automatically, recover from various error conditions independently, and entail immediate reporting of any problems.

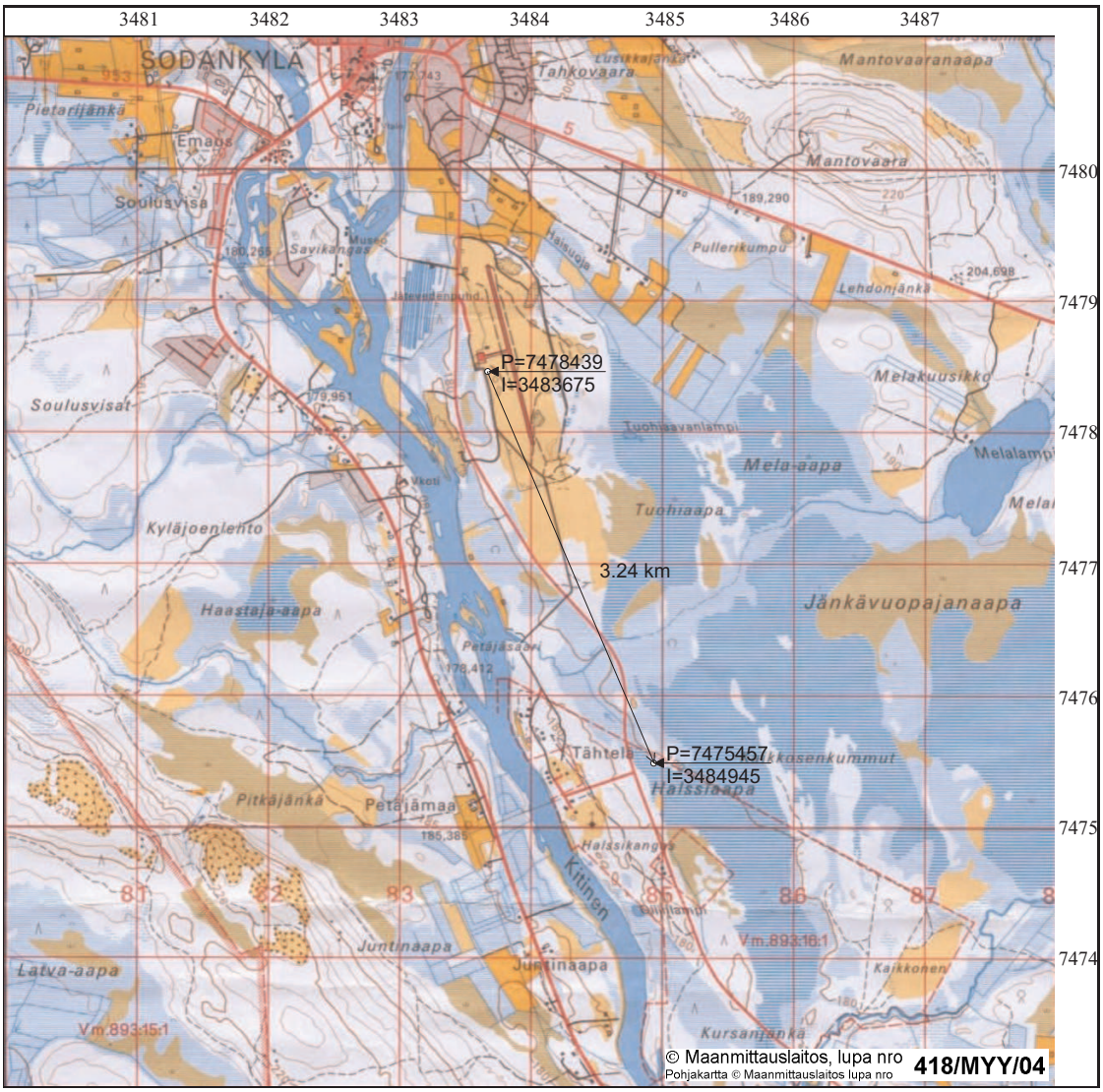

Fig. 3.2: A basic map of the measurement environment and co-ordinates for sound source and fixed receiving station. Source at P = 7478439, I = 3483675 and microphones at P = 7475457, I = 3484945, with sound propagation angle 157° (wind-rose equivalent: SSE).

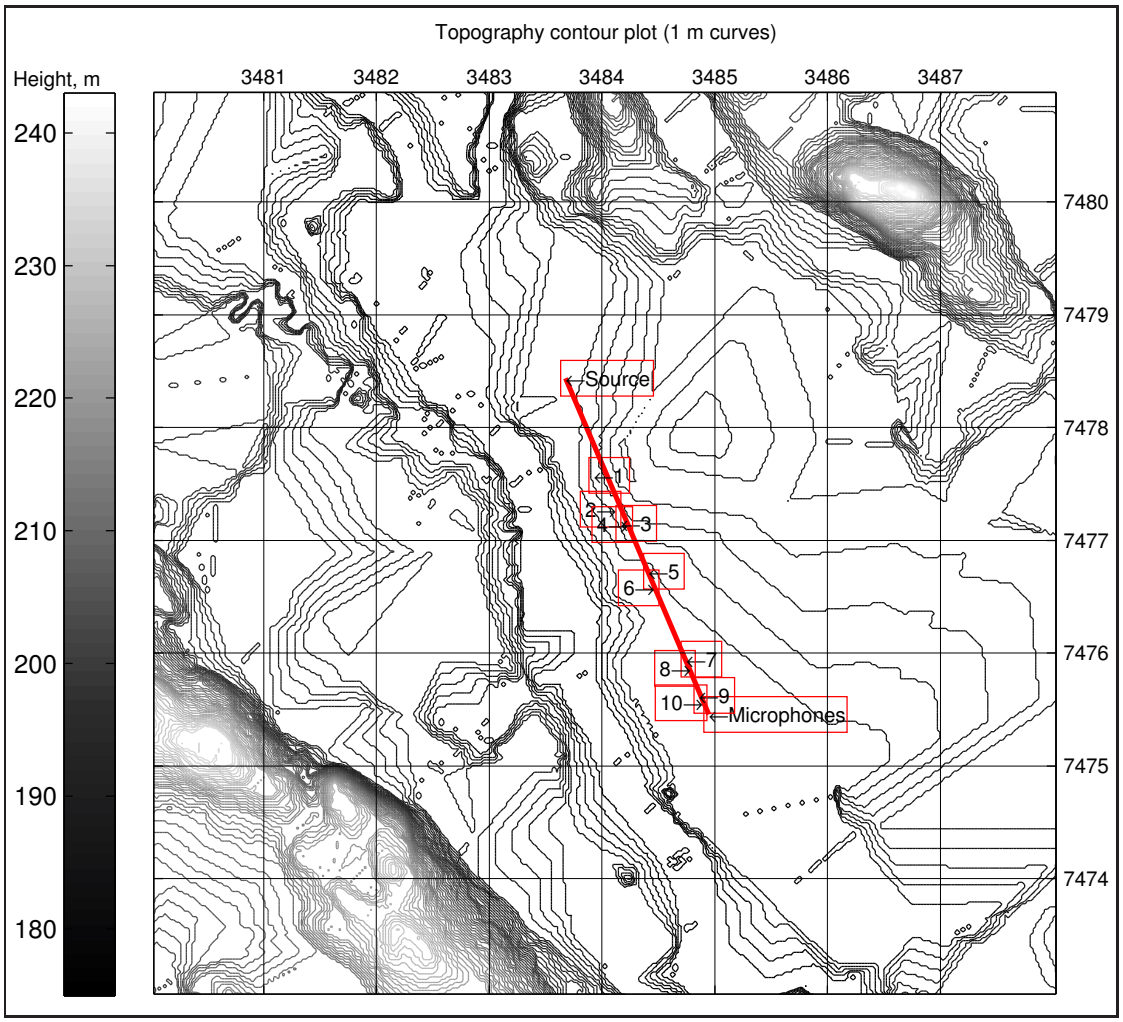

Fig. 3.3: The topography of the research area in terms of rectangular KKJ grid co-ordinates. Height (174 m – 244 m) from sea level and numbered locations 1–10 correspond to Table 3.2. The locations are depicted in exact evaluation positions and are slightly off the direct path.

3.2 Measurement facilities

3.2.1 Acoustic facilities

The sound source was at the Sodankylä airport[1], and the microphone antenna on a bog near Tähtelä, at the FMI's Arctic Research Centre[2], (see Fig. 3.4), 3.24 kilometres from the source.

The acoustic measurement devices consisted of an array of weather-proof measure-

[1] In KKJ (Finland Uniform Coordinate System) rectangular grid co-ordinates, P = 7478439, I = 3483675, or, in geographical KKJ co-ordinates (latitude, longitude) 67.39311837, 26.61961002 / 67° 23.587′, 26° 37.177′ / 67°23′ 35.226″, 26° 37′ 10.596″.

[2] P = 7475457, I = 3484945 / 67.36644932, 26.64959391 / 67° 21.987′, 26° 38.976′ / 67°21′ 59.218″, 26° 38′ 58.538″.

ment microphones (see Fig. 3.5), a four-metre-high horn stack, and a high-power subwoofer as a sound source (see Fig. 3.6), along with all of the other hardware needed for functionality.

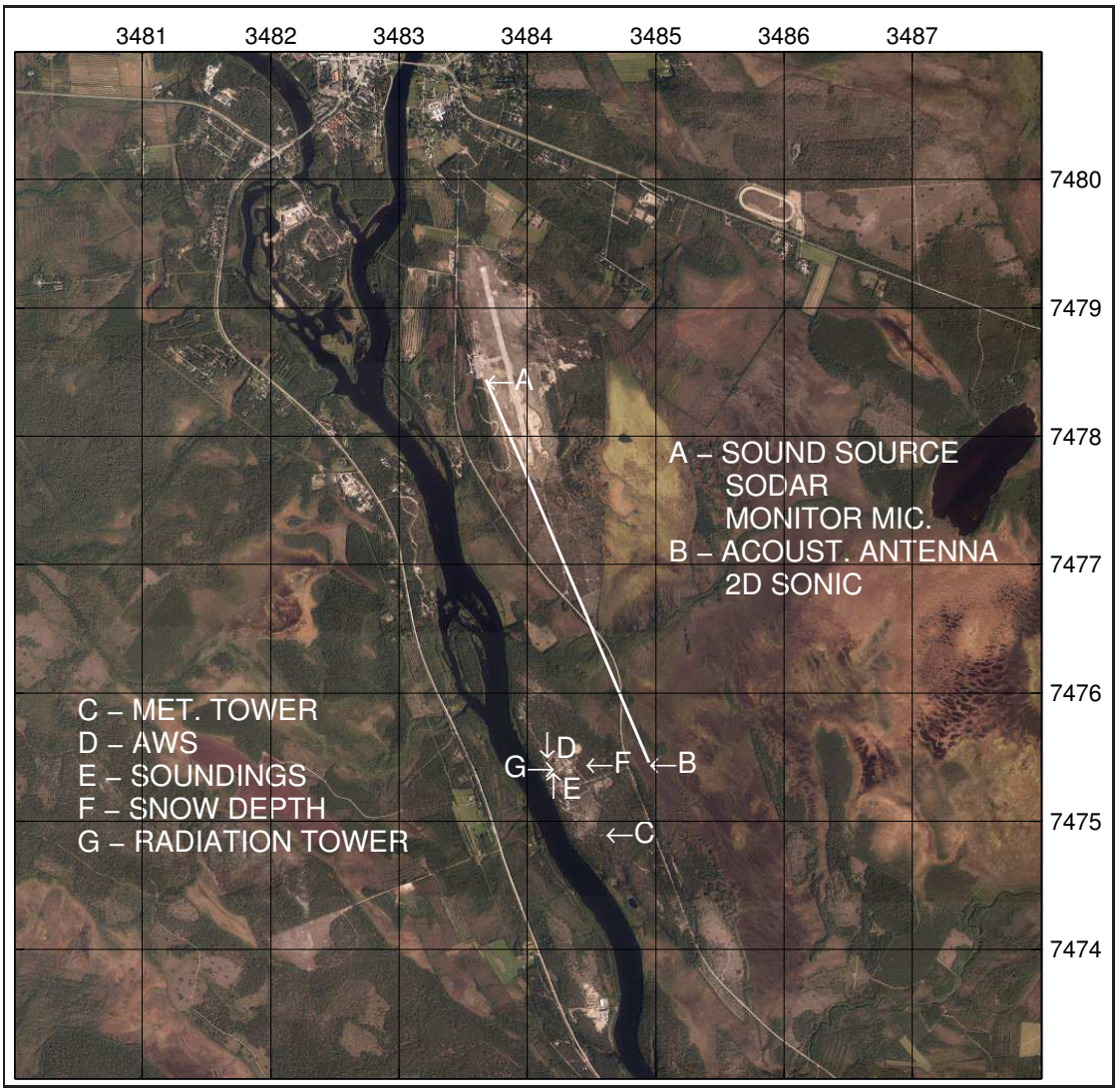

Fig. 3.4: An orthophoto of the measurement area. The measurement locations and direct sound propagation path are shown. Meteorological observations labeled from C to G were provided by the FMI. Rectangular grid co-ordinates are in accordance with the Finnish national adjustment of the ED50 co-ordinate system. NLS database 04/2013 data.[202]

The seven microphones were arranged as a combination of a tetrahedron and a linear array (see figures 3.7 and 3.8) to allow determination of the incident angle of sound. However, the angle of incident sound was not analysed and is not covered by this thesis. All the original audio data are available and will be analysed by a colleague in another project. Initially, there was one more microphone (R5), a few metres away from the antenna frame, but it was soon replaced by an acoustic anemometer (2D sonic).

The horn stack consisted of eight high-power compression drivers attached to horns

Fig. 3.5: The acoustic antenna with seven weather-proof microphones. There is a 2D sonic behind the acoustic antenna.

with 1 m $\times$ 1 m mouths, covering a radiation area of 8 m^2. Frequencies of 200 to 1600 Hz were reproduced by the horn stack. A subwoofer handled the frequencies from 40 to 200 Hz. The horn stack was of fully weather-proof design, but the subwoofer was only weather-protected, which means special waterproofing treatment on the loudspeaker cone. A special rigid weather case was planned and acoustically modelled to protect the subwoofer during the measurement campaign (see Fig. 3.6). The weather case was equipped with a large dehumidification device, capable of keeping a volume of 500 m^3 dry. The opening of the weather case was covered by sack material.

A weather-proof microphone was installed in front of the sound source (see Fig. 3.9) for automatic source condition monitoring and sound pressure level checks.

Sound source validation

The calculation of the most important result of the measurements, excess attenuation A_{env} (see Eq. 1.2), is based on the known sound power level L_W of a source and sound pressure level L_p captured by a microphone with known characteristics (see Eq. 3.1):

$$A_{\text{env}} = L_p - \left(L_W + 10\lg \frac{Q}{4\pi r^2}\ \text{dB} + D(f) \right), \tag{3.1}$$

Fig. 3.6: The back side of the sound source.

where $r = 3240$ m (distance between source and receiver), $Q = 2$ (source on a reflective surface), and $D(f)$ is the measured directivity (in dB) of the sound source to the direction of the receiving microphone; see Eq. 3.5.

The characteristics of a high-quality measurement microphone satisfy the accuracy requirements for this type of measurement, and the response of the microphone can routinely be checked and calibrated reliably again and again. However, there are many more challenges with sound sources. In this study, great care was taken to validate the sound source.

Sound power measurements following the ISO 3744[203] standard were performed three times during the trials: on 18 August 2003, 14 May 2004, and 19 September 2005. For the measurement, the sound sources were transferred to a concrete-surfaced wide area by a Hiab loader crane. Both narrowband and wideband excitations were used, and all the necessary characteristics of the sound sources were acquired as a result.

The most relevant information on the sound source is shown in Table 3.1, and an example of the directivity characteristics can be seen in Fig. 3.10. Since the approach in the ISO 3744[203] standard provides only 120° resolution for the directivity by means of the 'key microphone' positions, additional microphone positions were used, to yield 60° resolution. Also, the front-half sector was scanned for local variations, to 15° resolution.

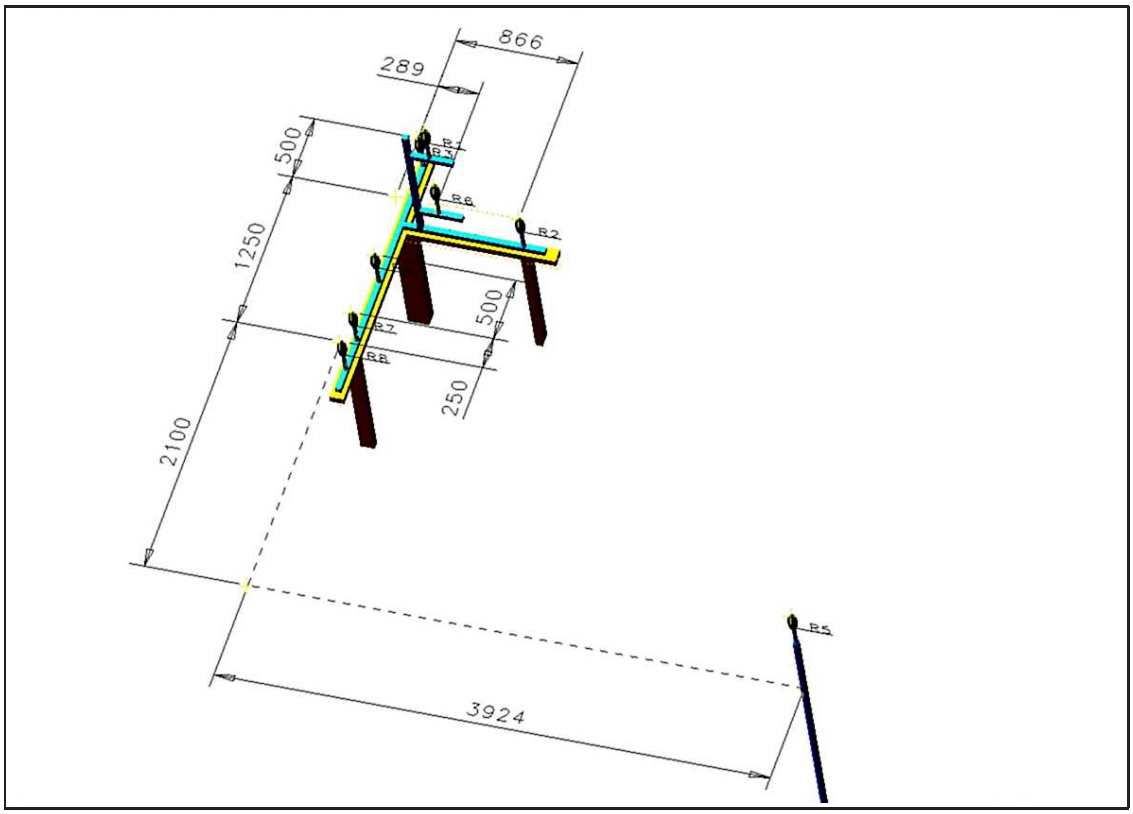

Fig. 3.7: Dimensions of the microphone antenna. Initially there were eight microphones, but the microphone outside the frame (R5) was soon replaced with an acoustic anemometer.

The sensitivities were found by means of $U_{\mathrm{RMS}} = 6.00$ V sinusoidal excitation signals at all of the one-third-octave centre frequencies.

Analysis of the sound power measurement was begun with the two time-averaged sound pressure levels, $L_{pi1}(f)$ and $L_{pi2}(f)$, where i is the microphone position number[3], between 1 and 20: two distinct measurements were used for every microphone position at distinct one-third-octave-band centre frequencies by means of sinusoidals adjusted to give $L_{\mathrm{RMS}} = 6.00$ V at the loudspeaker input contacts.

The logarithmic average $\overline{L_{pi}(f)}$ of $L_{pi1}(f)$ and $L_{pi2}(f)$ was calculated via Eq. 3.2:

$$\overline{L_p} = 10\lg\left(\frac{1}{n}\sum_{i=1}^{n} 10^{0.1L_{pi}}\right)\ \mathrm{dB}, \tag{3.2}$$

where n is the number of distinct sound pressure levels (or microphone positions) to be averaged and L_{pi} is the corresponding sound pressure level.

Calculated next was the logarithmic average $\overline{L_p(f)}$ of all the measurement points, via Eq. 3.2, and the hemisphere correction L_{hc} (see Eq. 3.3) for a reflecting hard surface

[3] Numbering in accordance with ISO 3744 [203, pp. 21–22].

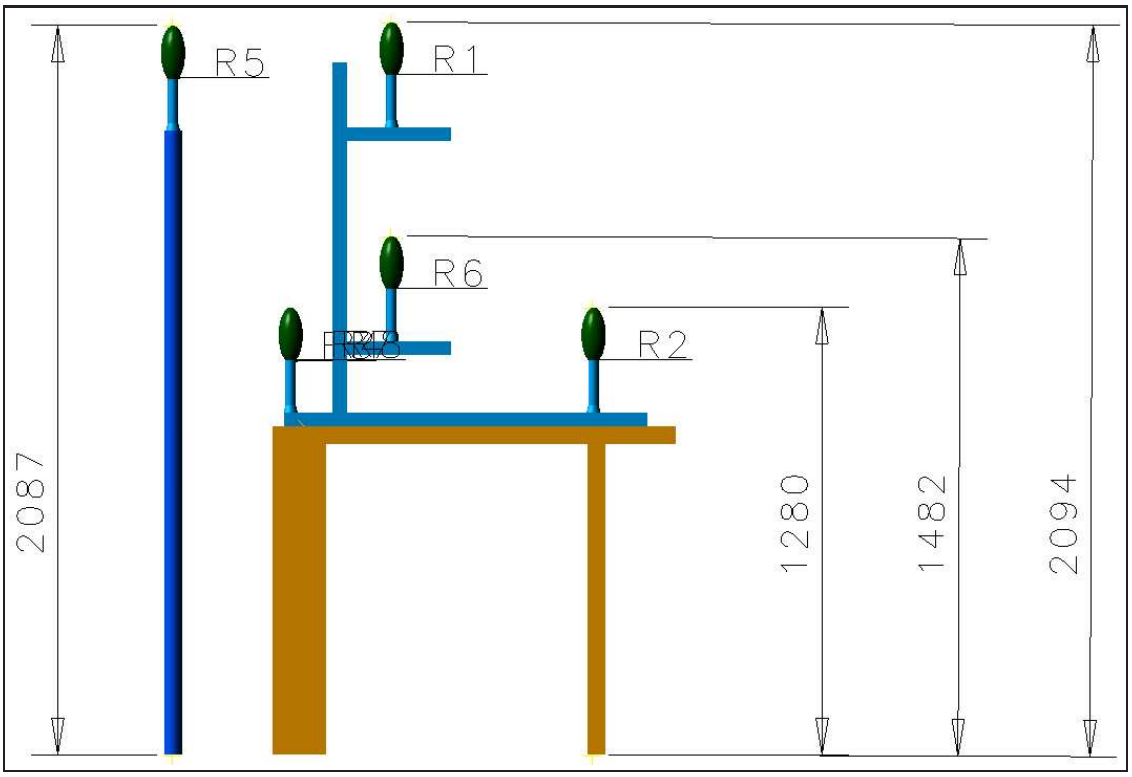

Fig. 3.8: The height of the microphones. The height of microphone R1 corresponds to that of the acoustic anemometer near the microphones.

($Q = 2$) with a radius $r = 8$ m:

$$L_{\mathrm{hc}} = -10\lg\frac{Q}{4\pi r^2}\ \mathrm{dB} \approx 26.04\ \mathrm{dB}. \tag{3.3}$$

This allowed determination of the sound power levels $L_W(f)$ as a function of frequency:

$$L_W(f) = \overline{L_p(f)} + L_{\mathrm{hc}}. \tag{3.4}$$

The *directivity* was approximated as a function of frequency (in Eq. 3.5):

$$D(f) = \max(\overline{L_{pi}(f)}) - \overline{L_p(f)}. \tag{3.5}$$

To allow approximation of the front-sector average sound pressure level, the logarithmic average for microphone positions 11, 6, and 18 ($L_{p11}(f)$, $L_{p6}(f)$, and $L_{p18}(f)$, respectively) was calculated by means of Eq. 3.2, to produce $\overline{L_{p\mathrm{front}}(f)}$. Then, using the sound power level (see Eq. 3.4), we calculated the sound pressure level at a distance of $r = 8$ m from the source, using Eq. 3.6 and $Q = 2$:

$$L_{p8\mathrm{m}}(f) = L_W(f) + 10\lg\frac{Q}{4\pi r^2}. \tag{3.6}$$

The directivity (see Eq. 3.5) was added to the averaged three microphone positions from the front to produce

$$L_{p\mathrm{front}}(f) = D(f) + \overline{L_{p\mathrm{front}}(f)}, \tag{3.7}$$

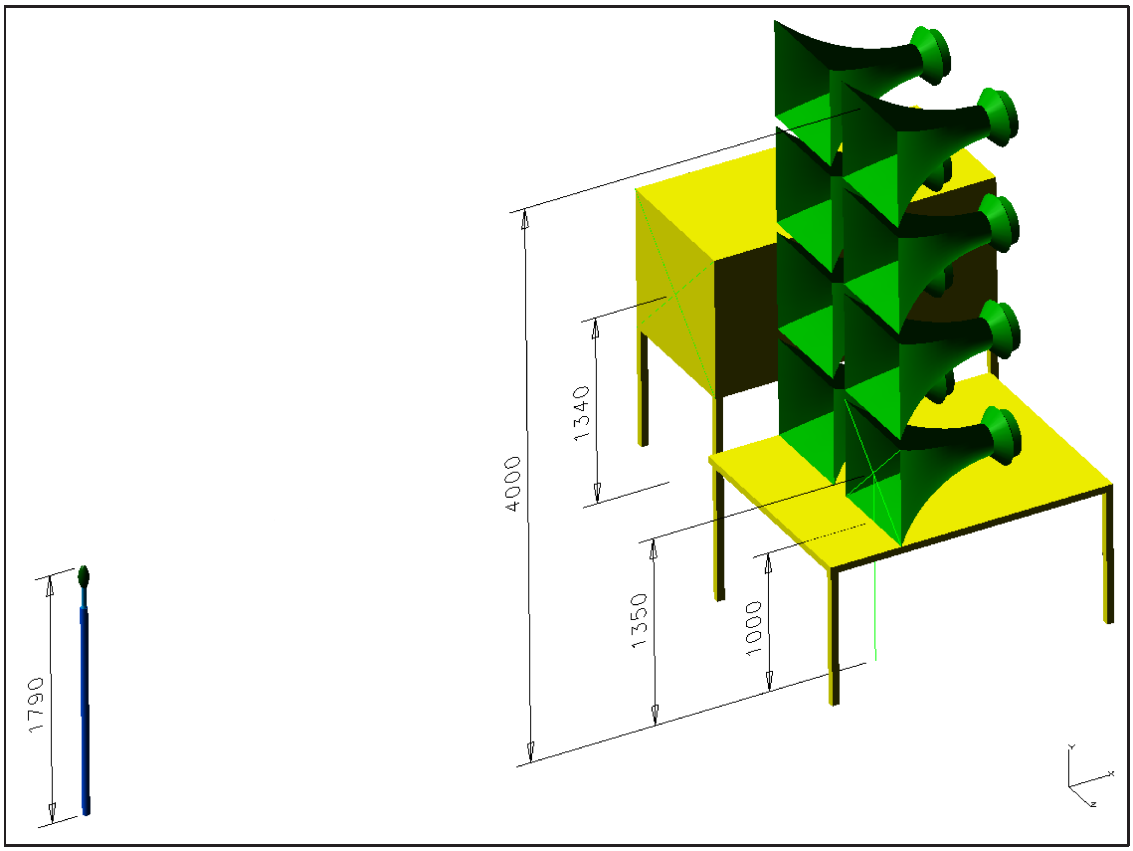

Fig. 3.9: Sound source dimensions. The control microphone was 5120 mm from the horizontal centre of the horn stack.

and, finally, we subtracted the sound power level calculated the traditional way (see Eq. 3.6) at a distance of 8 m from the directivity-corrected and averaged three front microphone positions' sound pressure level to obtain the level of 'shape error':

$$L_{\text{shape error}} = L_{p\text{front}}(f) - L_{p8\text{m}}(f). \tag{3.8}$$

Another approach, perhaps more practical, for estimating the effect of directivity of a source on results, is the following. Because all of the 20 microphones are associated with equal areas on the surface of a hemisphere of radius $r = 8$ m over a reflecting hard surface ($Q = 2$), we can calculate the hemisphere correction L_{hcfront} (see 3.9) for the area for which the three front microphones are responsible:

$$L_{\text{hcfront}} = -10\lg\left(\frac{20}{3}\frac{Q}{4\pi r^2}\right)\ \text{dB} \approx 17.80\ \text{dB}. \tag{3.9}$$

The sound power to the front sector can be calculated by adding of the surface correction to the logarithmic average for microphone positions 11, 6, and 18:

$$L_{W\text{front}}(f) = L_{\text{hcfront}} + \overline{L_{p\text{front}}(f)}. \tag{3.10}$$

Table 3.1: Some characteristics of the sound source, from sound power measurement on 14 May 2004 (the frequencies for the subwoofer are 40–200 Hz and for the horn speaker 200–1600 Hz, indicated by two 200 Hz lines in the table; the subwoofer was measured with the weather case)

Frequency, Hz	Directivity, dB	Divergence, dB	Sound power, dB
40	2.5	-5.3	100
50	2.9	-5.3	106
63	3.9	-4.7	106
80	4.9	-3.7	110
100	5.3	-4.1	110
125	6.5	-3.7	111
160	7.6	-3.2	113
200	9.0	-2.5	110
200	6.8	-2.9	110
250	5.6	-2.6	114
315	7.6	-1.0	115
400	9.0	-0.6	121
500	7.7	-0.6	119
630	9.7	-0.3	125
800	9.9	-0.1	125
1000	9.6	-0.2	125
1250	9.4	-0.3	117
1600	7.6	-0.5	110

Now, an indicator that measures how much the acoustic power emitted to the desired direction differs from the total acoustic power of the source can be obtained:

$$G(f) = L_{W\,\mathrm{front}}(f) - L_W(f). \tag{3.11}$$

This indicator, G, was called '*divergence*'. Divergence values are between 0 and minus infinity: the magnitude of the negative value will increase if the sound power to the desired sector is decreased in comparison to that in other directions. And, naturally, divergence approaches 0 dB, if the source emission to the desired sector is raised when compared to that toward other directions, and it comes to 0 dB if all the acoustic energy is concentrated in the desired sector.

In this sound propagation study, the sound source was placed in an open area at an airport and there were no vertical reflective surfaces nearby. The sound power emitted from the source can be used in determination of the excess attenuation with sufficient accuracy as long as the directivity of the source is taken into account. The error estimate could be determined via reverse modelling: what are the directions from the sound

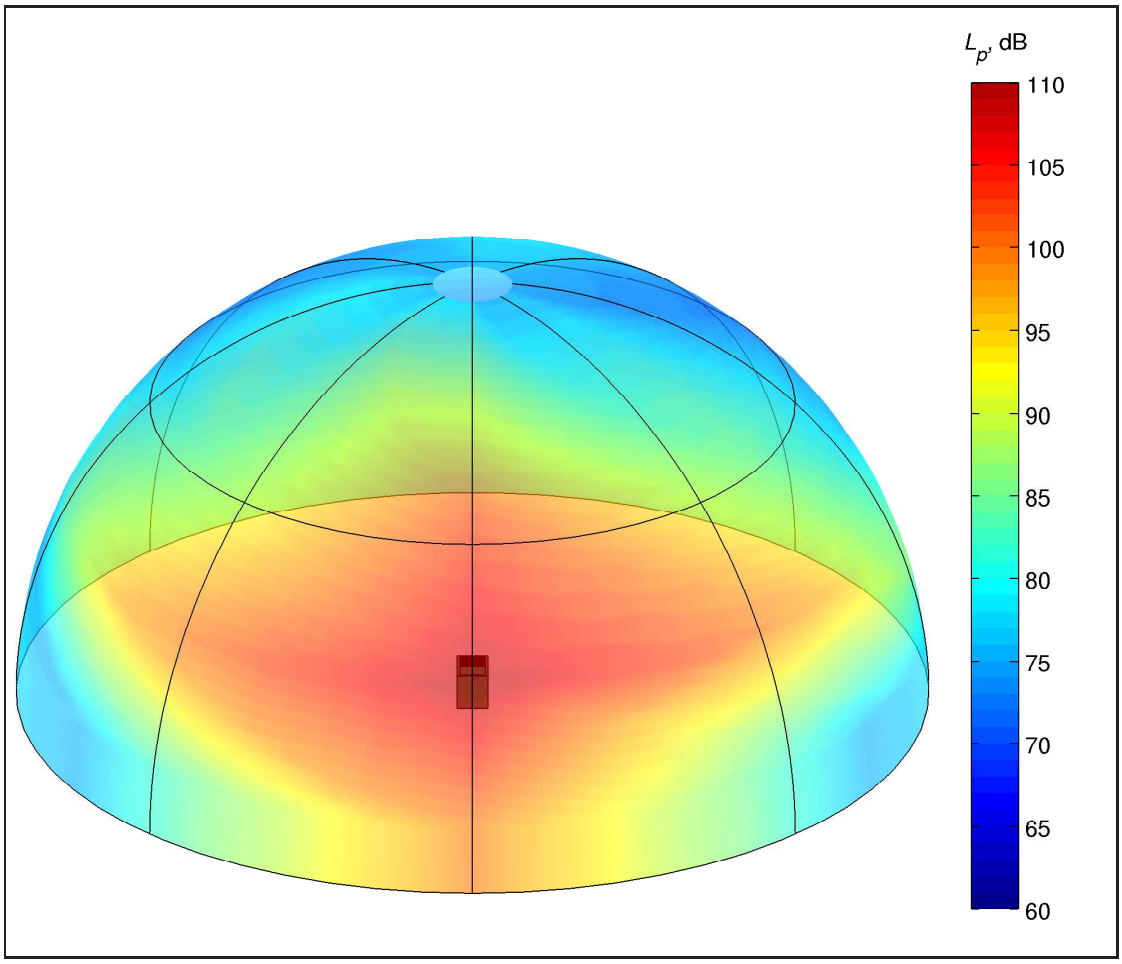

Fig. 3.10: The directivity of the horn speaker at a frequency of 1000 Hz. Standard ISO 3744[203] sound power measurement on 19 September 2005. Measurement radius $r = 8$ m and excitation signal level $U_{\mathrm{RMS}} = 6.00$ V.

source from which the energy is transmitted to the location of interest? If the modelling of the weather condition in question indicates that also the uneven part of the directivity of the source contributes to the total immission, the uncertainty value should be increased. However, this is very hard to estimate and the best option would be to implement an omnispherical sound source for the entire frequency range of interest. At the same time, the directivity of the sound source in this study, 3 dB, should remain satisfactory.

The frequency response of the horn loudspeaker remained unchanged throughout the study period, but the subwoofer created some problems. Apparently, the variations in temperature and moisture-related stress caused the subwoofer to go silent on 17.10.2005 between 17:02 and 18:47 (the automatic calibration system issued an alarm). The subwoofer was not replaced, which is why low-frequency excess attenuation values are absent from the database for the last month of the measurement campaign.

Data acquisition

The data-acquisition hardware for the sound measurements needed special attention, on account of the requirements of the sound propagation delay measurements. The excitation signal and the data acquisition had to be synchronised to an uncertainty of less than 1 ms.

It was quite easy to synchronise the computer clocks with atomic clocks. Instead, the challenges arose from latencies of the operating systems. Utilising a real-time operating system would have solved the latency problem, but this idea was abandoned on account of other limitations. The solution was to program recording and playback routines suitable for our purposes. The sum of all system-dependent time errors was minimised at less than 1 ms (mean: 0.69 ms).

Acoustical excitation

The source excitation signal was a combination of sinusoidals with one-third-octave-band centre frequencies of 160 to 1600 Hz and also lower-octave frequencies 40 and 80 Hz with a duration of 30 s. Additionally, there was an optimised series of sine sweeps to make calculation of sound propagation delays possible.

3.2.2 Meteorological facilities

The observation station of the FMI was near the receiving station (see Fig. 3.4). Meteorological data and acoustic data both were recorded constantly, around the clock. The vertical gradients of wind and temperature were determined by means of ultrasonic anemometers at different heights in a 50-metre-high meteorological tower (see Fig. 3.11) and a SODAR[204] (see Fig. 3.12) near the sound source. In addition to the data from automatic weather stations, the personnel made standard synoptic observations every third hour and sent a helium balloon with a radiosonde at midnight and midday UTC. The atmosphere was covered by the sounding data to a height of 30 km. Some of the parameters measured were processed afterwards.

The SODAR was used to measure the lapse rates and wind profiles over a 30-minute integration time up to a 750-metre height with a step resolution of 25 metres.

At the height of the highest microphone in the receiving antenna, there was a sonic near the microphones. The purpose of this sonic was to give an instant estimate of the wind conditions at the height of the microphones. The sonic was read 10 times per second to capture all of the gusts.

Finally, after observations of the ground surface's character, snow depth, visibility, cloud types and heights, weather codes, heat fluxes, and various wind and turbulence measurands, many calculated measurands were archived — for example, Pasquill sta-

bility classes (see Table 2.3) and friction velocity $u_\star$ (see Eq. 3.12)[124, (2.10)b]:

$$u_\star = \sqrt[4]{\overline{u'w'}^2 + \overline{v'w'}^2}, \tag{3.12}$$

where u' is the component of wind in the direction of wind flow, v' is the component of wind perpendicular (horizontal) toward the direction of wind flow, and w' is the component of wind perpendicular (vertical) in the direction of wind flow. Also archived was

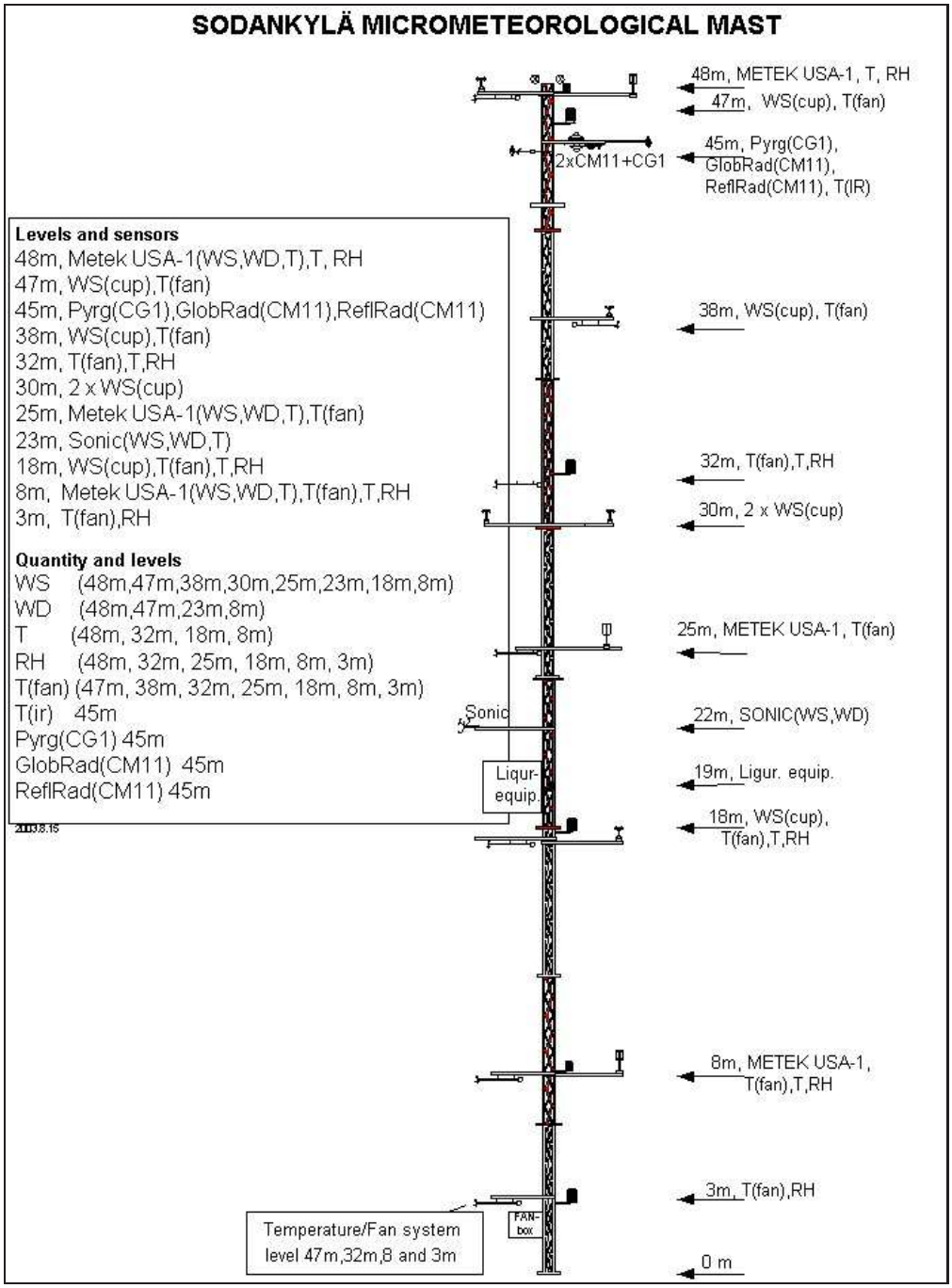

Fig. 3.11: The meteorological tower was close to the microphone antenna. Image © 2003 FMI. Reprinted with permission.

Fig. 3.12: The SODAR was near the sound source at the Sodankylä airport.

Obukhov length[4] (L_0)

$$L_0 = \frac{-u_\star^3 \Theta}{g \kappa Q_0}, \tag{3.13}$$

where $u_\star$ is the friction velocity, Θ is the potential temperature, g is the acceleration of free fall, κ is von Kármán's constant, and Q_0 is the kinematic heat flux.

3.3 System automation

The biggest issue before and during the measurements was how to control the signal-to-noise ratio (SNR) of the measurement signal. The system was able to provide a very high SNR. The very distinguishable signal was in the audible range, and there was fixed habitation nearby. The SNR had to be low enough not to disturb people but also high enough to allow automatic detection of the measurement signal as distinct from background noise. In addition, there was quite a lot of traffic on a road close to

[4] In the literature, Obukhov length is often incorrectly referred to as Monin–Obukhov length (and Obukhov's name is sometimes transliterated without the 'k' or 'h'). Alexander Obukhov (Алексáндр Óбухов) (1918–89) defined his turbulence quantity in 1946. Later, in 1954, he published the famous surface-layer Monin–Obukhov similarity theory with Monin [205].

the research area, and it was hard to discriminate the lowest sine signals from the road noise.

3.3.1 Measurement procedure

A tolerable solution for automatic SNR control was to calculate proper transmission power on the basis of the day of the week, the time of day, and the average of 10-minute-interval wind speeds captured just before measurement. The wind speed had the greatest weight in the control algorithm. There were four levels of the transmission power: 0, 6, 12, and 18 dB. The power was at its lowest level during calm nights and turned to the maximum for a windy day. Afterward, in the analysis, the transmission power had to be considered individually for each measurement. At the same time, the deviations in the response of the sound source (see Fig. 4.2) were corrected, resulting a stable sound power source with a flat frequency response.

Every hour, just before the measurement, a 200 Hz test signal was sent and captured by means of a monitoring microphone in front of the sound source. Abnormal sound levels were automatically reported to the GSM phone of the administrator. At the same time, at the receiving station, every microphone was checked via a computer-controlled charge injection calibration (CIC) method. The CIC method does not address accuracy but does indicate whether there are problems with the microphone, preamplifier, cables, measurement amplifier, or AD converter or with how these function together. The microphones were manually calibrated about four of times a year with a multifunction acoustic calibrator through the frequency range of interest.

After the measurement was triggered, the timestamps for the actual time was written to log files along with the transmitted-power level.

3.3.2 Archival procedure

Every hour, after the measurement, the signals were downsampled and checksums were calculated. The files were transferred to the archiving servers, located in central Finland, and the checksums were compared. The original recording at the receiving station was deleted only if the checksums were in agreement. All the audio and weather data, along with the log files, were mirrored once a day to another server.

3.3.3 Community liaison activities

The area was almost perfect for this kind of research; the disadvantage lay in the residential areas around the district. The nearest residential area was less than one kilometre away from the sound source, and there was a high risk of annoying a third party.

Many actions were taken to minimise any disturbances. Local media were informed in advance, briefings were given, and a person responsible for communications with the public was appointed. The main emission from the sound source was directed away from all residential areas, and the sound power was controlled automatically to keep it at its lowest feasible level. The automatic power control took into account the 10-minute-average wind speed, the time of day (lower power was used from 6pm to 8am), and the day of the week (lower power was used on Sundays). There were no complaints from residents of the municipality of Sodankylä but some complaints from the university campus near the receiver station. These were taken seriously and handled on an individual basis. Also, environmental noise measurement campaigns were carried out in all residential areas repeatedly.

3.4 Summary of the measurements

The measurement environment and the facilities for the long-term sound propagation measurements were presented. The measurement arrangement consisted of a large number of acoustical and meteorological instrumentation and a series of specific software that fully automatised the system. The objective of the measurements was to determine the effect of the environmental conditions on excess attenuation and sound propagation delay. In addition to the hourly sound propagation measurements, background noise measurements were carried out every 15 minutes. The measurements were continued for 612 days without interruption on a site, which was practically flat and relatively homogenous in acoustic terms, mostly with low vegetation. The sound source was a stable sound power source and a total of eight measurement microphones were used to capture the signals which were archived in time domain format to a database. The playback and the recording events were synchronised together so that the the error in timing was less than 1 ms. A meteorological tower, sonic anemometers in several heights, a SODAR, automatic weather stations, and radiosonde soundings provided the meteorological data, which was captured simultaneously with the acoustic data.

Fig. 3.13: The variation of the ground surface in the sound propagation area in the research location, explained in detail in Table 3.2. Photos taken on 15 May 2004.

Table 3.2: Research-area ground characteristics, location number ('no.'), distance ΔL from previous location, height, and flow resistivity during summer σ_s and winter σ_w, corresponding to Fig. 3.14

Loc. no.	ΔL, m	Height, m	σ_s, kPa·s/m^2	σ_w, kPa·s/m^2	Depiction, characteristics
-	0	180	630	40	*Source location*, airport, coarse gravel and sparse grass.
1	899	183	225	40	Airport fenced area ends, spacious rough pasture area begins — Fig. 3.13 (a), view to the north.
2	357	182	160	40	Spacious logging area begins — Fig. 3.13 (b), view to the south-east.
3	130	182	100	37	Logging area ends, half-logging area begins (east side full logging, west half of the region sparsely covered by pine stand, height 3–5 m).
4	61	182	70	20	Denser pine forest with 4-6-metre-tall trees begins.
5	452	180.3	100	37	Pine forest ends and silt, half-logging area begins (west side sparsely covered by high pine trees of 15–25 m) — Fig. 3.13 (c), view toward the west, Fig. 3.13 (d), view to the east.
6	152	180	225	63	Crossing the street, dense dwarf birch tree area begins, following next to the street.
7	693	180	100	37	Crossing the street, region covered with dense dwarf birch trees growing in moist swamp, near the street — Fig. 3.13 (e), view to the east.
8	85	180	40	37	Spacious region covered by sparse dwarf birch trees and some small pine trees growing in a wet swamp begins — Fig. 3.13 (f), view to the east.
9	255	180	40	37	Spacious wet swamp region without trees begins.
10	70	180	40	37	Wet swamp partially covered with water, grass growing here and there — Fig. 3.13 (g), view to the north-west.
-	117	180	63	40	*Acoustic antenna location*, wet swamp partially covered with water — Fig. 3.13 (h), view toward the south.

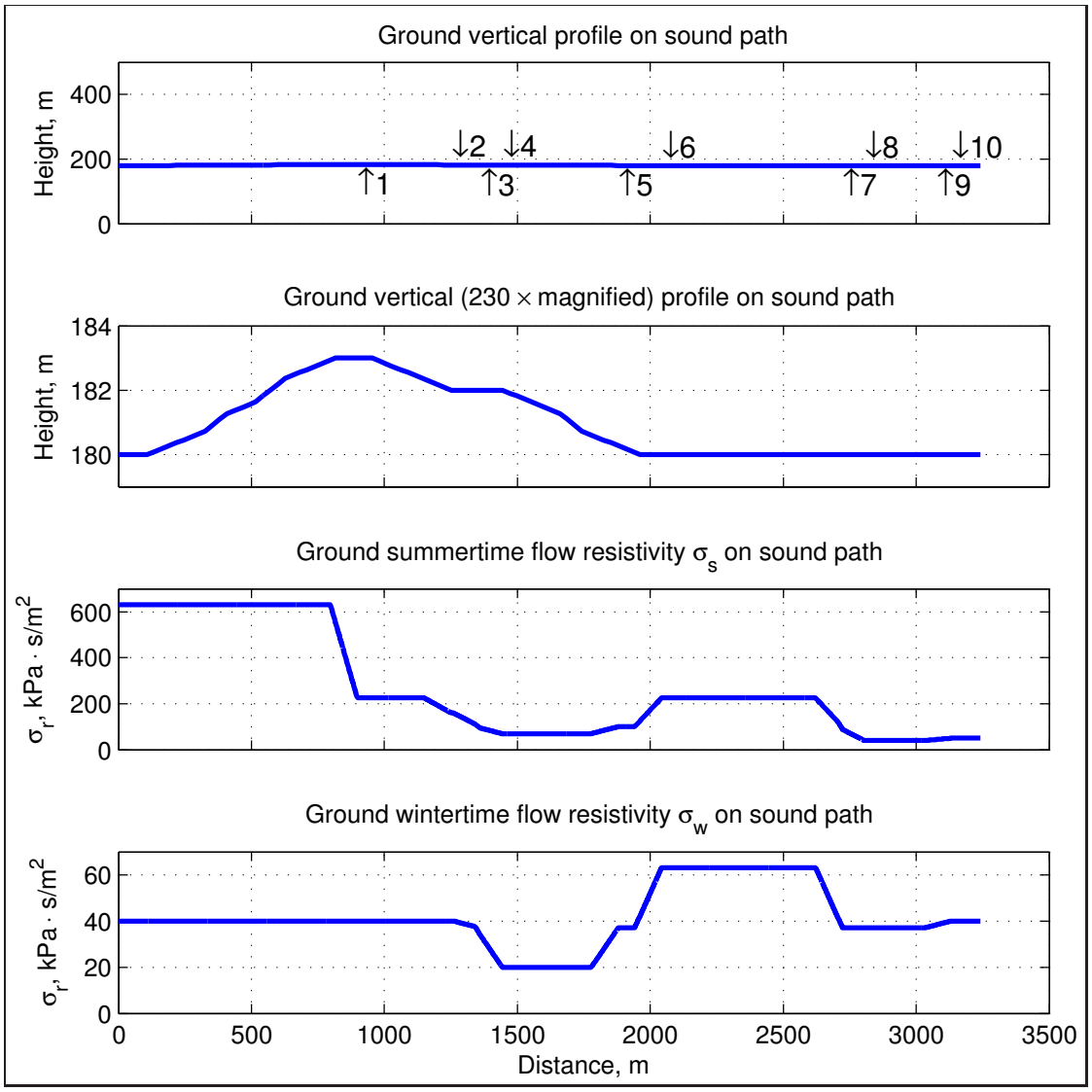

Fig. 3.14: Vertical profile of the research area and the ground flow resistivity along the sound path. Symmetric axis in the upper profile figure, vertical axis magnified in the lower profile figure, and height from sea level. The distance from the sound source in metres is common to all horizontal axes, and the numbered arrows correspond to the locations in Table 3.2. Flow resistivity values are averaged with a 100-metre-wide sliding window.

Chapter 4

Analysis and results

ANALYSIS of the sound propagation data was a computationally demanding operation, because of the huge quantity of data. Many characteristics were calculated: excess attenuation as a function of time[1], the mean, and the variance are only a few examples. The results were written to files, every third octave's frequency on its own line. The one-third-octave frequencies analysed were 40 to 5000 Hz, yielding 22 lines in each file, and 300 values per line (60 s sample divided into 200 ms time windows). Every row starts with the value of the frequency, followed by the decibel values for every 200 ms, with the values separated by a '$', as in this example:

```
0040$0045.1$0044.6$0049.5$0048.8$0053.9$0051.9$...
0050$0052.1$0045.9$0056.1$0055.9$0052.9$0055.4$...
...
```

Every 24 hours, 1920 files were produced, and the analysis of one day's measurements took up to 36 hours on a powerful workstation. Because the time required for the full analysis was estimated to be 874 days, some actions were taken to speed up the process: the samples were downsampled to 6 kHz and a computer cluster was deployed. Later, calculation from the data used the full 48 kHz sampling frequency.

The first two sections of this chapter explain how all the data from the sensors were pre-processed and summarised in 2,996,352 fields in a database, which begins and ends in the following manner:

```
Index$TimeStmp$DateTime$MonthNo$WeekNo$...
...
014687$200511142200$14-11-2005  22:00$11$46$...
014688$200511142300$14-11-2005  23:00$11$46$...
```

The statistical analysis of sound is given the main focus in this chapter, but the environmental conditions are summarised also, Section 4.9. The main objective of the chapter is to explain what the new model is and what it is capable of.

[1] During the 60-second measurement.

4.1 Data pre-processing

The four-level automatic power control described in Section 3.3, was optimised to keep the SNR as low as possible, to minimise any disturbances. On the other hand, the data had to be analysed automatically, and such analysis of audio data requires a better SNR than manual analysis does: there is a much greater risk in automatic analysis of some external distraction affecting the results. Truck noise, a helicopter fly-by, or a snowmobile passing by is an example of sources of distraction. In this section, the background for the selection of the limits and the validation process of audio data is explained.

The measured signals had a very low SNR. There were 1895 measurements between 1 January 2005 and 20 March 2005. If we consider all of the one-third-octave frequencies between 40 and 1600 Hz and set the SNR limit to 3 dB, 98.7% of the measurements must be rejected, but an SNR limit reduced to 1 dB would still lead to 98.1% being rejected. Limiting the frequencies to 250–1000 Hz and setting the SNR limit to 1 dB causes rejection of 75% of the measurements. If only measurements during 00:00–04:00 UTC are considered, 100% of the measurements must be abandoned — the only acceptable measurements were made during the daytime! If we look at all the measurements for which the average signal level was higher than the background noise level in the 363 days between 17 November 2004 and 14 November 2005:

- With the frequency range 40–1600 Hz, 96.7% must be rejected.
- With the frequency range 250–800 Hz, 72.5% must be rejected.
- With the frequency range 400–630 Hz, 62.1% must be rejected.

These comparisons led to the conclusion that we had to implement *frequency-dependent* SNR analysis for automated selection of valid measurements. The SNR of a measurement was determined from two equivalent sound pressure levels ($L_{\mathrm{eq,10\,s}}$), calculated from a measurement signal at one-third-octave centre frequencies: *background noise level* just before the excitation signal was captured and *signal level during the excitation signal*. The SNR limits for the validation were determined iteratively: the analysis application was run repeatedly, measurement signals near the limit values were listened to, and the threshold values were changed, until only measurements without distractions were accepted by the algorithm. The following SNR limits were required for acceptance of the measurement as valid: 40 Hz (+16 dB), 80 Hz (+12 dB), 160 Hz (+7 dB), and 200–1600 Hz (+1 dB). The higher threshold values for the lower frequencies were mainly due to the noise of trucks driving on a road at one kilometre's distance.

Regardless of frequency-dependent validation algorithm, quite a small percentage of the measurements were accepted for the database (see Fig. 4.1). The magnitude of the sound pressure levels from the subwoofer was the same as that with the horn stack, but environmental noise masked it more often. Up to 95% of the 14,688 measurements

in the 40 Hz frequency band were abandoned, while 46% in the 630 Hz frequency band were valid. Obviously, many more measurements would have been acceptable if the validation had been done manually, measurement by measurement. It must be emphasised that the excitation signal is audible also in almost all of the abandoned samples. A smarter validation algorithm would have saved more samples.

Sound propagation delays were easily determined through use of a cross-correlation method.

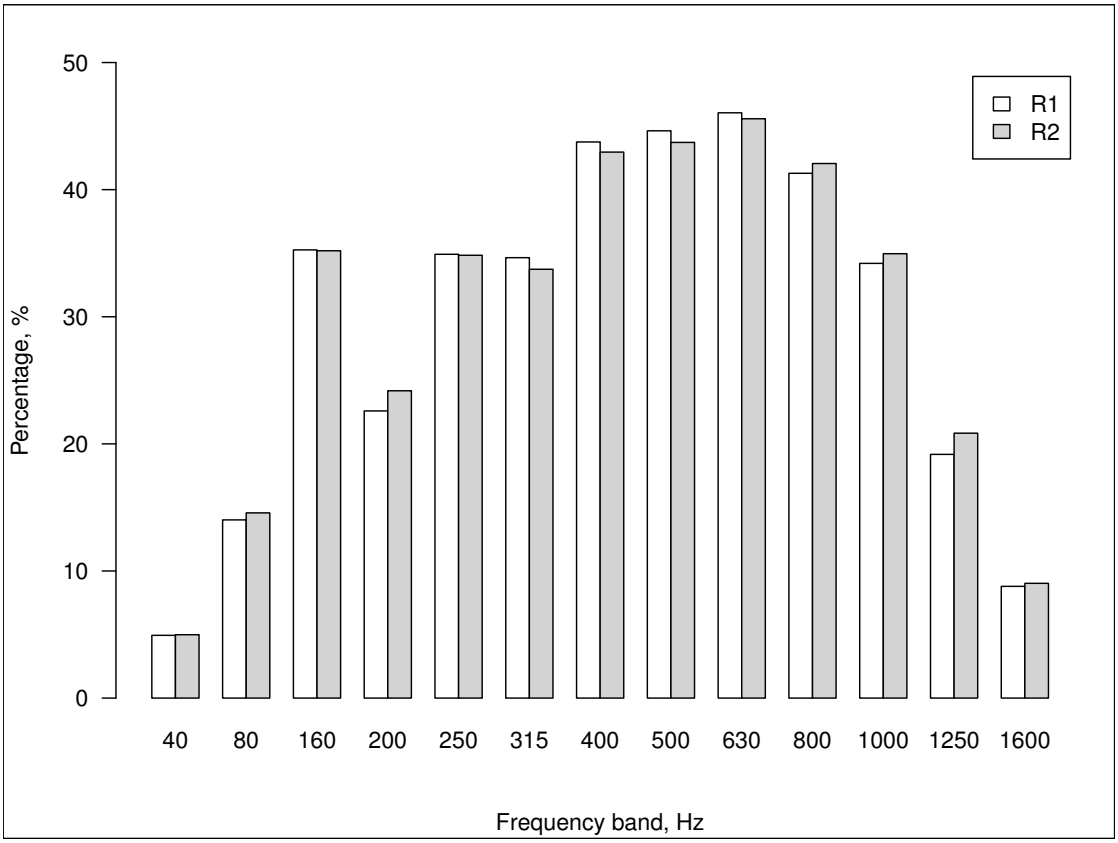

Fig. 4.1: The percentage of measurements between 13 March 2004 and 11 November 2005 from microphones R1 and R2 that were valid.

4.2 Creation of the database

The database created consists of eight channel 24-bit audio data with sample rates of 6 kHz to 48 kHz and millions of files with meteorological data from various sensor systems, along with log files generated by the measurement system. The log files contain information about, for example, automatically controlled sound transmission power levels and accurate[2] timestamps for the measurement moments. All the data were archived with UTC timestamps.

[2]Resolution of the time in the log files: 1 μs, uncertainty 690 μs.

The audio signals in the database are the responses captured by seven microphones to the excitation of a combination of sinusoidals with one-third-octave centre frequencies from 160 to 1600 Hz and also lower-octave frequencies 40 and 80 Hz with a duration of 30 s. Additionally, there is an optimised series of fast sine sweeps to make calculation of sound propagation delays possible.

In the analysis phase, the calibrated, absolute one-third-octave SPL values for the raw audio data were saved to text files.

Next, all the values of the parameters listed in Subsection 4.2.1 were added to the one-third-octave values. This procedure had to be adjusted slightly for different excitation signals. On the basis of the content of the excitation signal, the amplification gain, and the results of the sound power measurements for the sound source, emitted acoustic sound power level L_W was calculated. A summary of the source sound power measurements described in Subsection 3.2.1 is shown in Fig. 4.2; the L_W values with case were used as initial data. Finally, subtraction of the geometrical attenuation from the real acoustic emission yielded the *excess attenuation*; see Eq. 3.1.

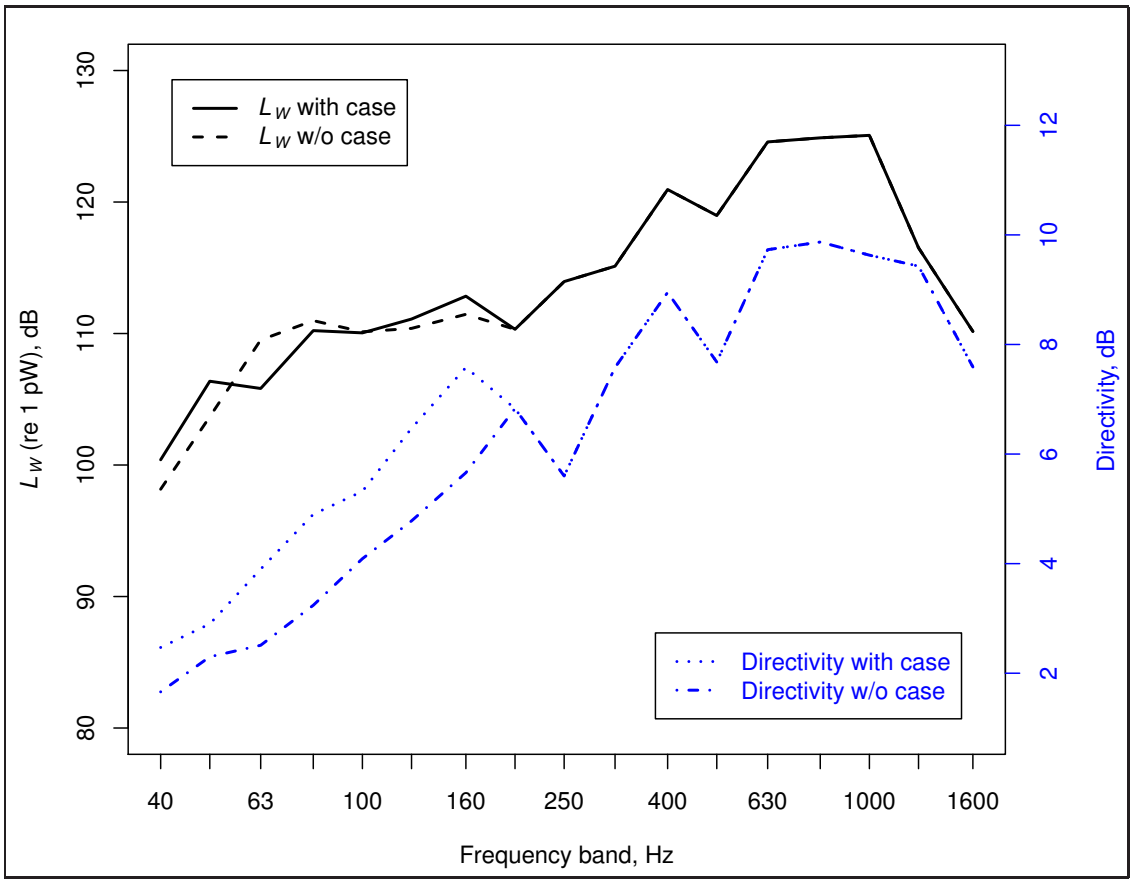

Fig. 4.2: Sound power level and directivity of the sound source(s). ISO 3744[203] standard measurements performed on 14 May 2004. Excitation level $U_{\mathrm{RMS}} = 6.0$ V. Subwoofer with and without the weather case.

4.2.1 Data in the log files

The log files produced by the measurement system are very important in the analysis of the sound data, because not only did the environmental parameters change; the measurement system parameters did too.

The following parameters showed changes over the 612 measurements days:

1. **Automatically adjusted transmission power**, which is saved to 'T'-named log files. The transmitted acoustic power was changed with the environmental conditions — mainly wind properties — to avoid disturbance to the neighbourhood. The measurement signal sound level was kept as low as reasonably possible. The range was 0 to 18 dB.

2. **Transmitted signal**, the measurement (*or excitation*) signal. This was changed for various reasons in the course of the period. The relationship between the frequencies and also the timings were changed 11 times, to improve the sound propagation delay analysis, in the early phase more frequently. The dates are 040309, 040310, 040311, 040312, 040313, 040513, 040517, 040521, 040526, 040906, and 050225.

3. **Transmission power of the main amplifier**, changed a couple of times, because the main amplifier was changed. The transmission power was controlled during calibrations and can be found in the log files. The range was 0 to 18 dB.

4. **The sound power of the sound source** as a function of frequency. This was frequently adjusted during the measurements in line with the ISO 3744[203] standard. Each one-third-octave frequency range was measured individually via up to 15 microphones in the front sector (0 to 60°) and nine microphones at minimum. The compensation value as a function of frequency was between 0 and 37 dB.

5. **Settings of the microphone amplifiers** such as the gain and filter settings. The microphones were calibrated frequently, and also the time data of the calibration response signals were archived. The filters were changed only once: high-pass filtering for channels 1–4 was changed from 0.1 Hz to 20 Hz on 1 February 2005. The filter setting 'linear' for channels 5–8 remained the same throughout. The filtering did not have any effect on the sound propagation measurements; the change was made to avoid clipping in certain background measurement situations. The range of amplification gains was 0 to 20 dB.

6. **Time error for the source computer** at the moment of transmission, saved to 'F' log files. The range was 10 ms.

7. **Time error for the receiver computer** at the moment of transmission, saved to 'G' log files. The range was 10 ms.

8. **Playback delay for the source computer**, saved to 'T'-named log files. The playback routine was written and compiled such that the last command before sending of the first byte to the DA converter was to capture the OS time. The range was 2000 ms.

9. **Recording delay for the receiver computer**, saved to 'R' log files. The recording routine was written and compiled such that the last command before receipt of the first byte at the AD converter was to capture the OS time. The range was 2000 ms.

All the values of the above-mentioned parameters had to be taken into account if correct analysis results were to be obtained. With attention paid to the time error and both the playback and the recording delays, the error in timing was less than 1 ms even in the worst case — without the log files, the error could even reach seconds.

4.2.2 Traceability of sound pressure levels

To preserve validity, the measured sound pressure levels had to be the best estimate of the actual value. This was confirmed through the use of appropriate measuring equipment.

The sensitivity of each microphone is always unique, and it is possible for the sensitivities to change on account of a fault. Moisture is one of the most important sources of faults, but the microphones used in this study proved to be very reliable, and no defects were found. This was confirmed via frequent calibration. The time-domain signals of the calibrations were archived also. Additionally, twice every year, a multifunction calibrator was used to test the microphones over the octave-bandwidth frequency range from 32 to 8000 Hz. The deviations measured between seasons were less than 0.3 dB. The calibration signals in the database occupy about 10 GB.

In the beginning, the eight-channel measurement signals were archived as Waveform Audio File Format (WAV) files at a 48 kHz sampling rate. In the data acquisition, a lower sample rate was tested too, but the Linux audio functionality (ALSA) capture routine lacked a proper low-pass filter, so it was abandoned. Because analysis of the 48 kHz WAV files took a lot of time and the high bandwidth did not yield any extra information, we searched for an automated downsampling solution. The commonly used *Secret Rabbit Code* (SRC) library[3] was tested thoroughly with diverse test signals and a defect was found: if there was a clipping signal on any of the channels, *all* the channels were multiplied by a coefficient of `1/max_amplitude`. To maintain the traceability of sound pressure levels, the source code of the SRC library was modified to save the attenuation values for possible occurrences of clipping and possible changes in gain to a log file. The magnitude of the changes was -0.08 dB at maximum.

[3] Versions: libsamplerate-0.1.2 and libsndfile-1.0.11.

All signals were resampled before archiving, via the SRC library, such that sound propagation (SP) measurements were downsampled to 6 kHz and background noise (BG) measurements to 12 kHz, both with the '`-c 0`' option, which causes use of the highest-quality, 'Best Sinc Interpolation' conversion.

The full signal path from the microphone to decibel levels in the database was tested through creation of a test directory structure similar to that of the 'hard' database and recording of calibration signals at different frequencies just as in the real measurement case, with full log files and automation algorithms — the automatic analysis and archival routines. The correct, 94 dB values of sound pressure levels were found at the correct frequencies in the respective channels in the 'test' database.

4.3 Description of the variables

The authors of the *Cambridge Dictionary of Statistics*[206] suggest using the term '*explanatory variable*' for an independent variable, because the variables are rarely independent of each other. Following the suggested naming for the dependent variable, we used the term '*response variable*'. The response variables of this study were the excess attenuation at one-third-octave centre frequencies and the sound propagation delay. The excess attenuation was considered on both logarithmic and linear scales. The distributions of response variables are shown in figures B.1–B.7, in Appendix B.

The statistical data processing was performed primarily via MATLAB®[207] and R[208]. A number of basic meteorological variables are described in this section of the thesis, the definitions of which can also be found in the textbooks of this field. *An Introduction to Boundary Layer Meteorology*, written by Stull[124], has been the primary source of definitions. Some of the meteorological variables are defined more specifically, as they are relevant to the interpretation of the model. All the names of the variables and their corresponding descriptions can be found in Table A.1, in Appendix A.

All of the categorical variables, such as *current weather*, were dummy-coded for the regression analysis but were also included without the coding. The dummy coding too is shown in Table A.1. Current weather (see Fig. B.9; the variable *curwea*) was obtained from the FMI as a code number, 1–100. Code 2, for 'No change in weather', dominated the statistics (39.7%) and was replaced with a reference to the preceding weather event. The frequencies of the weather events are shown in Table B.1, in Appendix B. The distributions of selected meteorological variables are presented in figures B.8–B.19.

'Contribution of wind direction', a new variable (*srcvwdir*), was defined by means of Eq. 4.1:

$$srcvwdir = \cos\frac{2\pi\,(iwindir - srcdir)}{360}, \tag{4.1}$$

where $srcdir = 157^\circ$, the geographical direction of sound propagation, and *iwindir* was

the measured wind direction. In a full tailwind, the variable *srcvwdir* received a value of 1, changing to -1 for a full headwind. A crosswind changes the value to 0. The effect of wind speed was omitted, because it would be added to the model through a separate coefficient.

The properties of the boundary layer can be described in terms of a multitude of quantities. There were many measured parameters in this study, and a number of derived quantities were calculated. Pasquill index was one of these, also chosen for the regression analysis. For information on determination of the index, see Subsection 2.4.3. The Pasquill index describes the stability of the ABL, and Obukhov length L_0, defined in Eq. 3.13, can be interpreted as the height at which the generation of turbulence by the buoyancy force exceeds the generation by the mechanical forces (heating vs. friction)[124]. The dimensionless derivative of L_0, the *Monin–Obukhov stability parameter* (see Eq. 4.2)[124, Eq. 5.7b], was used to describe the turbulence. This stability parameter, ζ, was also referred to as the variable *mmos*.

$$\zeta = \frac{z}{L_0}, \tag{4.2}$$

where z is height above the surface and L_0 is Obukhov length. The ABL is said to be *unstable* if the heat flux is upward ($L_0 \ll 0$), as in the summer when the sun heats the earth's surface and the mechanical turbulence becomes stronger, with efficient mixing. In *stable* stratification, the heat flux is positive (as is L_0), the buoyancy forces dampen the mechanically generated turbulence, and mixing is low. If the heat flux is small, there is no thermally generated turbulence and stratification is *neutral*.

The height of the ABL varies with the weather conditions: from 100 m (in stable stratification) to 2000 m (in unstable)[109]. No explanatory variable was dedicated to the height of the ABL in this study, but the height of the temperature gradient (*gradthgt*) and the maximum temperature gradient below 1000 m (*gradt*) were calculated.

Cross-tabulation of the explanatory variables revealed some strong correlation, the reason for which is obvious: they have the same source of energy, the sun. This *collinearity* would make the model unstable, and, on the basis of the principal component analysis and the correlation tables, the most representative variable was selected from among the strongly correlating variables. However, the principal component analysis was not used to form a new, orthogonal variable based on the set of strongly correlating variables. If some variables were equal, the most frequently acquired variable was chosen. Also, several variables were omitted for reason of irrelevance or for some other reason. Table B.5 (on page 130) lists the variables that were abandoned and the corresponding variables selected.

The final selection of the variables (Table 4.1) was done through combination of the data in tables B.5 and 6.1, the most representative variables of the explanatory variables with the highest linear correlation between the response variables.

Table 4.1: Selected explanatory variables in the final regression model

Frequency, Hz	Explanatory variables					
40	*iwspd*	*pasq*	*gradthght*	*gradt*	*ispress*	
80	*iwspd*	*cldness*				
160	*iwspd*	*pasq*	*spress*	*snowd*	*itempc*	
200	*mtq*	*ihum*	*gradthgt*	*itempc*		
250	*ihum*	*gradt*	*gradthgt*	*mtq*	*itempc*	
315	*gradt*	*ihum*	*itempc*	*gradthgt*	*mtq*	
400	*gradt*	*ihum*	*gradthgt*	*itempc*	*mtq*	
500	*gradthgt*	*gradt*	*ihum*	*itempc*	*mtq*	
630	*gradt*	*ihum*	*iwspd*	*mtq*	*srcvwdir*	
800	*gradt*	*ihum*	*srcvwdir*	*iwspd*	*gradt*	*itempc*
1000	*gradt*	*ihum*	*mtq*	*mhf*	*itempc*	
1250	*gradt*	*ihum*	*mhf*	*mtq*	*gradthgt*	*srcvwdir*
1600	*mhf*	*mtq*	*ihum*	*itempc*		

4.4 Selection of models for variables

The dependencies between the chosen explanatory variables and excess attenuation as a function of frequency were tested with different mathematical models.

The models tested were linear:

$$Y = b_0 + b_1 \cdot t, \tag{4.3}$$

logarithmic:

$$Y = b_0 + b_1 \cdot \ln(t), \tag{4.4}$$

inverse:

$$Y = b_0 + \frac{b_1}{t}, \tag{4.5}$$

quadratic:

$$Y = b_0 + b_1 \cdot t + b_2 \cdot t^2, \tag{4.6}$$

cubic:

$$Y = b_0 + b_1 \cdot t + b_2 \cdot t^2 + b_3 \cdot t^3, \tag{4.7}$$

power:

$$Y = b_0 \cdot t^{b_1} \text{ or } \ln(Y) = \ln(b_0) + b_1 \cdot \ln(t), \tag{4.8}$$

compound:

$$Y = b_0 \cdot b_1^t \text{ or } \ln(Y) = \ln(b_0) + \ln(b_1) \cdot t, \tag{4.9}$$

'S' shape, also known as sigmoid:

$$Y = e^{b_0 + \frac{b_1}{t}} \text{ or } \ln(Y) = b_0 + \frac{b_1}{t}, \tag{4.10}$$

growth:

$$Y = e^{b_0 + b_1 \cdot t} \text{ or } \ln(Y) = b_0 + b_1 \cdot t, \tag{4.11}$$

exponential:

$$Y = b_0 \cdot e^{b_1 \cdot t} \text{ or } \ln(Y) = \ln(b_0) + b_1 \cdot t, \tag{4.12}$$

and logistic:

$$Y = \frac{1}{\frac{1}{u} + b_0 \cdot b_1^t} \text{ or } \ln(\frac{1}{Y} - \frac{1}{u}) = \ln(b_0 + \ln(b_1) \cdot t), \tag{4.13}$$

where u is the upper boundary value separately selected for each explanatory variable. It is a positive number greater than the biggest response variable.

The process for selection of the models for the explanatory variables applied scoring. The statistics for the variables were examined one by one, and the models were scored on the basis of the overall measurand of the strength of association (R^2), the p value, and the F value best describing the response variable. There were 13 response variables for each of the microphone heights: *x40ch1*, ... , *x1600ch1*, so for each explanatory variable there were 26 points to be assigned to the models. The classifying variables, dummy variables *curwea0*, *curwea1*, ... (see Table 4.2), were not scored.

The scoring followed this procedure: First, the models with the largest R^2 values were chosen, then the F and p values were examined. If the p value was smaller for a model with a larger F value, the selection was based on the F value — however, if the R^2 value was two (or more) times lower, the model with a higher R^2 value was chosen, if, in addition, the p value was about the same. If two or more models had the same strength, p value, and F value, the principle of majority was followed: preference was given to the model with the highest score. Finally, if none of the above rules applied, the point was given to the linear model. Scoring of models was performed manually, and in some cases the scoring was non-obvious, as can be seen in this example output:

```
Independent:  ivisib
  Dependent Model Rsq  d.f.       F  Sigf
   x500ch1  LIN  .048    70    3.51  .065
   x500ch1  LOG  .023    70    1.65  .203
   x500ch1  INV  .005    70     .34  .563
   x500ch1  QUA  .108    69    4.19  .019
   x500ch1  CUB  .115    68    2.95  .039
   x500ch1  COM  .044    70    3.23  .076
   x500ch1  POW  .023    70    1.64  .205
   x500ch1  S    .004    70     .29  .590
   x500ch1  GRO  .044    70    3.23  .076
   x500ch1  EXP  .044    70    3.23  .076
   x500ch1  LGS  .045    70    3.33  .072
```

In this example, the cubic model (CUB) has the best strength (Rsq $= R^2 = .115$), but the F and p values indicate that the quadratic model (QUA) could be better. Because the strengths are about the same, the point was given to the quadratic model.

The result of the scoring is shown in Table B.6 (on page 130). The variables were found to fit four out of the 11 equations in general (equations 4.3 to 4.13). Linear, inverse, quadratic, and cubic equations accounted for 97% of the best fitting equations. The explanatory power of the equations describes their percentage of coverage as depicted in Fig. 4.3.

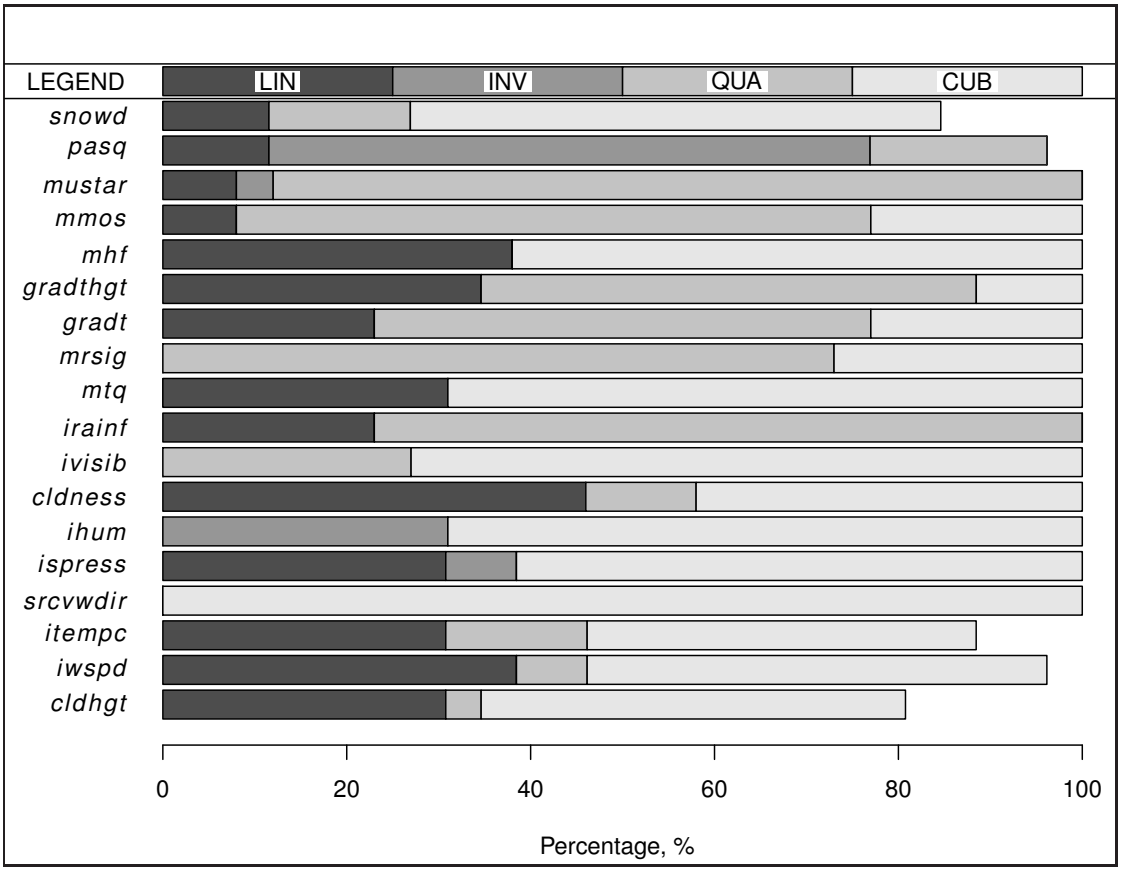

Fig. 4.3: Percentage of the data points covered by the four best fitting equations for each explanatory variable. The equations not included in this figure (see Table B.6) cover the remainder of the full 100%.

The final result of the process of selection of models for all the explanatory variables chosen, also for the dummy variables, and the main percentages are shown in Table 4.2.

4.5 Regression analysis

Many elimination methods were used in testing the explanatory power of various combinations of variables. The response variables were the logarithmic (in decibels) and

Table 4.2: The explanatory variables chosen, with their models and statistics (the p values for the class-2 dummy variables are small, because the explanation capacity is split on account of use of the linear model for them)

Variable	Model (best statistics and the corresponding response variable)
cldhgt	CUB (R^2 .095, p value .085, F value 2.30, x80ch1)
iwspd	CUB (R^2 .154, p value .010, F value 4.11, x1600ch2)
itempc	CUB (R^2 .196, p value .002, F value 5.51, x1600ch2)
srcvwdir	CUB (R^2 .329, p value .000, F value 11.12, x800ch1)
curwea	*dummy* LIN (R^2 .204, p value .000, F value 17.43, x630ch2)
ispress	CUB (R^2 .048, p value .186, F value 1.72, x160ch1)
ihum	CUB (R^2 .226, p value .000, F value 10.06, x500ch1)
gndtype	*dummy* LIN (R^2 .054, p value .041, F value 4.32, x40ch2)
cldness	LIN (R^2 .078, p value .019, F value 5.74, x400ch1)
ivisib	CUB (R^2 .235, p value .000, F value 6.98, x400ch1)
irainf	QUA (R^2 .187, p value .004, F value 6.08, x630ch1)
mtq	CUB (R^2 .192, p value .000, F value 6.96, x1250ch1)
mrsig	QUA (R^2 .099, p value .010, F value 4.87, x1600ch1)
gradt	QUA (R^2 .807, p value .003, F value 14.67, x1600ch2)
gradthgt	QUA (R^2 .528, p value .072, F value 3.91, x500ch2)
hicldt	*dummy* LIN (R^2 .086, p value .066, F value 3.59, x40ch2)
micldt	*dummy* LIN (R^2 .145, p value .003, F value 9.83, x1600ch1)
locldt	*dummy* LIN (R^2 .123, p value .004, F value 8.84, x160ch1)
mhf	CUB (R^2 .273, p value .000, F value 11.04, x800ch2)
mmos	QUA (R^2 .146, p value .003, F value 6.32, x800ch1)
mustar	QUA (R^2 .205, p value .000, F value 11.48, x800ch1)
pasq	INV (R^2 .140, p value .001, F value 12.23, x500ch1)
snowd	CUB (R^2 .307, p value .000, F value 12.97, x80ch2)
time	CUB (R^2 .163, p value .001, F value 5.71, x200ch2)
weekno	CUB (R^2 .149, p value .003, F value 5.13, x40ch1)

linear (in pascals) excess attenuation. There were some minor differences in regression strength between the microphones, but the behaviour of the variables was very similar. Appendix C provides a summary of the regression analysis rounds for microphone R1. The most complete summary can be found in the technical report[30].

The ‘forward’, ‘backward’, and ‘stepwise’ methods were chosen as the elimination methods. The variables were compared against each other in pairs (via the ‘pairwise’ and ‘backward’ methods) and also such that the missing values were replaced with the mean value of the variable (mean substitution). The criteria for elimination of vari-

ables were p values greater than 0.01, variable-addition criteria of more than 0.005, and confidence interval above 95%. The selection of thresholds was stringent[4] because the objective was to minimise the number of explanatory variables in the final model.

It is worth noting that the strength of association in tables C.1 and C.2 is a poor measure in this type of time-series model. The value of R^2 could be increased, through, for example, adding of explanatory variables (*over-parameterisation*[5]). The relative standardised beta coefficients are also shown, to make direct comparison of models to each other possible. For example, the results of regression analysis for the sound propagation delay presented in Table 4.3 show that temperature (the variable *itempc*) has the best explanatory power in all of the models, as a result of various elimination methods. For results for excess attenuation, see Appendix C's Table C.1. The negative sign of the beta coefficient indicates that an increase in the variable's value decreases the excess attenuation. The beta coefficients are not the coefficients of the regression equations. During the last iterative rounds, the coefficients did not change, but they may have changed order, if the values were close to each other. Furthermore, the values shown are the results of the four selection methods. The values were completely different during the iterations but, in most cases, the same at the end of the iterations.

Table 4.3: Explanatory variables selected for the sound propagation delay and the methods of their elimination, where the numerical values in brackets are standardised beta coefficients

Response	**Explanatory variables**
delay, BWMP	*itempc* (-.585), *srcvwdir* (-.333) Model F value: 136.1(***), R^2: 0.45, adjusted R^2: 0.45, DW: 1.59
delay, FWMP	*itempc* (-.585), *srcvwdir* (-.333) Model F value: 136.1(***), R^2: 0.45, adjusted R^2: 0.45, DW: 1.59
delay, SWMP	*itempc* (-.585), *srcvwdir* (-.333) Model F value: 136.1(***), R^2: 0.45, adjusted R^2: 0.45, DW: 1.59
delay, BWMM	*itempc* (-.487), *srcvwdir* (-.248), *mrsig* (-.049), *iwspd* (.048), *cldness* (.048), *mtq* (.032), *micldt* (-.029), *ispress* (.023), *hicldt* (-.022) Model F value: 693.3(***), R^2: 0.30, adjusted R^2: 0.30, DW: 1.43

[4]Usually, the criteria are less strict: the threshold values are 0.05 and 0.1, for elimination and addition, respectively.

[5]Entering more variables for the model increases the R^2 value even if the variables added do not have any explanatory power.

4.6 Results

The height of microphone R1 from the ground was about 2 m, and microphone R2 was 80 cm lower (see Fig. 3.8). Because of the difference in height, the decision was taken to perform full analysis of the signals captured by these two microphones. Fig. 4.4 shows the excess attenuation measured over the course of the whole period from 13 March 2004 to 14 November 2005. The attenuation values are spread over a dynamic range of 80 dB. The middle 50s are mostly the same size but show a shift, which depends on the frequency. Because the histograms for the excess attenuation are normally distributed (see figures B.1–B.7), the σ values can be interpreted as percentages of the distribution and the whiskers extending to 3σ in Fig. 4.4 cover 99.7% of the values. Also, the most common value, 2.7σ (the default in many analyses), has been used in some figures; it covers 99.3% of the distribution.

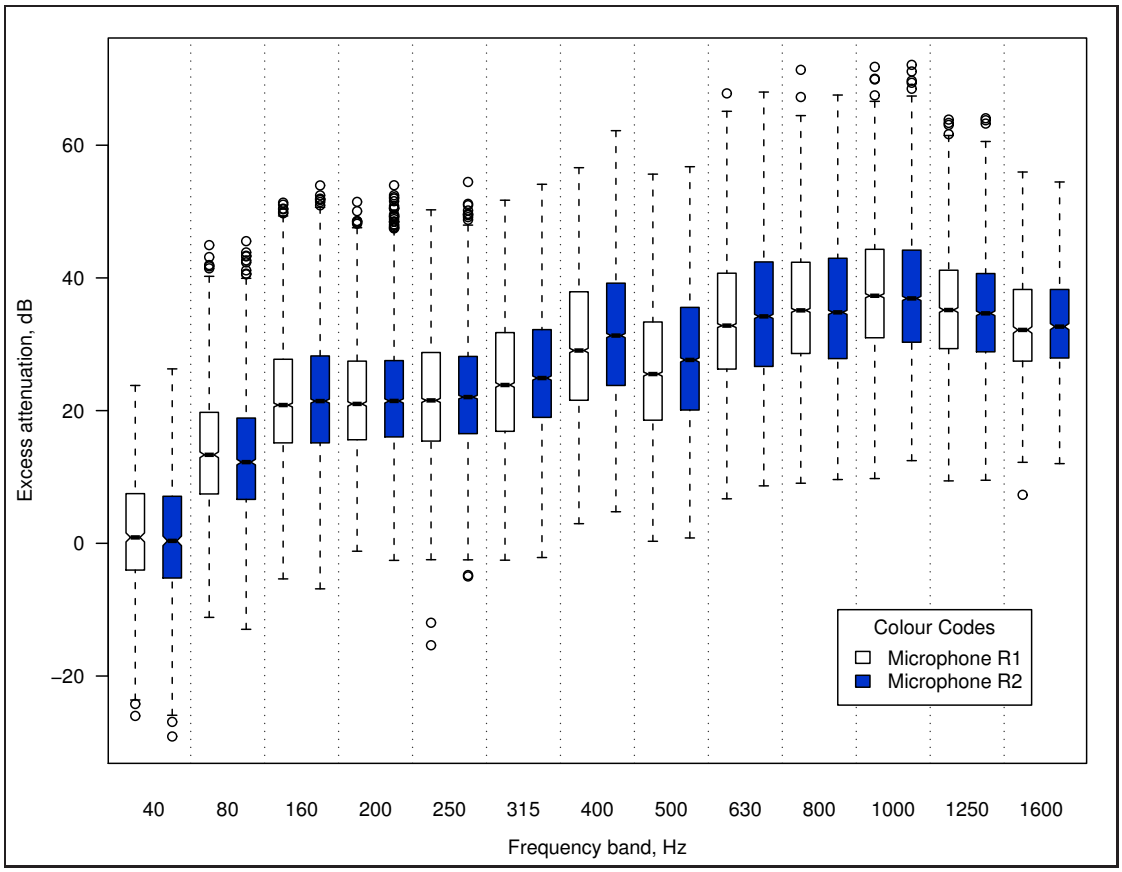

Fig. 4.4: Excess attenuation measured by two separate microphones at different heights from the ground. IQR boxed with median line; whiskers extend to 3σ.

If the excess attenuation is compared between seasons, differences of 10 dB can be found (see Fig. 4.5). It is noticeable that higher frequencies (over 400 Hz) never showed negative excess attenuation. On the other hand, even the median of the lowest frequency captured was negative during the fourth period (October to December). A

possible explanation might be that during that time over 80% of soundings revealed an inverse temperature profile; see Table 4.7.

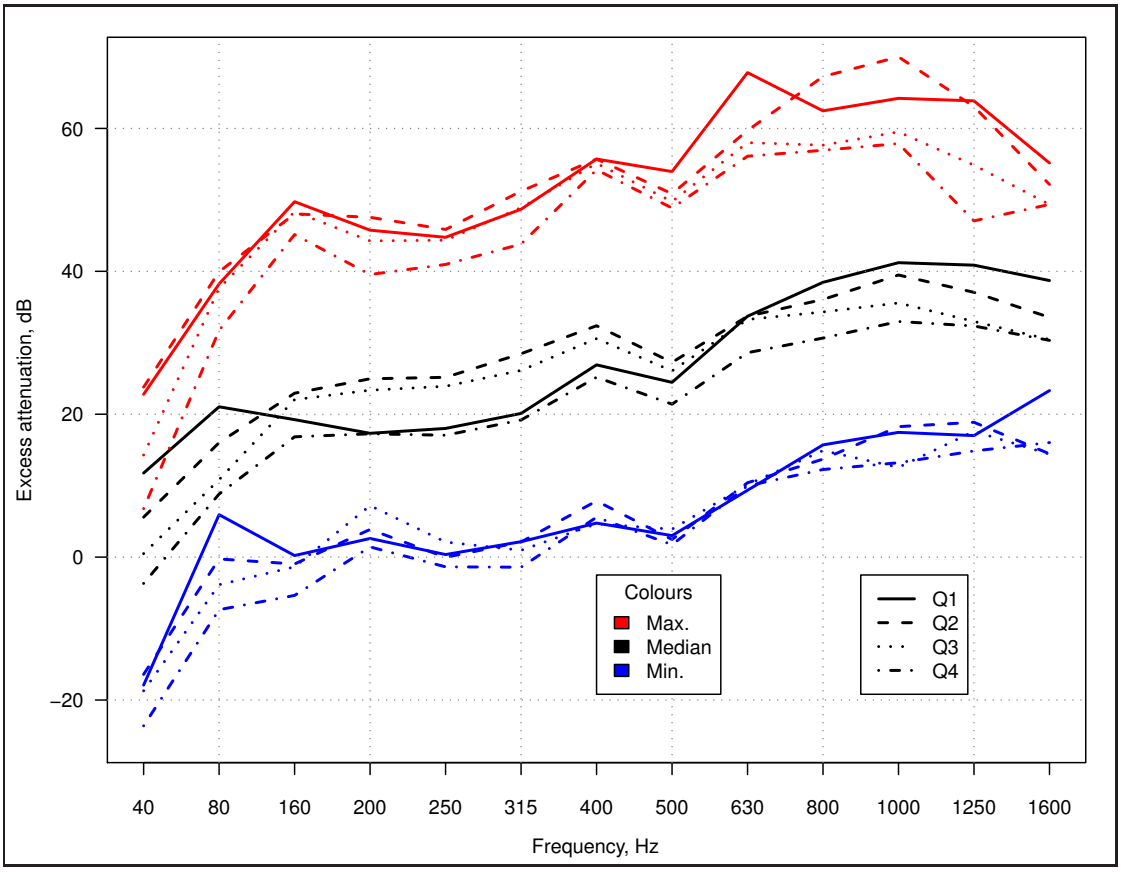

Fig. 4.5: Excess attenuation and quarters of the year: Jan.–Mar. (Q1), Apr.–Jun. (Q2), Jul.–Sep. (Q3), and Oct.–Dec. (Q4).

4.6.1 Cross-tabulation of correlation

Significant differences can be found when one compares the correlations of excess attenuation between low and high frequencies. If the bilateral correlation coefficients shown in Table B.4 are averaged for low frequencies 40–800 Hz and for high frequencies 1000–1600 Hz, then plotted as shown in Fig. 4.6, the mean curve of the low frequencies is found to have lower correlation values at high frequencies than at lower frequencies, and vice versa for the mean curve of the high frequencies. In other words, the values for excess attenuation at low frequencies does not follow the values for excess attenuation at the high frequencies fully. This indicates that the explaining variables differ between the high and low frequencies.

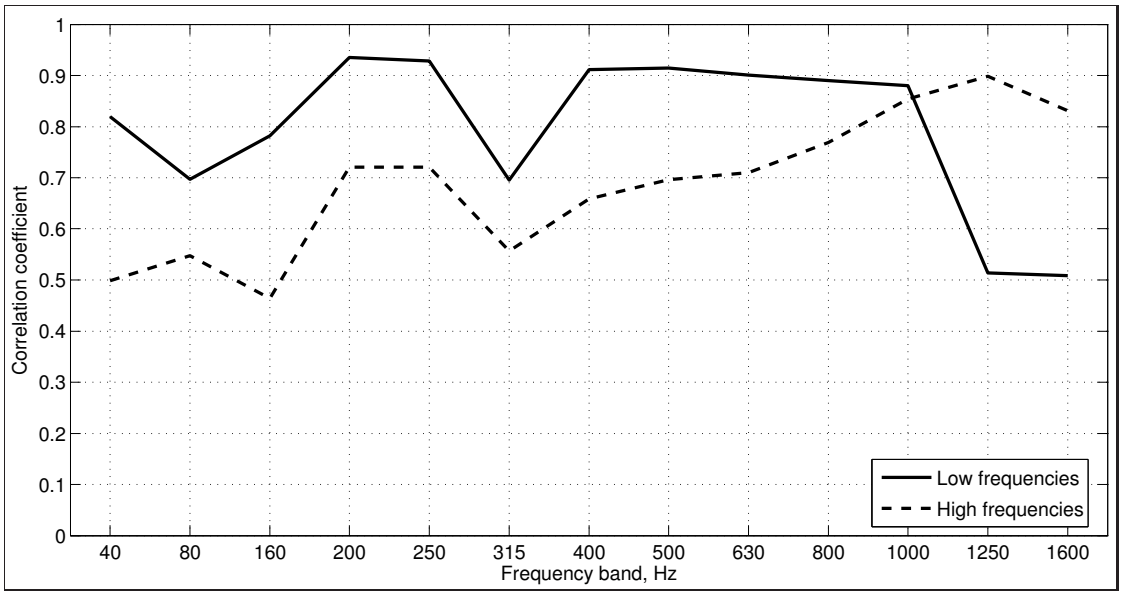

Fig. 4.6: Comparisons of the correlations of excess attenuation between high and low frequencies (see body text).

4.6.2 Excess attenuation in relation to time

The time of day has a significant effect on excess attenuation. It is well known that sound is attenuated more during the daytime. There are several physical phenomena that explain this. When the morning sun begins to warm the atmosphere between 4:00 and 5:00 UTC, a large increase in excess attenuation can be seen[6]. In Fig. 4.7, the excess attenuation at all frequencies during this campaign is plotted against time of day. There is a rapid increase of 10 dB in attenuation between 4 and 6 UTC and a slightly slower decrease toward the evening. Variations are slightly stronger in the daytime too. However, if individual frequencies are examined, this phenomenon is revealed to be strongest at higher frequencies; see Fig. 4.8.

In the above-mentioned figures, the values for excess attenuation at all the frequencies were taken together as a single variable, which is a statistically appropriate approach. However, from the stand-point of signal theory, the values should be incoherently averaged as power signals, in this manner:

$$L_{\text{avg}} = 10 \lg \frac{1}{N} \sum_{i=1}^{N} 10^{L_i/10}. \tag{4.14}$$

The medians and variance changed slightly if the values for all frequencies were averaged by means of Eq. 4.14; see Fig. 4.9.

[6] This corresponds to 6–7 GMT or, while Summer Time is in effect, 7–8 GMT.

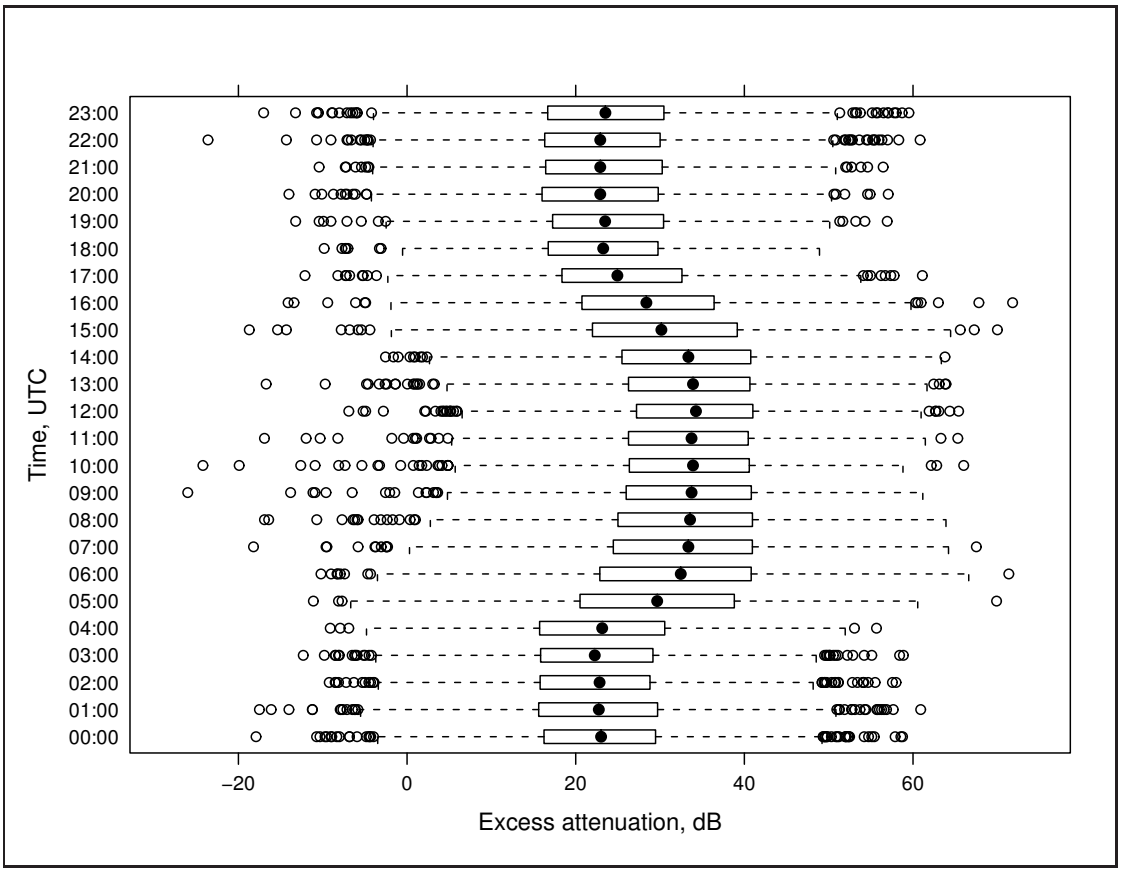

Fig. 4.7: Excess attenuation plotted against time of day, with all frequencies treated as one variable. IQR boxed with median dot; whiskers extend to 2.7σ.

4.6.3 Excess attenuation in relation to Pasquill index

The data on excess attenuation were compared to Pasquill indices/classes. A statistically highly significant dependency was found; see Fig. 4.10. Under convection and very unstable boundary-layer conditions, a strong attenuation can be seen, while a stable atmosphere shows almost 20 dB less attenuation. Windy days with a neutral atmosphere cause the range of excess attenuation to spread across a wide range of values while calm days with a strong unstable atmosphere cause less variation in the attenuation values. The smallest deviation in the excess attenuation values can be found under unstable conditions. This behaviour is similar — and systematic — across all of the frequencies, though the median values for excess attenuation do not decrease similarly when the Pasquill index value raises; see Fig. 4.11.

4.6.4 Wind speed and excess attenuation

Local wind speed was measured with a 2D sonic positioned a few metres from the microphones, at the height of the highest microphone (R1). The linear correlation between

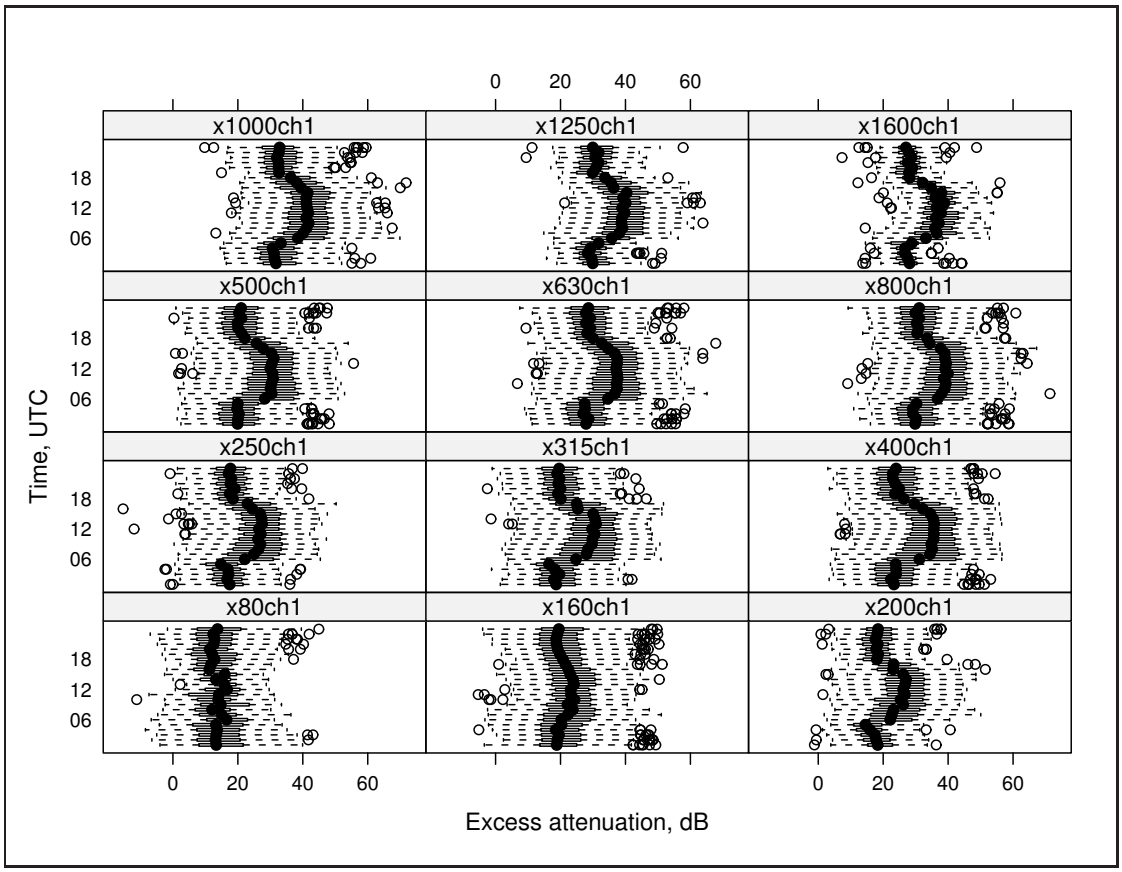

Fig. 4.8: Excess attenuation plotted against time of day. IQR boxed with median dot; whiskers extend to 2.7σ.

the local wind speed and excess attenuation was high, especially for the low frequencies: for the 40 Hz band, -0.914(***).

The wind directions and speeds, in particular, differ significantly in comparison of the measured data from different heights in this study (see Fig. 4.14).

4.6.5 Sound propagation delay

One of the application interests was sound propagation delay. This delay was automatically calculated to a resolution of 1 ms.

The best linear correlation between sound propagation delay and its explanatory variables was found between the temperature-dependent variables (see Table B.3). It was surprising that the effect of the wind speed and direction is much less, though still statistically highly significant. The movement of the air does not explain the deviation of the delays.

In calm weather, the deviation of the sound propagation delay is diminished and the correlation coefficient increases from -0.575 to -0.777. Windier weather reduces the correlation coefficient to -0.440 and the deviation increases. All three of these cases

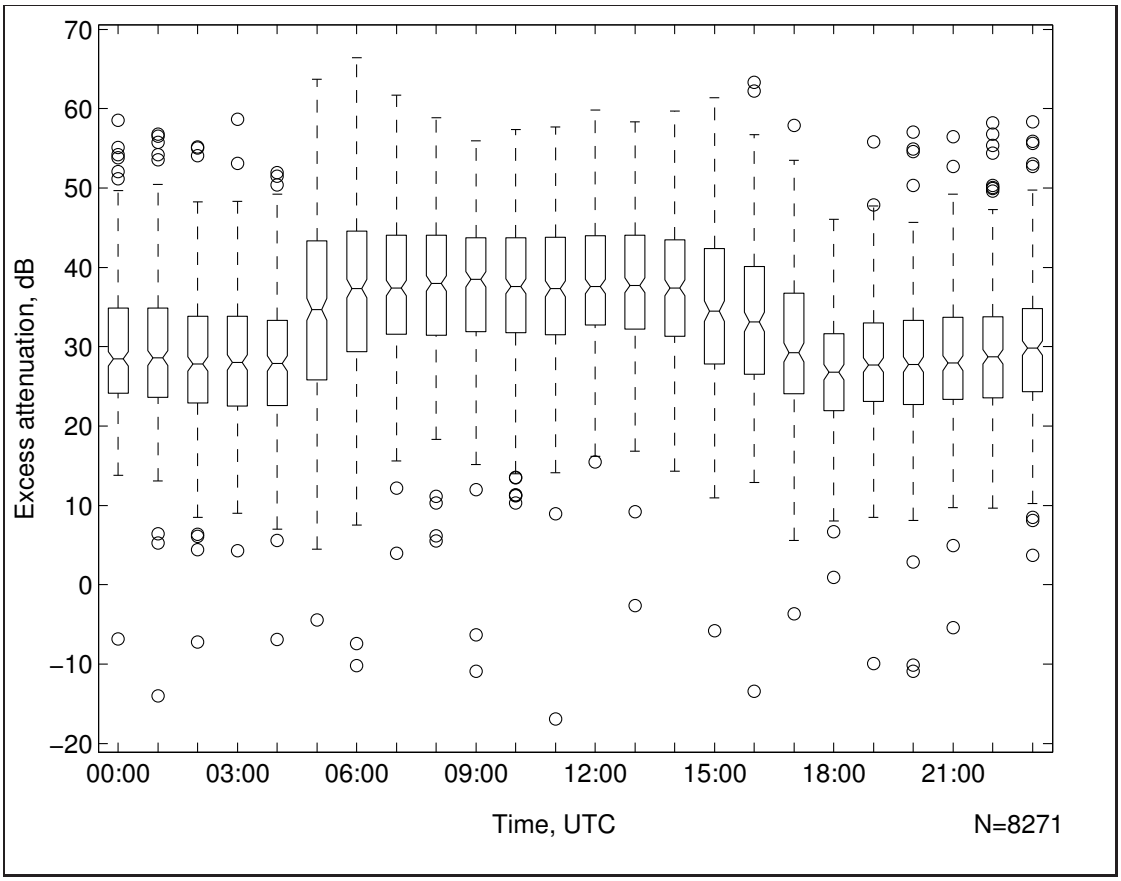

Fig. 4.9: Time of day and the averaged excess attenuation for the entire frequency band. IQR boxed with notched median line; whiskers extend to 2.7σ.

show statistically highly significant correlation.

Also *air pressure, the standard deviation of the vertical wind component, longitudinal turbulence intensity, and cloudiness* had a statistically significant effect on delay changes, but their coefficients are about 10 times smaller. The average surface wind speed during this campaign was about 2.5 m/s, leading to no sensible coefficients in the regression analysis.

From the results of the linear regression analysis, we can find an equation for sound propagation delay on the propagation path used in this study:

$$delay = 9.899\ \mathrm{s} - 0.01486 \cdot itempc \frac{\mathrm{s}}{^\circ\mathrm{C}} - 0.001621 \cdot srcvwdir \cdot \mathrm{s}, \tag{4.15}$$

where *itempc* is the air temperature (°C) and *srcvwdir* is the 'contribution of wind direction', as defined in Eq. 4.1. Eq. 4.15 can then be written as

$$delay = 9.9\ \mathrm{s} - 0.015 \cdot itempc \frac{\mathrm{s}}{^\circ\mathrm{C}} - 0.0016 \cdot \cos \frac{2\pi(windir - srcdir)}{360^\circ}\ \mathrm{s}, \tag{4.16}$$

where *windir* is the wind direction and *srcdir* is the geographical direction of the sound source from the receiver, in degrees.

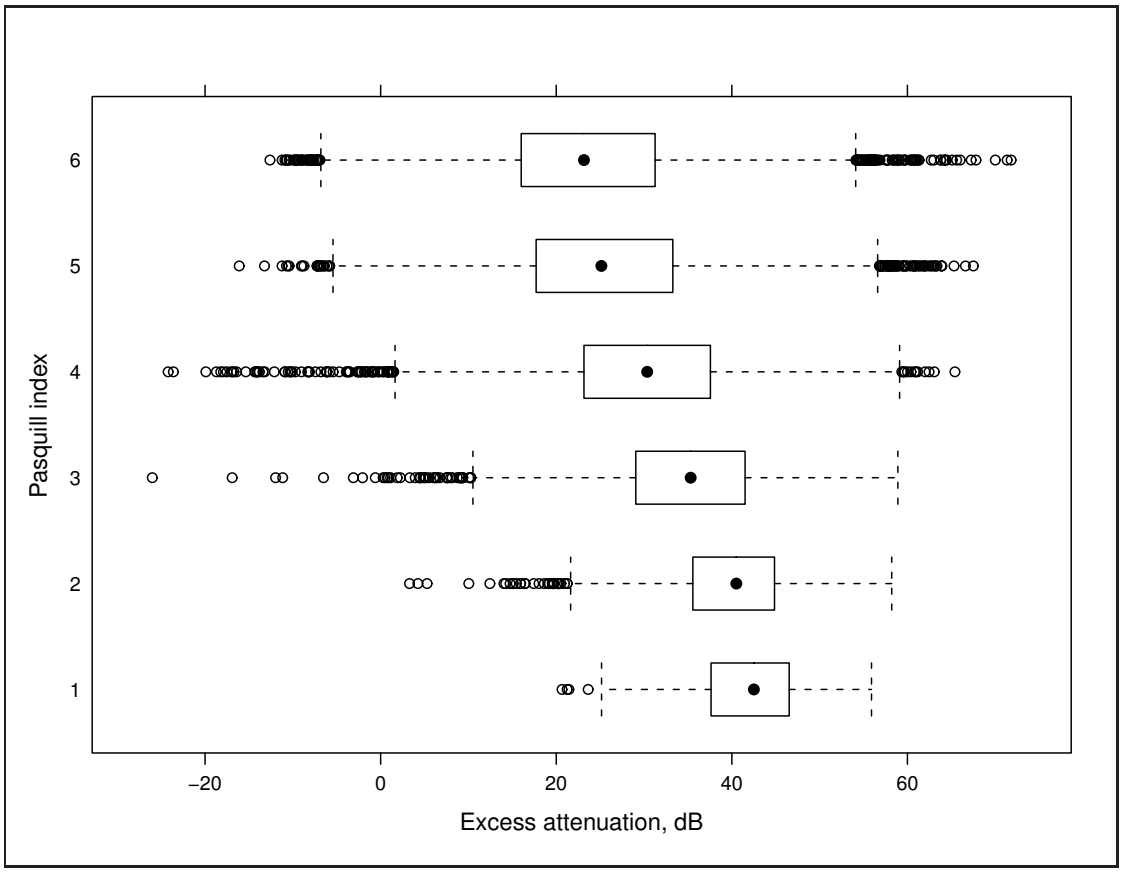

Fig. 4.10: Atmospheric stability and the excess attenuation for the entire frequency band. IQR boxed with median dot; whiskers extend to 2.7σ.

Sound propagation delay d as a function of temperature can be approximated for the propagation path of this study via Eq. 4.17:

$$d(t) = \frac{3240\ \mathrm{m}}{(331.4 + 0.6 \cdot t\frac{1}{^\circ\mathrm{C}})\frac{\mathrm{m}}{\mathrm{s}}}. \tag{4.17}$$

The calculated delays seem to follow the season of the year quite reasonably (see Fig. 4.12). The winter season shows as an increase in the delay, and, starting in autumn 2004, a clear upper limit seems to emerge, while there is much greater deviation for the lower values. A more in-depth view of the data might reveal whether the deviation profiles for the headwind and tailwind differ and cause this or, instead, the reason can be found in the temperature variation.

4.7 Deductions

The changes in excess attenuation are explained with quite traditional and sensible variables. One can state, as a conclusion based on correlation analysis, that the low frequencies are affected mainly by wind speed and various turbulence parameters. For the

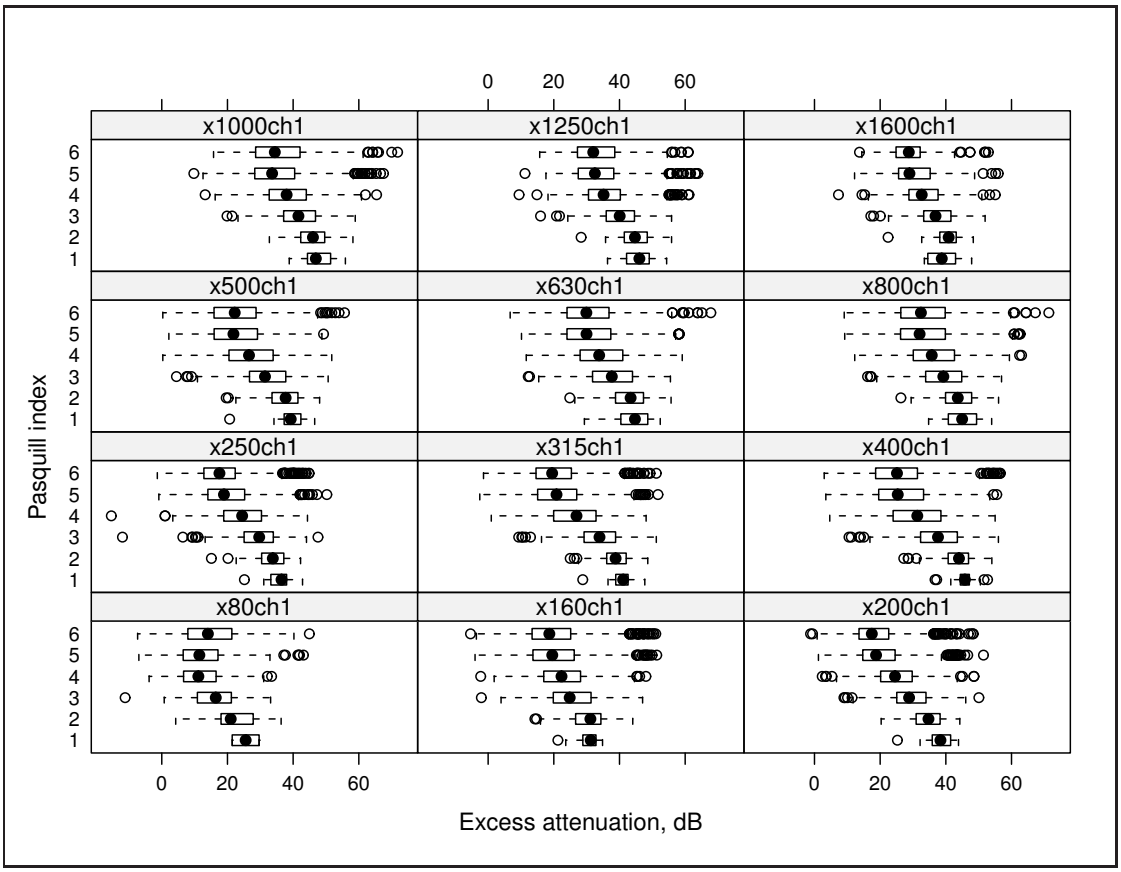

Fig. 4.11: Atmospheric stability and the excess attenuation at different frequencies. IQR boxed with median dot; whiskers extend to 2.7σ.

higher frequencies, the most important parameters are humidity and temperature lapse rate, but also sensible heat flux and longitudinal, transverse, and vertical turbulence intensities explain excess attenuation statistically significantly. These and some other variables explaining excess attenuation statistically significantly are listed in Table 6.1, above.

As a simplified summary of this analysis, the models were generated by a brute-force method via the following steps:

- The explanatory variables were chosen on the basis of the results from the correlation analysis.
- Performing various linear and nonlinear regression analyses with the chosen explanatory variables provided better understanding of the significance of the variables and their different combinations.
- The variables of the models tested were changed multiple times, and those variables that proved to be unnecessary were removed from the model. Both the addition and removal of variables from the models were tested with many meth-

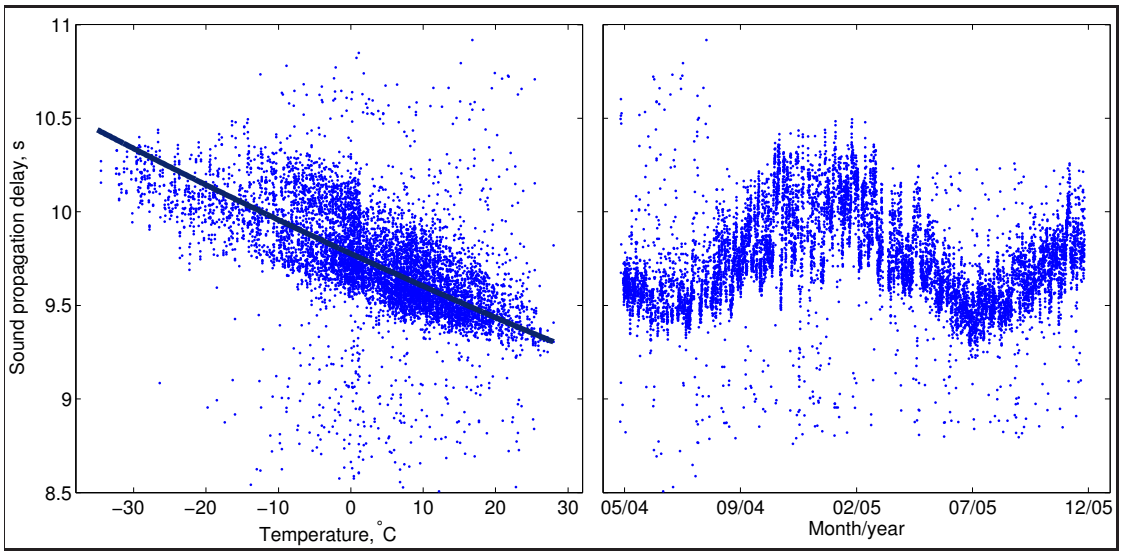

Fig. 4.12: Sound propagation delay as a function of temperature at a height of 2 m from the ground and as a function of month. The two plots share the same vertical axis. The dark line represents the theoretical delay (see Eq. 4.17).

ods. The results from the pairwise combinations were finally forced to listwise comparison, wherein all the variables were added in the initial phase and one of the variables was manually removed from the model in every round of analysis. This was continued until the performance of the model did not improve further.

- The collinearity was controlled for in every round of analysis, and models with Durbin–Watson (DW) values close to 2 were preferred. Models with values below 1 were critically reviewed.
- The exclusion criterion (p value) was 0.05. In the last round of regression analysis, all of the explanatory variables were statistically highly significant.
- The analysis was applied to two microphones, at different heights. Small differences were found, but confidence intervals were not affected.
- In total, about 18,000 pages (PDF/A4) of analysis reports were evaluated.
- Finally, the models, their respective regression coefficients, and other statistical characteristics for each frequency were coded into a software module, which is explained in Section 4.8.

4.8 Uncertainty modelling

The statistical model described in this section of the thesis is based on the measurement results from the specified environment and a fixed sound propagation path. It was not

designed to be a general tool for analysis of uncertainty in environmental noise assessments, though it can be applied to many similar cases. It is a demonstration model of one possible implementation of the application. The model does some scaling to different propagation distances, but it lacks information on how to scale properly, and this is the most obvious reason to avoid modelling of various distances. The validation of the model is shown in Section 4.9.

Analysis of the measurements revealed many statistically highly significant dependencies, which made it possible to develop the equations behind the model. The Pasquill index is a very good example: an unstable atmosphere causes less variation, which predicts less uncertainty, while a neutral atmosphere indicates very high uncertainty in the results; see Subsection 4.6.3. The idea is to use the most important quantities and their combinations: under the condition of inversion, there is practically no turbulence, and lapse rate is the key measurand. In neutral and stable conditions, the wind profile and turbulence measurands are essential. When the key variables are discovered, their various combinations are employed in equations (e.g., linear, logarithmic, inverse, cubic, and quadratic), and the best fit is chosen by statistical means. Increasing the number of input parameters to the model gives the model access to more variations of combinations and usually result in greater accuracy.

The best aspects of this approach are found in the short-term measurements. When the key environmental variables are measured along with the noise levels, also the uncertainty of the measured noise levels can be introduced. For calculation of the uncertainty, another of the key variables, in addition to the most basic quantities (such as the wind speed and direction), the Pasquill index, can be easily determined. Additionally, the Pasquill class indicates whether more advanced characterisation of the atmosphere is needed. This can be done by means of profilers such as a SODAR and weather balloons.

4.8.1 The statistical model

The initialisation of the algorithm of the statistical model begins with reading from the database of the regression models; see Fig. 4.13. Currently, there are up to 27 combinations of regression models for each frequency, but there could be any number of models. The input data to the statistical model are the environmental data available — for example, the synoptic data in Table 4.10 and the sounding data in Fig. 4.16. The software reads the standard format from balloon soundings carried out by the FMI. Also, the propagation conditions are needed (see Fig. 4.13): the variable *srcdir* for the geometrical direction of the source, *srcdist* for the distance of the source, *CurAngle* for the angle under calculation, and finally the frequencies for which to calculate the uncertainty. If the frequencies do not match the built-in frequencies of the model, the closest frequencies are selected.

There are one main loop and two sub-loops. In the main loop (1), the calculation

runs through the requested frequencies and one sub-loop (2) selects the appropriate variables and the corresponding statistics for the model loop (3), wherein the variables are applied to various regression equations and the best equation is selected, on the basis of calculation of the residual. After calculation that runs through all of the models and frequencies, the results are formatted for the desired propagation conditions. If the distance of the source is different from the model distance, a simple distance correction is applied. The correction just scales the values in accordance with the difference in distance between the model reference and the immission point from the source. The output of the software consists of the average, maximum, and minimum sound pressure levels, alongside their probability. The probabilities are based on the significance levels of each model that was selected as the best representative for each frequency.

An example from the output from the end of the implemented Atmosaku statistical algorithm reveals how the fitting process runs through various combinations of available environmental parameters to find the best fit, and it calculates an estimate for the excess attenuation and uncertainty (see Table 4.4). The example run is based on the yearly-average values for the Sodankylä site; see Table 4.6. In the example, the contribution of the square of the humidity (*ihump2*) varied from -7.30 dB to -10.5 dB, and this was the only variable determining the final value of the excess attenuation (*Xatten*) for the frequency 1600 Hz, with a contribution of -9.0 dB. However, it should be noted that this output value is not necessarily the attenuation caused by the physical phenomenon of humidity, which also can be calculated for the yearly-average values: $t = 2.7$ °C, RH $= 78\%$, and $P = 1010$ hPa yields an attenuation of 8.15 dB/km for 1600 Hz. As a result of the regression analysis, the excess attenuation is divided between the constant and the explanatory variables, which in this case consists of only the humidity.

4.9 Validation of the model

This section describes the validation case and the results of the validation. The objective of the validation was to test the accuracy, reliability, and transparency of the new model. The validation was carried out through comparison of the performance of the model developed to two other models currently used in environmental noise assessments. The P2P sound propagation path described Chapter 3 was selected to make the results directly comparable with the long-term measurements, and the case was calculated with all the models used in the selected conditions.

Two scientist colleagues[7] received an e-mailed request to perform the calculation in line with instructions attached to the e-mail message. The instructions described the environment of the sound propagation conditions as closely as possible, and the recipients were asked to perform the calculations for five distinct environmental cases.

[7] Dr Guillaume Dutilleux (CETE de l'Est, France) and Mr Denis Siponen (VTT, Finland).

Table 4.4: A demonstration test run for the frequency 1600 Hz

```
...
-> NEXT PROPOSED Xatten for 1600 Hz is 28.5659+-6.1583 dB.
Trying following variables for the frequency 1600 Hz:
+constant (+4.49e+01 dB)
+ihump2 (-1.05e+01 dB)
+mtq (+3.37e+00 dB)
+srcvwdir (-2.27e+00 dB)
+cldhgt (-7.09e+00 dB)
-> NEXT PROPOSED Xatten for 1600 Hz is 28.4206+-6.4308 dB.
Trying following variables for the frequency 1600 Hz:
+constant (+3.69e+01 dB)
+ihump2 (-7.74e+00 dB)
+mtq (+3.71e+00 dB)
+srcvwdir (-2.39e+00 dB)
-> NEXT PROPOSED Xatten for 1600 Hz is 30.4428+-5.5311 dB.
Trying following variables for the frequency 1600 Hz:
+constant (+3.69e+01 dB)
+ihump2 (-7.30e+00 dB)
+mtq (+3.62e+00 dB)
-> NEXT PROPOSED Xatten for 1600 Hz is 33.1792+-5.2116 dB.
Trying following variables for the frequency 1600 Hz:
+constant (+4.24e+01 dB)
+ihump2 (-9.03e+00 dB)
-> NEXT PROPOSED Xatten for 1600 Hz is 33.3633+-1.3426 dB.
-> Xatten for 1600 Hz is 33.1792+-6.2309 dB.
-> The best fitting model was number 2.
```

Both scientists were professionals in modelling of environmental acoustics, and two separate algorithms, the NMPB 2008 method[100] and the ISO 9613[36, 89] approach, were applied.

Both a brief and a fuller version of the instructions were provided in the request

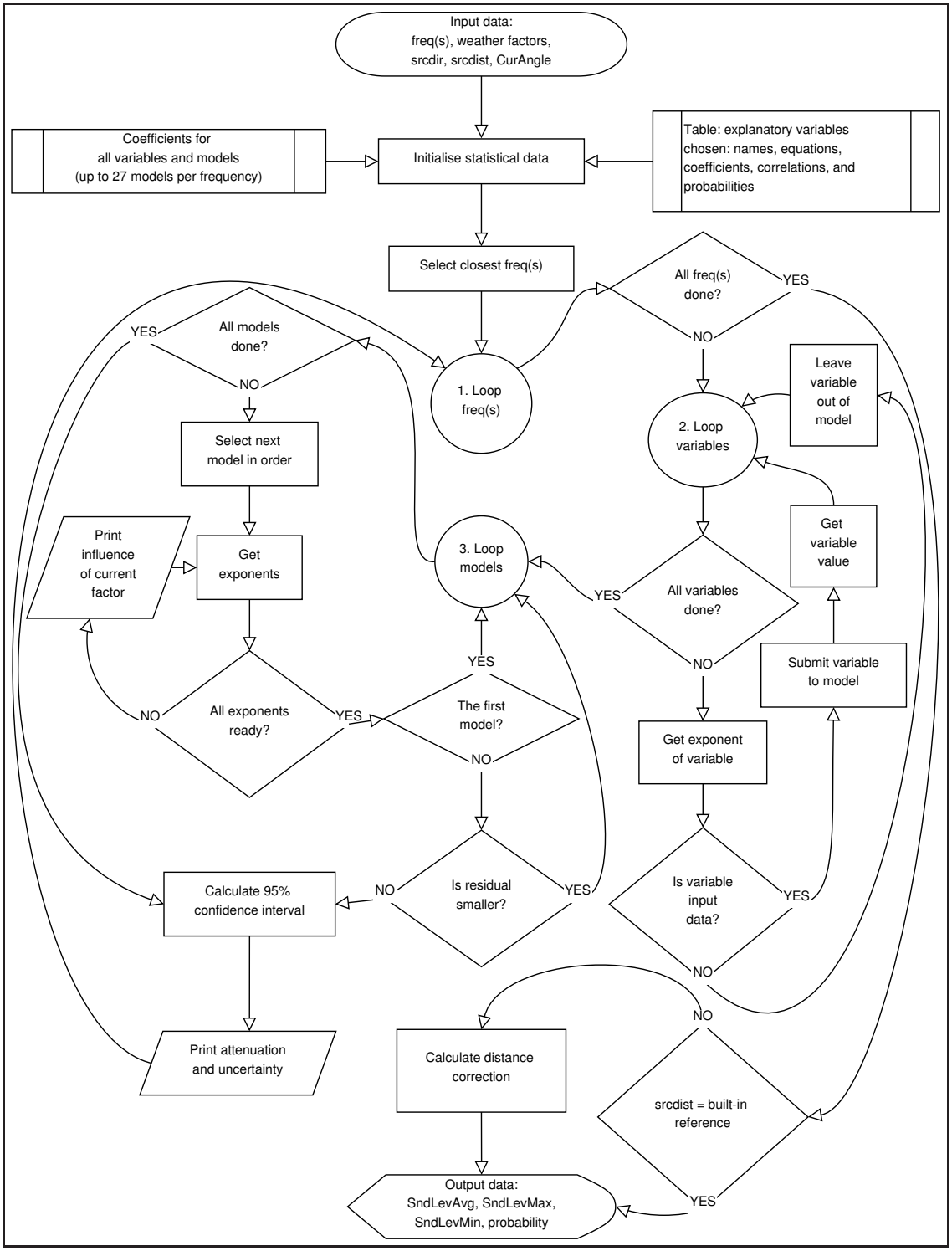

Fig. 4.13: Flowchart of the statistical model.

e-mail. The short version featured the following steps:

- In Table 3.2, the characteristics of the sound propagation path are defined.
- *The source, or emission*, is at the zero point, at a height of 2 m from the ground. The relative height of the ground is 0 m. The sound power spectrum of the source shall be flat; select the appropriate level. The only output needed is the attenuation at the immission point.
- *The receiver, or immission point*, is at a distance of 3240 m from the emission point, at a height of 2 m from the ground. The relative height of the ground is 0 m.
- If the software is able to use topography, the 3 m rise described in Fig. 3.14 can be implemented.
- If the software can exploit vegetation and ground characteristics, follow the depiction in Table 3.2. If only one reflection coefficient is allowed, use $R_s = 0.812$ for the year's average and the summertime (quarters Q2 and Q3) and $R_w = 0.659$ for the wintertime (quarters Q1 and Q4). It is also possible to define reflection coefficient as a function of distance from the emission point by following the data in Table 4.5.
- The modelling should be done for the year's average (L_{den}) and for the four quarters of the year (Q1, Q2, Q3, and Q4). The mean values of the weather parameters are shown in Table 4.6. Wind-rose data are shown in Table B.2. If the software is capable of using vertical temperature profiles, one positive value for the wintertime (for Q1 and Q4) and one positive (Q2) and one negative value (Q3) are given for the summertime in Table 4.6. For details, see Subsection 4.9.1 (these vertical profiles were also included as an attachment to the e-mail).
- *The results* will be the attenuation at the immission point for the year and the four individual quarters of the year. The attenuations values should be delivered in table form, in octave (or one-third-octave, if available) bands from 40 Hz to 1600 Hz for these five calculations all together. All the parameters exploited in the modelling, such as the calculation method, the given parameters, and the software name and version, are to be documented.

4.9.1 Detailed instructions

Two groups of parameters were selected to be varied in the comparison: basic meteorological and ground-specific parameters. *Wind speed and direction, temperature at a*

Table 4.5: Ground parameters for validation, where the numbers in the first column ('No.') correspond to location numbers in Table 3.2, L is the distance from the source, H is the relative height of the location, R_s is the summertime ground reflection coefficient, and R_w is the equivalent for wintertime

No.	L, m	H, m	R_s	R_w
-	0	0	0.902	0.663
1	899	3	0.842	0.663
2	1256	2	0.816	0.663
3	1386	2	0.773	0.653
4	1447	2	0.735	0.562
5	1899	0.3	0.773	0.653
6	2051	0	0.842	0.722
7	2744	0	0.773	0.653
8	2839	0	0.663	0.653
9	3082	0	0.663	0.653
10	3154	0	0.663	0.653
-	3271	0	0.722	0.663
Distance-weighted values:			0.812	0.659

Table 4.6: Meteorological parameters for the validation cases

	Mean values over the time period						
Description	Year	Q1	Q2	Q3	Q4	Unit	Details in Fig.
Wind speed	2.5	2.7	2.5	2.3	2.7	m/s	B.14
Wind direction	177	179	172	172	197	°	B.13
Temperature	2.7	−8.6	5.5	13	−5.3	°C	B.12
Relative humidity	78	83	70	78	89	%	B.11
Surface pressure	1010	1011	1012	1011	1004	hPa	B.14
Temp. gradient*	33	53	19	17	64	°C/km	B.10
Temp. grad. height**	308	353	163	332	406	m	B.10

* Wintertime: +44 °C/km, summertime: +29 °C/km and −11 °C/km; see (4.9.1).

** Wintertime: 514 m, summertime: 354 m; see Subsection 4.9.1.

height of 2 m and the vertical profile, surface pressure, relative humidity, and ground reflection coefficient (or flow resistivity) were selected for this comparison, and the calculation was performed with those parameters that the software was able to exploit.

The values of the parameters were averaged for the year and also for the four quarters of the year; see Table 4.6. Some of the values change very little with time, but the mean values were provided to make the results as comparable as possible with the

measurement data. Also, wind roses were provided if the software was able to make use of them. In the long-term measurements, only a few records of wind speeds higher than 9 m/s were encountered (one ‰ of the records), and those cannot be seen in either of the wind roses (Fig. 4.14) or in the wind statistics, shown in Table B.2. There were calm winds 2.9% and 0.3% of the time at heights 22 m and 48 m, respectively. The dominant wind-speed category was 0–3 m/s, with winds from the south-south-east (8.1%), south-east (6.6%), and south (5.6%). For the 3–6 m/s class, winds from the south were most common (5.0%). If the calculation method exploited the vertical temperature profile, the very common inversion phenomena were taken into account (for details, see Subsection 4.9.1).

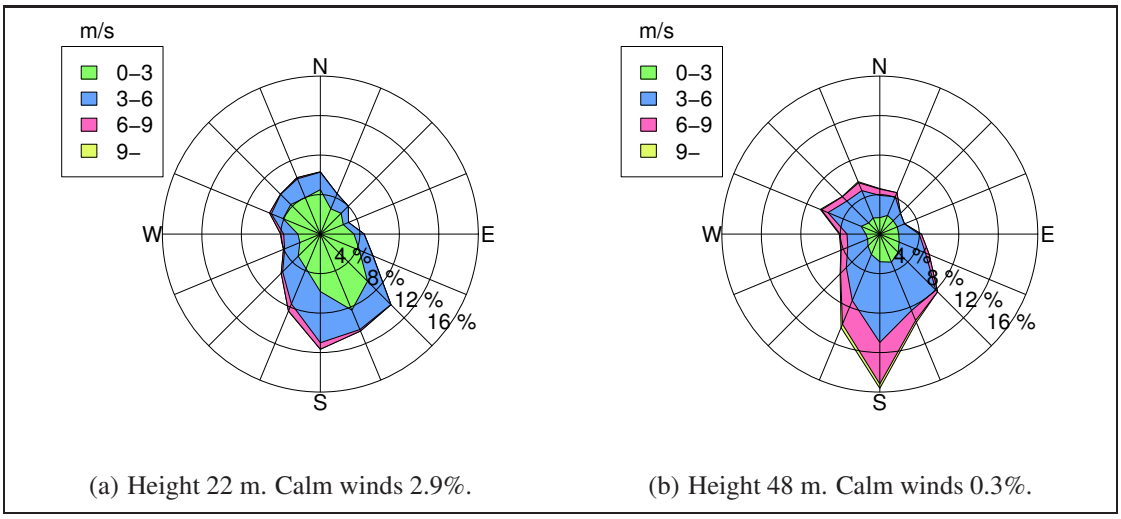

(a) Height 22 m. Calm winds 2.9%.

(b) Height 48 m. Calm winds 0.3%.

Fig. 4.14: Wind roses for the data from the meteorological tower for the whole study period.

Wintertime and summertime reflection coefficients were selected to characterise the ground (see Table 4.5). The reflection coefficient was obtained as a function of distance from the sound source, but if the software made use of only one value, the distance-weighted values $R_s = 0.812$ for the year's average and the summertime (quarters Q2 and Q3), and $R_w = 0.659$ for the wintertime (quarters Q1 and Q4) were used. All of the reflection coefficient values were calculated from the flow resistivity presented in Table 3.2 by means of the equations provided by Delany and Bazley [209] with the corrections suggested by von Mechel [210], such that the values present the arithmetic mean of reflection coefficients of all the one-third-octave centre frequencies from 40 to 1600 Hz.

Temperature profiles

All soundings during this measurement campaign were analysed, and from October to March, more than 80% of the time a positive lapse rate was found. The percentage

presence of a positive lapse rate was lowest during the summer; see Table 4.7. Also, the mean values for the individual quarters of the year were calculated, and typical profiles were found (see Table 4.6).

Table 4.7: Positive temperature gradients, as a percentage of all successful soundings

Jan.	Feb.	Mar.	Apr.	May.	Jun.	Jul.	Aug.	Sep.	Oct.	Nov.	Dec.
87%	91%	83%	66%	66%	50%	61%	66%	71%	80%	97%	85%

Averaging of the vertical wind speed, wind direction, and temperature profiles proved to be very challenging, and it was decided to select the most representative profiles for the seasons. The sounding data from 6 February 2005 at 23:00 UTC represent the most typical wintertime vertical temperature profile, with quite strong inversion. The temperature rises from −15.5 °C to −0.6 °C between the heights 179 m and 514 m, which means +44 °C/km. In the beginning (from 179 m to 211 m), the temperature increase is as great as +166 °C/km (see Fig. 4.15).

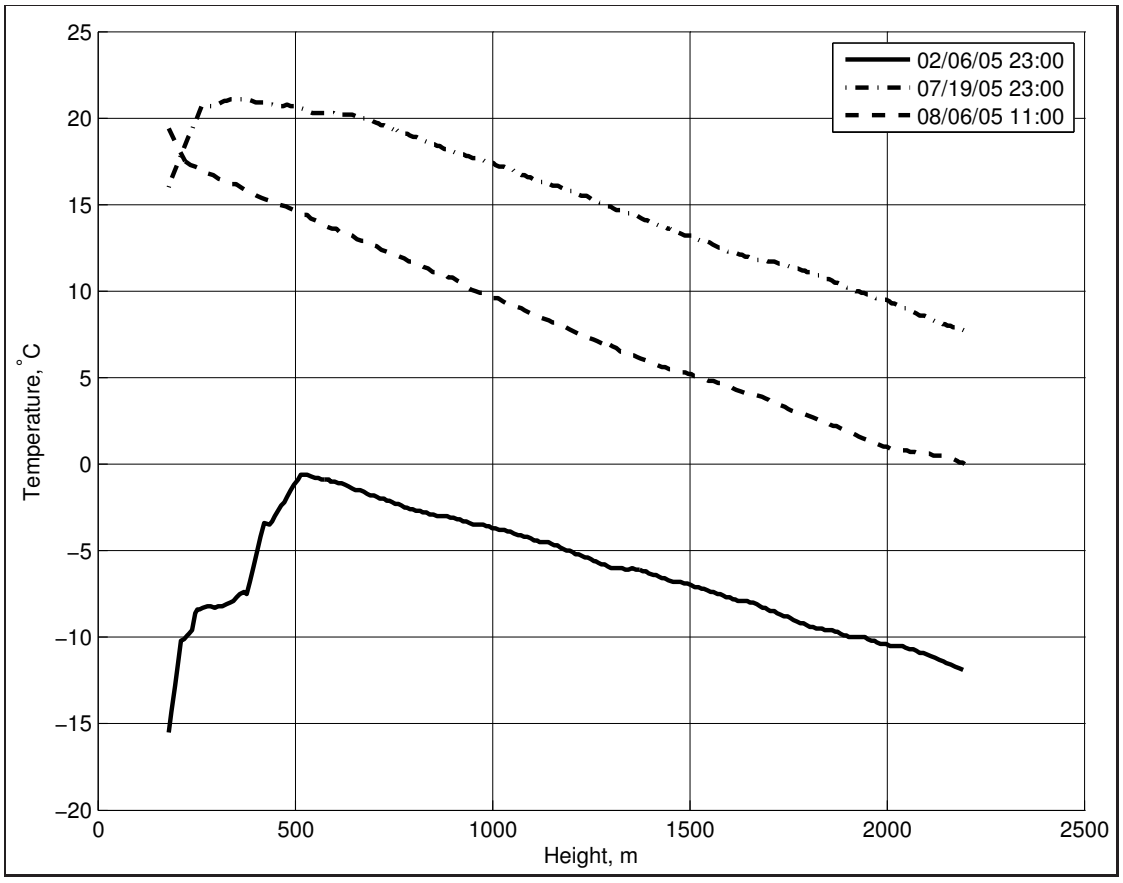

Fig. 4.15: The statistically selected most representative real (measured) temperature profiles for the wintertime (6 February) and summertime (19 June and 6 August).

It was more usual to see a negative lapse rate in summertime than in wintertime.

However, the sounding data indicate that half of the time there was also an inversion condition. The sounding on 6 August 2005 at 11:00 UTC shows the most representative profile for the negative lapse rate: the temperature drops from 19.4 °C to 0.0 °C between the heights of 179 m and 2197 m, for −10 °C/km. The positive lapse rates were not as strong as in the wintertime soundings, but they still cannot be neglected. The 19th of June 2005 at 23:00 UTC represents a very typical summertime sounding during the campaign — the temperature gradient height is at a lower altitude than during wintertime — from 179 m to 354 m in height, the temperature rises from 16.0 °C to 21.1 °C, making the temperature gradient +29 °C/km (from 179 m to 263 m, +56 °C/km, also in Fig. 4.15).

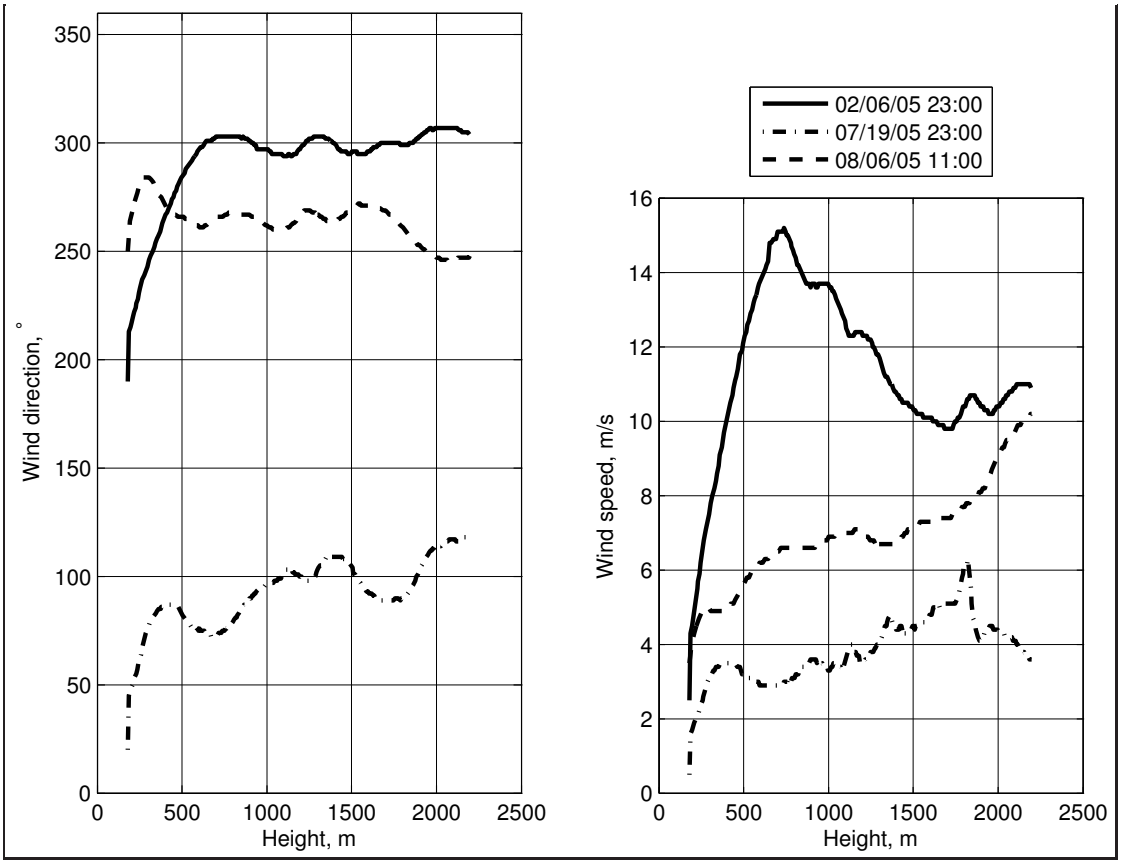

Fig. 4.16: Wind direction and speed in selected soundings for the wintertime (6 February) and summertime (19 June and 6 August).

To keep the lapse rates consistent with the best-matching real profiles in figures 4.15 and 4.16, the values determined from the real profiles were used in the modelling (see Table 4.6), in line with the following rules:

- The year's average was calculated in keeping with the profile measured on 19 June 2005 at 23:00 UTC or a value of +29 °C/km.

- The first-quarter (Q1) and fourth-quarter (Q4) values were calculated from the wintertime profile obtained on 6 February 2005 at 23:00 UTC or the value +44 °C/km.
- The calculations for the second quarter (Q2) used the same summertime profile as the year (that of 19 June 2005 at 23:00 UTC) or the value +29 °C/km.
- The third quarter (Q3)'s values were calculated in line with the profile measured on 6 August 2005 at 11:00 UTC, with a value of −10 °C/km.

4.9.2 Modelling and the results of validation

The environmental conditions applied by all the models were the topography and ground absorption as a function of propagation path and time. The σ_s and σ_w values defined in Table 3.2 were applied to the Atmosaku and the NMPB 2008[100] methods. The ISO 9613[36, 89] calculation was carried out by means of a commercial software application in which the ground was characterised by the reflection coefficient as a function of propagation path; the mean meteorological values for the four quarters of the year; and the year's average, as defined in tables 4.5 and 4.6.

In the NMPB 2008 method, the calculation of sound levels is carried out in *favourable conditions* and in *homogenous conditions*. Long-term level L_{LT} is calculated[100, p. 18] as a sum of levels in favourable conditions L_F and homogenous conditions L_H weighted by the *probability of occurrence of favourable conditions* (see Eq. 4.18):

$$L_{LT} = 10\lg\left(p_f 10^{L_F/10} + (1-p_f)10^{L_H/10}\right), \tag{4.18}$$

where p_f is the probability of occurrence of downward-refraction conditions in the long term.

The probability of occurrence for the Sodankylä site was calculated from the mast data and for a sound propagation angle of 157 degrees. The calculation was based on the existing wind and temperature data measured at ground level (only temperature), and at the heights of 2 m, 22 m, and 48 m. The sounding data and SODAR data were not used. The gradient values varied greatly with the heights of determination. The gradients between the heights 0 m and 2 m were as great as +14,000 °C/km, and there also were negative values. The altitudes 2 m and 48 m were found to give a moderate gradient for the temperature. For the determination of the wind speed and direction, both combinations of the higher altitudes were used (see Fig. 4.17). Sound speed gradient values of > 0.07 were used in determination of two distinct probability-of-occurrence values: $p_f = 0.0752$ and $p_f = 0.3077$. These two values are much lower than the probability of a favourable temperature gradient, which is between 0.5 and 0.97 (see Table 4.7). The wind characteristics seem to change the conditions significantly.

Both homogenous and favourable conditions were calculated for summertime and wintertime, and the long-term values also. Also, an estimate for L_{den} was calculated, by

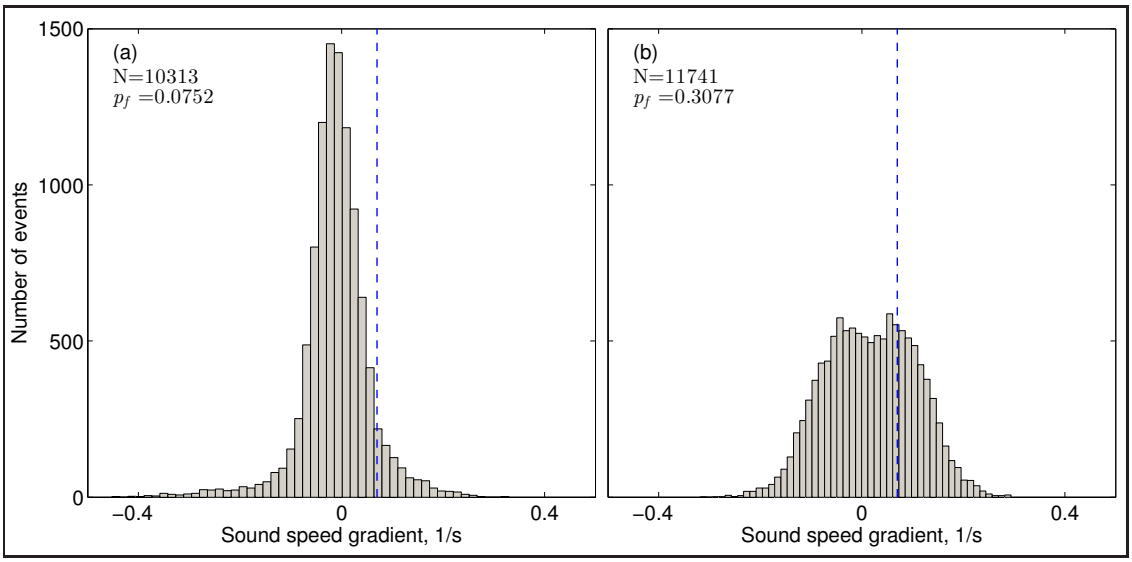

Fig. 4.17: Sound speed gradients and probability of occurrence. The temperature gradient is determined in both histograms between heights 2 m and 48 m and wind gradient determined between heights 2 and 22 m (pane a) and 22 and 48 m (pane b).

means of logarithmic averaging from the long-term values for summertime and wintertime. The lower value for probability of occurrences ($p_f = 0.0752$) was used because it gave results closer to the long-term values obtained from the measurements.

The NMPB 2008 system is not intended to be used for ranges beyond 2000 m from the source, so the test for this range in the calculation had to be removed — in other words, the algorithm applied was no longer NMPB 2008. There was no such restriction in ISO 9613.

Atmosaku is a combination of a physical and a statistical model. All the data available for the environment were exploited, but, because of the problem described in Subsection 4.9.1, above, only instantaneous data for the vertical profiles were utilised in the physical model. On the other hand, because the propagation path and the environment of the modelling case were exactly the same as in the statistical core of the software, the weighting coefficient for the physical model was zero. Both the physical and the statistical model were exploited, to demonstrate the differences between the approaches. However, for calculation of the yearly average, only the result with application of the statistical model is shown.

The calculation requirements for the statistical and physical model are very different. An example of the requirements for calculation of an inverse atmospheric condition, specifying the number of elements, the memory required, and approximate calculation times for the physical model, is shown in Table 4.8. The values are from the calculations for the validation case: distance 3240 m, GTPE, and turbulence enabled. XGrid is the number of calculation points in the horizontal direction and ZGrid vertically. Without

inversion, the size of the ZGrid value dropped to half. Without the turbulence model, the times were about a third of those reported in the table. At 1600 Hz, the initialisation of the turbulence model alone took about 3568 minutes, but only 92 GB of memory was needed in this phase. The statistical model operations are completed in seconds on any computer that can run a modern version of some software capable of handling matrix computations, such as MATLAB®.

Table 4.8: Atmosaku, calculation requirements of the physical model

	Frequency, Hz				
	40	100	400	800	1600
XGrid	4046	10,116	40,462	80,924	161,848
ZGrid	1499	2738	9454	18,408	36,316
Elements	6,064,954	27,697,608	382,527,748	1.490e+09	5.878e+09
CPU min.*	2	10	226	924	9800
GB**	2–3	6–7	80–90	300–320	850

* The wall time on an Intel® Xeon® CPU E5-4650 (32 cores) for 1600 Hz is 302 min.
** The virtual image size depends on the runtime environment.

The more detailed meteorological data for the three statistically selected, most representative dates are shown in Table 4.10. The vertical temperature profiles are depicted in Fig. 4.15 and the wind direction and speed as a function of height in Fig. 4.16. Also, the varying values of ground flow resistivity (see Table 3.2) and topography as shown in Fig. 3.14 were used as input data.

The modelling was done over the frequency range 40–1600 Hz in the 17 one-third-octave band centre frequencies, by means of the CNPE solver without the turbulent atmosphere and also the GTPE solver with the turbulent atmosphere, to produce some results comparable with those of the physical models. In the GTPE method, von Kármán spectrum[115, pp. 222–227] was selected and assigned the initial values shown in Table 4.9. The effect of turbulence can be seen in the GTPE calculations for 2000 Hz that are shown in Fig. 2.1, on page 19. The turbulence scattering of the sound field is very clear when one compares the excess attenuation curves determined at the same heights with both solvers. In Fig. 4.18, the excess attenuation curves of frequencies between 40 and 1600 Hz are shown for the winter favourable condition. The curves in pane b have been calculated by means of the CNPE solver without turbulence. The curves in panes a and c have been solved for via the GTPE solver with turbulence, and in pane c the values were height-averaged between 1.5 and 2.5 metres — note also the more than 20 dB lower levels in comparison to values determined at a height of 2 m.

In addition to L_{den} values, results for three instantaneous cases are shown. The wintertime inversion profile measured on 6 February 2005 at 23:00 UTC presents the *winter favourable* condition for the NMPB 2008 model and the first quarter (Q1) for

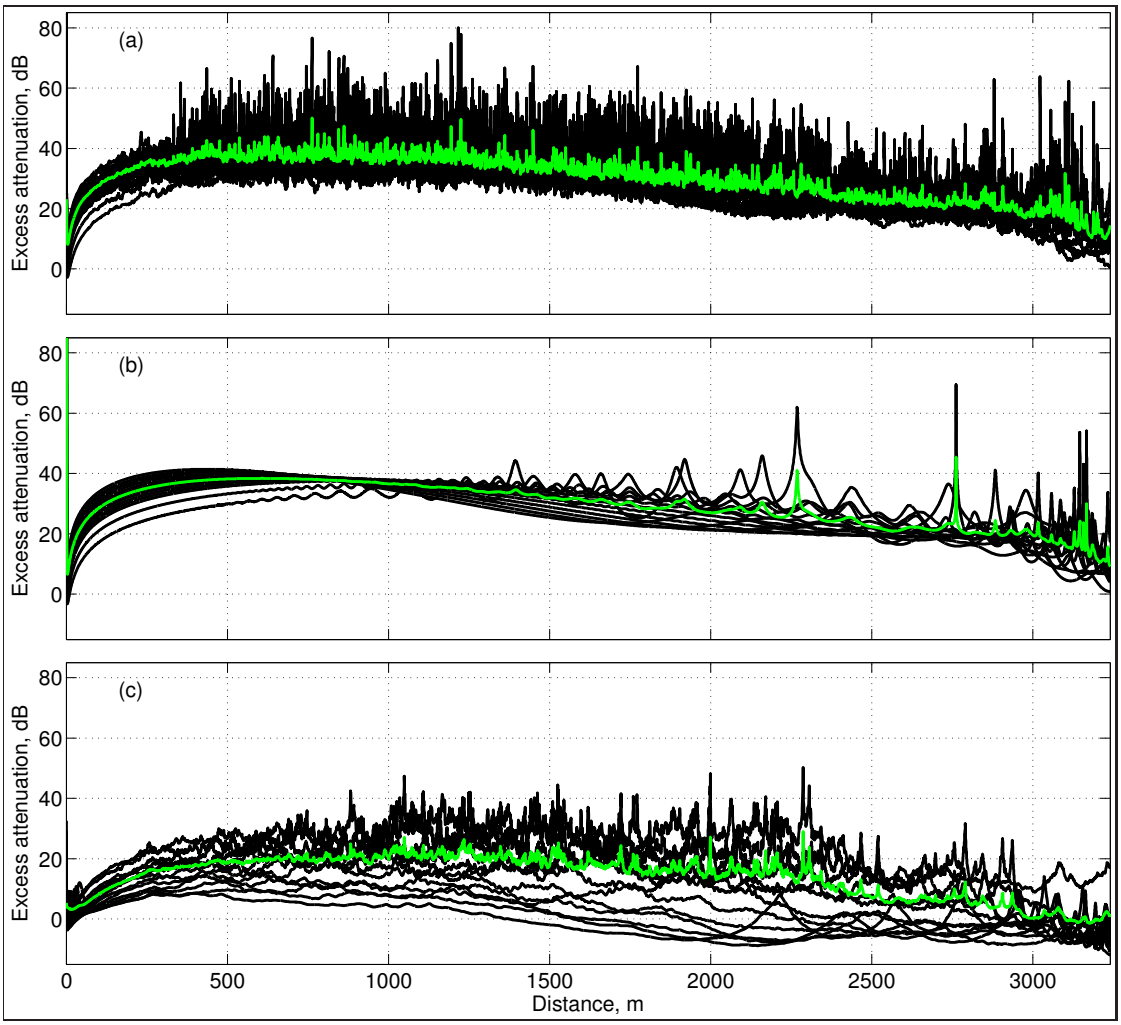

Fig. 4.18: Winter favourable condition, excess attenuation curves for all frequencies, a) GTPE, height 2 m; b) CNPE, height 2 m; and c) GTPE, values averaged between heights 1.5 and 2.5 m. Green lines represent the logarithmic average.

Table 4.9: Turbulence model initialisation parameters — for details, see the work of Salomons (2001)[115, p. 227]

Param.	Unit	Value	Description
a	m	20π	Outer scale of turbulence.
C_T^2/T_0^2	$m^{-2/3}$	10^{-7}	Scaled temperature structure-function parameter.
C_v^2/c_0^2	$m^{-2/3}$	10^{-6}	Scaled velocity structure-function parameter.
N	-	200	Number of discretised fluctuation values.
$k_{n,max}$	m^{-1}	10	Maximum wave number used in the fluctuation spectrum.

ISO 9613. The summertime inversion profile measured on 19 June 2005 at 23:00 UTC is the *summer favourable* and Q2, and the summertime normal profile measured on 6

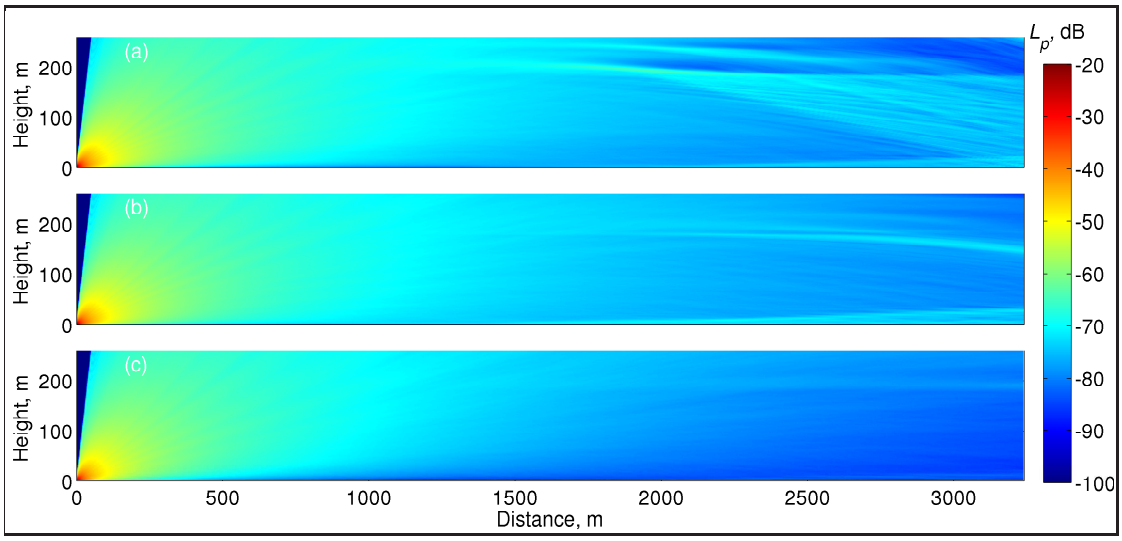

Fig. 4.19: Total averaged sound fields from the GTPE solver for frequencies between 40 and 1600 Hz: a) winter favourable, b) summer favourable, and c) summer homogenous.

August 2005 at 11:00 UTC is equivalent to *summertime homogenous* and Q3. Also the sound fields solved for via GTPE are shown in Fig. 4.19. The final results of the comparison can be seen from figures 4.20–4.23. Atmosaku follows the statistical model in all these conditions, because the distance from the evaluation point is the same as the built-in reference distance of the statistical model. However, also the results from the physical models are shown: the GTPE method with the turbulence calculation and CNPE without topography and turbulence. The values determined at 2 m height were used for the GTPE and CNPE curves.

Generally, the statistical model is able to find the best estimate in all of the cases and the average (semi-dashed line) follows the measurement results. The uncertainty for each frequency model is shown by a grey area surrounding the average line.

For the winter favourable condition, the standardised algorithms, ISO 9613 and NMPB 2008, gave a fairly good estimate in comparison to the measured values, but the wave-equation-based algorithms produced much greater excess attenuation, especially for the higher frequencies (see Fig. 4.21).

The average of the GTPE and CNPE methods matches better with the measurements for the summer favourable conditions than with the standardised algorithms, which underestimate the excess attenuation (see Fig. 4.22).

It was expected that the NMPB 2008 results for homogenous conditions would go well beyond the real values in Fig. 4.23 — since the system was designed this way. In a real situation, this result is just an upper limit value for the excess attenuation and is weighted with the probability-of-occurrence value (see Subsection 4.9.2) in relation to the other limit: for the favourable condition. The ISO 9613 approach underestimates the excess attenuation over 20 dB and the state-of-the-art algorithms overestimate for

Table 4.10: More detailed meteorological data for the modelling

Date	6 February	19 June	6 August
Time (UTC)	23:00	23:00	11:00
Surface pressure, hPa	1024.9	1004.5	1009.5
Temperature at height of 2 m, °C	−08.6	+19.6	+18.4
Temperature at 0 m, snow surface, °C	−18.5	+11.1	+5.4
Dew point, °C	−11.6	+15.6	+10.2
Relative humidity, %	76	72	50
Wind direction (0–360), °	250	290	250
Wind speed, m/s	3	2	3
Rainfall, mm	0	0	0
Snow depth, cm	75	0	0
Cloud cover, eighths	3	7	4
Low cloud class, code (see Table A.1)	0	3	2
Middle cloud class, code (see Table A.1)	4	6	4
High cloud class, code (see Table A.1)	8	8	1
Cloud altitude, code (see Table A.1)	8	6	5
Visibility, m	50,000	40,000	50,000
Present weather, code (see tables A.1–A.1)	1	2	2
Pasquill stability class	6	5	2
Temperature gradient height, m	239	250	0
Max. temperature gradient below 1 km altitude, °C/km	+143	+80	−4
Mean wind direction below 1 km altitude (0–360), degrees	282	80	268
Standard deviation of the wind component vertically perpendicular to the mean wind direction, m/s	0.382	0.072	0.705
Transverse turbulence intensity	0.227	0.185	0.197
Friction velocity, m/s	+0.182	+0.063	+0.568
Monin–Obukhov stability parameter, 1/m	+0.064	−0.012	−0.004
Sensible heat flux, an integer from −200 to +700	−38	0	+67
Ground type, code (see Table A.1)	2	7	4

frequencies over 500 Hz.

However, not all noise consultants have access to ceilometers, SODARs, and soundings, or even to the 3D sonics that are needed for provision of the turbulence parameters. When the input data are limited, Atmosaku uses simpler and less accurate regression

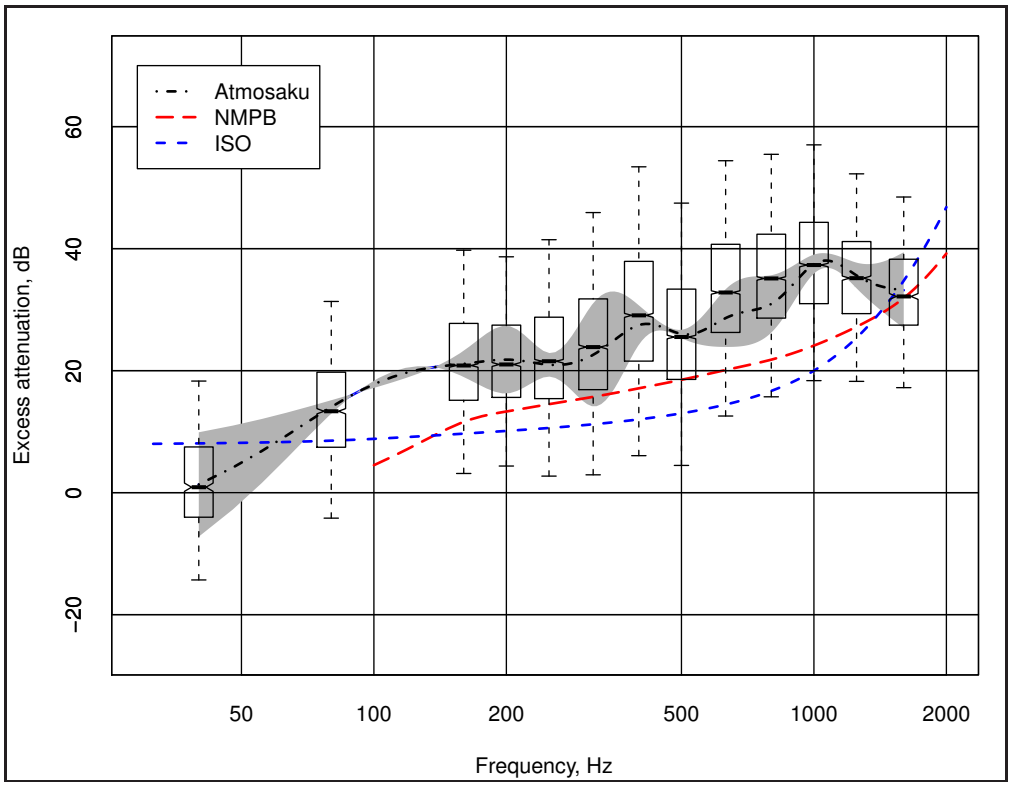

Fig. 4.20: L_{den}, with the measurements and validation models. IQR boxed with median line; whiskers extend to 2σ. Also, the confidence interval for Atmosaku is shown, in the grey area.

models. A test was prepared wherein only some synaptic observations were used and those variables that demand more advanced and more expensive equipment were omitted. However, to keep the uncertainty within appropriate limits, it was expected that the Pasquill index can be determined. Examples of other variables that were allowed are temperature, humidity, wind speed, ground type, snow depth, and surface pressure. The results from comparison with the limited input variables can be seen in figures 4.24 to 4.27. Uncertainty values increase, and the average values deviate more from the measured: the ability of the statistical model to estimate the measured values is impaired because of the inadequacy of the input information.

4.10 Validity and reliability

The documentation of the measurements was prepared in more detail than typically, making the internal validity easier to determine and enhancing the external validity of the research. The measurement facilities and software, the measurement area, the procedures in creation of the database, and a guide for utilisation of the database can be found in the software's documentation.

Neither of the standardised algorithms were intended for calculation of long dis-

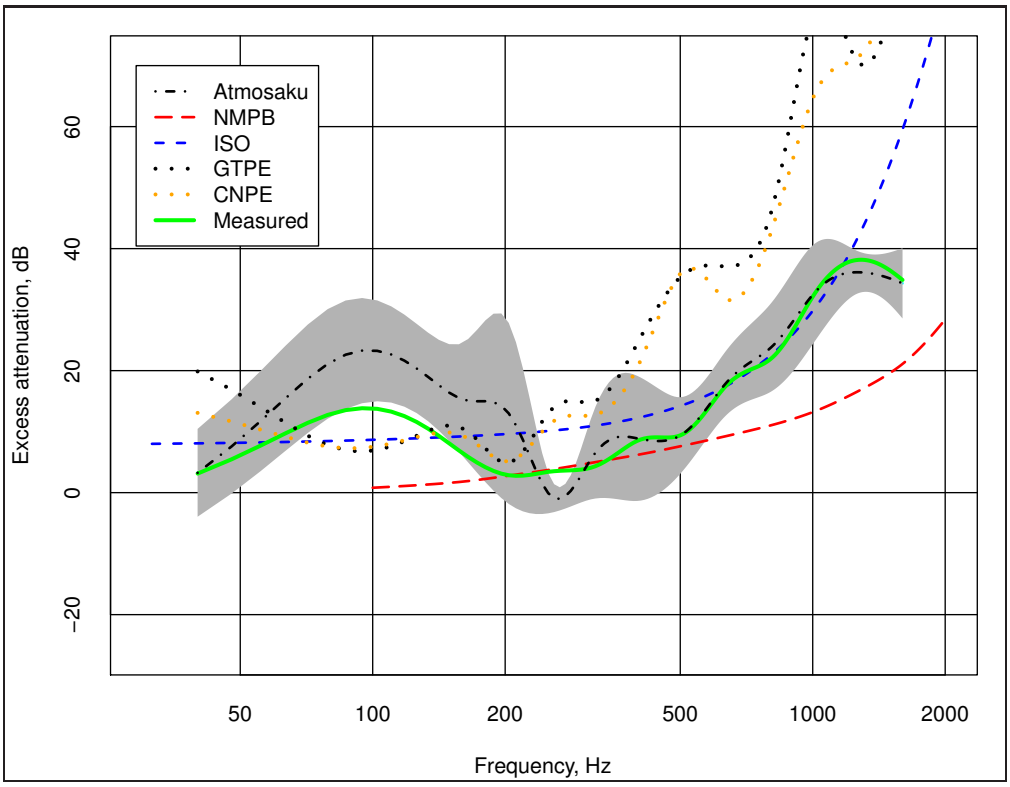

Fig. 4.21: Winter favourable, measurements and validation models.

tances. In the NMPB 2008 method, there was a restriction to a 2000 m maximum, which had to be overridden for this calculation. With the ISO 9613 approach, there was no such restriction, but the results of neither method should be considered to be references. Nonetheless, the ISO 9613 method is commonly used for long-range simulations.

Acoustic data

The acoustic data were normally distributed (see figures B.1–B.7), and the standard deviation of the measurement can be calculated as in Eq. 4.19:

$$s = \sqrt{\frac{1}{N-1}\sum_{i=1}^{N}(x_i - \bar{x})^2}, \tag{4.19}$$

where x_i is a single measurement value, $\bar{x}$ is the mean value, and N is the number of repetitions. Through introduction of s and N, random error ε_r can be introduced (4.20):

$$\varepsilon_r = \frac{s}{\sqrt{N}}. \tag{4.20}$$

In this research, there were almost 15,000 repetitions, but not all of the repetitions led to a valid measurement (see Section 4.1). The value of N for the valid acoustic data

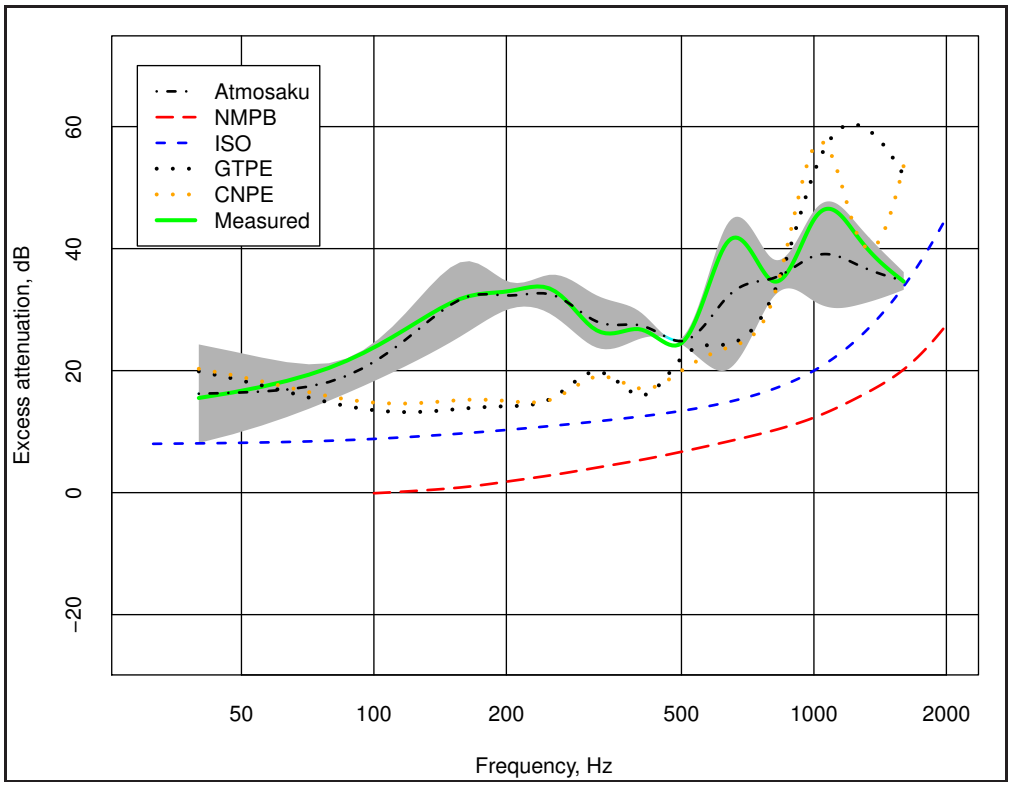

Fig. 4.22: Summer favourable, measurements and validation models.

varied between 725 (see Fig. B.1) and 6763 (see Fig. B.5). The effect of the random error on measured sound pressure level L_p can be calculated via Eq. 4.21:

$$L_{\varepsilon_r} = \pm 20 \lg \left(\varepsilon_r 10^{\frac{L_p}{20}} \right). \tag{4.21}$$

With this method, the random error for a given sound pressure level $L_p = 50$ dB in this research was $L_{\varepsilon_r} = \pm 0.3$ dB and $L_{\varepsilon_r} = \pm 0.1$ dB, for the two N values given, respectively. In light of the huge number of repetitions, the measurement may be considered to have good internal reliability.

It was expected that people passing by would disturb the measurements somehow. This was one of the factors behind the archival of all of acoustic data: anomalies and deviating results could be tracked down through listening to the samples. Because of the minimal-disturbance principle in relation to the measurements, the measured signals had a very low signal-to-noise ratio, but, through the frequency-dependent validation procedure described in Section 4.1, the anomalies were removed from the database before analysis — though at the expense of abandonment of many of the measurements, especially at low frequencies (see Fig. 4.1). The external reliability can be determined by means of the existing database.

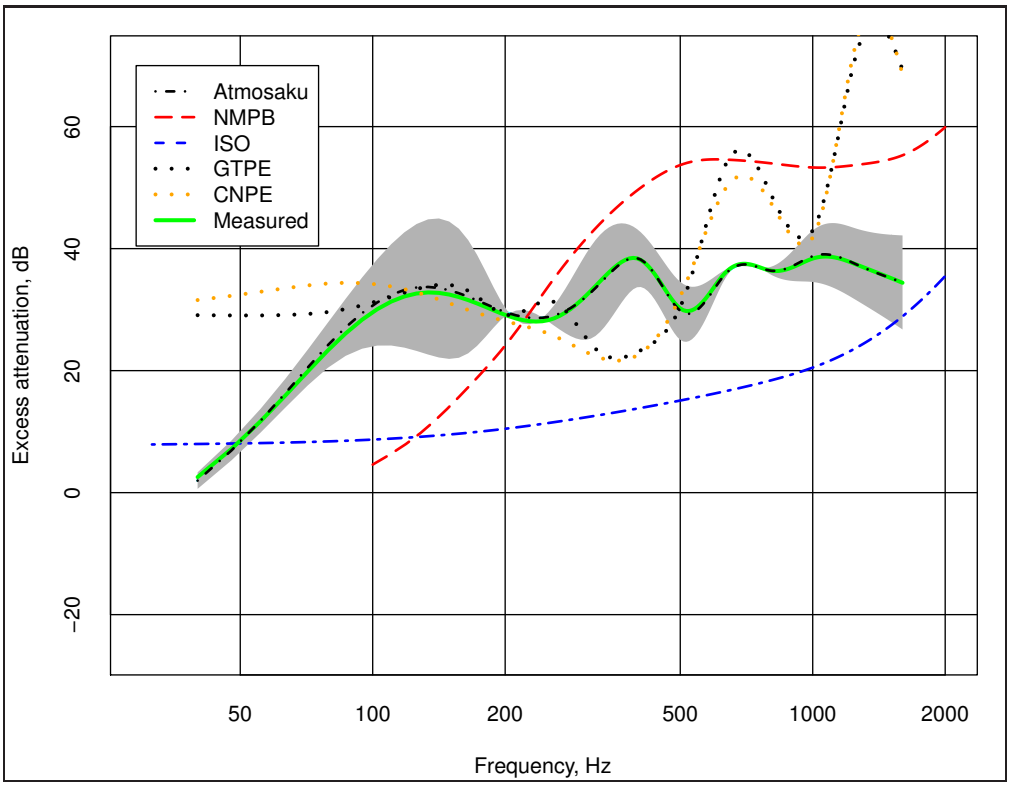

Fig. 4.23: Summer homogenous, measurements and validation models.

Meteorological data

The Sodankylä site was flat on both small and large scale, so the effect of topography on flow statistics was negligible. The areas around the sound source, where the SODAR was located, and the microphones, where one sonic was positioned, were large open spaces. However, the micrometeorological mast was slightly to the side of the path of sound propagation, and there was sparse tree distribution around that area.

A meteorologist with the FMI evaluated the representativeness of the meteorological data for the research area[109]. It was found that it is possible to correlate the sound data with the mast data but that there were some conditions for which extra care had to be applied. In the north-west direction, the surface was an open area with very sparse distribution of trees and the wind profile was less influenced by the roughness elements. An estimate for roughness length z_0 was calculated as a function of height and wind directions (see Fig. 4.28) on the basis of simultaneous data at three measurement levels (22, 25, and 47 m, with $N = 9166$). The values agree with the estimate made for the same area by Joffre et al. in 2001 [211].

The wind and temperature gradients calculated from the sounding data are representative, because the measurements were made above the roughness sublayer and the footprints of the momentum and heat fluxes grow at higher levels, such that the measured parameters are the result of the contribution of a greater area.[109]

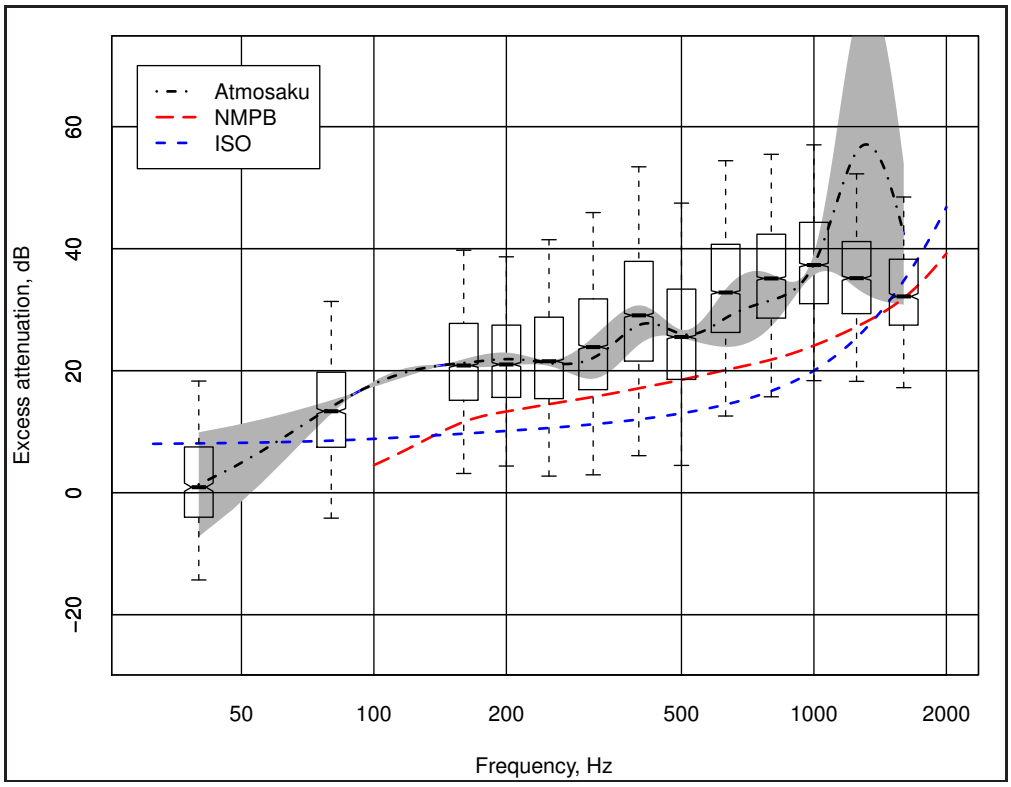

Fig. 4.24: L_{den}, comparison with the limited input data. IQR boxed with median line; whiskers extend to 2σ. Also, the confidence interval for Atmosaku is shown, in the grey area.

The SODAR results were found to be problematic when compared to the mast data and data from a numerical weather model (HIRLAM). However, the SODAR unit was 3 km from the mast, so the comparison can be called into question. The SODAR data were not used in this thesis project and need further investigation before they can be utilised in practice.

Finally, the features of the research area could permit application of the Monin–Obukhov similarity theory[124, pp. 357 *ff*] for generation of surface-layer profiles in various stratification conditions.

4.11 Summary of the analysis and the results

The signal processing and the statistical analysis of the sound and the weather data was presented. The data pre-processing included several steps, but all the routines were automatised. This was a computationally intense phase in taking two and a half years CPU time. The traceability of the sound power levels at the source and the measured sound pressure levels at the receiving station was maintained with great care.

The total variation of measured excess attenuation was 80 dB, while the medians were found to fluctuate by 10 dB with the season of the year and by 15 dB as a func-

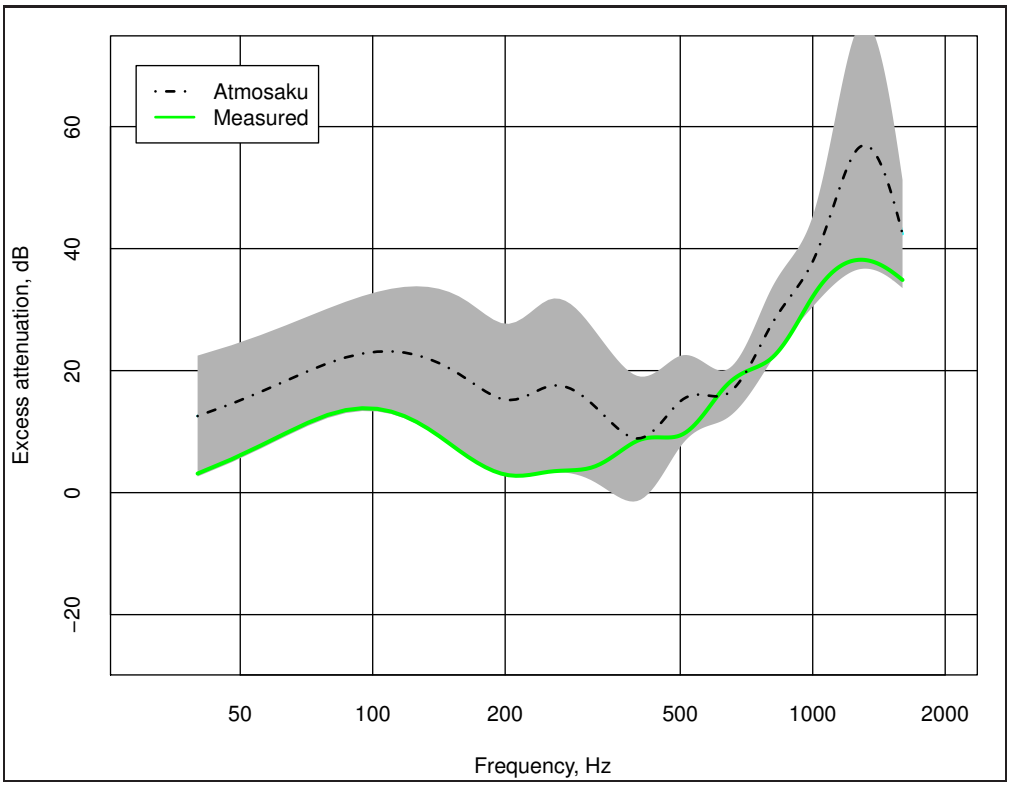

Fig. 4.25: Winter favourable, comparison with the limited input data.

tion of time of day. The values for excess attenuation were normally distributed, but most of the weather variables showed anomalies in the distributions: only some wind-, turbulence-, and temperature-related variables were almost normally distributed. On the other hand, many of the meteorological parameters were coded categorical variables, such as cloud type or weather code, which should not be normally distributed either. Statistical analysis showed that the most important meteorological variables affecting excess attenuation were frequency-dependent. Also, the height of the microphone affected the strength of the linear correlation between the variables and the excess attenuation, and the order of explanatory variables changed at most frequencies with the microphone height.

The dependencies between the meteorological variables and excess attenuation as a function of frequency were tested with many mathematical models, from linear to curves of various shapes. Most of the variables followed a cubic curve, turbulence variables fitted quadratic curves, and a linear model applied for cloudiness and for almost all of the dummy-coded categorical variables — of which Pasquill index was also tested as a continuous numerical variable. An inverse equation explained the continuous behaviour of the Pasquill index much better: statistically highly significantly.

Generally, at low frequencies, excess attenuation increases when both the height of the temperature gradient and the positive value of the gradient increase along a quadratic

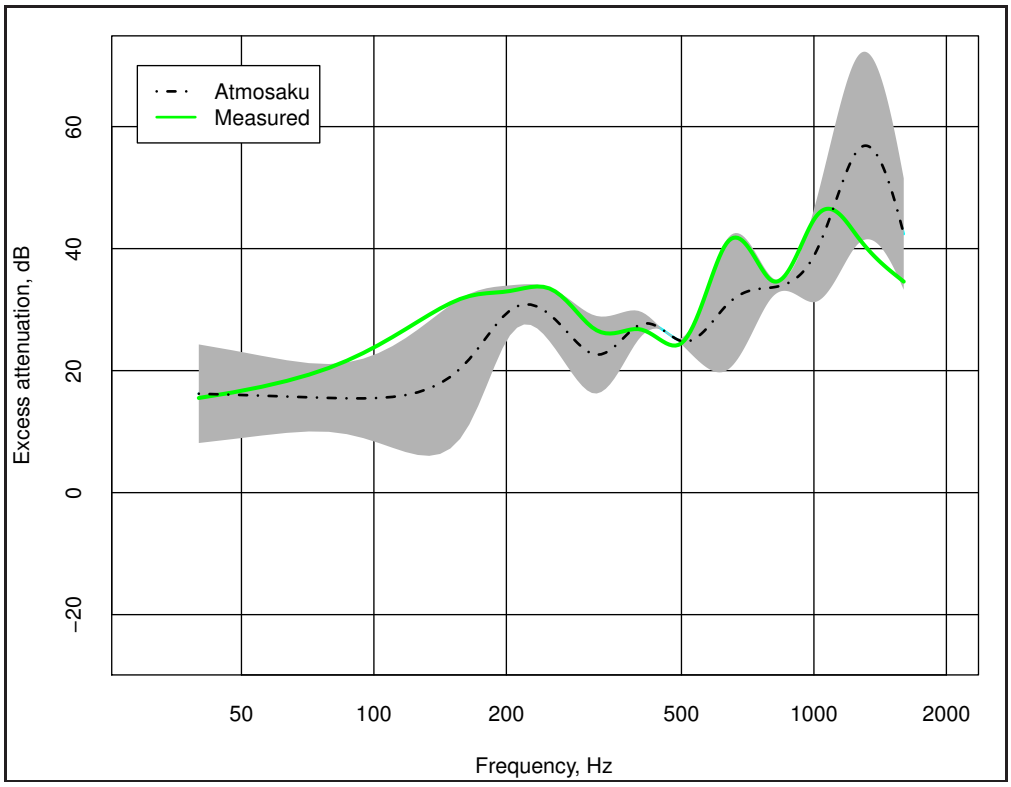

Fig. 4.26: Summer favourable, comparison with the limited input data.

curve. However, the best fitting was achieved at the higher frequencies and the strength of association for the temperature gradient was $R^2 = 0.807$ at 1600 Hz. For snow depth on the ground, the greatest effect on excess attenuation was found to follow a cubic curve at low frequencies ($R^2 = 0.307$ at 80 Hz). Time of day ($R^2 = 0.163$ at 200 Hz), and season ($R^2 = 0.149$ at 40 Hz) had highly significant explanatory power for the lower frequencies, with a cubic relationship. Low cloud type, as a dummy variable, behaved linearly with strength $R^2 = 0.123$ at the low frequencies.

At frequencies over 200 Hz, the atmospheric temperature profile had a very strong but opposite effect on excess attenuation: increasing the values decreased the excess attenuation. At most frequencies, the value of the temperature gradient was the best value explaining the excess attenuation, and second best was humidity. The effect of humidity, which has been known for a long time, was a strong negative correlation with the excess attenuation — especially at higher frequencies. The strongest linear correlation at the highest frequencies was with sensible heat flux: increasing the value of heat flux increased excess attenuation, but the best performance was for explaining excess attenuation cubically at 800 Hz, with a strength of $R^2 = 0.273$. Visibility did not have any statistically significant linear explanatory power but fitted a cubic equation at 400 Hz ($R^2 = 0.235$) statistically highly significantly.

Wind speed contributed almost equally for all frequencies, and a wind-derived vari-

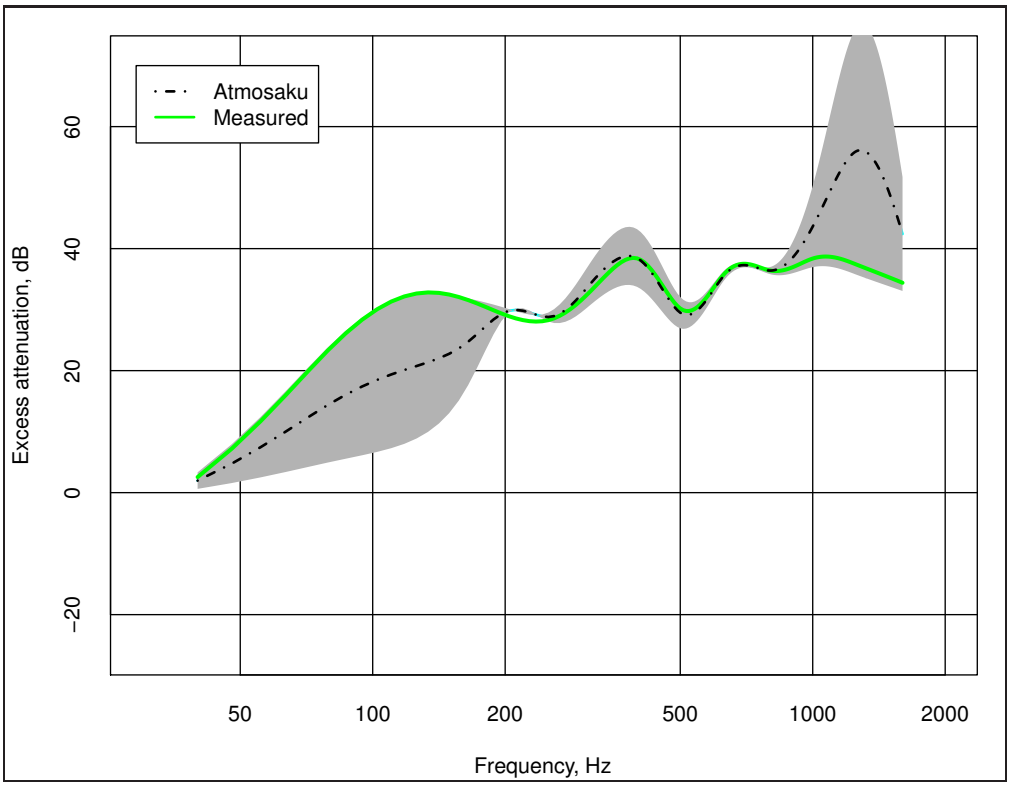

Fig. 4.27: Summer homogenous, comparison with the limited input data.

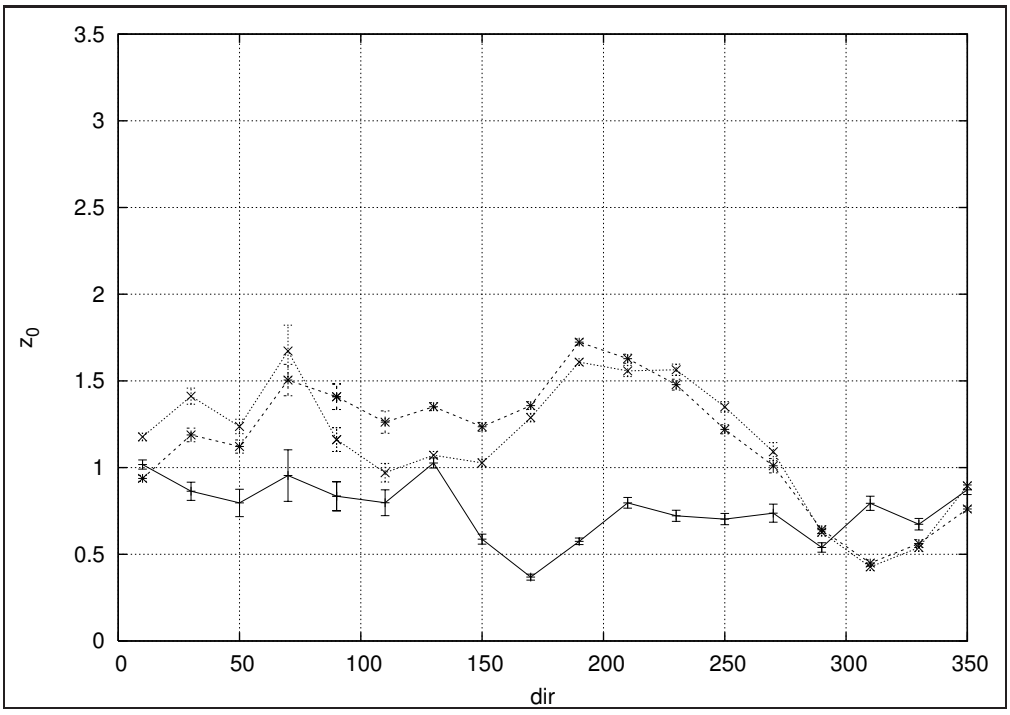

Fig. 4.28: The dependence of z_0 on wind direction at 47 m (solid line), 25 m (dotted line), and 22 m (dashed line).[109]

able, 'contribution of wind direction', the wind component toward the direction of sound propagation, was the best explanatory variable, with a strength of $R^2 = 0.329$ at 800 Hz. The very strongly wind-connected turbulence parameter, the transverse turbulence intensity, was also evident in the equations for most frequencies but reached its highest cubic explanatory power at 1250 Hz ($R^2 = 0.192$).

Friction velocity $u_\star$, the Pasquill index, and the Monin–Obukhov stability parameter (ζ) were selected to describe the atmospheric stability condition. The friction velocity is in the equation for the value ζ, but this relationship did not show up in the collinearity analysis. However, both the $u_\star$ and the ζ had quadratic explanatory power, of $R^2 = 0.205$ and $R^2 = 0.146$, respectively at 800 Hz — $u_\star$ with a two times higher F value (11.48) than ζ. Pasquill index was among the best explaining variables only for the lowest frequencies, though it achieved the best statistics for 500 Hz with an inverse behaviour ($R^2 = 0.140$).

The database, one result of these long-term measurements, makes possible many other studies too. In addition to weather data, the database contains the original acoustical data in waveform audio file format — i.e., as WAV files, which were recorded in sync with the sound source, with a time uncertainty of 0.69 ms. Also, there were seven microphones, which were arranged in a combination of a tetrahedron and a linear array, thus enabling analysis of the incident angle of sound. There were separate optimised excitation signals to make possible determination of both momentary impulse responses and short-term changes in the propagation path. Maximum length sequence, frequency-modulated chirp, and random-coded phase-modulation excitation were tested, but stationary and swept sinusoidals were found to yield the most reliable results. These further capabilities were used in a study of the effect of meteorological parameters on sound propagation delay. No surprises emerged: a strong linear correlation of -0.595 was found between the delay and the temperature. The delay was normally distributed and followed a sinusoidal curve as a function of date, reaching its maximum in winter and its minimum in summer. This research only scratched the surface of the material in the database — many interesting phenomena have been left for further research.

Chapter 5

Discussion

ALMOST all possible surface- and boundary-layer weather data provided by the Arctic Research Centre of the Finnish Meteorological Institute were utilised, and the interdependencies with long-range sound propagation were studied. Not all of the data were relevant, so some items were omitted from the final model. If we had known before starting this project what we know now, would we have reached even better results? In this chapter, the usability of the results, how the measurements and analysis could have been improved, and a future work scenario are discussed.

5.1 Usability and portability

In determination of a model on the basis of the measured environmental variables, the interdependencies among the environmental variables presented one of the most complicated issues. All of the variables have the same source of energy, the sun, and collinearities can be found. Wind properties were measured at different heights and positions, in 10 locations in all, with two additional places where the full atmospheric wind profile was measured. The same was true of the measurements of temperature. It is clear that there is a very strong correlation between these quantities, though captured at different heights or locations. Incorporating two or more collinear variables into a regression model could lead to an unstable model, and the only solution is to select the most representative variable for each group of quantities. At the same time, in a model that represents a large area, the variables should also reflect the differences within the area and have different values around the model space. Even the smallest deviations in the sound speed profile of the atmosphere may change the sound propagation path substantially.

These questions make *portability* of the approach presented in this thesis challenging, and portability is clearly one of the key questions for more general use. A statistical model based on measurements from a certain environment with specific meteorolog-

ical conditions might not be representative in another environment. The topography, vegetation, and climate should be as similar as possible in terms of sound propagation. All of this comes together to mean a need for many measurements, representative both spatially and in the time domain, from different environments.

Feasibility of a statistical model for more general use is not beyond reach. In a few years, low-power and low-cost 'smart' networked sensors will allow the measurement needs found to be met. Also, the social, commercial, and research needs create an impetus, with good examples of realisations already existing in the Helsinki Testbed[212], whose measurements commenced in 2005 with hundreds of weather stations in the Helsinki area, and the rapidly growing number of installations of noise-monitoring stations — offered by many commercial suppliers. All of these datasets are networked and available to all network-users. When the quantity of data is great enough from a statistical point of view, a statistical model can be implemented in the area and put into service. A weather model could be used as input to a statistical noise model, and real *noise predictions* could be introduced. There are diverse applications for these predictions. The model could be exploited by a manager of a port in a large city where there is action 24 hours a day: in planning of the noisiest actions, times of favourable conditions for that noise spreading could be avoided. An operator of a wind-power farm could also benefit from noise forecasts, because the noise generated by the turbines and its directivity pattern can be controlled through turning of the blades or the whole tower, via adjustment of the speed of rotation, and through the phasing of rotation of individual windmills.

5.2 Discussion of the measurements

This research was both very challenging and laborious. The technical implementation of the measurement system was a success and worked as planned throughout the data-acquisition period. The only drawback was the modest performance of the subwoofer: the power-handling capacity was below that specified by the manufacturer, and, regardless of the moisture-proof elements and the efficient dehumidifier in the weather shelter of the subwoofer, the variations in temperature and humidity did it in. On the positive side, the horn stack was found to be a reliable and a very stable source of sound power.

Another of the challenges in the study involved the research environment and its side effects, the continuous struggle to produce sound levels that were high enough to allow results while keeping the levels low enough not to annoy people. Some more advanced measurement methods were tested to minimise the annoyance: maximum length sequence (MLS), frequency-modulated chirp (FM-CHIRP), and random-coded phase-modulation (RPM) were used as excitation signals, but we had to abandon these because of inadequate allocation of resources for validation of the methods. The results of this work are presented in the report by Kero (2004)[108].

The amount of information acquired was as expected, but the resources required for management of the data exceeded predictions.

An automatic error condition reporting system was utilised: an error caused a report to be sent by e-mail, along with a text message to the researcher's phone. This feature was found to be valuable. The measurements were managed at a distance of more than 800 km from the research area, and there were many blackouts, so it was vital to have the messages be as detailed as possible. There were local personnel, who were able to solve most of the problems rapidly when they appeared. The reasons for the blackouts ranged from cable breaks due to excavators to unaware outsiders' unplugging of a power cable.

It was expected that the measurements would not be completed without some disruptions. Saving of the time-domain data enabled listening to the measurement signals afterward. Some measurements were found to contain speech of passers-by, but the values calculated for excess attenuation were not affected. As a curiosity, one outlier in the results was found: on 23 September 2005 at 14:00, the excess attenuation at microphone R1 was found to be over 80 dB. Because all the excess attenuation for the other microphones was as usual, this outlier was removed. It was concluded, on the basis of log files, that this outlier resulted from a halted calibration — the measurement signal from the sound source was suddenly heard during the calibration and the calibrator was left — powered off — on microphone R1. Of course, this measurement should have been removed at the moment of calibration, but it was forgotten for some reason. No other outliers were found, and all the other data were left intact.

The experience from the long-term sound propagation measurement can be summarised in the following guidance:

- Find a place where no humans can be disturbed by the measurement signal. If there is habitation nearby, automatic control of emission power is needed. Pay special attention to the linearity of the system: how many watts of acoustic power are emitted with different input power settings? Is the necessary SNR attainable enough for the worst-case weather? How will the inversion be taken into account — a condition, wherein the sound may travel dozens of kilometres instead of a few hundred metres?

- Plan everything in advance: traceable calibration chains, sound power measurements during the trials and their scheduling, the analysis, etc. In our case, many personnel were needed for completion of the sound power measurements and we performed the measurements in a slightly different way each time, which caused a lot of extra work in the analysis phase.

- Remember that the sound pressure levels recorded might be caused by someone or something else. Archive the captured acoustic signals as a function of time, to allow filtering out of bogus signals.

- Long-term measurements produce huge quantities of data, and the only way to manage this is to automate everything. All procedures from the conditioning of source and receivers to archiving of data have to be automatic.

- One cannot be prepared for everything. In addition to the automation, the properties of sensors and actuators need regular attention. Professional measurement microphones retain their properties and settings very well, but the sound sources in particular should be looked into.

- Give preference to Open Source software. Commercial software may have errors in programming that cannot be addressed and might require attention and later recovery efforts. In our case, the SODAR control program was found to crash frequently and could not be restarted without rebooting of the computer. We wrote a short program to check whether the SODAR was alive and, if not, automatically reboot the computer.

- Obtain the expertise of specialists in metrology, meteorology, and acoustics. Get a meteorologist to evaluate the meteorological quantities. As in other fields of science, not all measurements in meteorology are valid, and some may represent something other than what they are expected to indicate.

5.3 Analysis-related considerations

Previous measurements on this scale were not found in the literature, and it was assumed that all the measurable quantities were equal in the analysis. In a new round of analysis, only the problematic quantities or phenomena should be subject to analysis, with the effect of turbulence being an example. The well-known phenomena, such as humidity, could be omitted from the analysis — provided that these have no effect on the variables subject to analysis.

The selection of models for explanatory variables in regression analysis was carried out by means of scoring, and all the frequencies were treated as equal (see Section 4.4). However, the highly significantly explanatory variables were different, for the most part, between the cases of excess attenuation at lower and at higher frequencies (see Table 4.1), and handling those frequency bands separately might have resulted in a set of more powerful regression models.

5.4 Future work

Another source of uncertainty, not covered specifically in this thesis, is the human response to noise. This particularly nonlinear interface is dependent on many variables, which are discussed in the field of psychoacoustics[213]. Environmental noise has not been a traditional area of research in the field of psychoacoustics, but that changed in the

2000s[214–218]. The answer to the fundamental question of why psychoacoustics should be involved in environmental acoustics can be demonstrated by way of a few common noise samples as examples: In Fig. 5.1, four environmental noise signals recorded from a port and a sinusoidal (a dial tone of a wired phone) have been adjusted to give the same A-weighted equivalent sound pressure level. Because of the frequency content of the signals, differences in the *loudness* of the signals are heard. Broadband sound (a fan) is perceived to be louder than a narrowband sound (a warning signal).

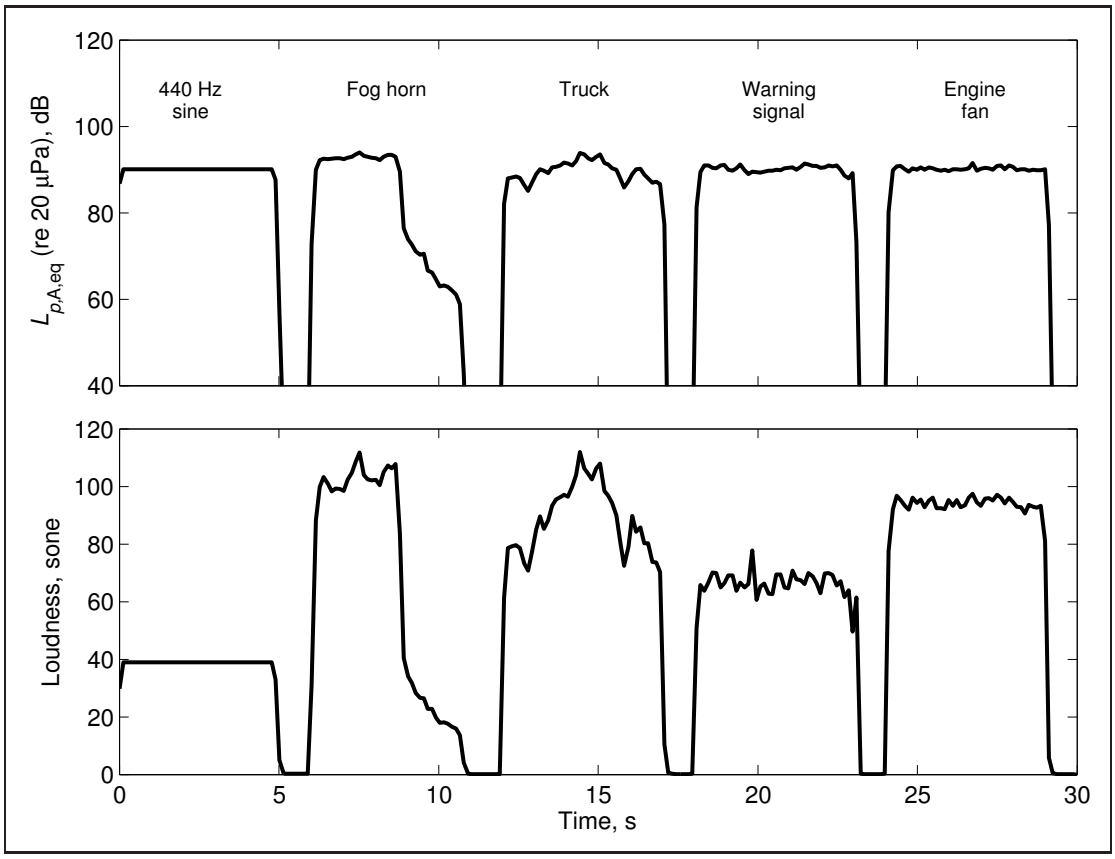

Fig. 5.1: Loudness and A-weighted sound pressure levels of various signals.

Loudness refers to a standardised[219], modern objective method of estimating how loud a sound is heard as being, and it has became a common method for evaluation of noise in many fields of noise engineering. A-weighting[72] is based on what was known about sensitivity of hearing in the 1930s but is still the most commonplace way to assess the effect of noise on humans. Even if loudness proved to be a much better approach than previous ones, it is not the best measurand of *annoyance*. For most noise sources, annoyance correlates with loudness, *sharpness*, and *roughness*[213]. There exist noise-source-specific annoyance models, also for sources of environmental noise[217, 220], but also more general objective measurands, such as unbiased annoyance (UBA), defined by Zwicker and Fastl[213, pp. 327 *ff*]. The uncertainty of an environmental noise assessment should be reflected in the annoyance descriptor, but, likewise, the uncertainty of the

annoyance descriptors should be summed to yield final uncertainty.

In future, the final outcome of an environmental noise assessment will be an annoyance map of an area, reported with the level of uncertainty. A complex environmental noise source could be assessed in the manner depicted in Fig. 5.2. Two major impediments to utilisation of better means for noise assessments, limited environmental data and computing power, will be resolved in the near future. It is obvious that the models will be developed to handle more details, in tandem with increases in computer capacity, and ability to collect more comprehensive environmental data is becoming a reality. When that day arrives, our ever-changing noisy environment will be simulated in the detail our senses provide. Until that day comes, there will be increasing demand for better and more relevant environmental noise measurements, and — maybe — development of statistical models based on the measurements.

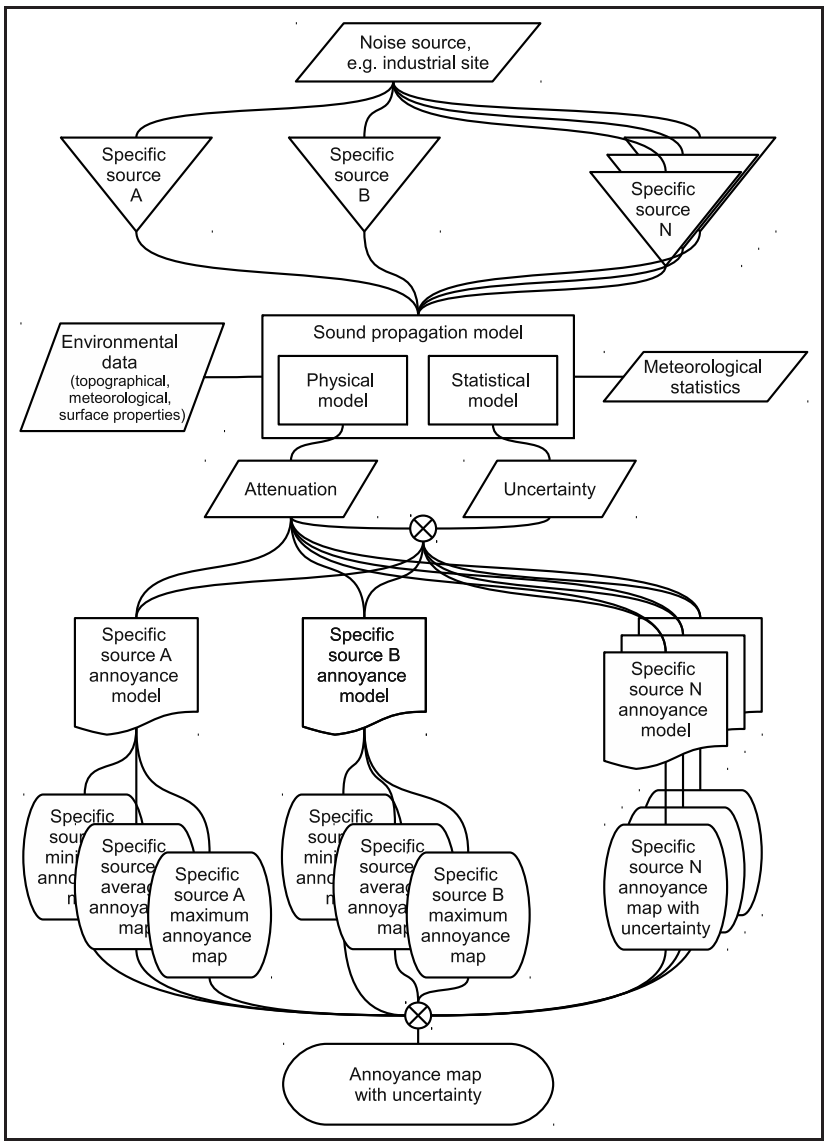

Fig. 5.2: An outline of a future noise mapping.

Chapter 6

Summary

LONG-RANGE environmental noise assessments can be carried out with known uncertainty by means of the approach presented in this thesis. The uncertainty in current computational models is based on a 'worst-case' scenario: the noise propagation occurs in the conditions wherein the noise is attenuated least, the so-called favourable condition. If the immission levels are overestimated, this may result in high additional costs for the operators and the industry, in the form of large buffer zones, costs of additional noise assessments and investments in noise-reduction actions, and even limited operation times. On the other hand, it has been found that there are environmental and meteorological conditions in which the calculation for favourable conditions yields lower immission levels than the real-world values. In these cases, a measurement-based statistical model gives a more relevant estimate, with known uncertainty limits.

The model described in this thesis takes environmental parameters or variables as input and returns an estimate of the uncertainty that meets the given condition. The variables may be simple, such as wind speed and direction, or more advanced ones — e.g., lapse rate and Pasquill index. More comprehensive and detail-level variables make the estimate of the uncertainty more appropriate.

Statistical analysis of simultaneous meteorological and sound propagation measurements form the core of this approach. Point-to-point measurements over a 3 km propagation path were carried out in a place where the terrain was quite homogenous and the topography was flat. A SODAR; multiple sonic anemometers, at different heights on a 50 m meteorological tower; weather balloon soundings; an automatic weather station; and synoptic observation provided meteorological data once an hour, around the clock, over a span of 20 months. Sound propagation data were validated with a frequency-dependent SNR detection algorithm, and excess attenuation was calculated from the measured sound data.

The medians of measured excess attenuation were found to fluctuate by 10 dB with the season of the year and by 15 dB as a function of time of day, and the total variation even reached 80 dB as a function of environmental conditions.

Many statistical tests were performed, and, of the more than 200 variables studied, 25 were selected for the statistical model. Most of the variables abandoned were collinear and correlated strongly with those selected.

Statistical analysis showed that the most important meteorological variables affecting excess attenuation were frequency-dependent. The most common frequency-dependency followed a cubic curve, but also quadratic curve, linear, and inverse dependencies were found.

Significant meteorological variables in explaining the excess attenuation are shown in Table 6.1. The enhancing tendencies — i.e., excess attenuation increases while the variable's value increases — are marked in green and with an upward arrow, while decreasing tendencies are indicated with red colour and a downward arrow. The value of the temperature gradient was the most important meteorological variable at most frequencies. Also, the effect of humidity is remarkable at frequencies above 200 Hz. Pasquill index was among the best explaining variables only for the lowest frequencies, though it achieved the best statistics for 500 Hz with an inverse behaviour.

Table 6.1: Highly significantly correlating meteorological variables for each frequency band

Hz	Explanatory variables
40	*lwspda*↓, *lwspdmax*↓, *pasq*↑, *gradthgt*↑, *gradt*↑, *spress*↑
80	*lwspda*↓, *lwspdmax*↓, *icldness*↓
160	*lwspdmax*↓, *lwspda*↓, *pasq*↑, *spress*↑, *snowd*↑, *idewpt*↓, *tempc*↓
200	*mtr*↑, *mtq*↑, *ihum*↓, *gradthgt*↓, *tempc*↑
250	*ihum*↓, *gradt*↓, *gradthgt*↓, *mtq*↑, *tempc*↑
315	*gradt*↓, *ihum*↓, *tempc*↑, *gradthgt*↓, *mtq*↑, *mtr*↑
400	*gradt*↓, *ihum*↓, *gradthgt*↓, *tempc*↑, *mtr*↑, *mtq*↑
500	*gradthgt*↓, *gradt*↓, *ihum*↓, *tempc*↑, *mtr*↑, *mtq*↑
630	*gradt*↓, *ihum*↓, *mu*↓, *mv*↑, *mtr*↑, *lvdira*↓
800	*gradt*↓, *ihum*↓, *lvdira*↓, *mu*↓, *gradt*↓, *mv*↑, *mintc*↓
1000	*gradt*↓, *ihum*↓, *mtq*↑, *mhf*↑, *mtr*↑, *mtp*↑, *mintc*↓
1250	*gradt*↓, *ihum*↓, *mhf*↑, *mtr*↑, *gradthgt*↓, *mtq*↑, *lvdira*↓
1600	*mhf*↑, *mtr*↑, *ihum*↓, *mtq*↑, *mtp*↑, *mintc*↓

gradt = max. temperature gradient
gradthgt = temperature gradient height
icldness = cloudiness
idewpt = dew point
ihum = humidity
lvdira = local wind direction, average
lwspda = local wind velocity, average
lwspdmax = max. wind velocity
mhf = sensible heat flux
mintc = minimum temperature
mtp = longitudinal turbulence intensity
mtq = transverse turbulence intensity
mtr = vertical turbulence intensity
mu = horizontal wind velocity
mv = vertical wind velocity
pasq = Pasquill index
snowd = snow depth
spress = surface pressure
tempc = surface temperature

6.1 Conclusions

The main findings of the thesis project are the following:

- A new approach for obtaining known uncertainty in noise assessments has been shown. The method introduces the effect of various meteorological variables on the magnitude and uncertainty in the long-range sound propagation. The procedure can be applied to the short-term measurements too.

- The most relevant meteorological parameters that should be taken into account in long-range noise assessments were determined. Also, new information on the interdependencies between the noise and meteorological variables were shown.

- The most important data items for long-range noise assessments are the vertical wind and temperature profiles, especially the magnitude of the temperature gradient and the height of the gradient.

- It was shown that some of the most complex meteorological variables, among them atmospheric turbulence, can be taken into account by statistical means.

- Changes in the sound speed profile and the stability condition of the atmosphere are responsible for the major sources of uncertainty.

- The measurement campaign yielded valuable information on the important meteorological parameters but also expertise in how to set up long-term sound propagation measurements.

- Comparison with two standardised noise modelling methods showed that the statistical model covers well a range of uncertainty not matched with the standardised methods.

- The measured excess attenuation fit well within the limits of the uncertainty predicted by the statistical model.

The objective of this research was to implement a statistical model with a competent sound propagation model, to make possible long-range noise assessments with a known level of uncertainty. Addressing changing environmental and atmospheric conditions is easy in the PE framework presented in this thesis. However, some of the condition models, such as those for turbulence, are not good enough. It was shown that the uncertainty arising from the models' deficiencies could be addressed with a combined or hybrid model of the sort proposed here.

A man with one watch knows what time it is;
a man with two watches is never quite sure.

—Lee Segall

A man with 100 watches
can calculate the uncertainty in his estimate of time.

—Panu Maijala

Appendix A

Variables and their description

In this appendix, the variables used in this thesis, the names, and their corresponding descriptions are shown. The naming of the sound variables is as follows: `{p or x}{frequency}ch{1 or 2}`, where the `p` element indicates excess attenuation in sound pressure and `x` refers to the equivalent sound pressure level. The number following `ch` is the channel (microphone) number. For example:
x80ch2 refers to excess attenuation in dB at 80 Hz, microphone R2.
p1000ch1 refers to excess attenuation in pascals at 1000 Hz, microphone R1.
The sound variables are not shown in the table below. In the regression analysis, also different exponent versions of the variables were used. The power was indicated with an extension, `p{1, 2, or 3}`: for example, humidity squared was *ihump2*. Also, inverse was marked with the extension `inv`; for example, the inverse of the Pasquill index was *pasqinv*.

Table A.1: Names of the variables and their description

Name	Description	Name	Description
cldhgt	Synop.: cloud altitude, code.	*cldhgt0*	0–49 m.
cldhgt1	50–99 m.	*cldhgt2*	100–199 m.
cldhgt3	200–299 m.	*cldhgt4*	300–599 m.
cldhgt5	600–999 m.	*cldhgt6*	1000–1499 m.
cldhgt7	1500–1999 m.	*cldhgt8*	2000–2499 m.
cldhgt9	2500 m or more, or cloudless.	*cldness*	Synop.: cloud cover, eighths.
curwea	Synop.: present weather (a major weather event within 3 hours), code.	*curwea0*	cloudless.
curwea1	Becoming clear.	*curwea10*	Mist, haze, not fog.
curwea14	Rain noticed, not reaching the ground.	*curwea15*	Raining noticed at over 5 km distance.
curwea16	Raining near but not at the observation point.	*curwea17*	Thunder but no rain.

Continued on next page

Table A.1 – continued from previous page

Name	Description	Name	Description
curwea2	No change in weather.	*curwea20*	Snowfall or drizzle that has just stopped.
curwea21	Rainfall (not freezing) that has just stopped.	*curwea22*	Snowfall that has just stopped.
curwea23	Sleet that has just stopped.	*curwea25*	Rain showers that have just stopped.
curwea26	Snow or sleet showers that have just stopped.	*curwea27*	Hail that has just stopped.
curwea29	Thunder that has just stopped.	*curwea3*	Getting cloudy.
curwea40	Fog noticed.	*curwea44*	Fog detected (the sky is visible).
curwea45	Fog (the sky is not visible).	*curwea46*	Fog (the sky is visible), thickening.
curwea47	Fog (the sky is not visible), thickening.	*curwea50*	Intermittent light drizzle, not freezing.
curwea51	Continuous light drizzle, not freezing.	*curwea53*	Intermittent moderate drizzle, not freezing.
curwea56	Light freezing drizzle.	*curwea58*	Light rain.
curwea59	Moderate to heavy rain.	*curwea60*	Occasional light rain, not freezing.
curwea61	Continuous light rain, not freezing.	*curwea62*	Intermittent moderate rain, not freezing.
curwea63	Continuous moderate rain, not freezing.	*curwea65*	Continuous heavy rain, not freezing.
curwea68	Light snow drizzle.	*curwea69*	Moderate snow drizzle.
curwea70	Light intermittent snowfall.	*curwea71*	Light continuous snowfall.
curwea73	Continuous moderate snowfall.	*curwea76*	Ice prism (with or without fog).
curwea77	Snowfall.	*curwea78*	Star-shaped snowflakes.
curwea80	Light rain showers.	*curwea81*	Heavy rain showers.
curwea85	Light snow showers.	*curwea86*	Heavy snow showers.
curwea91	Light rain, thunderstorm just finished.	*curwea95*	Thunderstorms and rain or snow. No granules.
curwea96	Thunderstorms and hail.	*curwea97*	Violent thunderstorms and rain, not hail.
curwea99	Violent thunderstorms and hail.	*date*	Date.
datetime	Date and time.	*delays*	Sound propagation delay, ms.
dewpt	Synop.: dew point, °C.	*gndtype*	Soil quality, code.
gndtype0	Ground dry (vegetation can be moist).	*gndtype1*	Ground moist.
gndtype2	Puddles on the ground.	*gndtype3*	Ground frozen or ice on the surface.
gndtype4	Open areas bare, snow in the forests.	*gndtype5*	Ground less than half covered with snow.
gndtype6	Ground more than half covered with snow.	*gndtype7*	Ground surface completely covered with hard-packed snow.
gndtype8	Ground more than half covered with dry and light snow.	*gndtype9*	Ground fully covered in light snow.
gradt	Sounding: max. temperature gradient below 1 km altitude, °C/km.	*gradthgt*	Sounding: temperature gradient height, m.

Continued on next page

Table A.1 – continued from previous page

Name	Description	Name	Description
gtemp	Synop.: temperature at 0 m or snow surface, °C.	*hicldt*	Synop.: high cloud class, code.
hicldt0	No high clouds.	*hicldt1*	Straddling cirrus clouds.
hicldt10	High clouds cannot be detected.	*hicldt2*	Dense plate-like cirrus clouds.
hicldt3	Block anvil-like cirrus clouds.	*hicldt4*	Fibrous cirrus clouds.
hicldt5	Cirrus and cirrostratus, less than half of the sky.	*hicldt6*	Cirrus and cirrostratus, more than half of the sky.
hicldt7	Cirrostratus clouds filling the sky.	*hicldt8*	Cirrostratus clouds not increasing.
hicldt9	Mostly cirrocumulus.	*hum*	Synop.: relative humidity, %.
icldhgt	Weather station: cloud altitude, m.	*icldness*	Weather station: cloud cover, eighths.
icurwea	Weather station: present weather, code.	*idewpt*	Weather station: dew point, °C.
igtemp	Weather station: temperature at 0 m or snow surface, °C.	*ihum*	Weather station: relative humidity, %.
ihumb	Weather station: moist / not moist (1/0).	*irainb*	Weather station: rain / no rain (1/0).
irainf	Weather station: rainfall, mm.	*ispress*	Weather station: surface pressure, hPa.
isunb	Weather station: sunshine / no sunshine (1/0).	*itempc*	Weather station: temperature at 2 m, °C.
ivisib	Weather station: visibility, m.	*ivisibp*	Weather station: prev. visibility, m.
iwindir	Weather station: wind direction (0–360), °.	*iwmax*	Weather station: max. wind speed, m/s.
iwspd	Weather station: wind speed, m/s.	*locldt*	Synop.: low cloud class, code.
locldt0	No low clouds.	*locldt1*	Low cumulus.
locldt10	Low clouds cannot be identified.	*locldt2*	High cumulus.
locldt3	Thunderclouds.	*locldt4*	Cumulus, wide form. Stratocumulus clouds.
locldt5	Stratocumulus clouds.	*locldt6*	Uniform stratus.
locldt7	Ragged stratus or cumulus clouds.	*locldt8*	Cumulus or stratocumulus clouds.
locldt9	Rain-shower clouds or thunderclouds.	*lvtmp*	Local virtual temperature (10 min average), °C.
lwdira	Local mean wind direction (10 min average), °.	*lwdirstd*	Local wind direction standard deviation, °.
lwspda	Local mean wind speed (10 min average), m/s.	*lwspdmax*	Local wind speed max. value (last 10 min), m/s.
lwspdstd	Local wind speed (10 min average), standard deviation, m/s.	*maxtc*	Synop.: max. temperature at 2 m, °C.
mdir	Metek: mean horizontal wind direction (0–360), °.	*mhf*	Metek: sensible heat flux, an integer from −200 to +700.
micldt	Synop: middle cloud class, code.	*micldt0*	No middle clouds.
micldt1	Transparent curtain clouds.	*micldt10*	Middle clouds cannot be identified.
micldt2	Curtain or rain clouds.	*micldt3*	Altocumulus clouds.

Continued on next page

Table A.1 – continued from previous page

Name	Description	Name	Description
micldt4	Block anvil-like altocumulus clouds.	*micldt5*	Thick altocumulus clouds.
micldt6	Cumulus become altocumulus clouds.	*micldt7*	Dense altocumulus clouds.
micldt8	Altocumulus clouds with tower-like projections.	*micldt9*	Altocumulus clouds at different altitudes.
mintc	Synop.: min. temperature at 2 m, °C.	*mmos*	Metek: Monin–Obukhov stability parameter, 1/m.
monthno	Month number, 1–12.	*mpsig*	Metek: standard deviation of the wind component parallel to the mean wind direction, m/s.
mqsig	Metek: standard deviation of the wind component horizontally perpendicular to the mean wind direction, m/s.	*mrsig*	Metek: standard deviation of the wind component vertically perpendicular to the mean wind direction, m/s.
msdq	Metek: quality of the measurement (normally 100).	*mt*	Metek: temperature at 48 m, °C.
mtp	Metek: longitudinal turbulence intensity.	*mtq*	Metek: transverse turbulence intensity.
mtr	Metek: vertical turbulence intensity.	*mu*	Metek: mean west–east wind component, m/s.
mustar	Metek: friction velocity, m/s.	*mv*	Metek: mean south–north wind component, m/s.
mvel	Metek: mean horizontal wind velocity, m/s.	*mw*	Metek: mean vertical wind component, m/s.
oldwea	Synop.: preceding the previous weather, code.	*pasq*	Pasquill stability class.
pasq1	Very unstable boundary layer, convection dominant.	*pasq2*	Unstable boundary layer.
pasq3	Almost neutral boundary layer.	*pasq4*	Neutral boundary layer.
pasq5	Almost stable boundary layer.	*pasq6*	Stable boundary layer.
prewea	Synop.: previous weather (see the definition of 'curwea'), code.	*rainf*	Synop.: rainfall, mm.
rainp	Synop.: rain period, hours.	*snowd*	Synop.: snow depth, cm.
spdelta	Synop.: surface pressure change, hPa.	*spress*	Synop.: surface pressure, hPa.
srcvwdir	Wind contribution — see Eq. 4.1.	*tempc*	Synop.: temperature at 2 m, °C.
tend	Synop.: surface pressure tendency.	*time*	Time.
timestmp	Timestamp (yyyymmddHHMM).	*visib*	Synop.: visibility, m.
wdir1km	Sounding: mean wind direction below 1 km altitude (0–360), °.	*wdirstd*	Sounding: wind direction standard deviation below 1 km altitude (0–360), °.
weekno	Week number, 1–53.	*windir*	Synop.: wind direction (0–360), °.
wmax	Synop.: max. wind speed, m/s.	*wspd*	Synop.: wind speed, m/s.

Appendix B

Statistical figures

In this appendix, some descriptive statistics for the most important variables represented in this thesis are shown. The most complete presentation of the statistics can be found in the original report on the Atmosaku software[30].

All statistics presented here are based on the measurements carried out between 13 March 2004 and 14 November 2005. The sound statistics are based on audio data recorded via microphone R1. Microphone R1 was the highest microphone in the antenna, and it shared its height with the acoustic anemometer (see Fig. 3.8). Microphone R2 was 80 cm lower. There were no significant differences in descriptive statistics between the microphones.

B.1 Sound variables

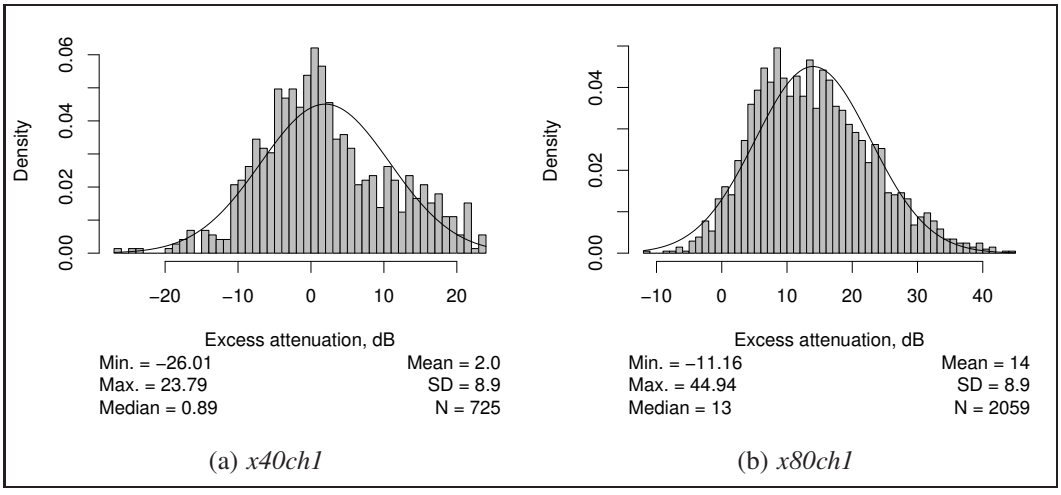

(a) *x40ch1* (b) *x80ch1*

Fig. B.1: Histograms for the variables *x40ch1* and *x80ch1*.

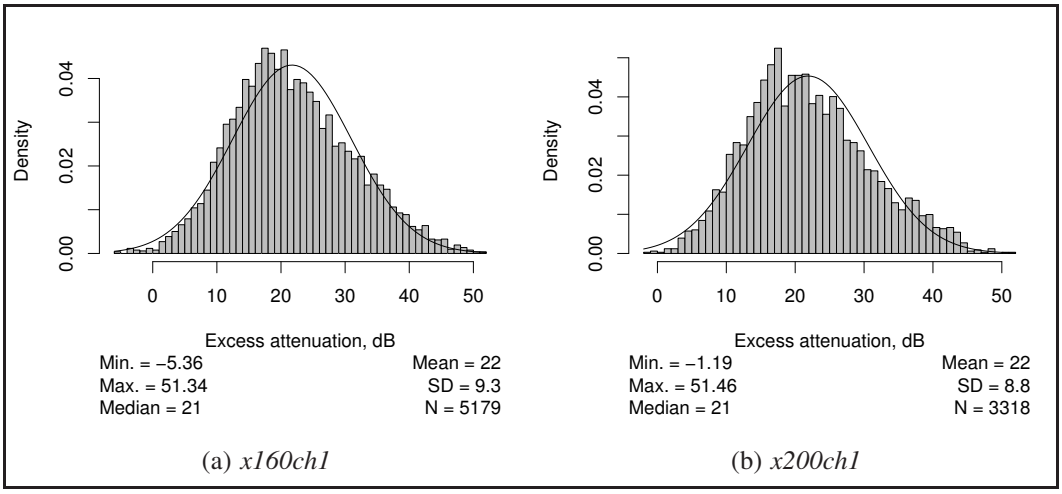

(a) *x160ch1* (b) *x200ch1*

Fig. B.2: Histograms for the variables *x160ch1* and *x200ch1*.

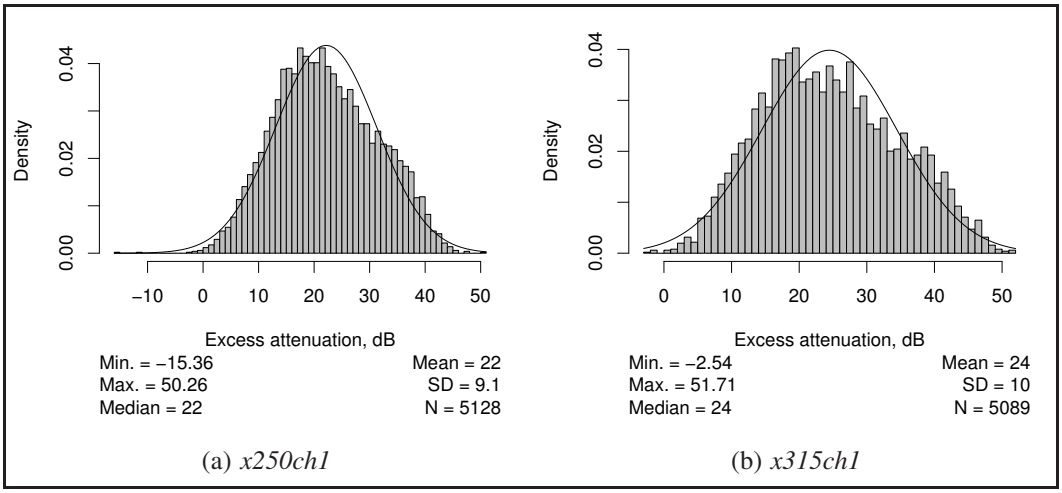

(a) *x250ch1* (b) *x315ch1*

Fig. B.3: Histograms for the variables *x250ch1* and *x315ch1*.

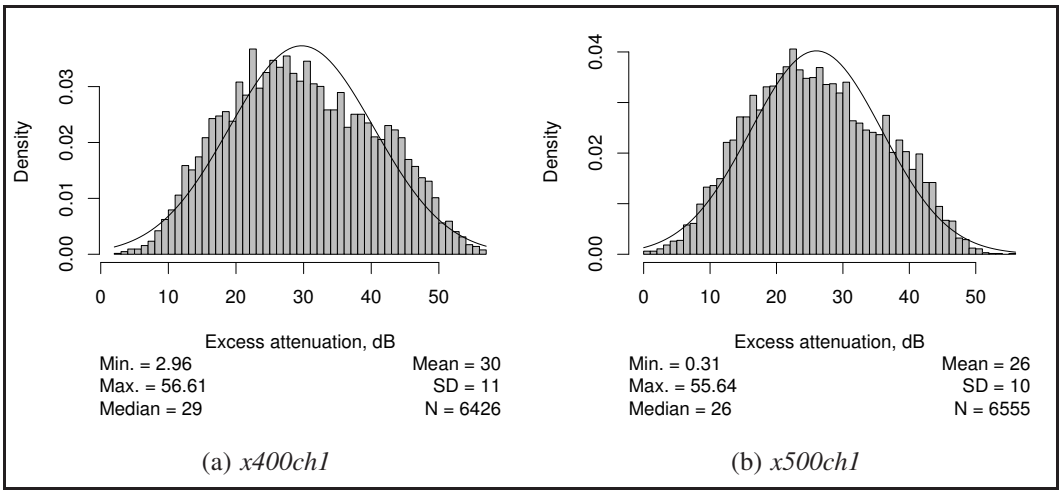

(a) *x400ch1* (b) *x500ch1*

Fig. B.4: Histograms for the variables *x400ch1* and *x500ch1*.

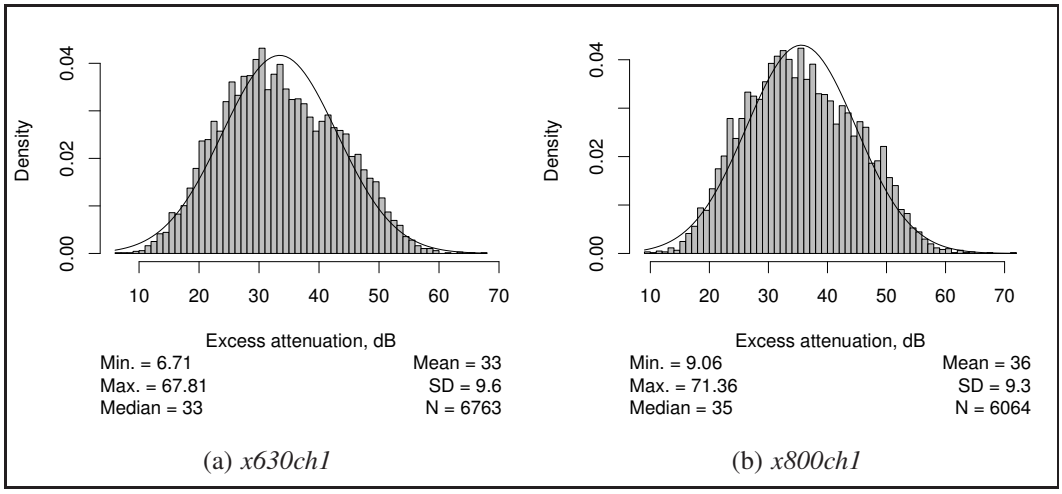

(a) *x630ch1* (b) *x800ch1*

Fig. B.5: Histograms for the variables *x630ch1* and *x800ch1*.

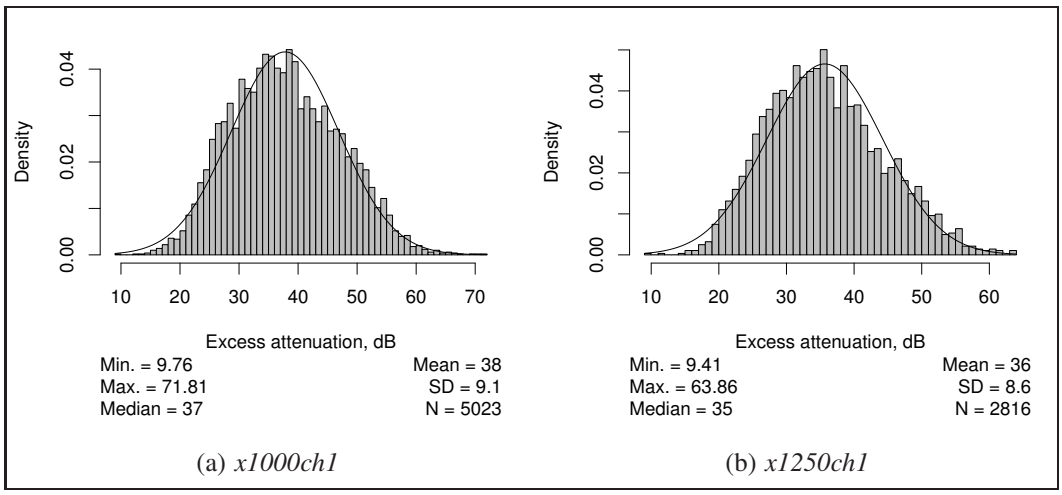

(a) *x1000ch1* (b) *x1250ch1*

Fig. B.6: Histograms for the variables *x1000ch1* and *x1250ch1*.

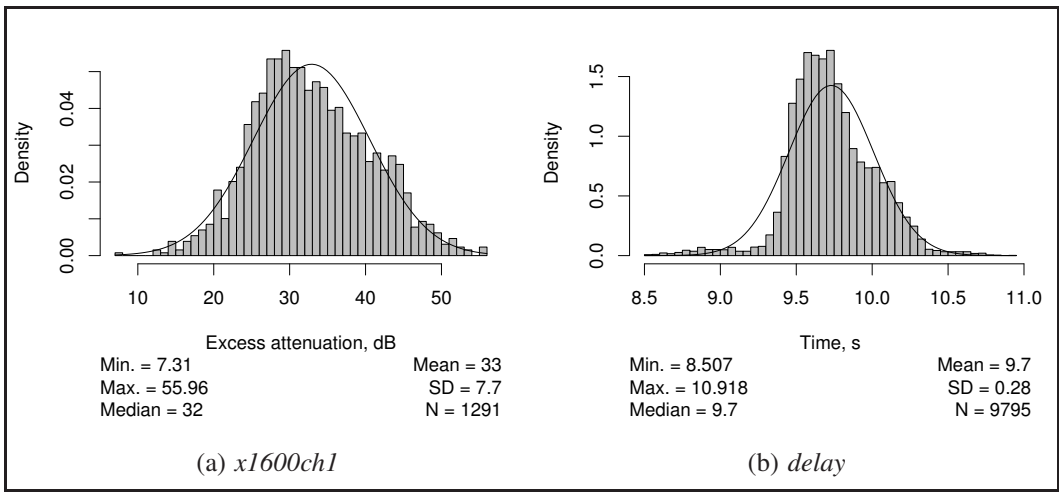

(a) *x1600ch1* (b) *delay*

Fig. B.7: Histograms for the variables *x1600ch1* and *delay*.

B.2 Weather variables

The frequency distribution figures are sorted in alphabetical order here.

In the calculation of frequency distributions for the temperature gradient heights (variable *gradthgt*; see Fig. B.10), heights below 200 m were discarded because of the technical issues in the sounding procedure[1]. Also, if the temperature did not increase in three or more calculation segments, *gradthgt* was marked as zero (no inversion).

Table B.1: Weather events during the study and their percentage shares ('No change in weather' events are changed to refer to the preceding weather event; see Section 4.3)

Description	Frequency	Percentage	% (valid)
Cloudless.	12	.1	.1
Becoming clear.	2775	18.9	23.8
Getting cloudy.	2445	16.6	21.0
Mist, haze, not fog.	504	3.4	4.3
Rain noticed, not reaching the ground.	33	.2	.3
Raining noticed at over 5 km distance.	48	.3	.4
Raining near but not at the observation point.	63	.4	.5
Thunder but no rain.	18	.1	.2
Snowfall or drizzle that has just stopped.	117	.8	1.0
Rainfall (not freezing) that has just stopped.	291	2.0	2.5
Snowfall that has just stopped.	150	1.0	1.3
Sleet that has just stopped.	33	.2	.3
Rain showers that have just stopped.	399	2.7	3.4
Snow or sleet showers that have just stopped.	60	.4	.5
Hail that has just stopped.	9	.1	.1
Thunder that has just stopped.	18	.1	.2
Fog noticed.	21	.1	.2
Fog detected (the sky is visible).	6	.0	.1
Fog (the sky is not visible).	12	.1	.1
Fog (the sky is visible), thickening.	6	.0	.1
Fog (the sky is not visible), thickening.	3	.0	.0
Intermittent light drizzle, not freezing.	39	.3	.3
Continuous light drizzle, not freezing.	297	2.0	2.5
Intermittent moderate drizzle, not freezing.	6	.0	.1
Light freezing drizzle.	36	.2	.3
Light rain.	69	.5	.6
Moderate to heavy rain.	18	.1	.2
Occasional light rain, not freezing.	111	.8	1.0
Continuous light rain, not freezing.	768	5.2	6.6
Intermittent moderate rain, not freezing.	18	.1	.2
Continuous moderate rain, not freezing.	198	1.3	1.7
Continuous heavy rain, not freezing.	6	.0	.1
Light snow drizzle.	150	1.0	1.3

Continued on next page

[1] The first altitude registered in balloon soundings is typically between 150 and 190 metres.

Table B.1 – continued from previous page

Description	Frequency	Percentage	% (valid)
Moderate snow drizzle.	6	.0	.1
Light intermittent snowfall.	48	.3	.4
Light continuous snowfall.	1314	8.9	11.3
Continuous, moderate snowfall.	174	1.2	1.5
Ice prism (with or without fog).	129	.9	1.1
Snowfall.	468	3.2	4.0
Star-shaped snowflakes.	219	1.5	1.9
Light rain showers.	345	2.3	3.0
Heavy rain showers.	48	.3	.4
Light snow showers.	102	.7	.9
Heavy snow showers.	3	.0	.0
Light rain, thunderstorm just finished.	3	.0	.0
Thunderstorms and rain or snow. No granules.	63	.4	.5
Observations	11,661	79.4	
Missing	3027	20.6	
Total	14,688	100.0	

Table B.2: Wind statistics for the data from an altitude of 22 m, from 13 March 2004 to 14 November 2005 (calm winds 2.9%)

	N	NNE	NE	ENE	E	ESE	SE	SSE
m/s					%			
0–3	4.4	2.7	2.9	2.4	3.3	4.2	6.6	8.1
3–6	1.7	1.6	1.0	0.6	1.0	1.4	3.2	2.1
6–9	0.0	0.0	0.0	0.0	0.0	0.0	0.0	0.2
9–	0.0	0.0	0.0	0.0	0.0	0.0	0.0	0.0
	S	SSW	SW	WSW	W	WNW	NW	NNW
m/s					%			
0–3	5.6	3.7	3.1	2.2	2.2	4.0	4.1	3.9
3–6	5.0	3.8	2.2	1.6	1.4	1.2	1.4	2.0
6–9	0.6	0.8	0.2	0.1	0.3	0.2	0.0	0.1
9–	0.0	0.0	0.0	0.0	0.0	0.0	0.0	0.0

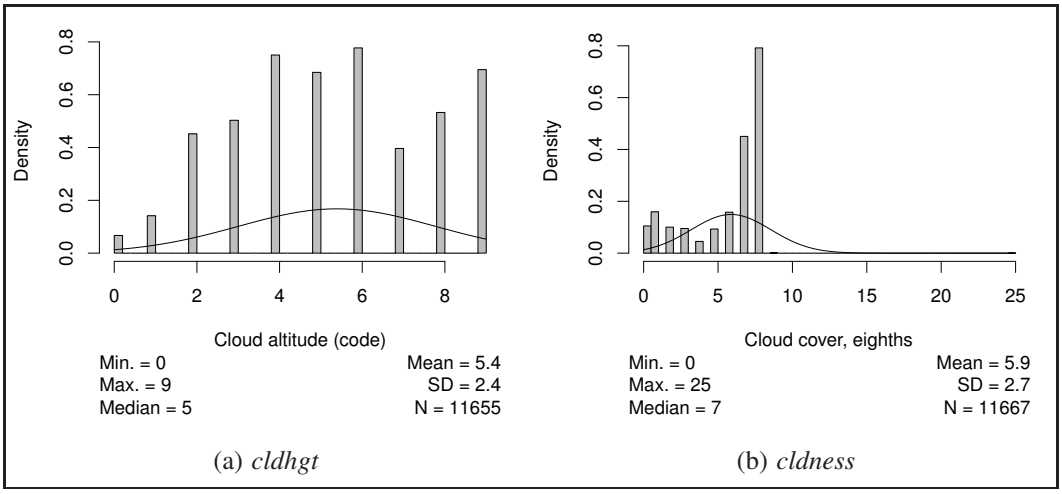

(a) *cldhgt* (b) *cldness*

Fig. B.8: Histograms for the variables *cldhgt* and *cldness*.

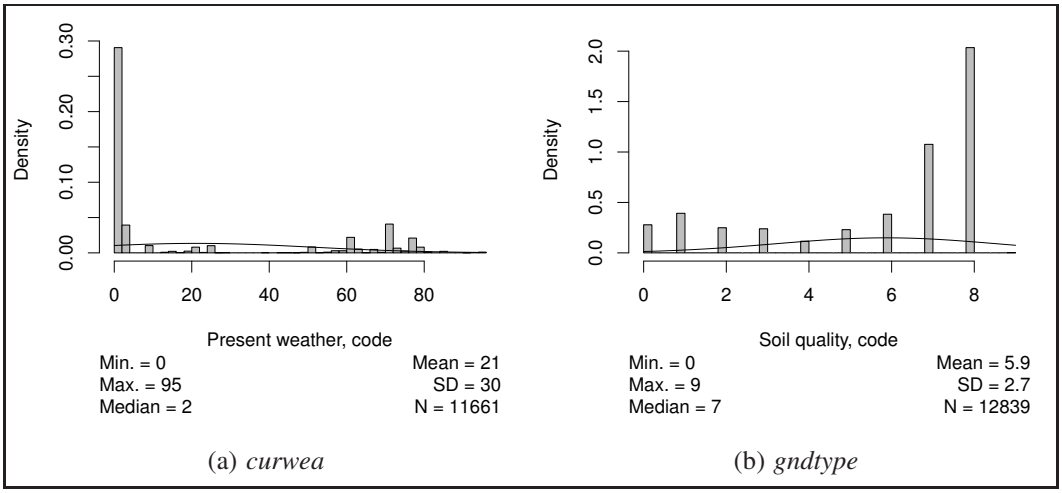

(a) *curwea* (b) *gndtype*

Fig. B.9: Histograms for the variables *curwea* and *gndtype*.

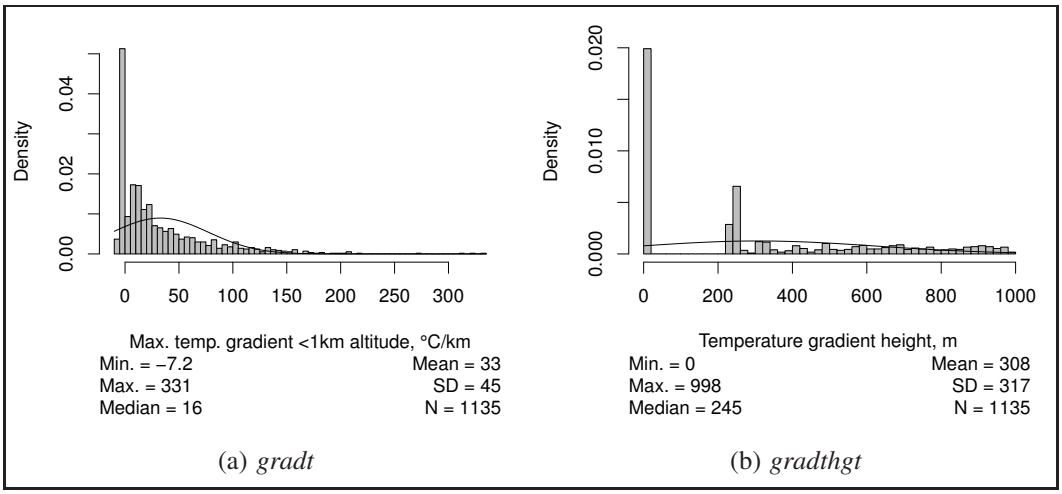

(a) *gradt* (b) *gradthgt*

Fig. B.10: Histograms for the variables *gradt* and *gradthgt*.

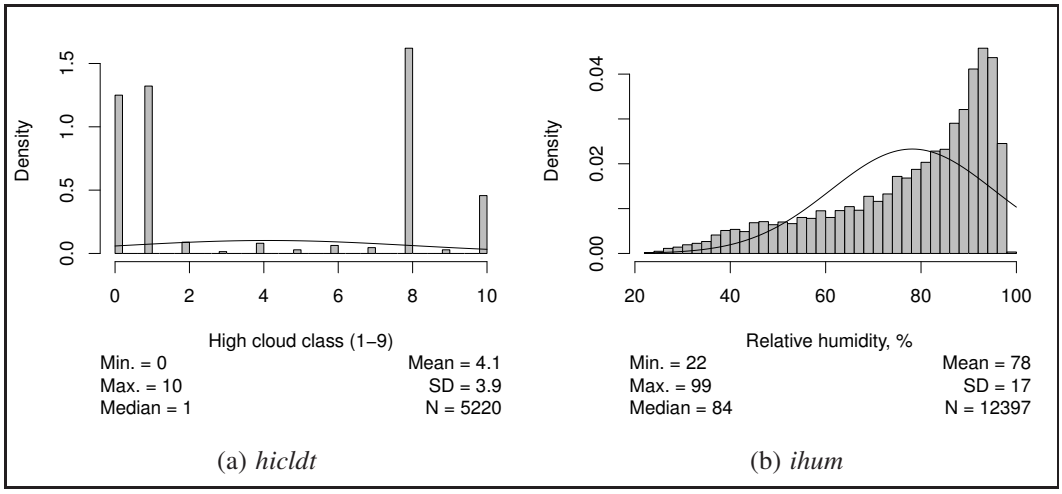

(a) *hicldt* (b) *ihum*

Fig. B.11: Histograms for the variables *hicldt* and *ihum*.

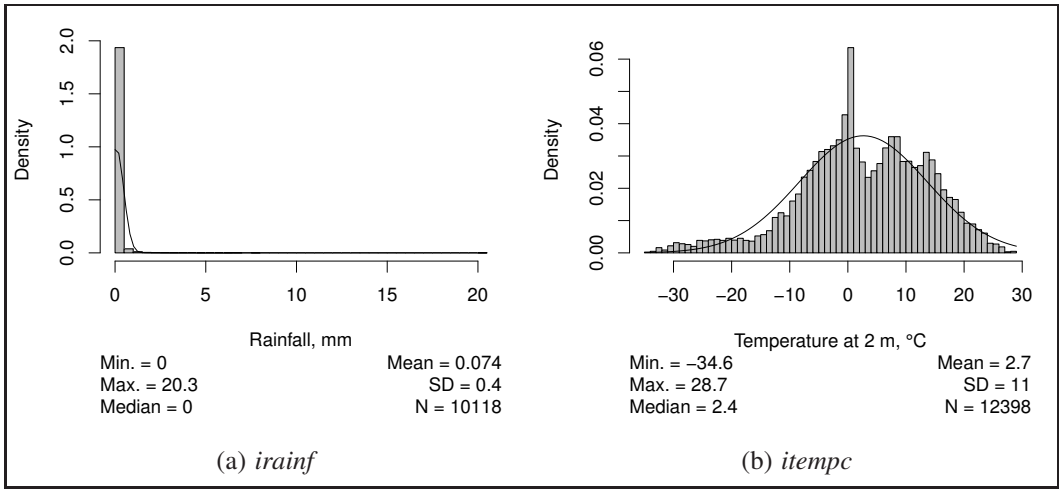

(a) *irainf* (b) *itempc*

Fig. B.12: Histograms for the variables *irainf* and *itempc*.

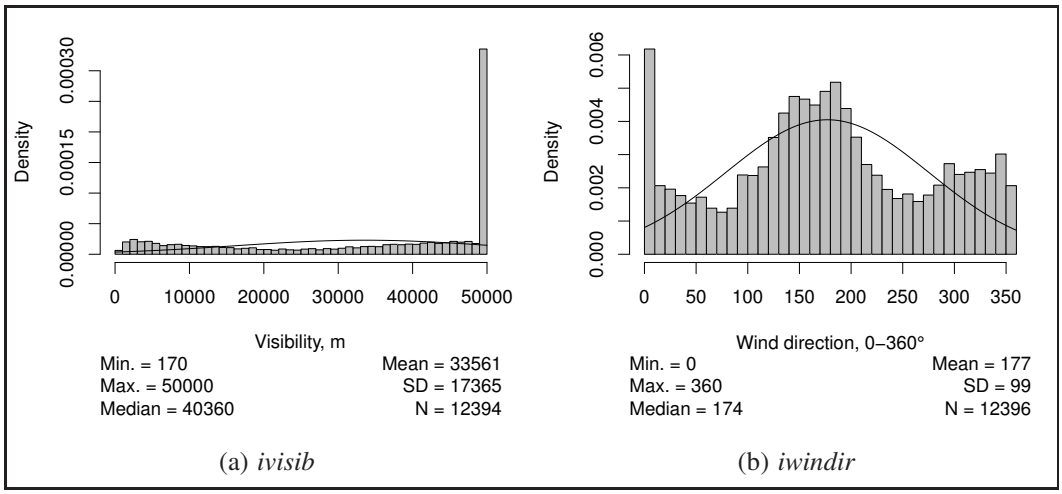

(a) *ivisib* (b) *iwindir*

Fig. B.13: Histograms for the variables *ivisib* and *iwindir*.

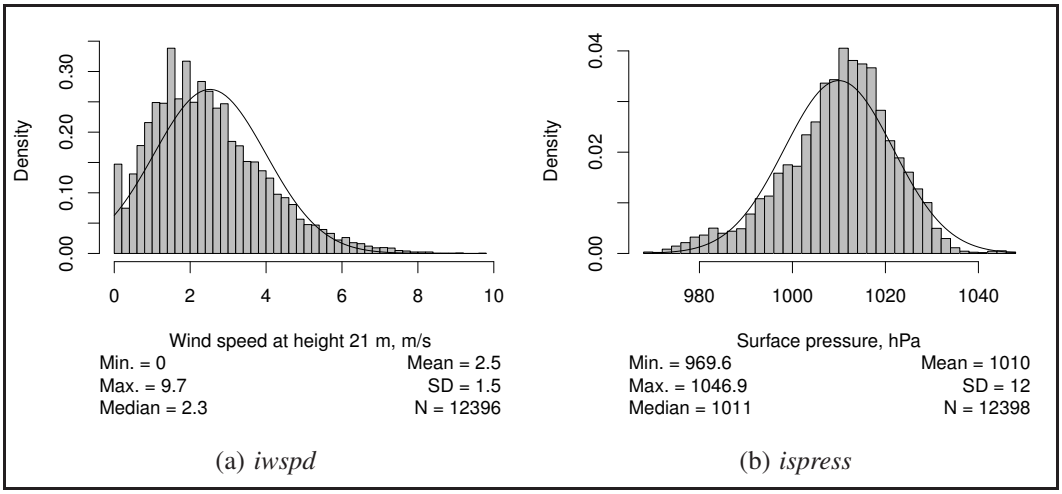

(a) *iwspd* (b) *ispress*

Fig. B.14: Histograms for the variables *iwspd* and *ispress*.

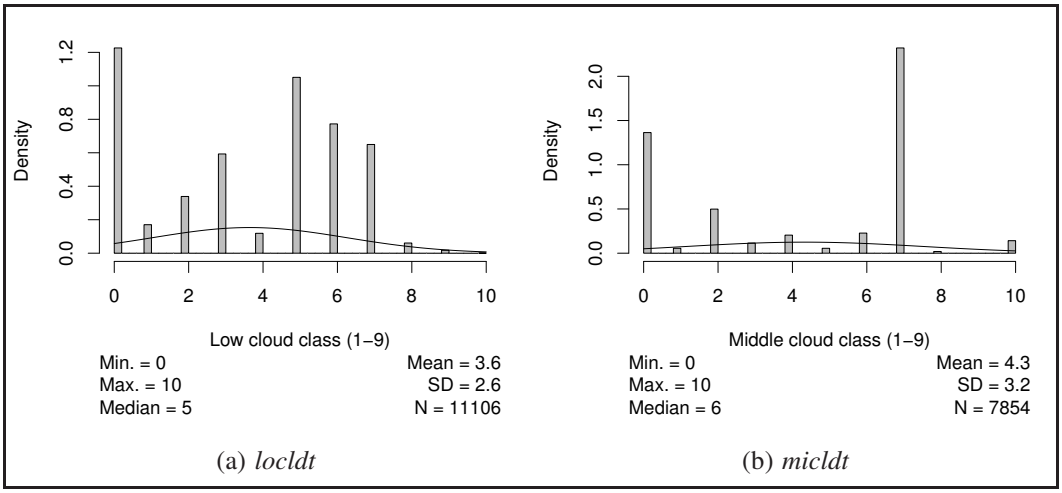

(a) *locldt* (b) *micldt*

Fig. B.15: Histograms for the variables *locldt* and *micldt*.

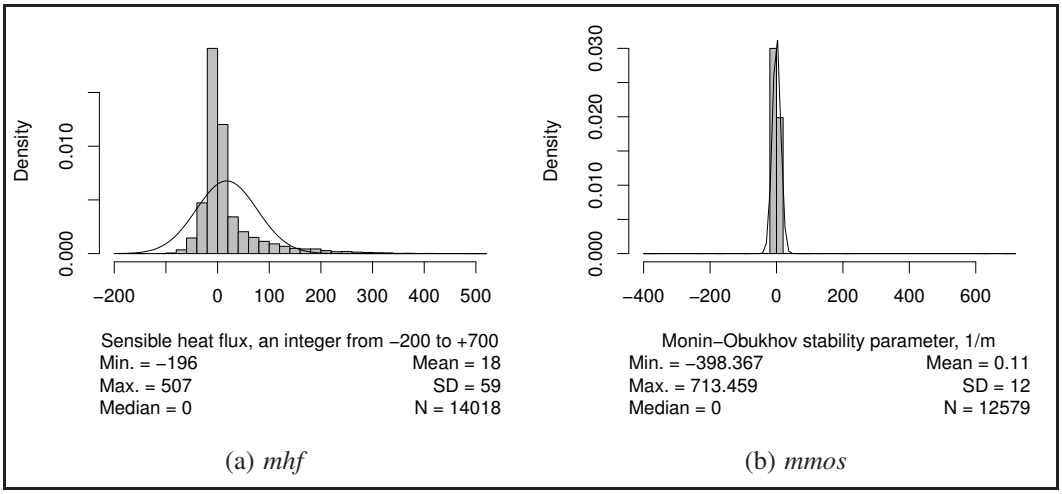

(a) *mhf* (b) *mmos*

Fig. B.16: Histograms for the variables *mhf* and *mmos*.

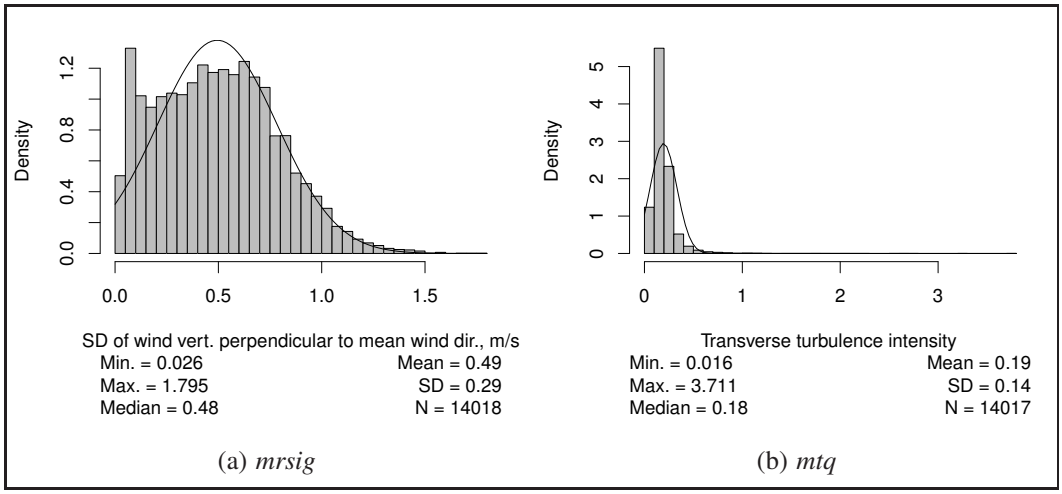

(a) *mrsig* (b) *mtq*

Fig. B.17: Histograms for the variables *mrsig* and *mtq*.

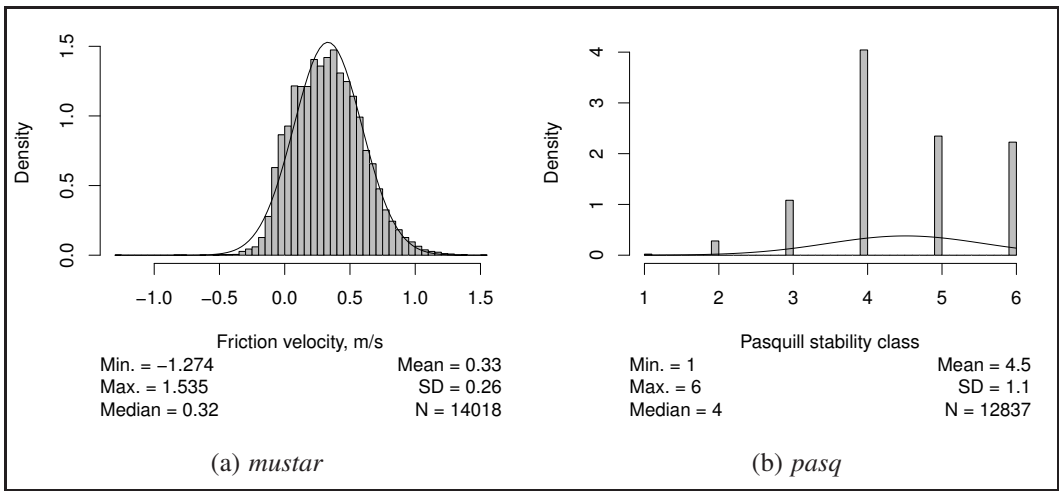

(a) *mustar* (b) *pasq*

Fig. B.18: Histograms for the variables *mustar* and *pasq*.

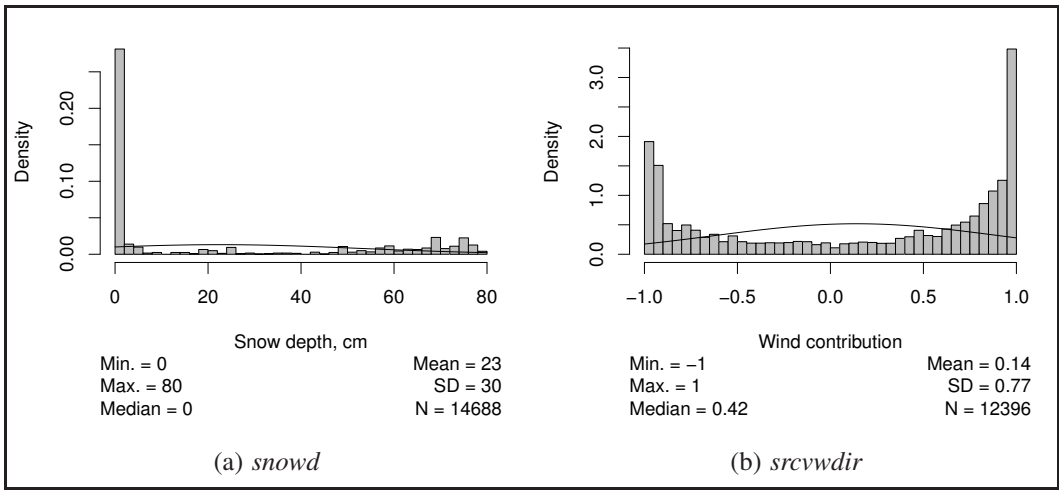

(a) *snowd* (b) *srcvwdir*

Fig. B.19: Histograms for the variables *snowd* and *srcvwdir*.

B.3 Linear correlation

Table B.3: Linear dependencies between the variable *delay* and explanatory variables, with $p < 0.05$ (the variable name is in boldface if the correlation coefficient exceeds 0.5)

Variable	Correlation coefficient	Variable	Correlation coefficient
tend	$0.035(**)$	*spdelta*	$-0.074(***)$
tempc	$-0.575(***)$	***gtemp***	$-0.549(***)$
maxtc	$-0.583(***)$	***mintc***	$-0.570(***)$
dewpt	$-0.514(***)$	*hum*	$0.281(***)$
windir	$-0.101(***)$	*rainf*	$-0.052(***)$
snowd	$0.375(***)$	*cldness*	$0.027(*)$
locldt	$0.091(***)$	*micldt*	$-0.062(***)$
hicldt	$0.109(***)$	*cldhgt*	$-0.075(***)$
visib	$-0.189(***)$	*curwea*	$0.182(***)$
prewea	$0.071(***)$	*oldwea*	$0.144(***)$
pasq	$0.276(***)$	*gradthgt*	$0.242(***)$
gradt	$0.367(***)$	*lwspda*	$-0.041(***)$
lwdira	$-0.187(***)$	*lwspdmax*	$-0.036(***)$
lwspdstd	$-0.103(***)$	*lwdirstd*	$-0.148(***)$
lvtmp	$-0.589(***)$	*msdq*	$-0.064(***)$
mt	$-0.595(***)$	*mpsig*	$-0.071(***)$
mqsig	$-0.100(***)$	*mrsig*	$-0.122(***)$
mtp	$-0.104(***)$	*mtq*	$-0.104(***)$
mtr	$-0.144(***)$	*mustar*	$-0.076(***)$
mhf	$-0.177(***)$	*mu*	$-0.139(***)$
mv	$0.361(***)$	*mw*	$0.150(***)$
mvel	$0.023(*)$	*mdir*	$-0.057(***)$
ispress	$-0.023(*)$	***itempc***	$-0.583(***)$
idewpt	$-0.570(***)$	*ihum*	$0.246(***)$
iwindir	$-0.072(***)$	*iwmax*	$-0.033(**)$
irainf	$-0.054(***)$	*icldness*	$-0.215(***)$
icldhgt	$-0.174(***)$	*ivisib*	$-0.172(***)$
icurwea	$0.176(***)$	*iwindir*	$-0.072(***)$
iwmax	$-0.033(**)$	*irainf*	$-0.054(***)$
icldness	$-0.215(***)$	*icldhgt*	$-0.174(***)$
ivisib	$-0.172(***)$	*icurwea*	$0.176(***)$

*** Statistically highly significant (level of significance 0.001).

** Statistically significant (level of significance 0.01).

* Statistically almost significant (level of significance 0.05).

Table B.4: Bilateral correlations between 'p' variables (microphone R1)

	p40ch1	*p80ch1*	*p160ch1*	*p200ch1*	*p250ch1*	*p315ch1*	*p400ch1*	*p500ch1*	*p630ch1*	*p800ch1*	*p1000ch1*	*p1250ch1*	*p1600ch1*
p40ch1	1.000	.768(**)	.803(**)	.953(**)	.929(**)	.145(**)	.919(**)	.912(**)	.874(**)	.891(**)	.926(**)	.264(**)	.305(**)
p80ch1	.768(**)	1.000	.738(**)	.804(**)	.704(**)	.262(**)	.655(**)	.660(**)	.674(**)	.703(**)	.731(**)	.358(**)	.553(**)
p160ch1	.803(**)	.738(**)	1.000	.845(**)	.824(**)	.387(**)	.804(**)	.811(**)	.803(**)	.806(**)	.816(**)	.270(**)	.305(**)
p200ch1	.953(**)	.804(**)	.845(**)	1.000	.991(**)	.848(**)	.978(**)	.980(**)	.981(**)	.972(**)	.963(**)	.593(**)	.606(**)
p250ch1	.929(**)	.704(**)	.824(**)	.991(**)	1.000	.934(**)	.982(**)	.985(**)	.966(**)	.967(**)	.958(**)	.589(**)	.614(**)
p315ch1	.145(**)	.262(**)	.387(**)	.848(**)	.934(**)	1.000	.925(**)	.900(**)	.828(**)	.722(**)	.573(**)	.550(**)	.548(**)
p400ch1	.919(**)	.655(**)	.804(**)	.978(**)	.982(**)	.925(**)	1.000	.993(**)	.940(**)	.920(**)	.942(**)	.541(**)	.493(**)
p500ch1	.912(**)	.660(**)	.811(**)	.980(**)	.985(**)	.900(**)	.993(**)	1.000	.964(**)	.942(**)	.952(**)	.603(**)	.533(**)
p630ch1	.874(**)	.674(**)	.803(**)	.981(**)	.966(**)	.828(**)	.940(**)	.964(**)	1.000	.975(**)	.961(**)	.630(**)	.540(**)
p800ch1	.891(**)	.703(**)	.806(**)	.972(**)	.967(**)	.722(**)	.920(**)	.942(**)	.975(**)	1.000	.981(**)	.743(**)	.584(**)
p1000ch1	.926(**)	.731(**)	.816(**)	.963(**)	.958(**)	.573(**)	.942(**)	.952(**)	.961(**)	.981(**)	1.000	.882(**)	.681(**)
p1250ch1	.264(**)	.358(**)	.270(**)	.593(**)	.589(**)	.550(**)	.541(**)	.603(**)	.630(**)	.743(**)	.882(**)	1.000	.813(**)
p1600ch1	.305(**)	.553(**)	.305(**)	.606(**)	.614(**)	.548(**)	.493(**)	.533(**)	.540(**)	.584(**)	.681(**)	.813(**)	1.000

** Statistically significant (level of significance 0.01, two-tailed).

* Statistically almost significant (level of significance 0.05, two-tailed).

B.4 The choice of the explanatory variables

Table B.5: The abandoned variables that correlate strongly with some chosen variables

Chosen variable	Strongly correlating (abandoned) variables
iwspd	*wspd*, *mvel*, *mu*, *mv*, *mw*, *wmax*, *iwmax*, *lwspda*, *lwspdmax*
itempc	*tempc*, *maxtc*, *mintc*, *mt*, *gtemp*, *lvtmp*, *idewpt*, *dewpt*
srcvwdir	*iwindir*, *windir*, *mdir*, *wdir1km*, *wdirstd*, *lwdira*
curwea	*icurwea*, *oldwea*, *prewea*
ispress	*spress*
ihum	*hum*
cldhgt	*icldhgt*
cldness	*icldness*
ivisib	*visib*
irainf	*rainf*
mtq	*mtp*, *mtr*
mrsig	*mpsig*, *mqsig*
weekno	*monthno*

Table B.6: The scoring for the explanatory variables (see Section 4.4)

Variable	LIN	LOG	INV	QUA	CUB	COM	POW	S	GRO	EXP	LGS
cldhgt	8			1	12	5					
iwspd	10			2	13	1					
itempc	8			4	11					2	1
srcvwdir					26						
ispress	8		2		16						
ihum			8		18						
cldness	12			3	11						
ivisib				7	19						
*irainf**	6			20							
mtq	8				18						
mrsig				19	7						
gradt	6			14	6						
gradthgt	9			14	3						
mhf	10				16						
mmos	2			18	6						
mustar	2		1	23							
pasq	3	1	17	5							
*snowd***	3			4	15	4					
time					26						
weekno	2	2	2	7	13						

* QUA and CUB are identical in some cases; the points are assigned to QUA (see Section 4.4).

** COM, GRO, and EXP are identical in some cases; the points are assigned to COM (see Section 4.4).

Appendix C

Results of the regression analysis

In this appendix, a summary of the regression analysis rounds for microphone R1 is shown. The most complete presentation of the analysis can be found in the original report for the Atmosaku software[30].

C.1 Excess attenuation, 'x' variables

Table C.1: Results of regression analysis with different elimination methods for the logarithmic excess attenuation variables, based on microphone R1 signals (the table continues on the following pages)

Response	Explanatory variables
x40ch1, BWMP	*snowd* (.458), *iwspd* (-.431), *itempc* (.408), *mrsig* (-.218) Model F value: 65.2(***), R^2: 0.44, adjusted R^2: 0.43, DW: 0.94
x40ch1, FWMP	*iwspd* (-.444), *snowd* (.395), *itempc* (.360), *mtq* (-.201), *weekno* (-.060) Model F value: 52.6(***), R^2: 0.44, adjusted R^2: 0.44, DW: 0.97
x40ch1, SWMP	*snowd* (.453), *iwspd* (-.450), *itempc* (.387), *mtq* (-.201) Model F value: 65.5(***), R^2: 0.44, adjusted R^2: 0.44, DW: 0.96
x40ch1, BWMM	*iwspd* (-.218), *itempc* (.201), *snowd* (.193), *mrsig* (-.152), *ihum* (-.079), *mustar* (-.071), *weekno* (-.063), *ivisib* (-.049), *cldhgt* (-.038), *pasq* (.034), *mtq* (.024) Model F value: 323.9(***), R^2: 0.20, adjusted R^2: 0.20, DW: 1.51
x80ch1, BWMP	*itempc* (.623), *snowd* (.598), *ihum* (-.423), *gradt* (.366), *iwspd* (-.275), *time* (-.242), *gradthgt* (.239), *locldt* (.230), *ivisib* (-.164) Model F value: 24.1(***), R^2: 0.40, adjusted R^2: 0.38, DW: 1.68
x80ch1, FWMP	*snowd* (.565), *itempc* (.409), *iwspd* (-.330), *srcvwdir* (-.161) Model F value: 32.8(***), R^2: 0.28, adjusted R^2: 0.28, DW: 0.72
x80ch1, SWMP	*snowd* (.565), *itempc* (.409), *iwspd* (-.330), *srcvwdir* (-.161) Model F value: 32.8(***), R^2: 0.28, adjusted R^2: 0.28, DW: 0.72
x80ch1, BWMM	*snowd* (.288), *iwspd* (-.192), *itempc* (.157), *ihum* (-.127), *mustar* (-.103), *srcvwdir* (-.102), *ivisib* (-.082), *mrsig* (.065), *cldhgt* (-.063), *mtq* (.055),

Continued on next page

Table C.1 – continued from previous page

Response	Explanatory variables
	pasq (-.036), *gradt* (.028), *micldt* (-.026), *time* (-.022) Model F value: 152.6(***), R^2: 0.13, adjusted R^2: 0.13, DW: 1.15
x160ch1, BWMP	*itempc* (.363), *srcvwdir* (-.312), *cldness* (.254), *iwspd* (-.239), *snowd* (.238), *ihum* (-.230), *ivisib* (-.216), *hicldt* (-.213) Model F value: 20.0(***), R^2: 0.33, adjusted R^2: 0.31, DW: 0.81
x160ch1, FWMP	*srcvwdir* (-.323), *itempc* (.297), *ihum* (-.239), *iwspd* (-.216), *cldhgt* (-.205), *ivisib* (-.188), *weekno* (-.165) Model F value: 22.1(***), R^2: 0.32, adjusted R^2: 0.31, DW: 0.68
x160ch1, SWMP	*srcvwdir* (-.323), *itempc* (.297), *ihum* (-.239), *iwspd* (-.216), *cldhgt* (-.205), *ivisib* (-.188), *weekno* (-.165) Model F value: 22.1(***), R^2: 0.32, adjusted R^2: 0.31, DW: 0.68
x160ch1, BWMM	*itempc* (.297), *srcvwdir* (-.224), *iwspd* (-.157), *ivisib* (-.141), *snowd* (.107), *ihum* (-.102), *cldhgt* (-.087), *mrsig* (.067), *mustar* (-.057), *weekno* (-.045), *curwea* (.031), *mhf* (.036), *mtq* (.035), *irainf* (-.030) Model F value: 224.7(***), R^2: 0.18, adjusted R^2: 0.18, DW: 0.94
x200ch1, BWMP	*mrsig* (.754), *iwspd* (-.516), *itempc* (.449), *ihum* (-.382), *mustar* (-.369), *locldt* (.279), *snowd* (.166), *ivisib* (-.165), *curwea* (.128), *mhf* (.126), *micldt* (.102) Model F value: 46.1(***), R^2: 0.63, adjusted R^2: 0.62, DW: 1.11
x200ch1, FWMP	*mrsig* (.747), *iwspd* (-.518), *itempc* (.471), *mustar* (-.357), *ihum* (-.351), *locldt* (.271), *snowd* (.174), *ivisib* (-.147), *curwea* (.139), *mhf* (.121) Model F value: 48.8(***), R^2: 0.62, adjusted R^2: 0.61, DW: 1.07
x200ch1, SWMP	*mrsig* (.794), *iwspd* (-.571), *itempc* (.488), *ihum* (-.419), *mustar* (-.346), *locldt* (.273), *snowd* (.190), *ivisib* (-.163), *curwea* (.144) Model F value: 52.6(***), R^2: 0.61, adjusted R^2: 0.60, DW: 1.05
x200ch1, BWMM	*itempc* (.228), *mrsig* (.190), *mustar* (-.162), *mhf* (.133), *iwspd* (-.107), *ihum* (-.089), *snowd* (.081), *ivisib* (-.081), *mtq* (.064), *pasq* (-.060), *cldhgt* (-.058), *locldt* (.041), *curwea* (.039), *micldt* (.033), *srcvwdir* (.029) Model F value: 189.9(***), R^2: 0.16, adjusted R^2: 0.16, DW: 1.28
x250ch1, BWMP	*mrsig* (.647), *iwspd* (-.538), *itempc* (.509), *ihum* (-.377), *cldhgt* (-.294), *mustar* (-.282), *snowd* (.210), *curwea* (.189), *srcvwdir* (-.170) Model F value: 47.4(***), R^2: 0.57, adjusted R^2: 0.56, DW: 0.92
x250ch1, FWMP	*mrsig* (.605), *itempc* (.493), *iwspd* (-.490), *ihum* (-.316), *mustar* (-.291), *cldhgt* (-.280), *snowd* (.193), *curwea* (.183), *srcvwdir* (-.170), *mhf* (.110) Model F value: 43.7 (***), R^2: 0.57, adjusted R^2: 0.56, DW: 0.94
x250ch1, SWMP	*mrsig* (.647), *iwspd* (-.538), *itempc* (.509), *ihum* (-.377), *cldhgt* (-.294), *mustar* (-.282), *snowd* (.210), *curwea* (.189), *srcvwdir* (-.170) Model F value: 47.4(***), R^2: 0.57, adjusted R^2: 0.56, DW: 0.92
x250ch1, BWMM	*itempc* (.249), *mrsig* (.164), *mhf* (.157), *iwspd* (-.154), *mustar* (-.150), *ihum* (-.122), *pasq* (-.102), *cldhgt* (-.102), *snowd* (.082), *ivisib* (-.072), *mtq* (.069), *srcvwdir* (-.063), *curwea* (.054), *micldt* (.034), *hicldt* (.026), *ispress* (-.025), *gradthgt* (.021) Model F value: 251.9(***), R^2: 0.23, adjusted R^2: 0.23, DW: 1.13

Continued on next page

Table C.1 – continued from previous page

Response	Explanatory variables
x315ch1, BWMP	*mrsig* (.718), *iwspd* (-.611), *ihum* (-.478), *itempc* (.438), *cldhgt* (-.340), *mustar* (-.335), *curwea* (.186), *snowd* (.167), *srcvwdir* (-.153), *hicldt* (.113) Model F value: 52.8(***), R^2: 0.62, adjusted R^2: 0.61, DW: 1.03
x315ch1, FWMP	*mrsig* (.623), *iwspd* (-.558), *ihum* (-.390), *itempc* (.383), *mustar* (-.329), *cldhgt* (-.310), *curwea* (.170), *snowd* (.154), *srcvwdir* (-.149), *pasq* (-.104), *hicldt* (.104), *mhf* (.100) Model F value: 46.8 (***), R^2: 0.64, adjusted R^2: 0.62, DW: 1.03
x315ch1, SWMP	*mrsig* (.718), *iwspd* (-.611), *ihum* (-.478), *itempc* (.438), *cldhgt* (-.340), *mustar* (-.335), *curwea* (.186), *snowd* (.167), *srcvwdir* (-.153), *hicldt* (.113) Model F value: 53.8(***), R^2: 0.62, adjusted R^2: 0.61, DW: 1.03
x315ch1, BWMM	*mrsig* (.185), *mustar* (-.178), *itempc* (.175), *iwspd* (-.175), *mhf* (.156), *ihum* (-.139), *pasq* (-.137), *cldhgt* (-.106), *ivisib* (-.073), *mtq* (.066), *srcvwdir* (-.055), *curwea* (.050), *snowd* (.037), *weekno* (-.032), *micldt* (.031), *hicldt* (.029), *ispress* (-.028) Model F value: 252.8(***), R^2: 0.28, adjusted R^2: 0.23, DW: 1.08
x400ch1, BWMP	*iwspd* (-.591), *mrsig* (.553), *ihum* (-.339), *srcvwdir* (-.328), *itempc* (.297), *mustar* (-.259), *cldhgt* (-.243), *snowd* (.194), *pasq* (-.180), *curwea* (.160) Model F value: 38.5(***), R^2: 0.54, adjusted R^2: 0.53, DW: 0.78
x400ch1, FWMP	*iwspd* (-.539), *mrsig* (.503), *ihum* (-.322), *srcvwdir* (-.321), *itempc* (.281), *mustar* (-.262), *cldhgt* (-.206), *pasq* (-.167), *snowd* (.161), *curwea* (.138), *ivisib* (-.099), *mhf* (.095) Model F value: 33.5(***), R^2: 0.56, adjusted R^2: 0.54, DW: 0.79
x400ch1, SWMP	*iwspd* (-.565), *mrsig* (.530), *ihum* (-.399), *srcvwdir* (-.339), *pasq* (-.277), *mustar* (-.255), *cldhgt* (-.228), *ivisib* (-.156) Model F value: 42.2(***), R^2: 0.51, adjusted R^2: 0.50, DW: 0.77
x400ch1, BWMM	*iwspd* (-.189), *srcvwdir* (-.163), *mustar* (-.163), *pasq* (-.163), *mhf* (.162), *itempc* (.154), *mrsig* (.144), *ihum* (-.123), *cldhgt* (-.095), *snowd* (.078), *ivisib* (-.075), *mtq* (.068), *curwea* (.061), *hicldt* (.025), *tend* (.022) Model F value: 309.3(***), R^2: 0.24, adjusted R^2: 0.24, DW: 0.95
x500ch1, BWMP	*iwspd* (-.545), *ihum* (-.389), *itempc* (.375), *srcvwdir* (-.363), *mrsig* (.334), *snowd* (.268), *cldhgt* (-.243), *gradt* (.214), *pasq* (-.175), *curwea* (.154), *time* (-.137) Model F value: 29.8(***), R^2: 0.50, adjusted R^2: 0.49, DW: 1.97
x500ch1, FWMP	*iwspd* (-.553), *srcvwdir* (-.410), *mrsig* (.328), *pasq* (-.310), *mhf* (.190), *weekno* (-.125) Model F value: 40.2(***), R^2: 0.42, adjusted R^2: 0.41, DW: 0.82
x500ch1, SWMP	*iwspd* (-.553), *srcvwdir* (-.410), *mrsig* (.328), *pasq* (-.310), *mhf* (.190), *weekno* (-.125) Model F value: 40.2(***), R^2: 0.42, adjusted R^2: 0.41, DW: 0.82
x500ch1, BWMM	*srcvwdir* (-.205), *iwspd* (-.176), *pasq* (-.155), *mhf* (.153), *ihum* (-.138), *mustar* (-.125), *snowd* (.100), *mrsig* (.099), *itempc* (.098), *cldhgt* (-.081), *mtq* (.079), *ivisib* (-.066), *curwea* (.048), *tend* (.032), *micldt* (.020) Model F value: 278.3(***), R^2: 0.22, adjusted R^2: 0.22, DW: 0.98

Continued on next page

Table C.1 – continued from previous page

Response	Explanatory variables
x630ch1, BWMP	*iwspd* (-.559), *srcvwdir* (-.409), *mrsig* (.301), *ihum* (-.286), *snowd* (.260), *cldhgt* (-.225), *pasq* (-.173), *itempc* (.171) Model F value: 30.6(***), R^2: 0.43, adjusted R^2: 0.42, DW: 0.76
x630ch1, FWMP	*iwspd* (-.546), *srcvwdir* (-.417), *mrsig* (.311), *pasq* (-.301), *mhf* (.169), *snowd* (.165) Model F value: 33.7(***), R^2: 0.38, adjusted R^2: 0.37, DW: 0.80
x630ch1, SWMP	*iwspd* (-.546), *srcvwdir* (-.417), *mrsig* (.311), *pasq* (-.301), *mhf* (.169), *snowd* (.165) Model F value: 33.7(***), R^2: 0.38, adjusted R^2: 0.37, DW: 0.80
x630ch1, BWMM	*srcvwdir* (-.220), *iwspd* (-.175), *pasq* (-.132), *ihum* (-.132), *snowd* (.131), *mhf* (.125), *mustar* (-.097), *itempc* (.094), *mrsig* (.085), *cldhgt* (-.083), *mtq* (.067), *ivisib* (-.066), *curwea* (.044), *tend* (.036), *ispress* (.028) Model F value: 239.3(***), R^2: 0.20, adjusted R^2: 0.20, DW: 1.00
x800ch1, BWMP	*iwspd* (-.542), *ihum* (-.449), *mrsig* (.399), *srcvwdir* (-.384), *snowd* (.364), *itempc* (.361), *cldhgt* (-.247), *gradt* (.243), *time* (-.142), *curwea* (.138) Model F value: 28.1(***), R^2: 0.46, adjusted R^2: 0.45, DW: 1.75
x800ch1, FWMP	*iwspd* (-.530), *srcvwdir* (-.429), *mrsig* (.335), *weekno* (-.236), *pasq* (-.211), *mhf* (.166) Model F value: 35.6(***), R^2: 0.39, adjusted R^2: 0.38, DW: 0.79
x800ch1, SWMP	*iwspd* (-.530), *srcvwdir* (-.429), *mrsig* (.335), *weekno* (-.236), *pasq* (-.211), *mhf* (.166) Model F value: 35.6(***), R^2: 0.39, adjusted R^2: 0.38, DW: 0.79
x800ch1, BWMM	*srcvwdir* (-.197), *iwspd* (-.164), *snowd* (.162), *ihum* (-.150), *mhf* (.125), *pasq* (-.125), *mustar* (-.102), *mrsig* (.089), *cldhgt* (-.073), *ivisib* (-.062), *itempc* (.053), *mtq* (.050), *ispress* (.038), *curwea* (.034), *tend* (.032), *hicldt* (.022) Model F value: 145.8(***), R^2: 0.18, adjusted R^2: 0.18, DW: 1.03
x1000ch1, BWMP	*mrsig* (.643), *iwspd* (-.594), *srcvwdir* (-.391), *ihum* (-.363), *mustar* (-.265), *snowd* (.224), *cldhgt* (-.179), *pasq* (-.168), *weekno* (-.147) Model F value: 39.7(***), R^2: 0.52, adjusted R^2: 0.51, DW: 0.86
x1000ch1, FWMP	*mrsig* (.643), *iwspd* (-.594), *srcvwdir* (-.391), *ihum* (-.363), *mustar* (-.265), *snowd* (.224), *cldhgt* (-.179), *pasq* (-.168), *weekno* (-.147) Model F value: 39.7(***), R^2: 0.52, adjusted R^2: 0.51, DW: 0.86
x1000ch1, SWMP	*mrsig* (.643), *iwspd* (-.594), *srcvwdir* (-.391), *ihum* (-.363), *mustar* (-.265), *snowd* (.224), *cldhgt* (-.179), *pasq* (-.168), *weekno* (-.147) Model F value: 39.7(***), R^2: 0.52, adjusted R^2: 0.51, DW: 0.86
x1000ch1, BWMM	*ihum* (-.179), *snowd* (.166), *srcvwdir* (-.161), *iwspd* (-.155), *mrsig* (.134), *pasq* (-.131), *mustar* (-.121), *mhf* (.117), *ivisib* (-.065), *cldhgt* (-.060), *mtq* (.051), *ispress* (.030), *hicldt* (.024) Model F value: 237.6(***), R^2: 0.17, adjusted R^2: 0.17, DW: 1.08
x1250ch1, BWMP	*mrsig* (1.103), *iwspd* (-.769), *mustar* (-.595), *snowd* (.373), *srcvwdir* (-.348), *ihum* (-.450), *pasq* (-.178), *cldhgt* (-.167) Model F value: 82.1(***), R^2: 0.72, adjusted R^2: 0.71, DW: 1.04

Continued on next page

Table C.1 – continued from previous page

Response	Explanatory variables
x1250ch1, FWMP	*mrsig* (1.101), *iwspd* (-.751), *mustar* (-.593), *ihum* (-.432), *srcvwdir* (-.355), *snowd* (.280), *cldhgt* (-.173), *pasq* (-.152), *weekno* (-.124), *mtq* (.015) Model F value: 67.7(***), R^2: 0.73, adjusted R^2: 0.72, DW: 1.02
x1250ch1, SWMP	*mrsig* (1.103), *iwspd* (-.769), *mustar* (-.595), *ihum* (-.450), *snowd* (.373), *srcvwdir* (-.348), *pasq* (-.178), *cldhgt* (-.167) Model F value: 82.1(***), R^2: 0.72, adjusted R^2: 0.71, DW: 1.04
x1250ch1, BWMM	*mrsig* (.207), *mustar* (-.196), *snowd* (.152), *iwspd* (-.141), *ihum* (-.126), *pasq* (-.118), *srcvwdir* (-.102), *mhf* (.100), *mtq* (.074), *cldhgt* (-.045) Model F value: 218.1(***), R^2: 0.13, adjusted R^2: 0.13, DW: 1.24
x1600ch1, BWMP	*mrsig* (1.526), *iwspd* (-1.020), *mustar* (-.833), *gradt* (-.591), *itempc* (-.503), *srcvwdir* (-.452), *cldness* (-.311), *pasq* (-.292), *cldhgt* (-.286), *time* (.250), *mmos* (-.124), *hicldt* (.111), *gradthgt* (-.104), *ispress* (.100), *snowd* (.093), *weekno* (-.092), *locldt* (-.089), *ivisib* (.071), *ihum* (-.065), *tend* (-.052), *irainf* (-.039), *mhf* (.033), *mtq* (.032), *micldt* (.028), *curwea* (-.020) Model F value: NA(NA), R^2: 1.00, adjusted R^2: 1.00, DW: 1.74
x1600ch1, FWMP	*mrsig* (1.526), *iwspd* (-1.020), *mustar* (-.833), *gradt* (-.591), *itempc* (-.503), *srcvwdir* (-.452), *cldness* (-.311), *pasq* (-.292), *cldhgt* (-.286), *time* (.250), *mmos* (-.124), *hicldt* (.111), *gradthgt* (-.104), *ispress* (.100), *snowd* (.093), *weekno* (-.092), *locldt* (-.089), *ivisib* (.071), *ihum* (-.065), *tend* (-.052), *irainf* (-.039), *mhf* (.033), *mtq* (.032), *micldt* (.028), *curwea* (-.020) Model F value: NA(NA), R^2: 1.00, adjusted R^2: 1.00, DW: 1.74
x1600ch1, SWMP	*ihum* (-.370), *mtq* (.304), *srcvwdir* (-.261), *snowd* (.244) Model F value: 19.9(***), R^2: 0.38, adjusted R^2: 0.36, DW: 1.02
x1600ch1, BWMM	*mrsig* (.186), *mustar* (-.171), *snowd* (.129), *pasq* (-.128), *iwspd* (-.105), *mhf* (.075), *mtq* (.073), *srcvwdir* (-.058), *cldhgt* (-.044), *weekno* (.041), *ihum* (-.038), *cldness* (-.037) Model F value: 93.5(***), R^2: 0.07, adjusted R^2: 0.07, DW: 1.44

C.2 Excess attenuation, 'p' variables

Table C.2: Results of regression analysis with different elimination methods for the linear excess attenuation variables, based on microphone R1 signals (the table continues on the following pages)

Response	Explanatory variables
p40ch1, BWMP	*snowd* (.423), *iwspd* (-.313), *itempc* (.238) Model F value: 23.5(***), R^2: 0.18, adjusted R^2: 0.17, DW: 1.04
p40ch1, FWMP	*snowd* (.423), *iwspd* (-.313), *itempc* (.238) Model F value: 23.5(***), R^2: 0.18, adjusted R^2: 0.17, DW: 1.04
p40ch1, SWMP	*snowd* (.423), *iwspd* (-.313), *itempc* (.238) Model F value: 23.5(***), R^2: 0.18, adjusted R^2: 0.17, DW: 1.04

Continued on next page

Table C.2 – continued from previous page

Response	Explanatory variables
p40ch1, BWMM	*snowd* (.238), *itempc* (.141), *iwspd* (-.138), *pasq* (.072), *mustar* (-.068), *ihum* (-.060), *hicldt* (-.029) Model F value: 161.2(***), R^2: 0.08, adjusted R^2: 0.08, DW: 1.53
p80ch1, BWMP	*snowd* (.463), *itempc* (.321), *iwspd* (-.250) Model F value: 21.4(***), R^2: 0.16, adjusted R^2: 0.16, DW: 0.87
p80ch1, FWMP	*snowd* (.463), *itempc* (.321), *iwspd* (-.250) Model F value: 21.4(***), R^2: 0.16, adjusted R^2: 0.16, DW: 0.87
p80ch1, SWMP	*snowd* (.463), *itempc* (.321), *iwspd* (-.250) Model F value: 21.4(***), R^2: 0.16, adjusted R^2: 0.16, DW: 0.87
p80ch1, BWMM	*snowd* (.277), *itempc* (.181), *iwspd* (-.143), *mustar* (-.097), *mrsig* (.080), *ihum* (-.078), *pasq* (.058), *weekno* (.046), *ivisib* (-.059), *srcvwdir* (-.041), *locldt* (.032), *mtq* (.031) Model F value: 90.3(***), R^2: 0.07, adjusted R^2: 0.07, DW: 1.49
p160ch1, BWMP	*itempc* (.284), *srcvwdir* (-.258), *iwspd* (-.238), *snowd* (.232) Model F value: 14.6(***), R^2: 0.15, adjusted R^2: 0.14, DW: 0.78
p160ch1, FWMP	*srcvwdir* (-.276), *iwspd* (-.199) Model F value: 18.6(***), R^2: 0.10, adjusted R^2: 0.10, DW: 0.73
p160ch1, SWMP	*srcvwdir* (-.276), *iwspd* (-.199) Model F value: 18.6(***), R^2: 0.10, adjusted R^2: 0.10, DW: 0.73
p160ch1, BWMM	*itempc* (.225), *srcvwdir* (-.175), *iwspd* (-.152), *snowd* (.114), *ivisib* (-.089), *pasq* (.079), *cldhgt* (-.054), *ihum* (-.045), *weekno* (-.041) Model F value: 160.3(***), R^2: 0.09, adjusted R^2: 0.09, DW: 1.35
p200ch1, BWMP	*mrsig* (.942), *iwspd* (-.727), *mustar* (-.431), *itempc* (.402), *ihum* (-.290), *snowd* (.272), *locldt* (.226), *srcvwdir* (-.183), *curwea* (.160) Model F value: 32.2(***), R^2: 0.49, adjusted R^2: 0.48, DW: 1.11
p200ch1, FWMP	*mrsig* (.893), *iwspd* (-.674), *mustar* (-.441), *itempc* (.384), *snowd* (.254), *ihum* (-.231), *locldt* (.221), *srcvwdir* (-.182), *curwea* (.152), *mhf* (.116) Model F value: 29.8(***), R^2: 0.50, adjusted R^2: 0.48, DW: 1.12
p200ch1, SWMP	*mrsig* (.942), *iwspd* (-.727), *mustar* (-.431), *itempc* (.402), *ihum* (-.290), *snowd* (.272), *locldt* (.226), *srcvwdir* (-.183) Model F value: 32.2(***), R^2: 0.49, adjusted R^2: 0.48, DW: 1.11
p200ch1, BWMM	*mrsig* (.220), *mustar* (-.190), *itempc* (.182), *iwspd* (-.154), *mhf* (.114), *mtq* (.083), *ihum* (-.066), *locldt* (.065), *srcvwdir* (-.056), *curwea* (.044), *micldt* (.030) Model F value: 152.1(***), R^2: 0.13, adjusted R^2: 0.13, DW: 1.39
p250ch1, BWMP	*mrsig* (.660), *iwspd* (-.600), *itempc* (.429), *srcvwdir* (-.318), *mustar* (-.293), *ihum* (-.289), *snowd* (.237), *cldhgt* (-.201), *curwea* (.159) Model F value: 32.8(***), R^2: 0.48, adjusted R^2: 0.46, DW: 1.00
p250ch1, FWMP	*mrsig* (.654), *iwspd* (-.592), *itempc* (.426), *srcvwdir* (-.329), *ihum* (-.297), *snowd* (.222), *locldt* (.179), *curwea* (.148), *mhf* (.087) Model F value: 29.5 (***), R^2: 0.48, adjusted R^2: 0.46, DW: 1.03

Continued on next page

Table C.2 – continued from previous page

Response	Explanatory variables
p250ch1, SWMP	*mrsig* (.691), *iwspd* (-.632), *itempc* (.440), *srcvwdir* (-330), *mustar* (-.289), *ihum* (-.266), *snowd* (.236), *locldt* (.182), *curwea* (.154) Model F value: 32.3(***), R^2: 0.47, adjusted R^2: 0.46, DW: 1.02
p250ch1, BWMM	*itempc* (.218), *iwspd* (-.175), *srcvwdir* (-.148), *mustar* (-.140), *mrsig* (.138), *snowd* (.114), *pasq* (-.112), *mtq* (.099), *ihum* (-.097), *mhf* (.094), *cldhgt* (-.087), *ivisib* (-.055), *curwea* (.054), *hicldt* (.042), *micldt* (.041), *cldness* (-.033) Model F value: 212.7(***), R^2: 0.19, adjusted R^2: 0.19, DW: 1.26
p315ch1, BWMP	*mrsig* (.675), *iwspd* (-.648), *itempc* (.338), *mustar* (-.335), *srcvwdir* (-.322), *ihum* (-.280), *snowd* (.193), *cldhgt* (-.170), *pasq* (-.157), *curwea* (.141) Model F value: 37.4(***), R^2: 0.54, adjusted R^2: 0.52, DW: 1.01
p315ch1, FWMP	*iwspd* (-.651), *mrsig* (.633), *srcvwdir* (-.364), *mustar* (-.337) *ihum* (-.263), *pasq* (-.211), *gradt* (-.202), *cldhgt* (-.168) Model F value: 42.0 (***), R^2: 0.51, adjusted R^2: 0.50, DW: 2.01
p315ch1, SWMP	*iwspd* (-.651), *mrsig* (.633), *srcvwdir* (-.364), *mustar* (-.337) *ihum* (-.263), *pasq* (-.211), *gradt* (-.202), *cldhgt* (-.168) Model F value: 42.0(***), R^2: 0.51, adjusted R^2: 0.50, DW: 2.01
p315ch1, BWMM	*iwspd* (-.194), *itempc* (.191), *mustar* (-.166), *mrsig* (.162), *pasq* (-.149), *srcvwdir* (-.147), *ihum* (-.102), *mtq* (.095), *snowd* (.088), *mhf* (.085), *cldhgt* (-.078), *ivisib* (-.056), *curwea* (.054), *cldness* (-.045), *micldt* (.034), *hicldt* (.032) Model F value: 224.0(***), R^2: 0.20, adjusted R^2: 0.20, DW: 1.31
p400ch1, BWMP	*iwspd* (-.580), *srcvwdir* (-.405), *mrsig* (.291), *itempc* (.288), *pasq* (-.272), *snowd* (.199) Model F value: 37.4(***), R^2: 0.41, adjusted R^2: 0.40, DW: 0.83
p400ch1, FWMP	*iwspd* (-.580), *srcvwdir* (-.405), *mrsig* (.291), *itempc* (.288), *pasq* (-.272), *snowd* (.199) Model F value: 37.4(***), R^2: 0.41, adjusted R^2: 0.40, DW: 0.83
p400ch1, SWMP	*iwspd* (-.580), *srcvwdir* (-.405), *mrsig* (.291), *itempc* (.288), *pasq* (-.272), *snowd* (.199) Model F value: 37.4(***), R^2: 0.41, adjusted R^2: 0.40, DW: 0.83
p400ch1, BWMM	*srcvwdir* (-.232), *itempc* (.194), *iwspd* (-.186), *pasq* (-.152), *mustar* (-.099), *snowd* (.092), *mtq* (.084), *mhf* (.071), *mrsig* (.067), *ihum* (-.057), *curwea* (.055), *ivisib* (-.051), *cldhgt* (-.051), *time* (-.026), *ispress* (.023) Model F value: 237.6(***), R^2: 0.20, adjusted R^2: 0.20, DW: 1.22
p500ch1, BWMP	*iwspd* (-.539), *srcvwdir* (-.445), *mrsig* (.266), *itempc* (.243), *pasq* (-.233), *snowd* (.225) Model F value: 32.6(***), R^2: 0.37, adjusted R^2: 0.36, DW: 0.82
p500ch1, FWMP	*srcvwdir* (-.448), *iwspd* (-.311), *pasq* (-.303), mhf(.156) Model F value: 42.8(***), R^2: 0.34, adjusted R^2: 0.33, DW: 0.81
p500ch1, SWMP	*srcvwdir* (-.448), *iwspd* (-.311), *pasq* (-.303), *mhf* (.156) Model F value: 42.8(***), R^2: 0.34, adjusted R^2: 0.33, DW: 0.81

Continued on next page

Table C.2 – continued from previous page

Response	Explanatory variables
p500ch1, BWMM	*srcvwdir* (-.259), *iwspd* (-.163), *itempc* (.149), *pasq* (-.139), *snowd* (.101), *mtq* (.087), *mhf* (.067), *ihum* (-.060), *cldhgt* (-.059), *curwea* (.056), *ivisib* (-.043), *ispress* (.040), *cldness* (-.038), *mustar* (-.038), *time* (-.028), *hicldt* (.024), *tend* (.022) Model F value: 186.6(***), R^2: 0.18, adjusted R^2: 0.18, DW: 1.23
p630ch1, BWMP	*srcvwdir* (-.453), *gradt* (-.279), *iwspd* (-.246), *ispress* (.155) Model F value: 28.4(***), R^2: 0.26, adjusted R^2: 0.25, DW: 1.79
p630ch1, FWMP	*srcvwdir* (-.445), *iwspd* (-.267), *gradt* (-.212), *mhf* (.151) Model F value: 28.2(***), R^2: 0.26, adjusted R^2: 0.25, DW: 1.83
p630ch1, SWMP	*srcvwdir* (-.445), *iwspd* (-.267), *gradt* (-.212), *mhf* (.151) Model F value: 28.2(***), R^2: 0.26, adjusted R^2: 0.25, DW: 1.83
p630ch1, BWMM	*srcvwdir* (-.249), *iwspd* (-.162), *itempc* (.125), *snowd* (.120), *pasq* (-.085), *ihum* (-.068), *curwea* (.058), *mtq* (.055), *ispress* (.054), *cldhgt* (-.054), *ivisib* (-.043), *mhf* (.040), *cldness* (-.027), *time* (-.024), *tend* (.023) Model F value: 149.2(***), R^2: 0.13, adjusted R^2: 0.13, DW: 1.31
p800ch1, BWMP	*srcvwdir* (-.384), *snowd* (.241), *iwspd* (-.239), *ihum* (-.219), *itempc* (.199), *curwea* (.148) Model F value: 19.4(***), R^2: 0.26, adjusted R^2: 0.25, DW: 0.91
p800ch1, FWMP	*srcvwdir* (-.409), *ihum* (-.264), *iwspd* (-.219), *cldhgt* (-.164), *weekno* (-.160) Model F value: 22.1(***), R^2: 0.25, adjusted R^2: 0.24, DW: 0.91
p800ch1, SWMP	*srcvwdir* (-.409), *ihum* (-.264), *iwspd* (-.219), *cldhgt* (-.164), *weekno* (-.160) Model F value: 22.1(***), R^2: 0.25, adjusted R^2: 0.24, DW: 0.91
p800ch1, BWMM	*srcvwdir* (-.226), *iwspd* (-.140), *snowd* (.134), *ihum* (-.100), *itempc* (.075), *ispress* (.061), *pasq* (-.059), *cldhgt* (-.056), *curwea* (.056), *mhf* (.047), *mtq* (.044), *cldness* (-.043), *ivisib* (-.042), *hicldt* (.031), *mmos* (-.020) Model F value: 123.7(***), R^2: 0.11, adjusted R^2: 0.11, DW: 1.40
p1000ch1, BWMP	*iwspd* (-.505), *srcvwdir* (-.394), *mrsig* (.329), *snowd* (.271), *gradt* (-.179), *ihum* (-.169), *ispress* (.136) Model F value: 22.2(***), R^2: 0.32, adjusted R^2: 0.31, DW: 1.69
p1000ch1, FWMP	*iwspd* (-.477), *srcvwdir* (-.394), *mrsig* (.355), *weekno* (-.236), *ihum* (-.198) Model F value: 26.1(***), R^2: 0.28, adjusted R^2: 0.27, DW: 0.91
p1000ch1, SWMP	*iwspd* (-.477), *srcvwdir* (-.394), *mrsig* (.355), *weekno* (-.236), *ihum* (-.198) Model F value: 26.1(***), R^2: 0.28, adjusted R^2: 0.27, DW: 0.91
p1000ch1, BWMM	*srcvwdir* (-.171), *ihum* (-.136), *snowd* (.131), *iwspd* (-.117), *mhf* (.072), *mtq* (.057), *ivisib* (-.056), *pasq* (-.054), *ispress* (.049), *hicldt* (.029), *curwea* (.027), *mmos* (-.022) Model F value: 237.6(***), R^2: 0.10, adjusted R^2: 0.10, DW: 1.31

Continued on next page

Table C.2 – continued from previous page

Response	Explanatory variables
p1250ch1, BWMP	*mrsig* (1.020), *iwspd* (-.708), *mustar* (-.487), *srcvwdir* (-.357), *snowd* (.331), *ihum* (-.326) Model F value: 42.1(***), R^2: 0.50, adjusted R^2: 0.49, DW: 1.00
p1250ch1, FWMP	*mrsig* (1.020), *iwspd* (-.708), *mustar* (-.487), *srcvwdir* (-.357), *snowd* (.331), *ihum* (-.326) Model F value: 42.1(***), R^2: 0.50, adjusted R^2: 0.49, DW: 1.00
p1250ch1, SWMP	*mrsig* (1.020), *iwspd* (-.708), *mustar* (-.487), *srcvwdir* (-.357), *snowd* (.331), *ihum* (-.326) Model F value: 42.1(***), R^2: 0.50, adjusted R^2: 0.49, DW: 1.00
p1250ch1, BWMM	*mrsig* (.177), *mustar* (-.155), *snowd* (.134), *iwspd* (-.130), *ihum* (-.127), *srcvwdir* (-.111), *mhf* (.080), *mtq* (.059), *pasq* (-.044), *ivisib* (-.040) Model F value: 145.5(***), R^2: 0.09, adjusted R^2: 0.09, DW: 1.37
p1600ch1, BWMP	*mrsig* (1.461), *iwspd* (-.957), *mustar* (-.750), *srcvwdir* (-.349), *snowd* (.323), *ihum* (-.303), *cldhgt* (-.266), *cldness* (-.262), *hicldt* (.220), *gradt* (-.177) Model F value: 31.2(***), R^2: 0.74, adjusted R^2: 0.72, DW: 1.05
p1600ch1, FWMP	*mrsig* (1.469), *iwspd* (-.893), *mustar* (-.736), *srcvwdir* (-.349), *snowd* (.342), *ihum* (-.201), *mhf* (.092), *mtq* (.080) Model F value: 31.8(***), R^2: 0.70, adjusted R^2: 0.67, DW: 1.07
p1600ch1, SWMP	*mrsig* (1.506), *iwspd* (-.987), *mustar* (-.749), *snowd* (.379), *srcvwdir* (-.361), *ihum* (-.231), *gradt* (-.178) Model F value: 38.5(***), R^2: 0.71, adjusted R^2: 0.69, DW: 1.79
p1600ch1, BWMM	*mrsig* (.162), *mustar* (-.149), *snowd* (.123), *iwspd* (-.100), *mtq* (.077), *pasq* (-.076), *mhf* (.071), *srcvwdir* (-.063), *ihum* (-.046), *cldhgt* (-.042), *weekno* (.034), *cldness* (-.030), *micldt* (.029) Model F value: 67.7(***), R^2: 0.06, adjusted R^2: 0.06, DW: 1.58

Glossary

Accuracy In modelling, the deviation of calculated results from the values obtained by means of a measurement with negligible uncertainty. Also referred to as internal validity. 7, 31

Atmospheric acoustics The science of sound propagation (or sound waves) in the atmosphere (or open air). The structure of the atmosphere varies in both space and time, and these variations have effects on a propagating sound wave. 10

Beta coefficient The coefficients that one would obtain if standardising all of the variables in the regression, including the response variable, and running the regression. All of the variables are on the same scale, and the magnitude of the coefficients can be compared for determination of which one has a greater effect. The variables are standardised through subtraction of the mean, followed by division by the standard deviation. 71

Bragg's scattering A concept related to scattering that occurs when the wavelength of acoustic energy matches the half-wavelength of the electromagnetic signal from a radar (e.g., if the radar operates at 1000 MHz, the acoustic signal should be about 2 kHz). 29

Calm winds Wind speeds below 0.3 m/s, a generally accepted limit that has been used in this work too. 87, 123

Dummy variables Variables used because categorical variables with more than two categories need to be coded if used in regression analysis. In this work, ground type code and current weather code were examples of variables that involved dummy coding (see Table A.1). 65, 101

Durbin–Watson test A simple statistical test for autocorrelation of residuals in regression analysis. The value of the DW statistics ranges from 0 to 4, with a value of 2 meaning that the residuals are uncorrelated. Positive correlation is indicated by

values less than 2, and values approaching 4 represent a strong negative correlation. If the DW value is less than 1.0, there may be cause for concern. However, the test is not valid if there is higher-order autocorrelation or if the error distribution is not normal. 80

Emission Sound emitted by a source, usually defined in terms of sound power level, L_W. There are standard methods of determining the noise emissions of stationary and moving sources. See also 'Immission'. 9

Excess attenuation As presented in this work, the measured attenuation minus geometrical divergence. A negative excess attenuation means that the sound has attenuated less than would be expected in view of the $1/r$ law, possibly because of inversion or downwind effect. 9, 62

Explanatory variables Here, the independent variables. They are referred to as explanatory variables in this thesis since they are rarely independent of one another[206]; see 'Response variable'. These are also known as 'predictor variables', 'regressors', 'controlled variables', 'manipulated variables', 'exposure variables', 'risk factors', 'features', and 'input variables'. 65

External reliability A measure of whether someone else could repeat the test in another situation and get the same result. This is considered also to be reproducibility. 31, 98

External validity How well other scientists can understand and interpret the measurement or test from the documentation provided. 31, 96

***F* value** A result of a test with F statistics. The ratio of the between-groups variance to the within-groups variance, $F = (\text{ variance of the group means})/(\text{mean of the within group variances}) = (\text{explained variance})/(\text{unexplained variance})$. 68

Favourable conditions The atmospheric conditions in which sound is attenuated least. 'Downward-refracting' conditions, wherein the acoustic energy oriented toward the sky bends down to the ground, producing sound levels at the immission point higher than in homogenous conditions. 90, 106, 111

Fermat's principle The principle of least time — the path taken between two points by a ray of sound is the path that can be traversed in the least time. If c is the velocity at any point and ds an element of the length of the ray, the condition may be expressed as $\delta \int \frac{1}{c} ds = 0$[63, p. 126]. 4

Flow resistivity An element analogous to electrical resistance. A pressure difference over a porous material forces air to flow through the material, and the flow resistivity is the ratio of the pressure difference to the flow velocity. 15

Friction velocity The flow rate / velocity at a height, near the ground, where shearing stress caused by dynamic viscosity can be assumed to be independent of height and is proportional to the square of the mean velocity. 52

Geometrical divergence Also referred to as geometrical attenuation. The corresponding frequency-independent decrease in sound level with increasing distance r from the source due to sound energy is spread out over a larger area. Geometrical divergence can be calculated as $A_{\text{div}} = 10\lg\frac{Q}{4\pi r^2}$ dB, where Q is the directivity index of the sound source (for an omnidirectional source, $Q = 1$). 9

Homogenous conditions A homogenous atmosphere, wherein sound propagates in a straight line, producing sound levels at the immission point lower than in favourable conditions. 90

Immission The sound at a specific place due to one or more sound sources, usually defined as sound pressure level, L_p. See also 'Emission'. 9, 30, 111

Internal reliability A way of measuring whether the test can be repeated and produce the same result. Internal reliability increases with repetition. This is considered also to refer to repeatability. 31, 98

Internal validity How well the measurement represents what it should represent. This measures also whether the test performed was done as was documented. 31, 96

KKJ co-ordinates A system used in Finland. The Finland Uniform Coordinate System is based on the European Datum 1950 (ED50) co-ordinate system; it shifts and rotates the ED50 plane for optimally fitting national purposes. Co-ordinates can be presented in geographical terms (latitude, longitude) or as rectangular grid co-ordinates (P = northing, I = easting), with the latter being the presentation used in the present work. The National Land Survey of Finland (NLS) will migrate to the ETRS89 co-ordinate reference system and the plane co-ordinate systems ETRs-TM_{35}FIN and ETRS-GKn in the course of 2013 . 42

Lapse rate The rate of the change of an atmospheric variable as a function of height. The variable is temperature unless it is specified otherwise. 8, 9, 111

Monin–Obukhov similarity theory Similarity theory applying to the surface layer as presented by Monin and Obukhov [205]. It describes the vertical properties of wind and turbulence within the surface layer and enables transferring the measured vertical behaviour of the atmosphere to another place. 53, 100

Obukhov length The height where the generation of turbulence by the buoyancy force exceeds generation by the mechanical forces. A dimensionless Obukhov length (the height above surface divided by the Obukhov length) is used as a stability parameter. Although also known as Monin–Obukhov length, it was first presented by Obukhov alone, in 1946[222] so should not be called the Monin–Obukhov length. See also 'Monin–Obukhov similarity theory'. 53

Orthophoto Also called an orthoimage, an aerial photograph geometrically corrected to correspond to a map of the area. It can be used for measurement of true distances. 43

***p* value** Statistical significance level or risk level. In statistical testing, the probability of the first-class error that is the probability of the data showing a more extreme departure from the null hypothesis when the null hypothesis is true. 68

Pasquill index A six-class (sometimes seven) measurand for characterisation of atmospheric stability. It is designed to provide a semi-quantitative estimate of the mixing capabilities of the lower atmosphere in terms of the horizontal surface wind, the amount of solar radiation (sun incidence angle), and the fractional cloud cover (ceiling). 32, 51, 101, 111

Precision In modelling, a measure of the deviation of the results from various experts. Also considered to refer to external reliability. 31

RASS Radio Acoustic Sounding System[172, pp. 9–14], for measuring lapse rate up to an altitude of one kilometre. Its operation is based on Bragg's scattering. High wind velocities limit RASS altitude to a few hundred metres. The vertical resolution is 60 to 100 m. This functionality can be added to a SODAR. 23, 29

Reliability A measure of the repeatability of a test. For details, see 'Internal reliability' and 'External reliability'. 31

Response variable In this thesis, a term used for the dependent variables. The response variable is variable of primary importance, explained by independent variables or explanatory variables. Response variables are also known as 'regressands', 'measured variables', 'responding variables', 'explained variables', 'outcome variables', 'experimental variables', and 'output variables'. 65

Significance level The level of probability at which it is agreed that the null hypothesis shall be rejected; see also '*p* value'. The levels set in this thesis are 0.05 for 'statistically almost significant', 0.01 for 'statistically significant', and 0.005 (in some tables 0.001) for 'statistically highly significant'. 79, 82, 101

SODAR Sonic Detection and Ranging[172, pp. 9-9 *ff*], for profiling the atmosphere — e.g., measuring lapse rate. The vertical range depends on the power of the transmitter and the atmospheric conditions and may reach several kilometres. Vertical resolution depends on the signals transmitted and the computing power; it can be as great as under a metre (but is typically 50 m). An RASS is sometimes added, to enhance performance. 23, 98, 111

Sonic An anemometer applying acoustic measurement technique. There are no moving parts. The anemometer sends an acoustic pulse to the medium, and the wind speed is calculated from the changes in time or frequency of the acoustic pulse acquired by the same device. 43, 98, 111

Source Anything that emits acoustic energy into the adjacent medium. 5

Synoptic In this work, a term that refers to the regular meteorological weather observations. The synoptic observations were made by an experienced person, while weather-station data were acquired by a machine. 51, 111

Test Here, a generic term for a measurement or a case of modelling. 31

Uncertainty A factor encompassing the reliability and validity of a test. Sometimes it is divided into sub-categories such as aleatory uncertainty, resulting from, for example, random signal generation and scattering effects, and epistemic uncertainty, linked to the state of the environment. 10, 31, 111

Validity A feature determined by how well the test measures what it is meant to measure. For details, see 'Internal validity' and 'External validity'. 31

Bibliography

[1] PANU P. MAIJALA. *Binaural System for Evaluation of Sound Quality*. Master's thesis, Helsinki University of Technology, Espoo, Finland, 1997. (published in 1999). vii

[2] PANU P. MAIJALA. Binauraalinen äänitys ja toisto kuuntelukokeita varten ['Binaural Recording and Authentic Reproduction'], volume 41, pages 285–306. Laboratory of acoustics and audio signal processing, 1996. ISBN 951-22-3309-7. vii

[3] PANU P. MAIJALA. Parempia binauraalisia äänityksiä tosipäällä? ['Better Binaural Recordings Using the Real Human Head?']. In *Proceedings of the Acoustical Society of Finland, Espoo 8.–9.10.1997, (Akustiikkapäivät 1997)*, pages 12–24, Espoo, Finland, October 1997. Akustinen Seura.

[4] ANTTI JÄRVINEN AND PANU P. MAIJALA. On the Use of Real Head Recordings in Product Sound Design. In *Proceedings of the International Conference on Noise Control Engineering, Budapest, Hungary, Aug. 25–27, (Inter-noise 1997)*, volume 2, pages 1143–1146, Budapest, Hungary, August 1997. INCE.

[5] PANU P. MAIJALA. Better Binaural Recordings Using the Real Human Head. In *Proceedings of the International Conference on Noise Control Engineering, Budapest, Hungary, Aug. 25–27, (Inter-noise 1997)*, volume 2, pages 1135–1138, Budapest, Hungary, August 1997. INCE.

[6] HANNA JÄRVELÄINEN, PANU P. MAIJALA, AND MATTI KARJALAINEN. Noise Annoyance Study in the Cabin of Mobile Work Machines. In *Proceedings of the Nordic Acoustical Meeting (NAM'98)*, pages 185–189, 1998.

[7] HANNA JÄRVELÄINEN, MATTI KARJALAINEN, PANU P. MAIJALA, KARI SAARINEN, AND JUKKA TANTTARI. *Työkoneiden ohjaamomelun häiritsevyys ja sen vähentäminen* ['Reducing the Noise Annoyance in Mobile Work Machines'], volume 47. Laboratory of acoustics and audio signal processing, 1998. ISBN 951-22-3967-1. vii

[8] PANU P. MAIJALA. Factors on Perception of Simultaneous Sound Sources, volume 52 of Laboratory of acoustics and audio signal processing publication series, In MATTI KARJALAINEN, editor, *Measurements and Modeling in Acoustics and Audio*, pages 155–176. Laboratory of acoustics and audio signal processing, 1999. ISBN 951-22-4507-8. vii

[9] PANU P. MAIJALA. *Evaluation of Binaural Technology in Hydro-Acoustic Surveillance Systems*. Public research report A/99/6, MATINE, Helsinki, 1999. vii

[10] PANU P. MAIJALA. *Akustiset anturit. Teoria, toimintaperiaatteet, ominaisuudet, kaupalliset anturit ja varusteet sekä valinta käyttötarkoituksen mukaan* ['Acoustical Sensors: Theory, Principles of Operation, Properties, Commercial Sensors and Accessories, and Selection According to Use']. Technical Report TUR C030/1, Technical Research Centre of Finland (VTT), 2000. vii

[11] PANU P. MAIJALA. *Akustisten antureiden tuulisuojat* ['Wind Screens of Acoustic Sensors']. Technical Report TUR C060, Technical Research Centre of Finland (VTT), 2001.

[12] JUKKA LEKKALA, MIKA PAAJANEN, RISTO PORAMO, AND PANU P. MAIJALA. *Laajapinta-alainen akustinen sensori* ['An Acoustic Sensor with Large Surface Area']. Technical report, Technical Research Centre of Finland (VTT), 2000. vii

[13] PANU P. MAIJALA, KARI SAARINEN, AND VELIPEKKA MELLIN. *Äänen leviämistä mallintavan ohjelmiston käyttöönotto ja evaluointi* ['Deployment and Evaluation of a Piece of Sound Propagation Modeling Software']. Technical Report TUR C064, Technical Research Centre of Finland (VTT), 2001. vii, 26, 27

[14] PANU P. MAIJALA. *Maalin korkeuden vaikutus havaitsemisetäisyyteen, laboratoriomittaus* ['The Effect of the Height of a Target on the Detection Distance, Laboratory Measurement']. Technical Report TUO56-021767, Technical Research Centre of Finland (VTT), 2002. vii

[15] PANU P. MAIJALA AND VELIPEKKA MELLIN. *Maalin korkeuden vaikutus havaitsemisetäisyyteen, mallinnustarkastelu* ['The Effect of the Height of a Target on the Detection Distance, a Modelling Approach']. Technical Report TUR C067, Technical Research Centre of Finland (VTT), 2002. vii

[16] PANU P. MAIJALA. Measurements of Atmospheric Sound Propagation Near the Ground, volume 63 of Laboratory of acoustics and audio signal processing publication series, In MATTI KARJALAINEN, editor, *Measurements and modeling in acoustics and audio*, pages 65–84. Laboratory of acoustics and audio signal processing, 2002. ISBN 951-22-5943-5. vii

[17] PANU P. MAIJALA, VELIPEKKA MELLIN, ESA NOUSIAINEN, AND KARI SAARINEN. *Akustisen energian kytkeytyminen rakenteisiin* ['Coupling of Acoustic Energy with Buildings']. Technical Report TUO56-033409, Technical Research Centre of Finland (VTT), 2003. vii

[18] PANU P. MAIJALA. On Sound Radiated by a Fighter, volume 74 of Laboratory of acoustics and audio signal processing publication series, In MATTI KARJALAINEN, editor, *Acoustics and Modeling of Sound Sources*, pages 1–26. Laboratory of acoustics and audio signal processing, 2004. ISBN 951-22-7085-4. vii

[19] PANU P. MAIJALA. *Tutkimussuunnitelma Sodankylän koeasetelmaa varten* ['Research Plan for Sodankylä Trials']. Public research report TUO56-031187, Technical Research Centre of Finland (VTT), 2003. vii

[20] PANU P. MAIJALA. *Sodankylän mittausjärjestelyt* ['Measurement Set-up for Sodankylä Trials']. Public research report 201/IVE-2003, Technical Research Centre of Finland (VTT), August 2003. vii

[21] MERVI KARRU. *Development of Signal Analysis for the Sound Propagation Measurement*. Master's thesis, Helsinki University of Technology, Espoo, November 2004. vii, 10

[22] PANU P. MAIJALA. *ATMOSAKU-ohjelmistomodulin rajapintojen kuvaus* ['The Programming Interface of the ATMOSAKU Software']. Public research report TUO56-041293, Technical Research Centre of Finland (VTT), 2004. vii

[23] PANU P. MAIJALA. *ATMOSAKU-ohjelmistomoduli* ['The ATMOSAKU Software Module']. Public research report TUO56-041300, Technical Research Centre of Finland (VTT), 2004. vii

[24] PANU P. MAIJALA. *ATMOSAKU-ohjelmiston toiminnallinen määrittely* ['Functional Specification of the ATMOSAKU Software']. Public research report TUO56-051364, Technical Research Centre of Finland (VTT), 2005. vii, 16

[25] MERVI KARRU AND PANU P. MAIJALA. *Automaattinen ilmakehän akustiikan mittausjärjestelmä* ['Automatic Measurement System for Atmospheric Acoustics']. Public research report TUO56-041263, Technical Research Centre of Finland (VTT), 2004. vii, 39

[26] PANU P. MAIJALA. Järjestelmä äänen etenemisen mittaamiseen ['System for Measurements of Sound Propagation']. In *Proceedings of the Acoustical Society of Finland, Kuopio 26.–27.09.2005, (Akustiikkapäivät 2005)*, pages 129–134, Kuopio, 2005. Acoustical Society of Finland.

[27] PANU P. MAIJALA. A Set-up for Long Term Sound Propagation Measurements. In *Proceedings of the International Congress on Noise Control Engineering, Tampere, Finland, 30 May – 1 June, (Euronoise 2006)*, number SS20-390, page 6, Tampere, Finland, May 2006. EAA. vii, 23

[28] PANU P. MAIJALA. Excess Attenuation and Meteorological Data in a Long Term Measurement. In *Proceedings of the International Conference on Noise Control Engineering, Tampere, Finland, 30 May – 1 June, (Euronoise 2006)*, number SS20-392, page 6, Tampere, Finland, May 2006. EAA. vii, 23, 25

[29] PANU P. MAIJALA AND OSSI OJANEN. Long-Term Measurements of Sound Propagation in Finland (invited paper). In *Proceedings of the International Conference on Noise Control Engineering, Honolulu, Hawaii, Dec. 3–6 (Inter-noise 2006)*, number 326, page 10, Honolulu, Hawaii, USA, December 2006. INCE. vii

[30] PANU P. MAIJALA. *ATMOSAKU-ohjelmisto* ['The ATMOSAKU Software']. Public research report VTT-R-02565-06, Technical Research Centre of Finland (VTT), 2007. vii, 9, 16, 18, 70, 119, 131

[31] PANU P. MAIJALA. Criterion to Select Meteorological Factors to Evaluate Uncertainties in Sound Propagation. *The Journal of the Acoustical Society of America*, 123(5):3149–3149, June 2008. ISSN 0001-4966. doi: 10.1121/1.2933156. vii

[32] PANU P. MAIJALA. *Noise Propagation in the Atmosphere from Wind Power Plants*. Public research report VTT-R-00030-11, VTT Technical Research Centre of Finland, January 2011. viii

[33] PANU P. MAIJALA, LASSE LAMULA, JOHANNES HYRYNEN, AND DENIS SIPONEN. *Set-up Plan of Facilities for Annoyance Evaluation*. Technical Report EFFORTS project report D.2.4.2., Technical Research Centre of Finland (VTT), February 2008. viii

[34] DIRECTIVE, EN. *Directive 2002/49/EC of the European Parliament and of the Council of 25 June 2002 Relating to the Assessment and Management of Environmental Noise*, June 2002. 1, 7, 12, 13, 171, 174

[35] MONICA GUARINONI, CATHERINE GANZLEBEN, ENDA MURPHY, AND KAROLINA JURKIEWICZ. Towards a Comprehensive Noise Strategy. In *Environment, Public Health and Food Safety*, number IP/A/ENVI/ST/2012-17, page 86. Directorate General for Internal Policies, Policy Department A: Economic and Scientific Policy, B-1047 Brussels, November 2012. 1

[36] ISO. Standard ISO 9613-2:1996. Acoustics — Attenuation of Sound during Propagation Outdoors — Part 2: General Method of Calculation. 1996. 1, 5, 6, 9, 84, 90

[37] JØRGEN KRAGH, BIRGER PLOVSING, S. STOREHEIER, AND HANS JONASSON. *Nordic Environmental Noise Prediction Methods, Nord2000*. Technical Report AV1719001, Delta Acoustics & Electronics, March 2001. 1

[38] WOLFGANG PROBST. Uncertainties in the Prediction of Environmental Noise and in Noise Mapping. In *INCE Europe Conference "Managing Uncertainty in Noise Measurement and Prediction", Le Mans, France*, 2005. 1, 7

[39] LIN FRITSCHI, A. LEX BROWN, ROKHO KIM, DIETRICH SCHWELA, AND STYLIANOS KEPHALOPOULOS, editors. *Burden of Disease from Environmental Noise*. WHO Regional Office for Europe, Scherfigsvej 8, DK-2100 Copenhagen Ø, Denmark, March 2011. ISBN 978-92-890-0229-5. 1

[40] WINAND SMEETS, ADDO VAN PUL, HANS EERENS, ROB SLUYTER, AND GUUS DE HOLLANDER. *Technical Report on Chemicals, Particulate Matter and Human Health, Air Quality and Noise*. Technical Report RIVM No. 481505015, Prepared by RIVM, EFTEC, NTUA, and IIASA in association with TME and TNO under contract with the Environment Directorate-General of the European Commission, RIVM, P.O. Box 1, 3720 BA Bilthoven, May 2000. 1

[41] STÅLE NAVRUD. *The State-of-the-Art on Economic Valuation of Noise*. Technical report, Department of Economics and Social Sciences, Agricultural University of Norway, Final Report to the European Commission, Environment Directorate-General, April 2002. http://ec.europa.eu/environment/noise/pdf/020414noisereport.pdf. 1

[42] ARISTOTLE. *De Anima*. Cambridge University Press, 1907. Translated into English by R. D. Hicks, 1907 (written in 350 BCE). 1, 2, 8

[43] ARISTOTLE OR STRATO OF LAMPSACUS. *De Audibilibus*. OXONII, 1837. Index translated into Latin by Immanuelis Bekkeri, 1837 (formerly attributed to Aristotle but now generally believed to be the work of Strato of Lampsacus). 1, 8

[44] M. R. COHEN AND I. E. DRABKIN. *Source Book in Greek Science*. First Edition edition, January 1948; Harvard University Press, 1 edition, January 1948. ISBN 978-0674823204. 1, 2

[45] PETRI GASSENDI. *Opera Omnia, Tomus Primus*, volume 1. Laurentius Anisson & Ioannes Baptista Devenet, Lyon, France, 1 edition, 1658. 2

[46] R. BRUCE LINDSAY. The Story of Acoustics. *The Journal of the Acoustical Society of America*, 39(4):629–644, 1966. ISSN 0001-4966. doi: 10.1121/1.1909936. 2, 4

[47] J. M. A. LENIHAN. Mersenne and Gassendi: An Early Chapter in the History of Sound. *Acustica*, 2:96–99, 1951. 2

[48] MARIN MERSENNE. *De l'utilité de l'Harmonie*, volume 1. Pierre Ballard, Paris, 1 edition, 1637. 2, 8

[49] J. M. A. LENIHAN. The Velocity of Sound in Air. *Acustica*, 2:205–212, 1952. 2

[50] SIR ISAAC NEWTON. *Philosophiæ Naturalis Principia Mathematica*, volume 1–3. Joseph Streater, for the Royal Society of London, London, 1 edition, July 1687. Newton's own copy of the first edition, in the Cambridge Digital Library. Classmark: Adv.b.39.1. 2, 3, 8

[51] GALILEO GALILEI. *Dialogues Concerning Two New Sciences* (originally 'Discorsi e Dimostrazioni Matematiche, Intorno à due Nuoue Scienze Attenenti alla Mecanica & i Movimenti Locali'). The Macmillan Company, New York, May 1914. Translated into English by Henry Crew and Alfonso De Salvio, 1914. Originally published by In Leida, appresso gli Elsevirii, 1638. 3

[52] SIR ISAAC NEWTON. *The Mathematical Principles of Natural Philosophy*, volume 2. Published Nov 10. 1802 by H. D. Symonds Paternoster Row, London, 3 edition, 1729. Translated into English by Andrew Motte. 3

[53] LEONHARD EULER. Dissertatio Physica de Sono. *Basel*, 1:1–16, February 1727. 3

[54] LEONHARD EULER. De la Propagation du Son ['The Propagation of Sound']. *Mémoires de l'académie des sciences de Berlin*, 15:185–209, November 1759. According to C. G. J. Jacobi, a treatise with this title was presented to the Berlin Academy on November 1, 1759. Number E305 in the series Digitalisierte Akademieschriften und Schriften zur Geschichte der Königlich Preußischen Akademie der Wissenschaften. 3, 4, 8

[55] JEAN (JOHN) LE ROND D'ALEMBERT. Recherches sur la Courbe que forme une Corde Tenduë mise en Vibration. *Histoire de l'Académie royale des sciences et belles-lettres de Berlin (HAB)*, pages 214–219, 1747. 4

[56] BERNARD S. FINN. Laplace and the Speed of Sound. *Isis*, 55(1):7–19, March 1964. 4

[57] PIERRE SIMON LAPLACE. *Traité de Mécanique Céleste, Tome Cinquième*, volume 5. Bachelier, 1825. 4

[58] LEONHARD EULER. Continuation des Recherches sur la Propagation du Son ['Continuation into the Propagation of Sound']. *Mémoires de l'académie des sciences de Berlin*, 15:241–264, November 1759. Number E307 in the series Digitalisierte Akademieschriften und Schriften zur Geschichte der Königlich Preußischen Akademie der Wissenschaften. 4

[59] SIMÉON DENIS POISSON. Sur l'Intégration de Quelques Équations Linéaires aux Différences Partielles, et Particulièrement de l'Équation Générale du Mouvement des Fluides Élastiques. *Mémoires de l'Académie Royale des sciences de l'Institut de France, Année 1818*, 3:121–176, 1820. 4, 8

[60] ALLAN D. PIERCE. *Acoustics: An Introduction to Its Physical Principles and Applications*. Acoustical Society of America, 1989. ISBN 0-88318-612-8. 4

[61] LEONHARD EULER. Supplement aux Recherches sur la Propagation du Son ['Supplement to the Research on the Propagation of Sound']. *Mémoires de l'académie des sciences de Berlin*, 15:210–240, November 1759. According to C. G. J. Jacobi, a treatise with this title was presented to the Berlin Academy on December 13, 1759. Number E306 in the series Digitalisierte

Akademieschriften und Schriften zur Geschichte der Königlich Preußischen Akademie der Wissenschaften. 4

[62] Ulrich J. Kurze and Grant S. Anderson. Outdoor Sound Propagation, In Leo L. Beranek and István L. Vér, editors, *Noise and Vibration Control Engineering: Principles and Applications, Second Edition*, chapter 5, pages 119–144. John Wiley & Sons, Inc., USA, 2006. ISBN 978-0-471-44942-3. doi: 10.1002/9780470172568.ch5. 4, 8

[63] Rayleigh (Strutt, John William), Lord. *The Theory of Sound*, volume 2. Dover Publications, New York, USA, 1945. The first edition of this volume was printed in 1878 and the second edition (revised and enlarged) in 1896. This is the first American edition. 4, 8, 142

[64] B. A. Poole, V. M. Ehlers, F. B. Elder, H. B. Gotaas, and Sol Pincus. Exploration of Research Needs in the Field of Environmental Sanitation. *American Journal of Public Health and the Nations Health*, 38(5_Pt_2):82–86, May 1948. doi: 10.2105/AJPH.38.5_Pt_2.82. 4

[65] Edward Elway Free. Noise Measurement. *Review of Scientific Instruments*, 4(7):368–372, 1933. ISSN 0034-6748. doi: 10.1063/1.1749147. 4

[66] Shirley W. Wynne. New York City's Noise Abatement Commission. *The Journal of the Acoustical Society of America*, 2(1):12–17, 1930. ISSN 0001-4966. doi: 10.1121/1.1915231. 4

[67] Edward Elway Free. Practical Methods of Noise Measurement. *The Journal of the Acoustical Society of America*, 2(1):18–29, 1930. ISSN 0001-4966. doi: 10.1121/1.1915232. 4

[68] Rogers H. Galt. Results of Noise Surveys Part I: Noise Out-of-doors. *The Journal of the Acoustical Society of America*, 2(1):30–58, 1930. ISSN 0001-4966. doi: 10.1121/1.1915233. 4

[69] Rexford S. Tucker. Results of Noise Surveys Part II: Noise in Buildings. *The Journal of the Acoustical Society of America*, 2(1):59–64, 1930. ISSN 0001-4966. doi: 10.1121/1.1915234.

[70] John S. Parkinson. Results of Noise Surveys Part III: Vehicle Noise. *The Journal of the Acoustical Society of America*, 2(1):65–67, 1930. ISSN 0001-4966. doi: 10.1121/1.1915235.

[71] John S. Parkinson. Results of Noise Surveys Part IV: Noise Reduction. *The Journal of the Acoustical Society of America*, 2(1):68–74, 1930. ISSN 0001-4966. doi: 10.1121/1.1915236. 4

[72] IEC. Standard IEC 61672-1:2002. Electroacoustics — Sound Level Meters — Part 1: Specifications. May 2002. 4, 12, 109, 173

[73] Karl Uno Ingard. A Review of the Influence of Meteorological Conditions on Sound Propagation. *The Journal of the Acoustical Society of America*, 25(3):405–411, 1953. ISSN 0001-4966. doi: 10.1121/1.1907055. 5, 8

[74] Hugh Saurenman, James P. Chambers, Louis C. Sutherland, Robert Bronsdon, and Hans Forschner. *Atmospheric Effects Associated with Highway Noise Propagation*. Technical Report FHWA-AZ-05-555, Arizona Department of Transportation, USA, October 2005. 5

[75] N. Blades, G. Marchant, and P. Greening. Impacts of Crushed Rock Quarries on Historic Villages and Cultural Landscapes. In *Proceedings of the 7th European Conference 'SAUVEUR', Safeguarded Cultural Heritage — Understanding & Viability for the Enlarged Europe*, pages 61–70, 2007. 6

[76] JOHN E. WESLER. *Noise Control and Compatibility Planning for Airports*. Technical Report AC 150/5020-1, Federal Aviation Administration, May 1983. 5

[77] RTA SOFTWARE PTY. LTD. Environmental Noise Model. *The Journal of the Acoustical Society of America*, 83(6):2461–2461, 1988. doi: 10.1121/1.396329. 5

[78] KEITH ATTENBOROUGH, S. TAHERZADEH, HENRY E. BASS, XIAO DI, RICHARD RASPET, G. R. BECKER, A. GÜDESEN, A. CHRESTMAN, GILLES A. DAIGLE, A. L'ESPÉRANCE, YANNICK GABILLET, Y. L. LI, MICHAEL J. WHITE, P. NAZ, JOHN M. NOBLE, AND H. A. J. M. VAN HOOF. Benchmark Cases for Outdoor Sound Propagation Models. *The Journal of the Acoustical Society of America*, 97(1):173–191, January 1995. ISSN 0001-4966. 5, 8, 23, 31

[79] YANNICK GABILLET, HARTMUT SCHROEDER, GILLES A. DAIGLE, AND ANDRÉ L'ESPÉRANCE. Application of the Gaussian Beam Approach to Sound Propagation in the Atmosphere: Theory and Experiments. *The Journal of the Acoustical Society of America*, 93(6): 3105–3116, June 1993. ISSN 0001-4966. 5

[80] M. WEST, KENNETH E. GILBERT, AND R. A. SACK. A Tutorial on the Parabolic Equation (PE) Model Used for Long Range Sound Propagation in the Atmosphere. *Applied Acoustics*, 37(1): 31–49, 1992. ISSN 0003-682X. doi: 10.1016/0003-682X(92)90009-H. 5

[81] R. A. SACK AND M. WEST. A Parabolic Equation for Sound Propagation in Two Dimensions over Any Smooth Terrain Profile: The Generalised Terrain Parabolic Equation (GT-PE). *Applied Acoustics*, 45(2):113–129, 1995. ISSN 0003-682X. doi: 10.1016/0003-682X(94)00039-X. 18

[82] ERIK M. SALOMONS. Improved Green's Function Parabolic Equation Method for Atmospheric Sound Propagation. *The Journal of the Acoustical Society of America*, 104(1):100–111, 1999. ISSN 0001-4966. doi: 10.1121/1.423260. 5, 16, 17

[83] RICHARD RASPET, S. W. LEE, E. KUESTER, D. C. CHANG, W. F. RICHARDS, R. GILBERT, AND N. BONG. A Fast-Field Program for Sound Propagation in a Layered Atmosphere above an Impedance Ground. *The Journal of the Acoustical Society of America*, 77(2):345–352, February 1985. ISSN 0001-4966. doi: 10.1121/1.391906. 5

[84] TIMOTHY VAN RENTERGHEM, ERIK M. SALOMONS, AND DICK BOTTELDOOREN. Efficient FDTD-PE Model for Sound Propagation in Situations with Complex Obstacles and Wind Profiles. *Acta Acustica united with Acustica*, 91(4):671–679, 2005. ISSN 1610-1928. 5

[85] MICHAEL MUNGIOLE AND D. KEITH WILSON. Prediction of Outdoor Sound Transmission Loss with an Artificial Neural Network. *Applied Acoustics*, 67(4):324–345, 2006. ISSN 0003-682X. doi: 10.1016/j.apacoust.2005.06.003. 5

[86] REINHARD BLUMRICH AND DIETRICH HEIMANN. A Linearized Eulerian Sound Propagation Model for Studies of Complex Meteorological Effects. *The Journal of the Acoustical Society of America*, 112(2):446–455, August 2002. ISSN 0001-4966. 6

[87] ISO. Standard ISO 1996-1:1982. Acoustics — Description and Measurement of Environmental Noise — Part 1: Basic Quantities and Procedures. 1982. 6, 8

[88] ISO. Standard ISO 3891-1:1978. Acoustics — Procedure for Describing Aircraft Noise Heard on the Ground. 1978. 6

[89] ISO. Standard ISO 9613-1:1993. Acoustics — Attenuation of Sound during Propagation Outdoors — Part 1: Calculation of the Absorption of Sound by the Atmosphere. 1993. 6, 84, 90

[90] Frank H. Brittain and Marlund E. Hale. Some Limitations of Ray-tracing Software for Predicting Community Noise from Industrial Facilities. In *NOISE-CON 2008, Dearborn, Michigan, USA, July 28–30 2008*. NOISE-CON, 2008. 6

[91] Tjeert Ten Wolde. The EU Noise Policy and the Related Research Needs. *Acta Acustica united with Acustica*, 89(5):735–742, 2003. ISSN 1610-1928. 7, 8

[92] Paul de Vos, Margreet Beuving, and Edwin Verheijen. *Harmonised Accurate and Reliable Methods for the EU Directive on the Assessment and Management of Environmental Noise–Final Technical Report*. Technical report, Technical report, 2005. http://www. harmonoise. org, February 2005. 7

[93] Margreet Beuving and Paul de Vos. *Improved Methods for the Assessment of the Generic Impact of Noise in the Environment (IMAGINE) – State of the Art*. Technical Report 2, http://www.imagine-project.org, October 2004. 7

[94] Margreet Beuving and Brian Hemsworth. *Improved Methods for the Assessment of the Generic Impact of Noise in the Environment (IMAGINE) — Guidance on the IMAGINE methods*. Technical report, http://www.imagine-project.org, November 2006. 7

[95] Carl-Christian Hantschk, Fabrice Junker, Dieter Knauss, Dirk van Maercke, Mathias Ringheim, Isabelle Schmich, and J. Rob Witte. *Improved Methods for the Assessment of the Generic Impact of Noise in the Environment (IMAGINE) — Guidelines for Producing Strategic Noise Maps on Industrial Sources*. Technical Report 14, http://www.imagine-project.org, February 2007. 7

[96] Stylianos Kephalopoulos, Balazs Gergely, Fabienne Anfosso-Lédée, and Marco Paviotti. Common Noise Assessment Methods in [the] EU: CNOSSOS-EU (Part I: The Roadmap). In *Proceedings of the 39th International Congress on Noise Control Engineering (Inter-noise 2010), Lisbon, Portugal*, June 2010. 7

[97] Fabienne Anfosso-Lédée, Marco Paviotti, Stylianos Kephalopoulos, and Balazs Gergely. Common Noise Assessment Methods in [the] EU: CNOSSOS-EU (Part II: Application for Strategic Noise Mapping and Action Planning). In *Proceedings of the 39th International Congress on Noise Control Engineering (Inter-noise 2010), Lisbon, Portugal*, June 2010.

[98] Simon Shilton, Nigel Jones, Thomas Werst, Dirk van Maercke, Paul de Vos, Fabienne Anfosso-Lédée, Marco Paviotti, and Stylianos Kephalopoulos. Common Noise Assessment Methods in [the] EU: CNOSSOS-EU (Part III: Guidance for the Competent Use for Strategic Noise Mapping Purposes). In *Proceedings of the 39th International Congress on Noise Control Engineering (Inter-noise 2010), Lisbon, Portugal*, June 2010.

[99] Stylianos Kephalopoulos, Balazs Gergely, Fabienne Anfosso-Lédée, Marco Paviotti, and Paul de Vos. Common Noise Assessment Methods in [the] EU: CNOSSOS-EU (Part IV: Aircraft Noise Prediction for the Purpose of Strategic Noise Mapping). In *Proceedings of the 39th International Congress on Noise Control Engineering (Inter-noise 2010), Lisbon, Portugal*, June 2010. 7

[100] François Abbaléa, Savine Andry, Marine Baulac, Michel C. Bérengier, Bernard Bonhomme, Jérôme Defrance, Jean Pierre Deparis, Guillaume Dutilleux, David Ecotière, Benoît Gauvreau, Vincent Guizard, Fabrice Junker, Hubert Lefèvre, Vincent Steimer, Dirk van Maercke, and Vadim Zouboff. *Road Noise Prediction, 2—Noise Propagation Computation Method Including Meteorological Effects (NMPB 2008)*. Technical Report EQ-SETRA–09-ED32–FR+ENG, Sétra report, June 2009. 7, 8, 84, 90

[101] D. Palazzuoli, Gaetano Licitra, Paul de Vos, J. L. Cueto, R. Hernandez, Guillaume Dutilleux, J. Rob Witte, R. Bütikofer, E. Ascari, Wolfgang Probst, Douglas Manvell, G. Brambilla, Stylianos Kephalopoulos, Marco Paviotti, P. McDonald, L. Maffei, and G. Memoli. *Noise Mapping in the EU—Models and Procedures*. CRC Press, 2012. ISBN 978-0-415-58509-5. doi: 10.1201/b12885-1. 8

[102] ISO. Standard ISO 1996-2:1987. Acoustics — Description and Measurement of Environmental Noise — Part 2: Acquisition of Data Pertinent to Land Use. 1987. 8

[103] ISO. Standard ISO 1996-3:1987. Acoustics — Description and Measurement of Environmental Noise — Part 3: Application to Noise Limits. 1987. 8

[104] J. E. Piercy, T. F. W. Embleton, and Louis C. Sutherland. Review of Noise Propagation in the Atmosphere. *The Journal of the Acoustical Society of America*, 61(6):1403–1418, 1977. ISSN 0001-4966. doi: 10.1121/1.381455. 8

[105] T. F. W. Embleton. Tutorial on Sound Propagation Outdoors. *The Journal of the Acoustical Society of America*, 100(1):31–48, 1996. ISSN 0001-4966. doi: 10.1121/1.415879.

[106] Louis C. Sutherland and Gilles A. Daigle. Atmospheric Sound Propagation, In M. J. Crocker, editor, *Handbook of Acoustics*, chapter 28, pages 305–329. John Wiley & Sons, Inc., New York, 1997. ISBN 0-471-80465-7.

[107] David A. Bies and Colin H. Hansen. *Sound Sources and Outdoor Sound Propagation (Chapter 5)*. Taylor & Francis, 4 edition, June 2009. ISBN 978-0-415-48706-1. 8

[108] Antti Kero. *Epälineaaristen ja aikavarianttien akustisten järjestelmien mittaukset* [‘Measurements of Nonlinear and Time-Variant Acoustical Systems’]. Atmosaku-osaprojektiraportti, Sodankylän geofysiikan observatorio, 2004. 11, 106

[109] Ivan Mammarella and Reijo Hyvönen. *The Structure of the ABL at Sodankylä*. Report of the FMI-ASI Group, Finnish Meteorological Institute, Energy and Environment, 2004. 11, 66, 99, 103

[110] JCGM. JCGM 100:2008. Evaluation of Measurement Data — Guide to the Expression of Uncertainty in Measurement (GUM). 2008. 12

[111] Raimo Eurasto. Ympäristömelun mittaaminen [‘Environmental Noise Measurements’]. In *Ympäristöministeriön ympäristönsuojeluosaston ohje 1/1995*, number 1/1995, page 82. Ympäristöministeriö, ympäristönsuojeluosasto, PL 399, 00121 Helsinki, 1 edition, March 1995. ISBN 951-731-082-X. 12

[112] ISO. Standard ISO 1996-1:2003. Acoustics — Description, Measurement and Assessment of Environmental Noise — Part 1: Basic Quantities and Assessment Procedures. 2003. 13

[113] K. DAVIDSON, N. GUTTMAN, C. ROPELEWSKI, N. CANFIELD, E. SPACKMAN, AND D. GULLETT. *Calculation of Monthly and Annual 30-Year Standard Normals*. Technical Report WMO-TD / No. 341, World Meteorological Organization, March 1989. 13

[114] JØRGEN JAKOBSEN. Danish Regulation of Low Frequency Noise from Wind Turbines. *The Journal of Low Frequency Noise, Vibration and Active Control*, 31(4):239–246, December 2012. ISSN 0263-0923. doi: 10.1260/0263-0923.31.4.239. 13

[115] ERIK M. SALOMONS. *Computational Atmospheric Acoustics*. Kluwer Academic Publishers, 2001. ISBN 0-7923-7161-5. 14, 15, 20, 92, 93

[116] KENNETH E. GILBERT AND MICHAEL J. WHITE. Application of the Parabolic Equation to Sound Propagation in a Refracting Atmosphere. *The Journal of the Acoustical Society of America*, 85(2):630–637, 1989. ISSN 0001-4966. doi: 10.1121/1.397587. 14

[117] C. I. CHESSELL. Propagation of Noise along a Finite Impedance Boundary. *The Journal of the Acoustical Society of America*, 62(4):825–834, 1977. ISSN 0001-4966. doi: 10.1121/1.381603. 15

[118] M. E. DELANY AND E. N. BAZLEY. A Note on the Effect of Ground Absorption in the Measurement of Aircraft Noise. *The Journal of Sound and Vibration*, 16(3):315–322, 1971. ISSN 0022-460X. doi: 10.1016/0022-460X(71)90589-X. 15

[119] T. F. W. EMBLETON, J. E. PIERCY, AND GILLES A. DAIGLE. Effective Flow Resistivity of Ground Surfaces Determined by Acoustical Measurements. *The Journal of the Acoustical Society of America*, 74(4):1239–1244, April 1983. ISSN 0001-4966. doi: 10.1121/1.390029. 16, 17

[120] ALEXANDER POHL, STEFAN DRECHSLER, UWE M. STEPHENSON, DIRK SCHRÖDER, DIRK SVENSSON, AND MICHAEL VORLÄNDER. openMat — an Open XML-database for Acoustical Properties of Materials and Objects. In *Proceedings of the 41st International Congress on Noise Control Engineering (Inter-noise 2012), New York, USA*, volume 2012, August 2012. 16

[121] NORDTEST. Method NT ACOU 104:1999. Ground Surfaces: Determination of the Acoustic Impedance. November 1999. ISSN 0283-7145. 17

[122] J. S. ROBERTSON, W. L. SIEGMANN, AND M. J. JACOBSON. Low-Frequency Sound Propagation Modeling over a Locally Reacting Boundary with the Parabolic Approximation. *The Journal of the Acoustical Society of America*, 98(2):1130–1137, 1995. ISSN 0001-4966. doi: 10.1121/1.413611. 16

[123] B. LANGE AND J. HÖJSTRUP. The Influence of Waves on the Offshore Wind Resource. In *Proceedings of the European Wind Energy Conference*, pages 1216–1219, 1999. 17

[124] ROLAND B. STULL. *An Introduction to Boundary Layer Meteorology*. Kluwer Academic Publishers, Dordrecht, The Netherlands, 1988. ISBN 90-277-2769-4. 18, 19, 52, 65, 66, 100

[125] S. R. HANNA, G. A. BRIGGS, AND R. P. HOSKER. *Handbook on Atmospheric Diffusion*. Report DOE/TIC-11223, National Oceanic and Atmospheric Administration, Atmospheric Turbulence and Diffusion Laboratory, Oak Ridge, TN, USA, January 1982. 19

[126] D. KEITH WILSON, JAMES G. BRASSEUR, AND KENNETH E. GILBERT. Acoustic Scattering and the Spectrum of Atmospheric Turbulence. *The Journal of the Acoustical Society of America*, 105(1):30–34, 1999. ISSN 0001-4966. doi: 10.1121/1.424594. 19

[127] GILLES A. DAIGLE, J. E. PIERCY, AND T. F. W. EMBLETON. Effects of Atmospheric Turbulence on the Interference of Sound Waves near a Hard Boundary. *The Journal of the Acoustical Society of America*, 64(2):622–630, August 1978. ISSN 0001-4966. doi: 10.1121/1.381998. 20

[128] VLADIMIR E. OSTASHEV, ERIK M. SALOMONS, STEVEN F. CLIFFORD, RICHARD J. LATAITIS, D. KEITH WILSON, PHILIPPE BLANC-BENON, AND DANIEL JUVÉ. Sound Propagation in a Turbulent Atmosphere near the Ground: A Parabolic Equation Approach. *The Journal of the Acoustical Society of America*, 109(5):1894–1908, May 2001. ISSN 0001-4966. doi: 10.1121/1.1356022. 20, 32

[129] A. N. KOLMOGOROV. The Local Structure of Turbulence in Incompressible Viscous Fluid for Very Large Reynolds Numbers [in Russian]. In *Doklady Akademii Nauk SSSR* ['Proceedings of the USSR Academy of Science'], volume 30, pages 299–303, 1941. 20

[130] A. N. KOLMOGOROV. The Local Structure of Turbulence in Incompressible Viscous Fluid for Very Large Reynolds Numbers. *Proceedings of the Royal Society of London. Series A: Mathematical and Physical Sciences*, 434(1890):9–13, 1991. ISSN 0962-8444. doi: 10.1098/rspa.1991.0075. 20

[131] VLADIMIR E. OSTASHEV, G. GOEDECKE, B. BRÄHLER, V. MELLERT, AND HARRY J. AUVERMANN. Coherence Functions of Plane and Spherical Sound Waves in the Turbulent Atmosphere with von Karman Spectra of Temperature and Wind Velocity Fluctuations. In *Seventh International Symposium on Long Range Sound Propagation, Écully, France, 24–26 July 1996*, pages 349–357, 1996. 20

[132] WOLF-CHRISTIAN MÜLLER AND DIETER BISKAMP. The Evolving Phenomenological View on Magnetohydrodynamic Turbulence. *Turbulence and Magnetic Fields in Astrophysics*, 614:3–27, 2003. doi: 10.1007/3-540-36238-X_1. 21

[133] D. KEITH WILSON, SERGEI N. VECHERIN, AND VLADIMIR E. OSTASHEV. Modeling Sound Fields from Directive Noise Sources in the Presence of Atmospheric Refraction and Ground Effects. In *Proceedings of the 41st International Congress on Noise Control Engineering (Inter-noise 2012), New York, USA*, volume 2012, August 2012. 20, 21

[134] SERGEI N. VECHERIN, D. KEITH WILSON, AND VLADIMIR E. OSTASHEV. Incorporating Source Directionality into Outdoor Sound Propagation Calculations. *The Journal of the Acoustical Society of America*, 130(6):3608–3622, 2011. ISSN 0001-4966. doi: 10.1121/1.3655881. 21

[135] LARS ROBERT HOLE AND H. M. MOHR. Modeling of Sound Propagation in the Atmospheric Boundary Layer: Application of the MIUU Mesoscale Model. *The Journal of Geophysical Research: Atmospheres*, 104(D10):147–174, 1999. ISSN 2156-2202. doi: 10.1029/1999JD900016. 21, 22

[136] DONALD G. ALBERT, LANBO LIU, PAUL R. ELLER, AND JING-RU C. CHENG. Fast Computations of Outdoor Sound Scattering Using Graphical Processing Hardware. In *Proceedings of the 41st International Congress on Noise Control Engineering (Inter-noise 2012), New York, USA*, volume 2012, August 2012. 22

[137] JIAN KANG. Sound Propagation in Street Canyons: Comparison between Diffusely and Geometrically Reflecting Boundaries. *The Journal of the Acoustical Society of America*, 107(3):1394–1404, 2000. ISSN 0001-4966. doi: 10.1121/1.428580. 22

[138] J. PICAUT, L. SIMON, AND J. HARDY. Sound Field Modeling in Streets with a Diffusion Equation. *The Journal of the Acoustical Society of America*, 106(5):2638–2645, 1999. ISSN 0001-4966. doi: 10.1121/1.428093. 22

[139] MARTIN SCHIFF, MAARTEN HORNIKX, AND JENS FORSSÉN. Excess Attenuation for Sound Propagation over an Urban Canyon. *Applied Acoustics*, 71(6):510–517, 2010. ISSN 0003-682X. doi: 10.1016/j.apacoust.2010.01.005. 22

[140] DIETRICH HEIMANN. Meteorological Aspects in Modeling Noise Propagation Outdoors. In *Proceedings of Euronoise*, 2003. 23

[141] DIETRICH HEIMANN AND ERIK M. SALOMONS. Testing Meteorological Classifications for the Prediction of Long-Term Average Sound Levels. *Applied Acoustics*, 65(10):925–950, October 2004. ISSN 0003-682X. doi: 10.1016/j.apacoust.2004.05.001. 23, 26

[142] DIETRICH HEIMANN, M. BAKERMANS, JÉRÔME DEFRANCE, AND DIETRICH KÜHNER. Vertical Sound Speed Profiles Determined from Meteorological Measurements near the Ground. *Acta Acustica united with Acustica*, 93(2):228–240, 2007. ISSN 1610-1928. 23, 28, 32

[143] PENTTI PIRINEN, HENRIIKKA SIMOLA, JUHA AALTO, JUHO-PEKKA KAUKORANTA, PIRKKO KARLSSON, AND REIJA RUUHELA. *Climatological Statistics of Finland 1981–2010 (Tilastoja Suomen ilmastosta 1981–2010)*, volume the 'Raportteja - Rapporter - Reports 2012:1' of *Finnish Meteorological Institute*. Finnish Meteorological Institute, Helsinki, Finland, Finnish and English edition, August 2012. ISBN 978-951-697-766-2. 23

[144] N. SHU, L. F. COHN, R. A. HARRIS, T. K. KIM, AND W. LI. Comparative Evaluation of the Ground Reflection Algorithm in FHWA Traffic Noise Model (TNM 2.5). *Applied Acoustics*, 68 (11-12):1459–1467, November 2007. ISSN 0003-682X. doi: 10.1016/j.apacoust.2006.07.004. 23

[145] P. CHEVRET, PHILIPPE BLANC-BENON, AND DANIEL JUVÉ. A Numerical Model for Sound Propagation through a Turbulent Atmosphere near the Ground. *The Journal of the Acoustical Society of America*, 100(6):3587, 1996. ISSN 0001-4966. doi: 10.1121/1.417224. 23

[146] P. H. PARKIN AND W. E. SCHOLES. The Horizontal Propagation of Sound from a Jet Engine Close to the Ground, at Radlett. *The Journal of Sound and Vibration*, 1(1):1–13, 1964. ISSN 0022-460X. doi: 10.1016/0022-460X(64)90003-3. 23, 32

[147] P. H. PARKIN AND W. E. SCHOLES. The Horizontal Propagation of Sound from a Jet Engine Close to the Ground, at Hatfield. *The Journal of Sound and Vibration*, 2(4):353–374, 1965. ISSN 0022-460X. doi: 10.1016/0022-460X(65)90115-X. 23, 32

[148] A. GARCÍA AND L. J. FAUS. Statistical Analysis of Noise Levels in Urban Areas. *Applied Acoustics*, 34(4):227–247, 1991. ISSN 0003-682X. doi: 10.1016/0003-682X(91)90007-2. 23, 24

[149] PAUL D. SCHOMER. A Statistical Description of Blast Sound Propagation. *Noise Control Engineering Journal*, 49(2):79–87, March 2001. 24

[150] PAUL D. SCHOMER AND MICHAEL J. WHITE. A Statistical Description of Sound Propagation: A Comparison of Elevated and Near-Ground Sources. *Noise Control Engineering Journal*, 54(3): 157–168, 2006. 24

[151] K. KONISHI, Y. TANIOKU, AND Z. MAEKAWA. Long Time Measurement of Long Range Sound Propagation over an Ocean Surface. *Applied Acoustics*, 61(2):149–172, 2000. ISSN 0003-682X. 25

[152] LARS ROBERT HOLE. *Sound Propagation in the Atmospheric Boundary Layer: An Experimental and Theoretical Study*. PhD thesis, Geophysical Institute, University of Bergen, 1998. 25

[153] BENOIT GAUVREAU. Long-Term Experimental Database for Environmental Acoustics. *Applied Acoustics*, 74(7):958–967, 2013. ISSN 0003-682X. doi: 10.1016/j.apacoust.2013.01.008. 25

[154] T. JUHANI NUOTIO. A Field Study on Sound Propagation Outdoors. 26
Licentiate thesis, Helsinki University of Technology, Department of Electrical Engineering, 1978.

[155] J. HOLMBERG, TAPIO LAHTI, AND T. JUHANI NUOTIO. Ympäristömelun mittaaminen ['The Measurements of the Environmental Noise']. In Laboratory of acoustics publication series, number 21, page 83. Helsinki University of Technology, November 1979. ISBN 951-751-902-8. 26

[156] OSSI OJANEN. *Refraction in a Layered Medium with Applications to Geodesy and to Atmospheric Acoustics*. PhD thesis, Helsinki University of Technology, Department of Surveying, March 1996. 26

[157] DIRK VAN MAERCKE AND JÉRÔME DEFRANCE. Development of an Analytical Model for Outdoor Sound Propagation within the Harmonoise Project. *Acta Acustica united with Acustica*, 93 (2):201–212, March 2007. ISSN 1610-1928. 26

[158] JÉRÔME DEFRANCE, ERIK M. SALOMONS, INGRID NOORDHOEK, DIETRICH HEIMANN, BIRGER PLOVSING, GREG WATTS, HANS JONASSON, XUETAO ZHANG, E. PREMAT, ISABELLE SCHMICH, FRANÇOIS-EDERN ABALLÉA, MARINE BAULAC, AND FOORT DE ROO. Outdoor Sound Propagation Reference Model Developed in the European Harmonoise Project. *Acta Acustica united with Acustica*, 93(2):213–227, 2007. ISSN 1610-1928. 26

[159] DIETRICH KÜHNER. Long-Term Leq Errors Expected and How Long to Measure (Uncertainty and Noise Monitoring). In *Proceedings, Forum Acusticum*, pages 1269–1274, 2005. 35

[160] BIRGER PLOVSING. *Nord2000. Validation of the Propagation Model Client: Danish Road Directorate*. Technical Report AV111706, Delta Acoustics & Electronics, March 2006.

[161] STYLIANOS KEPHALOPOULOS, MARCO PAVIOTTI, DIETER KNAUSS, AND MICHEL C. BÉRENGIER. Uncertainties in Long-Term Road Noise Monitoring Including Meteorological Influences. *Noise Control Engineering Journal*, 55(1):133–141, January 2007. ISSN 0736-2501. doi: 10.3397/1.2709621.

[162] WOLFGANG PROBST AND F. PROBST. Validation of Calculation Methods for Sound Propagation Outdoors. In *INTER-NOISE and NOISE-CON Congress and Conference Proceedings*, volume 2011, pages 449–458. Institute of Noise Control Engineering, 2011. 26

[163] M. GENESCÀ, J. ROMEU, T. PÀMIES, AND A. SÁNCHEZ. Real Time Aircraft Fly-over Noise Discrimination. *The Journal of Sound and Vibration*, 323(1–2):112–129, 2009. ISSN 0022-460X. doi: 10.1016/j.jsv.2008.12.030. 27

[164] M GENESCÀ, J. ROMEU, R. ARCOS, AND S. MARTÍN. Measurement of Aircraft Noise in a High Background Noise Environment Using a Microphone Array. *Transportation Research Part D: Transport and Environment*, 18(0):70–77, 2013. ISSN 1361-9209. doi: 10.1016/j.trd.2012.09.002. 27

[165] BURAK UZKENT, BUKET D. BARKANA, AND JIDONG YANG. Automatic Environmental Noise Source Classification Model Using Fuzzy Logic. *Expert Systems with Applications*, 38(7):8751–8755, 2011. ISSN 0957-4174. doi: 10.1016/j.eswa.2011.01.084. 27

[166] B. D. BARKANA AND B. UZKENT. Environmental Noise Classifier Using a New Set of Feature Parameters Based on Pitch Range. *Applied Acoustics*, 72(11):841–848, November 2011. ISSN 0003-682X. doi: 10.1016/j.apacoust.2011.05.008. 27

[167] CHRISTOPHE COUVREUR, VINCENT FONTAINE, PAUL GAUNARD, AND CORINE GINETTE MUBIKANGIEY. Automatic Classification of Environmental Noise Events by Hidden Markov Models. *Applied Acoustics*, 54(3):187–206, 1998. ISSN 0003-682X. doi: 10.1016/S0003-682X(97)00105-9. 27

[168] AKI HÄRMÄ, M. F. MCKINNEY, AND J. SKOWRONEK. Automatic Surveillance of the Acoustic Activity in Our Living Environment. In *IEEE International Conference on Multimedia and Expo, 2005. ICME 2005*, page 4 pp. IEEE, July 2005. ISBN 0-7803-9331-7. doi: 10.1109/ICME.2005.1521503. 27, 28

[169] TAKATOSHI YOKOTA, KOICHI MAKINO, YOSHIHIRO HIRAO, KOHEI YAMAMOTO, YASUAKI OKADA, AND KOICHI YOSHIHISA. Numerical Simulation on Outdoor Sound Propagation under the Influence of Wind Speed Gradient by the PE Method. In *Proceedings of the International Conference on Noise Control Engineering, Honolulu, Hawaii, Dec. 3–6 (Inter-noise 2006)*, volume 2006, pages 5480–5486. Institute of Noise Control Engineering, 2006. 28, 29, 30, 34

[170] YUI WEI LAM. Characterisation of Meteorological Conditions for Sound Propagation Predictions. In *Proceedings of the 8th International Congress on Sound and Vibration, 2–6 July 2001, Hong Kong, China*, pages 1281–1288. ICSV, July 2001. 28

[171] STUART G. BRADLEY, SABINE VON HÜNERBEIN, AND DAVID C. WADDINGTON. RASS Sound Speed Profile (SSP) Measurements for Use in Outdoor Sound Propagation Models. *IOP Conference Series: Earth and Environmental Science*, 1(1):6, 2008. doi: 10.1088/1755-1307/1/1/012005. 28, 29

[172] DESMOND T. BAILEY. *Meteorological Monitoring Guidance for Regulatory Modeling Applications*. Technical Report EPA-454/R-99-005, United States Environmental Protection Agency, Research Triangle Park, NC 27711, February 2000. Originally published as EPA-450/4-87-013 in 1987. 29, 144, 145

[173] N. J. CRAVEN AND GEOFFREY KERRY. *A Good Practice Guide on the Sources and Magnitude of Uncertainty Arising in the Practical Measurement of Environmental Noise*. University of Salford, May 2007. ISBN 0-9541649-0-3. This is the May 2007 version. The original edition was October 2001. 30

[174] ISO. Standard ISO 1996-2:2007. Acoustics — Description, Measurement and Assessment of Environmental Noise — Part 2: Determination of Environmental Noise Levels. 2007. 30

[175] GEOFFREY KERRY AND DAVID C. WADDINGTON. Considering Uncertainty When Performing Environmental Noise Measurements. In *Institute of Acoustics Autumn Conference 2005*, pages 1–10, October 2005. 30, 31

[176] D. KEITH WILSON AND CHRIS L. PETTIT. Uncertainty in Atmospheric and Terrain Effects on Battlefield Signal Propagation. In *27th Army Science Conference (ASC), JW Marriott Grande Lakes, Orlando, Florida, 29 November – 2 December 2010*, 2010. 31, 32

[177] I. NEWMAN AND C. R. BENZ. *Qualitative-Quantitative Research Methodology: Exploring the Interactive Continuum*. Southern Illinois Univ Pr, 1998. ISBN 0-8093-2150-5. 31

[178] J. KIRK AND M. L. MILLER. *Reliability and Validity in Qualitative Research*. Qualitative Research Methods Series 1. Sage Publications, Inc, 1986. ISBN 0-8039-2470-4.

[179] N. GOLAFSHANI. Understanding Reliability and Validity in Qualitative Research. *The Qualitative Report*, 8(4):597–607, December 2003. 31

[180] WOLFGANG PROBST. Accuracy and Precision of Prediction Models for Road Noise. In *Euronoise 2009, Edinburgh, Scotland, October 26–28, 2009*, October 2009. 31

[181] R. A. PUTNAM. Model Scale Testing of Outdoor Noise Propagation from a Power Plant. *The Journal of the Acoustical Society of America*, 83(S1):S93–S93, May 1988. ISSN 0001-4966. doi: 10.1121/1.2025594. 31

[182] TOM DE MUER AND DICK BOTTELDOOREN. Methods for Quantifying the Uncertainty in Noise Mapping. In *INCE Symposium: Managing Uncertainties in Noise Measurements and Prediction*, 2005. 31

[183] PETER LERCHER, BRAM DE GREVE, DICK BOTTELDOOREN, MARINE BAULAC, JÉRÔME DEFRANCE, AND JOHANNES RÜDISSER. The Effect on Annoyance Estimation of Noise Modeling Procedures. In *Proceedings of the 9th Congress of the International Commission on the Biological Effects of Noise (ICBEN 2008)*, page 670, 2008. 32

[184] SIMON SHILTON, HANS VAN LEEUWEN, AND RENEZ NOTA. Error Propagation Analysis of XPS 31-133 and CRTN to Help Develop a Noise Mapping Data Standard. In *Proceedings of ForumAcusticum 2005, Budapest*, 2005. 32

[185] OLIVIER BAUME, BENOIT GAUVREAU, MICHEL C. BÉRENGIER, FABRICE JUNKER, HANS WACKERNAGEL, AND JEAN-PAUL CHILÈS. Geostatistical Modeling of Sound Propagation: Principles and a Field Application Experiment. *The Journal of the Acoustical Society of America*, 126 (6):2894–2904, December 2009. ISSN 0001-4966. doi: 10.1121/1.3243301. 32

[186] R. H. BOLT, STEPHEN J. LUKASIK, A. WILSON NOLLE, AND A. D. FROST. *Handbook of Acoustic Noise Control. Volume 1. Physical Acoustics*. Technical Report WADC TR 52-204, DTIC document, December 1952. 32

[187] CAMPBELL STEELE. A Critical Review of Some Traffic Noise Prediction Models. *Applied Acoustics*, 62(3):271–287, 2001. ISSN 0003-682X. doi: 10.1016/S0003-682X(00)00030-X. 32

[188] RUFIN MAKAREWICZ AND M. GAŁUSZKA. Road Traffic Noise Prediction Based on Speed-flow Diagram. *Applied Acoustics*, 72(4):190–195, 2011. ISSN 0003-682X. doi: 10.1016/j.apacoust.2010.11.010. 32

[189] RUFIN MAKAREWICZ. The Annual Average Sound Level of Road Traffic Noise Estimated from the Speed-flow Diagram. *Applied Acoustics*, 74(5):669–674, 2013. ISSN 0003-682X. doi: 10.1016/j.apacoust.2012.11.008. 32

[190] ERIK M. SALOMONS, VLADIMIR E. OSTASHEV, STEVEN F. CLIFFORD, AND RICHARD J. LATAITIS. Sound Propagation in a Turbulent Atmosphere near the Ground: An Approach Based on the Spectral Representation of Refractive-index Fluctuations. *The Journal of the Acoustical Society of America*, 109(5):1881–1893, 2001. ISSN 0001-4966. doi: 10.1121/1.1356021. 32

[191] KARL UNO INGARD AND GEORGE C. MALING JR. On the Effect of Atmospheric Turbulence on Sound Propagated over Ground. *The Journal of the Acoustical Society of America*, 35(7):1056–1058, July 1963. ISSN 0001-4966. doi: 10.1121/1.1918657. 32

[192] S. CANARD-CARUANA, S. LEWY, J. VERMOREL, AND G. PARMENTIER. Long Range Sound Propagation near the Ground. *Noise Control Engineering Journal*, 34(3):111–119, May 1990. ISSN 0736-2501. 32

[193] D. BRUCE TURNER. *Workbook of Atmospheric Dispersion Estimates*. Environmental Protection Agency, Office of Air Programs, 4 edition, July 1971. 32, 33

[194] F. A. PASQUILL. *Atmospheric Diffusion*. Van Nostrand Co., London, U.K., 1962. 32, 33

[195] ALBERT W. WALDRON. *A Statistical Method of Calculating Turbulence Values for the Pasquill Stability Categories*. Technical Report 5-C0-402-000-051, DTIC document, March 1977. 32

[196] L. HASSE AND H. WEBER. On the Conversion of Pasquill Categories for Use over Sea. *Boundary-Layer Meteorology*, 31(2):177–185, February 1985. ISSN 0006-8314. doi: 10.1007/BF00121176. 33

[197] D. BRUCE TURNER. A Diffusion Model for an Urban Area. *The Journal of Applied Meteorology*, 3(1):83–91, February 1964. doi: 10.1175/1520-0450(1964)003<0083:ADMFAU>2.0.CO;2. 33

[198] DONALD GOLDER. Relations among Stability Parameters in the Surface Layer. *Boundary-Layer Meteorology*, 3(1):47–58, 1972. ISSN 0006-8314. doi: 10.1007/BF00769106. 33

[199] D. KEITH WILSON, EDGAR L. ANDREAS, JOHN W. WEATHERLY, CHRIS L. PETTIT, EDWARD G. PATTON, AND PETER P. SULLIVAN. Characterization of Uncertainty in Outdoor Sound Propagation Predictions. *The Journal of the Acoustical Society of America*, 121(5):177–183, May 2007. ISSN 0001-4966. doi: 10.1121/1.2716159. 33, 34, 35, 36, 37

[200] C. A. KRAJEWSKI. Uncertainty in Prediction of Environmental Noise Emission Due to Ground Effect. *The Journal of the Canadian Acoustical Association*, 21(3):43–44, 1993. 34, 35

[201] ISO. Standard ISO 8601:2004. Data Elements and Interchange Formats — Information Interchange — Representation of Dates and Times. December 2004. 40

[202] NLS. The National Land Survey of Finland Data Set Open License, Version 1.0, 1.5.2012 ('Maanmittauslaitoksen avoimen tietoaineiston lisenssi, versio 1.0, 1.5.2012'). 43 http://www.maanmittauslaitos.fi/avoindata_lisenssi_versio1_20120501. (Accessed on 27 June 2013).

[203] ISO. Standard ISO 3744:1994. Acoustics — Determination of Sound Power Levels of Noise Sources Using Sound Pressure — Engineering Method in an Essentially Free Field over a Reflecting Plane. 1994. 45, 46, 50, 62, 63

[204] S. VOGT AND P. THOMAS. SODAR — a Useful Remote Sounder to Measure Wind and Turbulence. *The Journal of Wind Engineering and Industrial Aerodynamics*, 54-55:163–172, February 1995. ISSN 0167-6105. doi: 10.1016/0167-6105(94)00039-G. 51

[205] A. S. MONIN AND A. M. OBUKHOV. Basic Laws of Turbulent Mixing in the Surface Layer of the Atmosphere. *Geofizicheskiĭ Institut: Trudy, Akademiia Nauk SSSR*, 151(24):163–187, 1954. 53, 143

[206] B. S. EVERITT AND A. SKRONDAL. *The Cambridge Dictionary of Statistics*. Cambridge University Press, 4 edition, August 2002. ISBN 978-0-521-76699-9. 65, 142

[207] THE MATHWORKS, INC. *MATLAB® Version 7.14.0.739 (R2012a) and Statistics Toolbox Version 8.0 and Signal Processing Toolbox Version 6.17*. Natick, Massachusetts, United States, February 2012. 65

[208] R DEVELOPMENT CORE TEAM. *R: A Language and Environment for Statistical Computing, Version 2.10.1*. R Foundation for Statistical Computing, Vienna, Austria, December 2009. 65

[209] M. E. DELANY AND E. N. BAZLEY. Acoustical Properties of Fibrous Absorbent Materials. *Applied Acoustics*, 3(2):105–116, April 1970. ISSN 0003-682X. doi: 10.1016/0003-682X(70)90031-9. 87

[210] F. P. VON MECHEL. Ausweitung der Absorberformel von Delany und Bazley zu tiefen Frequenzen. *Acustica*, 35:210–213, 1976. ISSN 1610-1928. 87

[211] SYLVAIN M. JOFFRE, MARKKU KANGAS, MARTTI HEIKINHEIMO, AND S. A. KITAIGORODSKII. Variability of the Stable and Unstable Atmospheric Boundary-Layer Height and Its Scales over a Boreal Forest. *Boundary-Layer Meteorology*, 99(3):429–450, 2001. ISSN 0006-8314. doi: 10.1023/A:1018956525605. 99

[212] JARKKO T. KOSKINEN, JANI POUTIAINEN, DAVID M. SCHULTZ, SYLVAIN M. JOFFRE, JARMO KOISTINEN, ELENA SALTIKOFF, ERIK GREGOW, HEIKKI TURTIAINEN, WALTER F. DABBERDT, JUHANI DAMSKI, NOORA ERESMAA, SABINE GÖKE, OTTO HYVÄRINEN, LEENA JÄRVI, ARI KARPPINEN, JANNE KOTRO, TIMO KUITUNEN, JAAKKO KUKKONEN, MARKKU KULMALA, DMITRI MOISSEEV, PERTTI NURMI, HEIKKI POHJOLA, PIRKKO PYLKKÖ, TIMO VESALA, AND YRJÖ VIISANEN. The Helsinki Testbed: A Mesoscale Measurement, Research, and Service Platform. *Bulletin of the American Meteorological Society*, 92(3):325–342, March 2011. doi: 10.1175/2010BAMS2878.1. 106

[213] HUGO FASTL AND EBERHARD ZWICKER. *Psychoacoustics: Facts and Models*. Springer-Verlag New York Inc, 3 edition, 2007. ISBN 978-3-540-23159-2. 108, 109

[214] KLAUS GENUIT. How to Influence Environmental Noise Based on Psychoacoustic Parameters. In *Proceedings of Inter-noise*, 2000. 109

[215] S. SANDROCK, B. GRIEFAHN, TOMASZ KACZMAREK, H. HAFKE, ANNA PREIS, AND T. GJESTLAND. Experimental Studies on Annoyance Caused by Noises from Trams and

Buses. *The Journal of Sound and Vibration*, 313(3-5):908–919, 2008. ISSN 0022-460X. doi: 10.1016/j.jsv.2007.12.003.

[216] PANU P. MAIJALA. A Concept to Model Environmental Noise Annoyance, In MATTI KARJALAINEN, editor, *Modeling of Acoustics and Audio*, page 25. Laboratory of acoustics and audio signal processing publication series. Laboratory of acoustics and audio signal processing, May 2009.

[217] JOHANNES HYRYNEN, PANU P. MAIJALA, AND DENIS SIPONEN. *Target Setting: Implementation Plan for Emission Control Based on Annoyance Evaluation*. Technical Report EFFORTS project report D.2.4.4., VTT Technical Research Centre of Finland, October 2009. 109

[218] TOMASZ KACZMAREK AND ANNA PREIS. Annoyance of Time-Varying Road-Traffic Noise. *Archives of Acoustics*, 35(3):383–393, December 2010. ISSN 0137-5075. doi: 10.2478/v10168-010-0032-2. 109

[219] ISO. Standard ISO 532:1989. Acoustics — Method for Calculating Loudness Level. 1989. 109

[220] JOHANNES HYRYNEN, VELIPEKKA MELLIN, AND PANU P. MAIJALA. *Source Ranking Data (Sound Power Level & Annoyance Data)*. Technical Report EFFORTS project report D.2.4.3., Technical Research Centre of Finland (VTT), November 2008. 109

[221] EBERHARD ZWICKER AND HUGO FASTL. *Psychoacoustics: Facts and Models*. Springer-Verlag Berlin Heidelberg, New York, 3 edition, 1990. ISBN 978-3-540-23159-2. 109

[222] A. M. OBUKHOV. Turbulence in an Atmosphere with a Non-Uniform Temperature. *Geofizicheskiĭ Institut: Trudy, Akademiia Nauk SSSR*, 1:95–115, 1946. 144

[223] ISO. Standard ISO/TR 25417:2007. Acoustics. Definitions of Basic Quantities and Terms. 2007. 173

[224] ISO. Standard ISO 80000-8:2007. Quantities and Units. Part 8: Acoustics. 2007. 173

[225] ISO. Standard ISO 1683:2008. Acoustics — Preferred Reference Values for Acoustical and Vibratory Levels. August 2008. 173

List of figures

List of tables

List of abbreviations and acronyms

ABL	Atmospheric boundary layer.
AWS	Automatic weather station.
BC	Before Christ.
BEM	Boundary element method.
BWMM	Backward missing mean substitution, an elimination method in regression analysis.
BWMP	Backward missing pairwise, an elimination method in regression analysis.
CNOSSOS	Common noise assessment methods.
CNPE	Crank–Nicolson parabolic equation.
COM	Compound, an elimination method in regression analysis.
CUB	Cubic, an elimination method in regression analysis.
CUDA	Compute Unified Device Architecture.
d.f.	Degrees of freedom.
DSM	Directional starter method.
DSTs	Decision-support tools.
DTM	Digital terrain model.
DW	Durbin–Watson statistical test quantity.
END	Environmental Noise Directive, 2002/49[34].
ENM	Environmental Noise Model.
EXP	Exponential, an elimination method in regression analysis.
FAA	United States Federal Aviation Administration.
FM-CHIRP	Frequency-modulated chirp.
FMI	Finnish Meteorological Institute.
FWMP	Forward missing pairwise, an elimination method in regression analysis.
GB	Gigabyte, 10^9 bytes.
GIS	Geographic information system.
GMT	Greenwich Mean Time.
GPU	Graphics processing unit.

GRO	Growth, an elimination method in regression analysis.
GTPE	Generalized Terrain Parabolic Equation.
INM	Integrated Noise Model.
INV	Inverse, an elimination method in regression analysis.
IQR	Interquartile range.
KKJ	Finland Uniform Coordinate System.
LES	Large-eddy simulation.
LIDAR	Light detection and ranging.
LIN	Linear, an elimination method in regression analysis.
LGS	Logistic, an elimination method in regression analysis.
LOG	Logarithmic, an elimination method in regression analysis.
MET	Meteorological.
MLS	Maximum length sequence.
MS	The EU member states.
NLS	The National Land Survey of Finland (or 'Maanmittauslaitos').
P2P	Point-to-point.
PE	Parabolic equation.
PF	Paris feet, referring to an ancient French unit of length, 0.3248 m.
POW	Power, an elimination method in regression analysis.
QUA	Quadratic, an elimination method in regression analysis.
RASS	Radio Acoustic Sounding System.
RH	Relative humidity.
RPM	Random-coded phase-modulation.
Rsq	A statistical measure of the strength of association, R^2.
SD	Standard deviation.
SGO	Sodankylä Geophysical Observatory.
Sigf	Statistical significance level, p value.
SNR	Signal-to-noise ratio.
SODAR	Sound Detection and Ranging.
SSP	Sound speed profile.
SPL	Sound pressure level.
SRC	Secret Rabbit Code library, a library for sample-rate conversion.
SVM	Support vector machine.
SSP	Synthetic sound speed profile.
SWMP	Stepwise missing pairwise, an elimination method in regression analysis.
Ts	Toise, an ancient French unit of length, 6 PF (Paris feet), or 1.949 m.
UBA	Unbiased annoyance.
UTC	Coordinated Universal Time.
WAV	Waveform Audio File Format.

List of symbols

The definitions are based on ISO/TR 25417[223] and are consistent in essence with ISO 80000-8[224]. Frequency weightings are specified in IEC 61672-1[72]. Reference values for acoustic levels follow ISO 1683[225].

Vector symbols

are boldface upright Roman characters. Examples are $\mathbf{r} = (x, y, z)$ and matrix

$$\mathbf{D} = \begin{pmatrix} \xi_1 & \xi_2 \\ \xi_3 & \xi_4 \end{pmatrix}.$$

Notation for differentials

$\partial_x f$	$\equiv \partial f / \partial x$,	Partial derivative of the function f with respect to x.
$\partial_x^2 f$	$\equiv \partial^2 f / \partial x^2$,	Second partial derivative of the function f with respect to x.
$f'(x)$	$\equiv df/dx$,	Derivative of the function $f(x)$.
∇	$\equiv (\partial_x, \partial_y, \partial_z)$,	Nabla operator in a rectangular co-ordinate system.
∇f	$= (\partial_x f, \partial_y f, \partial_z f)$,	Gradient of the scalar function f.
$\nabla \cdot \mathbf{v}$	$= \partial_x v_x + \partial_y v_y + \partial_z v_z$,	Divergence of the vector function $\mathbf{v} = (v_x, v_y, v_z)$.

Roman symbols

C_T^2	Temperature structure-function parameter — see Table 4.9, $K^2/m^(2/3)$.
C_v^2	Velocity structure-function parameter — see Table 4.9, $(m/s)^2/m^(2/3)$.
D	Directivity — see Eq. 3.5.
G	Divergence — see Eq. 3.11.
H	Relative height.

L	Distance.
L_0	Obukhov length — see Eq. 3.13.
L_{den}	The day-evening-night level as introduced in the END[34, p. 7].
L_1	A percentile level — the sound level exceeds this threshold 1% of the time.
L_{10}	A percentile level — the sound level exceeds this threshold 10% of the time.
L_{50}	A percentile level — the sound level exceeds this threshold 50% of the time.
L_{90}	A percentile level — the sound level exceeds this threshold 90% of the time.
L_{99}	A percentile level — the sound level exceeds this threshold 99% of the time.
L_{eq}	Equivalent sound pressure level.
L_F	Level for favourable conditions, defined in Section 4.9.2.
L_H	Level for homogenous conditions, defined in Section 4.9.2.
L_{LT}	Long-term level, defined in Section 4.9.2.
L_p	Sound pressure level.
$L_{p,\text{A}}$	A-weighted sound pressure level.
$L_{p,\text{A,eq}}$	A-weighted equivalent sound pressure level.
L_W	Sound power level.
N	A reference to the number of events, also to compass point North.
P	Gas (or atmospheric) pressure.
Q	Effect of environment on the directivity of the source — see Eq. 3.1.
Q1	First quarter of the year.
Q2	Second quarter of the year.
Q3	Third quarter of the year.
Q4	Fourth quarter of the year.
Q_0	Kinematic heat flux, $\langle w'T' \rangle$.
$\mathscr{R}$	Gas constant, 8.3145 $\text{J}/(\text{mol}\cdot\text{K})$.
R1 to R8	Microphones 1 to 8.
R^2	Statistical measurand of the strength of association.
R_d	Gas constant, 287.04 $\text{J}/(\text{kg}\cdot\text{K})$.
R_s	Reflection coefficient for summertime.
R_w	Reflection coefficient for wintertime.
T	Air temperature, K.
T_0	Mean temperature near the ground, K.
U_{RMS}	Root mean squared voltage.
c	The speed of sound.
c_0	The speed of sound near the ground, m/s.
g	Acceleration of free fall, ≈ 9.81 m/s.
h	Solar altitude.
i	Imaginary unit.
k	Wave number, ω/c

p_f	Probability of occurrence — see Eq. 4.18.
p_c	Complex sound pressure amplitude.
r	Distance.
t	Temperature of air, °C.
t_0	Temperature near the ground, °C.
u	Uncertainty.
$u_\star$	Friction velocity — see Eq. 3.12.
u'	Wind component of the direction of wind flow.
v'	Wind perpendicular (horizontal) component of the direction of wind flow.
w'	Wind perpendicular (vertical) component of the direction of wind flow.
z_0	Aerodynamic roughness value for the ground.
z	Height above ground.

Greek symbols

Θ	Potential temperature.
α	Gradient of wind speed profile.
β	Geometrical angle.
γ	Adiabatic ratio / constant of gases, for air 1.4.
ζ	Monin–Obukhov stability parameter, also the variable *mmos* in the analysis — see Eq. 4.2.
κ	Von Kármán's constant (≈ 0.4).
ρ	Gas (air) density.
ρ_0	Static density of air.
σ	Normal standard deviation.
σ_r	Flow resistivity.
σ_s	Flow resistivity during summer.
σ_w	Flow resistivity during winter.
θ	Angle between horizontal wind and the sound propagation directions.
$\psi(x,z)$	Function for sound pressure field, shown as a function of x and z, also other variables.
ω	Angular velocity.

Index

Series title and number
VTT Science 48

Title	**A measurement-based statistical model to evaluate uncertainty in long-range noise assessments**
Author(s)	Panu Maijala
Abstract	Carefully validated long-range sound propagation measurements with extensive meteorological instrumentation were continued for 612 days without interruption, around the clock, resulting in a database with millions of files, terabytes of sound and environmental data, and hundreds of pages of documentation. More than 100 environmental variables were analysed by statistical means, and many statistically highly significant dependencies linked to excess attenuation were found. At a distance of 3 km from the source, excess attenuation was spread over a dynamic range of 80 dB, with differences of 10 dB between individual quarters of the year; also, negative excess attenuation at frequencies below 400 Hz existed. The low frequencies were affected mainly by the stability characteristics of the atmosphere and the lapse rate. Humidity; lapse rate; sensible heat flux; and longitudinal, transverse, and vertical turbulence intensities explain excess attenuation at higher frequencies to a statistically highly significant extent. Through application of a wide range of regression analyses, a set of criteria for frequency-dependent uncertainty in sound propagation was created. These criteria were incorporated into a software module, which, together with a state-of-the-art physical sound propagation calculation module, makes it possible to perform environmental noise assessments with known uncertainty. This approach can be applied to the shortterm measurements too and it was shown that some of the most complex meteorological variables, among them atmospheric turbulence, can be taken into account. Comparison with two standardised noise modelling methods showed that the statistical model covers well a range of uncertainty notmatched with the standardisedmethods and themeasured excess attenuation fit within the limits of predicted uncertainty.
ISBN, ISSN	ISBN 978-951-38-8109-2 (Soft back ed.) ISBN 978-951-38-8110-8 (URL: http://www.vtt.fi/publications/index.jsp) ISSN-L 2242-119X ISSN 2242-119X (Print) ISSN 2242-1203 (Online)
Date	December 2013
Language	English, Finnish abstract
Pages	178 p.
Keywords	acoustic wave propagation, aeroacoustics, atmospheric acoustics, environmental acoustics, environmental noise, noise assessments, uncertainty, statistical model
Publisher	VTT Technical Research Centre of Finland P.O. Box 1000, FI-02044 VTT, Finland, Tel. +358 20 722 111

Julkaisun sarja ja numero
VTT Science 48

Nimeke	**Mittauksiin perustuva tilastollinen malli ympäristöolosuhteiden aiheuttaman epävarmuuden arvioimiseksi ympäristömelun kartoituksissa**
Tekijä(t)	Panu Maijala
Tiivistelmä	Ympäristömelun vuosittaiset kustannukset EU:ssa ovat 38 miljardia ja Suomessa 4 miljardia euroa. Terveydelliset ja taloudelliset vaikutukset kohdistuvat yksilöihin ja yrityksiin, mm. aiheuttaen sydän- ja verisuonitauteja, laskien asuntojen arvoa, rajoittaen tuotannon toiminta-aikoja ja maa-alueiden käyttöä. Sää ja ympäristöolosuhteet vaikuttavat monin tavoin ympäristömeluun ja nykyisin käytössä olevat melumallit eivät ota monia vaikutuksia huomioon, jolloin laskennalliset tulokset täytyy usein kyseenalaistaa. Uudet lait ja säädökset asettavat haasteita myös melun mittaamiselle. Väitöstyössä on esitetty tilastollinen malli, jonka avulla ympäristöolosuhteiden aiheuttaman epävarmuuden arvioiminen ympäristömelun kartoituksissa on mahdollista. Myös monimutkaiset meteorologiset tekijät, kuten turbulenssi, voidaan melun mallinnuksessa ottaa huomioon. Tutkimuksessa mitattiin melun leviämistä samanaikaisesti yli sadan ympäristöön ja säähän liittyvän parametrin kanssa. Ilmakehän ominaisuuksia mitattiin mm. radiosondeilla ja tutkalla. Aineistoa kerättiin ympäri vuorokauden kahden vuoden ajan. Pitkäaikaismittaustuloksia verrattiin kahden standardoidun melumallin ja väitöskirjassa esitetyn tilastollisen mallin laskennallisiin tuloksiin. Tilastollinen malli kattoi mitattujen arvojen vaihtelun, standardoidut mallit eivät. Lisäksi meteorologisten suureiden ja melun välille löytyi uusia riippuvuussuhteita.
ISBN, ISSN	ISBN 978-951-38-8109-2 (nid.) ISBN 978-951-38-8110-8 (URL: http://www.vtt.fi/publications/index.jsp) ISSN-L 2242-119X ISSN 2242-119X (painettu) ISSN 2242-1203 (verkkojulkaisu)
Julkaisuaika	Joulukuu 2013
Kieli	Englanti, suomenkielinen tiivistelmä
Sivumäärä	178 s.
Avainsanat	aeroakustiikka, ilmakehän akustiikka, ympäristöakustiikka, ympäristömelu, melukartoitus, epävarmuus, tilastollinen malli
Julkaisija	VTT PL 1000, 02044 VTT, puh. 020 722 111

A measurement-based statistical model to evaluate uncertainty in long-range noise assessments

In addition to restricting land use and causing real estate to lose value, environmental noise has become a health issue: cardiovascular disease and cognitive impairment are among the identified effects of environmental noise. Including disturbance and annoyance, the social significance of this question is of major economic importance today.

Weather and environmental conditions affect environmental noise. Because not all these effects have been implemented in the existing noise models, resulting predictions must often be called into question. New laws and regulations pose challenges for the noise measurement also.

The model presented in this thesis allows to evaluate the uncertainty created by changing environmental and atmospheric conditions. Even complex meteorological variables, among them atmospheric turbulence, can be taken into account in noise predictions.

Comparison with two standardised noise modelling methods showed that the approach presented in this thesis covers well a range of uncertainty not matched with the standardised methods and the measured values fit within the limits of predicted uncertainty. Also, new information on the interdependencies between the noise and meteorological variables were shown.

ISBN 978-951-38-8109-2 (Soft back ed.)
ISBN 978-951-38-8110-8 (URL: http://www.vtt.fi/publications/index.jsp)
ISSN-L 2242-119X
ISSN 2242-119X (Print)
ISSN 2242-1203 (Online)